Performance Analysis and Characterisation of a High Concentrating Solar Photovoltaic Receiver

Ali Omar Mohamed Maka

Submitted for the degree of Doctor of Philosophy

Heriot-Watt University

School of Engineering and Physical Sciences

Institute of Mechanical Process and Energy Engineering

December 2019

ABSTRACT

Solar energy is deemed to be one the most efficient and clean energy resources to generate electricity. Photovoltaic technologies have a promising future in space and terrestrial applications. Photovoltaic concentrating is a technique to increase the conversion efficiency of high-efficiency solar cells. Multi-junction solar cells are designed to exploit a larger range of solar spectrum photons and convert to electricity. In this study, triple-junction III–V solar cells compound consisting of GaInP/GaInAs/Ge semiconductor materials is considered.

This work investigates terrestrial multi-junction solar cells performance characterisation, which is important for the design of high concentration photovoltaic systems. The research has developed a model of a III–V solar cell operating at high flux conditions induced by light concentration. The thermal management on such an assembly is a focus of this work. This research also presents the effects of Air Mass (*AM*) on solar cell performance. This atmospheric parameter has a strong influence on the behaviour of high concentrating photovoltaic solar cells. As air mass increases, the corresponding Direct Normal Irradiance (*DNI*) and Cell Temperature (T_c) decrease. The effects of air mass (*AM* =1–10D) atmospheric changes on triple-junction solar cells have been assessed. For High Concentration Photovoltaic (HCPV) the light concentration on to a relatively small solar cell area leads to high power densities.

Effective thermal management is essential to avoid damaging high temperatures. A thermal model by using a convergent iterative technique has been developed; the predicted convergent cell temperature limit is $\leq 80^{o}$C. The proportion of the incident radiation not converted to electricity leads to the generation of heat; this is a function of material temperature coefficients and current mismatch in variable atmospheric conditions and results in an increase in cell temperature. The rate of heat loss by convective transfer is also considered for air mass values *AM* =1.5, 4 and 8D. In addition, a Finite Element Method (FEM) model is developed in COMSOL Multiphysics® in order to predict the temperature distribution of the PV cells and thermal behaviour of the receiver assembly.

Furthermore, in this study, a transient model of the HCPV cell has been developed using MATLAB® Live-Link with COMSOL Multiphysics. In order to characterise the behaviour of a triple-junction solar cell, it is essential to find the transient cell operating temperature. The behaviour of electrical parameters of the J_{sc}, V_{oc}, FF and conversion

efficiency are considered. However, in the proposed model, a dynamical efficiency is compared with constant efficiency and the error is about 12%.

The research has given a better understanding of the overall daily/annual performance prediction of CPVs and is important for future system design in variable environment conditions. At higher values of *DNI*, T_{amb} and lower *AM* the thermal response needs enhanced/forced convection to maintain cell operation within/below safe operating temperature and to optimise energy yield. For long-term performance evaluation, the average of monthly variations of atmospheric parameters throughout the year is considered. Thus, during the summer months, a higher record of the atmospheric parameters values in which need more consideration. The annual cell operating temperature of > 80^{o}C represents about 13% of the time, which happened during the Summer season. As is noted, the cell temperature between 65 – 70^{o}C is predominate in the Spring and Autumn seasons and represent about 24%, (the highest frequency).

Dedication

This thesis is dedicated
To
Sprit of my Father and Mother
and
My Wife
and
My Children
and
My Brothers and Sisters
and
My Friends

Acknowledgements

First of all, I thank “Allah”, the most gracious and the most merciful for directing me to the right path and for enabling me to do this work. All praise is due to “Allah” for his guidance, blessing and assistance to me to complete my Thesis.

My honest gratitude is to my supervisor Prof. Tadhg S. O’Donovan for his support, guidance and patience to accomplish this research project. In addition, his suggestions and guidance have been invaluable. His expertise and knowledge have always been helpful for me to rectify my mistakes and to learn new things. I would like also to thank my Co-supervisor Dr Nick Bennat.

Many thanks to the School of Engineering and Physical Sciences, Heriot-Watt University and to my research group. I would like to give my sincerest thanks to thanks to Dr Marios Theristis, for his guidance, encouragement and support and for his useful technical comments. Also, thanks to L. Stefano from my research group.

Thanks to the Libyan government for funding and give me an opportunity to postgraduate study. Special thanks to stuff in Arab Centre for research and development of sharain community.

Special thanks to those people for their help and to my friend's grateful thanks. Also, extend my thanks to all my friends during my PhD study at Heriot-Watt University. Dr Tariq Nawaz, Dr Mohamed Farooq, Mahmud Mubasher, Salem Salem.

I would like to extend my thanks to my family for their prayers, continues support and engorgement, to my Brothers and Sisters in Libya; I will not forget their support and gaudiness in my life. In addition, many thanks to all my friends those always asking about me.

Lastly, but not the least, special grateful thanks to my Wife; and to my lovely daughters: Fatma and Alzahra, Furthermore, to my lovely Sons: Omar, Abdulminom and Akram for their continues support and patience during the journey of my doctoral study.

ACADEMIC REGISTRY

Research Thesis Submission

Name*:*	**Ali Omar Mohamed Maka**		
School:	Engineering and Physical Science		
Version: *(i.e. First, Resubmission, Final)*	**Final**	Degree Sought:	**Phd** **Mechanical Engineering**

Declaration

In accordance with the appropriate regulations, I hereby submit my thesis and I declare that:

1) The thesis embodies the results of my own work and has been composed by myself
2) Where appropriate, I have made acknowledgement of the work of others and have made reference to work carried out in collaboration with other persons
3) The thesis is the correct version of the thesis for submission and is the same version as any electronic versions submitted*.
4) my thesis for the award referred to, deposited in the Heriot-Watt University Library, should be made available for loan or photocopying and be available via the Institutional Repository, subject to such conditions as the Librarian may require
5) I understand that as a student of the University I am required to abide by the Regulations of the University and to conform to its discipline.
6) I confirm that the thesis has been verified against plagiarism via an approved plagiarism detection application e.g. Turnitin.

* *Please note that it is the responsibility of the candidate to ensure that the correct version of the thesis is submitted.*

Signature of Candidate*:*		Date:	

Submission

Submitted By *(name in capitals):*	ALI OMAR MOHAMED MAKA
Signature of Individual Submitting:	
Date Submitted:	11/01/2020

For Completion in the Student Service Centre (SSC)

Received in the SSC by *(name in capitals):*			
Method of Submission *(Handed in to SSC; posted through internal/external mail):*			
E-thesis Submitted (mandatory for final theses)			
Signature:		Date:	

Table of Contents

ABSTRACT i
Dedication iii
Acknowledgements iv
ACADEMIC REGISTRY v
Table of Contents vi
Lists of Figures x
Lists of Tables xv
Glossary xvi
Chapter 1 : Introduction 1
1.1 Introduction 1
1.2 Photovoltaic solar cells 4
1.2.1 First Generation 4
1.2.2 Second generation 4
1.2.3 Third generation 5
1.3 Solar cell principle 5
1.3.1 P-N Junction 5
1.3.2 Ideal Solar Cell Characteristics 6
1.4 Research Aims and Objectives 8
1.5 Thesis outline 9
Chapter 2 : Background and Literature Review 11
2.1 Introduction 11
2.2 Energy development 11
2.2.1 Historical development of CPV technology 12
2.2.2 Development of CPV Solar cells 15
2.3 Solar spectrum 23
2.3.1 Triple-junction solar cells spectral distribution 25
2.4 Concentration ratio 28
2.4.1 Geometric concentration ratio 28
2.4.2 Optical concentration ratio 29
2.5 Photovoltaic Concentrating Technique 30
2.5.1 Ultra-high concentration (CR > 2000 suns) 30
2.5.2 High concentration (CR > 100 < 2000 suns) 30

2.5.3 Medium concentration (10 suns > CR < 100 suns) 30
2.5.4 Low concentration (CR < 10 suns) 31
2.6 Thermal management requirement of CPV receiver 32
2.6.1 Passive heat dissipation 32
2.6.2 Active heat dissipation 32
2.7 Concentrating Photovoltaic Receivers 33
2.7.1 Substrate 33
2.8 Heat remover module 34
2.9 Prediction and measuring of cell temperature 36
2.10 Reliability Requirements 40
Chapter 3 : Triple-Junction Solar Cell Performance Modelling and Characterisation 48
3.1 Introduction 48
3.2 Electrical model 48
3.2.1 Modelling of single/triple junction cells at 1x 49
3.3 Modelling results and discussions 54
3.3.1 Single/triple junction J-V curve 54
3.3.2 Current limitation 57
3.3.3 Validation 60
3.3.4 J-V curve verification 61
3.4 Spectrum model 62
3.5 Effects of increases of *AM* in the solar spectrum 63
3.6 Effects of increases in the *AM* in the performance of Triple junction cell 64
3.7 Different Concentration Ratio 66
3.8 Validation of the model 67
Chapter 4 : Effect of Temperature on a Triple-Junction Solar Cells Performance Parameters 71
4.1 Introduction 71
4.2 Temperature dependent on energy Bandgap 71
4.3 Temperature dependent *J-V* curves parameters 76
4.4 Temperature-dependent EQE 82
4.5 Temperature-dependent Power 84
4.6 Temperature dependent Fill Factors (FF) of a Triple-junction Cell 86
4.7 Temperature dependent of Triple-junction cell efficiency 88
4.8 Sensitivity analysis 89

Chapter 5 : Thermal Modelling and Performance Analysis of a High Concentrating Photovoltaic Receiver 92
5.1 Introduction 92
5.2 Methodology 92
5.3 MATLAB Thermal Model 93
5.4 (FEM) Finite Element thermal model 95
5.5 Results 98
5.5.1 Thermal model 98
5.5.2 Meshing convergence 98
5.6 Analysis of Performance convergence 100
5.6.1 Verification 103
5.7 Model development for different *AM* 104
5.7.1 Estimation of energy conversion yield 106
5.7.2 Convergence analysis 109
Chapter 6 : Transient Thermal-Electrical Behaviour of a Concentrating Solar Photovoltaic Receiver 116
6.1 Introduction 116
6.2 Methodology 118
6.3 Numerical modelling 119
6.3.1 Triple-junction cells electric model 119
6.3.2 Thermal FEM model 120
6.4 Results and discussions 122
6.4.1 Temperature-dependent on cell efficiency 122
6.4.2 Validation 123
6.4.3 Heat power 124
6.4.4 Receiver geometry and boundary condition 124
6.5 Thermal response analysis 125
6.6 Analysis of electrical parameters response 131
6.7 Effects of varying irradiance intensity on steady-state temperature 132
6.8 Effects of varying ambient temperature in the steady-state temperature 135
Chapter 7 : Dynamic Characterisation of Thermal-Electrical Model and Coupling with Climatic Conditions 138
7.1 Introduction 138
7.2 Model approach 139
7.3 Daily variation of Atmospheric Parameters 139

7.3.1 Effects of clouds on PV performance 142
7.4 Thermal dynamic characterisation 143
7.5 Estimation of annual cell steady- state temperature 147
7.6 Validation 147
7.7 Electrical dynamic characterisation 150
7.8 Estimation of energy yield 155
Chapter 8 : Conclusions and Recommendations 160
8.1 Conclusions 160
8.2 Recommendation for further work 163
References 165

Lists of Figures

Figure 1-1 Future production of global energy generation, solar is forecast to be at the forefront of energy resource in the decades to come [9]. 2
Figure 1-2 Worlds solar Direct normal irradiance map, this picture extracted from solargis.com (*DNI* Solar Map Solargis) [18]..... 4
Figure 1-3 Structure of the *p-n* junction and format of space region through diffusion of electrons [23]. 6
Figure 1-4 Typical *J-V* curve characteristic of an ideal solar cell. 8
Figure 2-1 Anticipation of the development of III-V multijunction solar cells under CPV application[13, 36]. 14
Figure 2-2 Thermal transient measuring data and the calculated cell temperature are showing the CPV module [95]. 38
Figure 2-3 Predicted and measured cell temperature for triple-junction by using the RF models of cell 1 x1cm^2 [90]..... 39
Figure 2-4 Predicted and measured cell temperature for the triple-junction by using the cell model, *ANN* model of cell 1x1cm^2 [90]. 40
Figure 2-5 Experimental data of failure rate function of the triple-junction solar cells for a nominal operating temperature of 80^{o}C and 100^{o}C [102]. 41
Figure 2-6 An overview of performance analysis of HCPV receiver. 46
Figure 3-1 (a) The equivalent circuit of one-diode of three layers in series connection solar cell model, (b) represent equivalent circuit model for triple-junction cell. 50
Figure 3-2 The External Quantum Efficiency (EQE) of each layer of the triple-junction solar cell as a function of wavelength [121]. 54
Figure 3-3 One-sun results at temperature 25^{o}C, (a) top cell *J-V* curve (a) middle cell *J-V* curve (c) bottom cell *J-V* curve..... 55
Figure 3-4 (a) *J-V* curves and (b) *P-V* curves of three layers of solar cells. 56
Figure 3-5 *J-V* curve of a combination of the top, middle, bottom subcell of tandem three junctions the total current of solar cell limited by the top and middle cell. 58
Figure 3-6 *J-V* curve of a combination the top, middle, bottom subcell of tandem 3-J; the total current of solar cell limited by top cell. 59
Figure 3-7 *J-V* curve of the tandem triple-junction solar cell (b) *P-V* curve of the three cells of triple junction cell. 60
Figure 3-8 *J-V* curves of this model results in compression with A. Walker [130] model and Fernández, *et al.* model [54]. 62
Figure 3-9 Direct spectral irradiance generated by the SMARTS2 model for different *AM* value. 63
Figure 3-10 *DNI* integration versus *AM* Air Mass as a function of the zenith angle (z)..... 64

Figure 3-11 (a) *J-V* curves of triple-junction cells and the effects of a variety of air mass. (b) *P-V* curves of triple junction cells and effects of a variety of air mass..... 65
Figure 3-12 Influence of air mass variation in cell efficiency. 66
Figure 3-13 Comparisons of concentration ratio versus $V_{oc,}$ current study model and experimental data from (Spectro Lab) C1MJ [145]. 68
Figure 3-14 Comparison of concentration ratio versus J_{sc} current study model and experimental data from specter Lab C1MJ [145]. 69
Figure 4-1 (a) top cell-cell temperature rise versus bandgap of the (GaInP) top cell, (b) bandgap versus Current density of the top cell..... 73
Figure 4-2 (a) cell temperature versus bandgap of (GaInAs) middle cell, (b) bandgap versus current density of middle subcell. 74
Figure 4-3 (a) cell temperature versus bandgap of (Ge) bottom subcell, (b) bandgap versus current density of bottom subcell. 75
Figure 4-4 (a) current density increase due to a temperature rise of the top cell GaInP, (b) *J-V* curves of the top subcell GaInP as a function of temperature increase..... 78
Figure 4-5 (a) current density increase because of temperature rise of middle cell GaInAs, (b) *J-V* curves of middle subcell GaInAs as a function of temperature increase. 79
Figure 4-6 (a) current density increase as results of temperature rise of middle cell Ge, (b) *J-V* curves of middle subcell Ge as temperature increase. 80
Figure 4-7 (a) current density increase due to temperature rise, (b) *J-V* curve of tandem cell in triple junction cell as a function of temperature increase. 81
Figure 4-8 Temperature dependent on the open circuit voltage of the three layers GaInP/GaInAs/Ge. 82
Figure 4-9 Experimental data of EQE as a function of temperature rise, (a) top subcell (b) middle subcell (c) bottom subcell [154]. 83
Figure 4-10 *P-V* curve of a single layer for triple-junction cells respectively, (a) top subcell GaInP (b), middle subcell GaInAs and (c) bottom subcell Ge. As a function of temperature increase, where varies from 25 to 125ºC. 85
Figure 4-11 Triple junction cell *P-V* as a function of temperature from 25 – 125ºC..... 86
Figure 4-12 Fill factor of the three-layer cell at a temperature from 25 – 125ºC. 87
Figure 4-13 Cell temperature rise from 25 – 125ºC, versus decreases in fill factor. 87
Figure 4-14 Cell temperature versus single junction cell efficiency from 25 – 125ºC. 88
Figure 4-15 Cell temperature versus overall cell efficiency from 25 – 125ºC..... 89
Figure 4-16 Cell parameters changes due to temperature variation from 25 – 125ºC. 90
Figure 5-1 Flowchart diagram of model for cell temperature. 93
Figure 5-2 (a) Receiver assembly component structures and boundary condition, (b) schematic diagram of the receiver. 96
Figure 5-3 Receiver assembly of triangle normal size mesh (a) 3D mesh and (b) 2D mesh. 99

Figure 5-4 Mesh convergence verses cell temperature. 99
Figure 5-5 Steady-state cell temperature distribution, $h_{conv} \geq 2000$ W/m^{2}K. 101
Figure 5-6 Cell temperatureT_{c2} versus to iteration as a function of convection heat transfer coefficient at constant initial cell temperature h_{conv} from (2000 – 2400) W/m^{2}K. 102
Figure 5-7 Steady state cell temperature distribution, $h_{conv} \geq 2400$W/m^{2}K. 102
Figure 5-8 Cell temperature T_{c2} versus to cycle iteration at different initial cell temperature T_{c1} at constant h_{conv} = 2400W/m^{2}K. 103
Figure 5-9 Plot of thermal receiver assembly results, (a) FEM model done by Muron *el al*. [105], (b) Current study model. 104
Figure 5-10 Flow diagram of a process and the steps of the proposed modelling. 105
Figure 5-11 Estimation of portions energy absorbs and approximation of energy losses by each layer of triple-junction cells for *AM* 1.5D. 107
Figure 5-12 Estimation of portions energy absorbs and approximation of energy losses by each layer of triple-junction cells for *AM* 4D. 108
Figure 5-13 Estimation of portions energy absorbs, and an approximation of energy losses by each layer of triple-junction cells for *AM* 8D. 108
Figure 5-14 Cell temperature convergence versus iterations; this model of triple-junction cells, at the variation of h_{conv} between 2200 to 2400 W/m^{2}K to maintain a cell temperature below 80^{o}C. 109
Figure 5-15 *AM* as a function of irradiance versus heat power generated on the solar cell, also *AM* versus h_{conv} required to maintain a cell temperature below 80^{o}C. 110
Figure 5-16 2D plot of temperature distributions on CPV receiver, (a) *AM* 1.5D and at an ambient temperature of 25^{o}C, h_{conv} = 2400W/m^{2}K, (b) *AM* 1.5D at an ambient temperature of 45^{o}C and h_{conv} = 3000W/m^{2}K. 111
Figure 5-17, 2D plot of temperature distributions on CPV receiver, (a) *AM* 4D, h_{conv} = 2300W/m^{2}K and ambient temperature of 25^{o}C, (b) *AM* 4D and h_{conv} = 2800W/m^{2}K at ambient temperature of 45^{o}C. 112
Figure 5-18, 2D plot of temperature distributions on CPV receiver, (a) *AM* 8D and ambient temperature of 25^{o}C and h_{conv} = 2200W/m^{2}K, (b) *AM* 8D for ambient temperature of 45^{o}C and h_{conv} = 2600W/m^{2}K. 112
Figure 5-19 Variation values of h_{conv} as a function of variation T_{amb} for the different of *AM*... 113
Figure 6-1 Flow chart of the transient modelling process..... 119
Figure 6-2 Temperature dependent on cell electrical efficiency as a function of temperature from 25 – 80^{o}C at CR of 500x. 122
Figure 6-3 Measurement data of the performance curve of 3C42A, 2014 for different concentration ratio verses efficiency at a variable operating temperature [186]. 123
Figure 6-4 Temperature dependent on heat power generated by the temperature of the cell from 25 – 80^{o}C..... 124

Figure 6-5, 3D structure of receiver assembly. 125
Figure 6-6 Transient model and steady state, this to determine steady-state maximum cell temperature. 126
Figure 6-7 Transient model results in steady-state maximum temperature for both constant efficiency and dynamic efficiency. 127
Figure 6-8, 3D Temperature profile distribution patterns of the dynamic efficiency of receiver assembly for different intervals (a, b, c, d, e, f, g) time prospectively (0, 5, 10, 15, 20, 25, 30 seconds). 129
Figure 6-9, 3D temperature profile distribution, steady-state model at constant efficiency. ... 130
Figure 6-10 Electrical parameters versus to cell steady state condition at 500x, (a) Current density versus time (b) open circuit voltage versus time (c) fill factor verses to time (d) maximum power point verses to time intervals. 131
Figure 6-11 Conversion efficiency versus cell steady-state condition. 132
Figure 6-12 Effects of changes *DNI* in the maximum cell temperature at the dynamic efficiency of time for steady-state temperature. 133
Figure 6-13 Different *DNI* versus to maximum cell temperature at steady-state temperature. 134
Figure 6-14 Represents the values of various *DNI* and corresponding *AM*. 135
Figure 6-15 Steady states cell temperature at a variety of h_{conv} and ambient temperature. 136
Figure 7-1 Variation of air mass *AM* versus daytime. 140
Figure 7-2 Daily metrological data (a) *DNI* versus daytime (b) *DNI* verses to different *AM* Air Mass values. 141
Figure 7-3 Ambient temperature versus daytime. 142
Figure 7-4 (a) heat power (q_{heat}) versus daytime, (b) heat power versus difference *DNI* values. 144
Figure 7-5 Cell temperature at convection heat transfer coefficient of 1400W/m^{2}K for different days. 145
Figure 7-6 Cell temperature versus different values of direct normal irradiance. 145
Figure 7-7 Cell temperature with variable convection heat transfer coefficient h_{conv} = 1300, 1400 and 1500 W/m^{2}K for different days. 146
Figure 7-8 (a) annual beam irradiance *DNI* W/m^2 for NM Albuquerque [198], (b) an average of ambient temperature and *AM* of Albuquerque [190]. 148
Figure 7-9 Compared this model with modelling results of annual cell temperature for Albuquerque, New Mexico US, data from Theristis *et al.*[190]. 149
Figure 7-10 Typical year distribution percentage of predicted cell temperature. 150
Figure 7-11 Changes of current density, (a) current density versus time, (b) current density versus the values of *DNI*. 152
Figure 7-12 The open circuit's voltages depends on both the cell temperature and different *AM*. 153

Figure 7-13 (a) estimation of maximum power versus to *AM*, (b) maximum power versus time. 154
Figure 7-14 Estimations of daily energy yields of three days of summer 2015 produced from a single assembly. 156
Figure 7-15 Predicted the average monthly of energy yield as a function of *DNI* at the clear sky. 157
Figure 7-16 Predicted the average monthly of energy yield as a function of *DNI* at the partially cloudy sky. 157

Lists of Tables

Table 2-1 Summary of performance characterisation of CPV. 44
Table 3-1 Listed parameters used in the model [111]. 53
Table 3-2 Summarised simulated *J-V* parameters compared to world record values published in the literature for a lattice-matched (LM) MJSC by Green *et al*.[123]. Walker [122] triple cell model results, the temperature at 25 °C and concentration of one – sun. 61
Table 4-1 Temperature coefficient of J_{sc} and V_{oc} of single cells [84, 142, 143]. 77
Table 4-2 Detailed performance parameters of temperature rises from 25ºC to 125ºC with variation±. 89
Table 5-1 Listed boundary condition. 97
Table 5-2 Materials thermophysical properties. 97
Table 5-3 Dimensions of PV receiver assembly. 97
Table 5-4 Detailed mesh optimisation data. 99
Table 6-1 Comparison of cell efficiency resulted from this modelling and between empirical data extracted from 3C42A, AZUR–SPACE and current model at 500x. 123
Table 6-2 Detailed variations of *DNI* for maximum cell temperature, steady-state conversion efficiency and time. 134
Table 7-1 Table average daily sunshine hours [187]. 149
Table 7-2 Estimations of monthly single assembly cell average energy yields at clear sky and energy yields at the partially cloudy sky. 158

Glossary

Nomenclature

Symbol	Definition	Unit
A_c	Area of the cell	m^2
A_s	Convective area	m^2
CR	Concentrating Ratio	X
DNI	Direct Normal Irradiance	W/m^2
E_g	Energy band gap	eV
G	Solar irradiance	$W/m^2/nm$
h_{conv}	Convective heat transfer coefficient	W/m^2K
J_{sc}	Shot circuit current density	A/cm^2
J_o	Reverse saturation current	*A*
J_m	Maximum current density	*A*
K_b	Boltzmann constant	eV/K
m	Mass of the cell	g
n	Diode ideally factor	-
P_{out}	Amount of delivered power	W
P_{in}	Incident power	W
q	Electron charge	C
q_{con}	Conductive heat	
q_{conv}	Convective heat	
q_{rad}	Radiation heat	
q_{heat}	Heat power	W
Q	Amount of heat in cell after dissipation	W
Q_{out}	Heat dissipated from the cell	W

Q_{cm}	Heat generated due to current mismatch	W
P_m	Maximum power	W
R_s	Series resistance	Ω
SR	Spectrum response	A/W
T_{c1}	Intimal cell temperature	^oC
T_{amb}	Ambient temperature	^oC
T_o	Temperature at standard condition	^oC
T_c	Cell temperature	^oC
V_m	Maximum voltage	V
V_{oc}	Open circuit voltage	V
X_c	Cell thickness	
Δt	Time different	s
W_s	Wind speed	m/s
Z	Zeniyh angle	^{o}
K	Thermal conductivity	K(W/mK))
X	Suns	

Greek Symbols

ρ	Density
C_p	Heat capacity
λ	Wavelength
α	Materials constant
β	Materials constant
K	Materials constant
γ	Materials constant
β_{η}	Efficiency temperature coefficient
η_c	Cell efficiency
η_{opt}	Optical efficiency
ε	Surface emissivity
σ	Stefan-boltzman

Abbreviation

Al	Aluminuim
AF	Acceleration Factor
ANN	Artificial Neural Networks
ALT	Accelerated Life Tests
AM	Air Mass
ARC	Anti-Reflecting Coating
Al_2O_3	Aluminium Oxide
CPV	Concentrating Photovoltaic
DCB	Direct Copper Bended
1D	One Dimensional
2D	Two Dimensional
3D	Three Dimensional
EQE	External Quantum Efficiency
FF	Fill Factor
FEM	Finite Element Model
GaInP	Gallium Indium Phosphide
GaInAs	Gallium Indium Arsenide
Ge	Germanium
HCPV	High Concentrating Photovoltaic
IE	Integrated Error
LM	Lattice Matching
MBE	Mean Bias Error
RMSE	Root Mean Square Error
MJ	Multi-junction

NREL	National Renewable Energy Laboratory
PV	Photovoltaic
PV/T	Photovoltaic Thermal
RF	Random-Forest
RE	Renewable Energy
SAM	System Adviser Model
Si	Silicon
SMART	Simple Model of Atmospheric Radiative Transfer
TJ	Triple-Junction
UV	Ultraviolet
SEM	Single Expontial Model
UHCPV	Ultra-High Concentration Photovoltic

Physical constants

Electron charge	$q \approx 1.602 \times 10^{-19}$C (or A.s)
Plack's constant	$h \approx 6.626 \times 10^{-34}$ m^2.kg/s (or J.s)
Boltzman constant	$k \approx 1.381 \times 10^{-23}$ m^2 .kg.s^{-2}.K^{-1} (or J/K)
Speed of light in vacuum	$c \approx 2.998 \times 10^{8}$ m/s
Stefan-boltzman constant	$\sigma \approx 5.670 \times 10^{-8}$W/($m^2$.$K^4$)

List of Publications

Ali O. M. Maka, Tadhg S. O'Donovan, "Analysis of thermal response and electrical characterisation of triple-junction solar cells based on variable solar spectral irradiance and air mass" *Thermal Science and Engineering Progress.* Vol. 10, May 2019, pg.269-279.

Ali O. M. Maka, Tadhg S. O'Donovan, "Modelling of the Thermal Behaviour of Solar High Concentrating Photovoltaic Receiver" *Thermal Science and Engineering Progress.* Vol. 9, March 2019, pg. 281-288.

Ali O. M. Maka, Tadhg S. O'Donovan, "Transient thermal-electrical performance modeling of solar concentrating photovoltaic receiver" (under *review of Applied Thermal Engineering*).

Ali O. M. Maka, Tadhg S. O'Donovan, "A review of Performance Characterisation of a High Concentrating Photovoltaic Solar Receiver Assembly" (*submitted to Sustainable Energy Review*).

Ali O. M. Maka, Tadhg S. O'Donovan "Characterisation of dynamic performance for concentrating photovoltaic model and coupling with variable climatic conditions" (*in preparation to Renewable Energy*).

Conferences

Ali O. M. Maka, Tadhg S. O'Donovan, "Temperature dependence of energy band gaps In triple-Junction solar cell" *14th UK Heat Transfer Conference, (UKHTC-2015) Edinburgh.*

Ali O. M. Maka, Tadhg S. O'Donovan, "Thermal performance modelling of a solar concentrating photovoltaic CPV receiver" *15th UK Heat Transfer Conference (UKHTC-2017) London 4-5 September 2017.*

Ali O. M. Maka, Tadhg S. O'Donovan, "Effects of atmospheric parameters on the performance of concentrated photovoltaic receiver", *Solar conference and exhibition. Edinburgh 6th September 2017.*

Ali O. M. Maka, Tadhg S. O'Donovan, "Effects of climatic conditions variation on the performance behaviour of high-efficiency solar cell", *Solar conference and exhibition. Edinburgh 4th September 2018.*

Other publication does not include this thesis

Ali O. Mohamed, TN Chaudhary, M Akram "Econmic benefits of a gas turbine compressoer washing at different inerivals", *Journal of Faculty of Engineering & Technlogy*, vol. 24 Issue (2), 2017. pg. 21-33.

Ali O. M. Maka, TN Chaudhary, Abdulazez HASAN, Ahamed GATOU "In-situ performance evaluation of photovoltaic solar water pumping system in the rural region" *Journal of Mechanical and Energy Engineering.*Vol. 3(43) issue (1), 2019. pg. 69-76.

Chapter 1: Introduction

1.1 Introduction

The demand for clean and sustainable energy sources has increased in recent years. Governments around the world recognise the importance of clean energy resources for future planning, to decrease dependency on conventional energy resources, and replace them with green energy technology. The world is moving to exploit clean energy sources and decrease the reliance on conventional fossil fuel as energy sources [1, 2].

The pollutants and emissions with the largest environmental impact have been subject to a number of international and national legislations [3]. In the past decade, concern about the effects of an excessive amount of greenhouse gases in the atmosphere have been rising. Gases such as Carbon Dioxide (CO_2), Methane (CH_4) and Carbon Monoxide (CO) contribute most to the greenhouse effect. Furthermore, the burning of fossil fuel, such as Gasoline, Coal and Oil as well as Methane, are widely utilised to generate electricity or energy for transportation. This kind of energy is depleting energy resources, at an unsustainable rate [4-6].

Energy is inevitably necessary to sustain and develop human societies. Therefore, with the modernization of human civilisation, the demand for energy is increasing day-by-day. In addition, the rapid growth of the world's population and the development of technology has led to a growing demand for energy in the last few decades. Therefore, investment in other energy sources rather than fossil fuels are required, to fulfil the energy demand. In addition, the Renewable Energy (RE) sources play a significant role in supplying energy services in a sustainable way, particularly in alleviating climate change [1-3].

Fossil fuels still dominate and remain the main large energy sources for the time being. Nonetheless, clean energy ought to play a fundamental role in our energy's future. The framework of world energy is undergoing a transition towards sustainable energy resources [7, 8].

The energy generation has peaked for fossil fuels, while the forecast is for solar energy to be at the forefront of energy generation in the future, as depicted in Figure 1-1. The estimated global primary energy generation in 2019 is approximately 650 Joules in which the solar energy represents about 10-13%. However, in 2050, it is estimated that the solar

energy generation will exceed to 48% by forecasting economic growth and with the industrial development. It is expected that estimation will exceed to 64% by 2100 [8, 9].

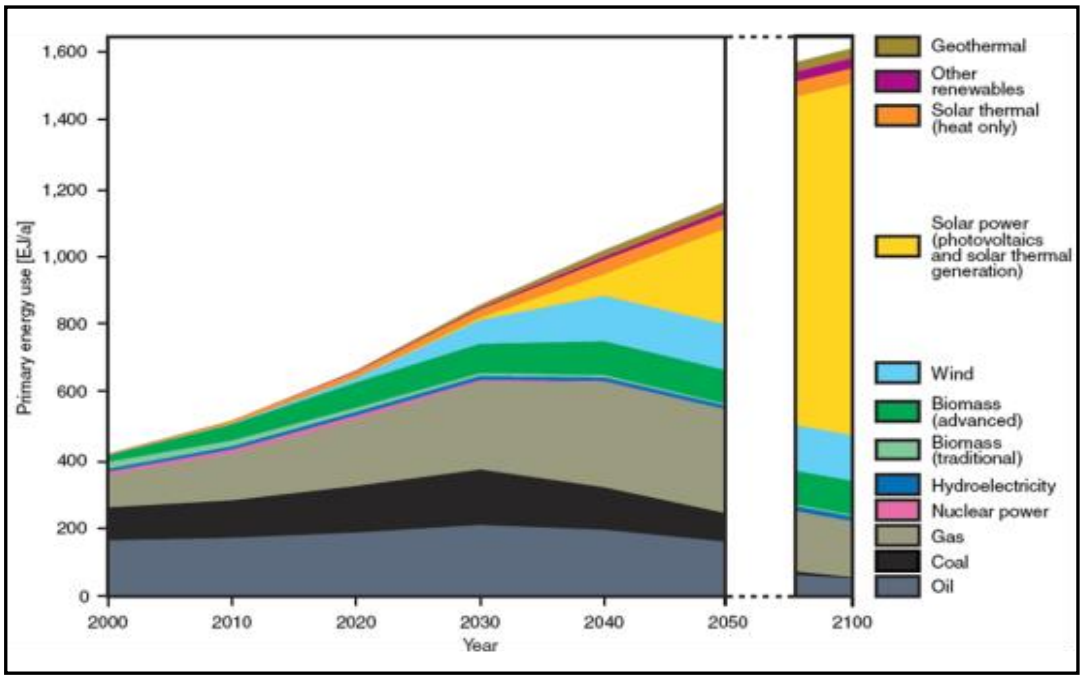

Figure 1-1 Future production of global energy generation, solar is forecast to be at the forefront of energy resource in the decades to come [9].

There are two types of application technologies that are widely-used to produce energy from the Sun: the direct approach, by using a "Photovoltaics" module to capture sunlight and convert it to electricity; another application is "solar thermal" which generates enough heat to turn the steam turbines, resulting in electricity generation.

As a result of the growing demand for renewable energy sources, the manufacture of solar cells has advanced in recent years and is expected to increase its percentage of power generation in the near future. This scenario is considered to be one of the motivations to reduce global carbon emissions and pollutants [1, 2, 9].

The contribution and potential of renewable energy sources cannot be underestimated with regard to providing energy services which will lead to a path of sustainable social and economic development in energy generation. That includes assessments of available renewable resources and technologies, costs of expansion, investment and integration, and the competition policy in the energy market [3].

The current PV installed capacity worldwide is approximately 403GW at the end of 2018. In addition, the global market in photovoltaic cells had become a substantial player within

the renewable energies sector via expanded production capacity, especially in the areas where highly automated production lines are prevelant. Moreover, the expanded worldwide production has led to considerable cost reductions, and have led to greater competition in the PV industry [10].

Photovoltaics (PV) affords an elegant approach, which converts the Sun's solar irradiation directly into electricity. Due to the rising demand, and supply, worldwide for renewable energy sources, the power produced from the solar cell sector has dramatically increased in recent years. Also, the research development in solar cells, reduction in materials cost and investment in the industry has led to a booming PV sector [2, 5].

Recently there was a drop in manufacturing materials for Photovoltaic devices, which is expected to compensate for the needs and growth of the world's energy demand [11]. Solar energy is a clean, sustainable energy source that is environmentally friendly. The technologies of solar photovoltaic applications are widespread. The theory of photovoltaic PV solar cells is converting the radiant energy from the sun directly to electrical power, although the technology of photovoltaic is always in continuous development for numerous usages, in both space and terrestrial applications [12].

There is a great potential to exploit solar energy, particularly *CPV*, in countries located in the "Sunbelt" area. There is plentiful solar *DNI* (Direct Normal Irradiance) in that particular area throughout the year [13]. Accordingly, countries in the Middle East, North Africa, South USA, South China, Southern Africa and Australia, to name but a few, have a great opportunity for solar conversion technology. The average daily solar intensity is >10.5 KWh/m^2 and the annual solar intensity >3800 KWh/m^2. Figure-1-2 shows the optimum regions for concentrating photovoltaic.

The Direct Normal Irradiance, *DNI*, is described as "the power received per unit of area normal to the sunlight" [14, 15]. Therefore, electricity generation of a CPV device is dependent on the *DNI* of sunlight components, as it does not absorb any of the Sun's diffuse radiation. Also, in CPV systems, one can only can use the *DNI*, due to the optical concentration [16]. The performance of solar cells in CPV systems can operate in high environmental temperature, compared to the conventional photovoltaic systems [17].

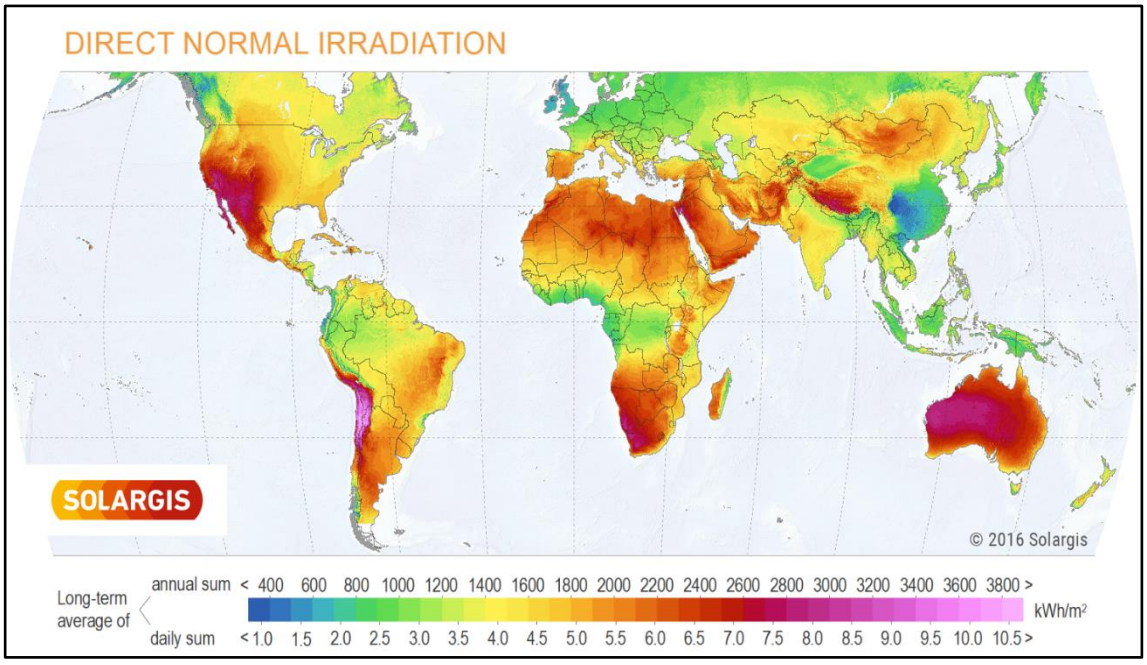

Figure 1-2 Worlds solar Direct normal irradiance map, this picture extracted from solargis.com (*DNI* Solar Map Solargis) [18].

1.2 Photovoltaic solar cells

Solar cells convert sunlight directly into electrical power; commonly used semiconductors materials from the basis of a PV solar cells assembly. The properties of these materials have atoms with four electrons in the outer shell or orbit. Therefore, those electrons are called “valence electrons”. Semiconductor elements are from both group “IV” in the periodic table or a mixture of group “IV” and group “II”, the latter called “II–VI” semiconductors [19]. Moreover, a combination of elements from group "III" and the “V” group in the periodic table, which can produce “III–V” materials.

1.2.1 First Generation

The first generation of photovoltaics is based on silicon cells, which still the most prevalent material for the solar industry. The usage of silicon is widespread in the industry and is inexpensive. The cells are comprised of large surface area, high-quality and single junction devices [20]. The silicon single junction cell has a limiting efficiency of about 22% at 1000 W/m^2, 25 ^{o}C [21].

1.2.2 Second generation

The Second-generation photovoltaic materials have been developed to meet energy requirements and reduce production costs of solar cells. The most successful second-generation materials have been Cadmium Telluride (CdTe), Copper Indium Gallium Arsenide, Amorphous Silicon, Micro-amorphous Silicon and Thin Film (Si,CIs,CdTe)

[20]. These technologies have conversion efficiencies of about 21% at 1000W/m^2, 25^{o}C and offers significantly cheaper production costs [21].

1.2.3 Third generation

The main aim of third-generation technologies is to enhance the electrical conversion efficiency of the second generation. The target conversion efficiencies range from between 34% at 1x, 25^{o}C [21], achieved by using high-efficiency solar cells and applying optical concentrations [22]. Concentrating photovoltaics are considered as one method to reduce solar electricity cost by substituting costly solar cells with cheap optical concentrators [16].

1.3 Solar cell principle

The basic working principle of the photovoltaic solar cell, acting as a semiconductor diode, is its ability to convert light energy into electricity using the principle of the photovoltaic effect. A charge is only generated if three principles are met: sufficient light must be absorbed to generate excitons or electron-hole pairs; the separation of opposite charge carriers occurs, and the ability of those charge carriers to allow the flow of current to an external circuit. The energy of the incident solar photon must be great enough to excite and separate covalent electrons from their semiconductor material. While sunlight has a large array of photons, which have a variety of energies dependent on their frequencies, to enable a PV effect, the photons must have sufficient energy, i.e. larger than the energy of the semiconductors' band-gap, to excite the PV cell's charge carriers. Since the charge carriers are restricted in how much energy they can absorb (equal to the band-gap energy), residual energy is transformed to heat energy in the cell, which increases its temperature [23].

1.3.1 P-N Junction

The (*P*-*N*) junction is a combination of a *P*-type semiconductor with an *N*-type semiconductor. The *P*-type has holes which have a positive charge and *N*-type that has an electron with a negative charge. The free hole available on *P*-type is positively charged, and the free electron is available at a negative charge. The region where *P*-*N* type is joined together called a *P*–*N* junction [23].

As functioning is based on the presence of sunlight, the electrons near *N*-type migrate toward the *P*-type semiconductor, and holes near *P*-type migrate toward the *N*-type

semiconductor. This phenomenon creates a space charge region (also, called depletion region) at the junction. Electrons available at the *P* region at space charge while holes are available in the *N* region at space charge. An electric field is created in this space region, some of the electrons move back from *N*-type to *P*-type, and some holes move back from *P*-type to *N*-type. This continues to happen until an equilibrium state is reached; this moving of electrons and holes in the space region gives a current, known as a diffusion current [23, 24]. Figure 1-3 illustrates the structure of the p-n junction format of the space region by the diffusion of electrons and holes.

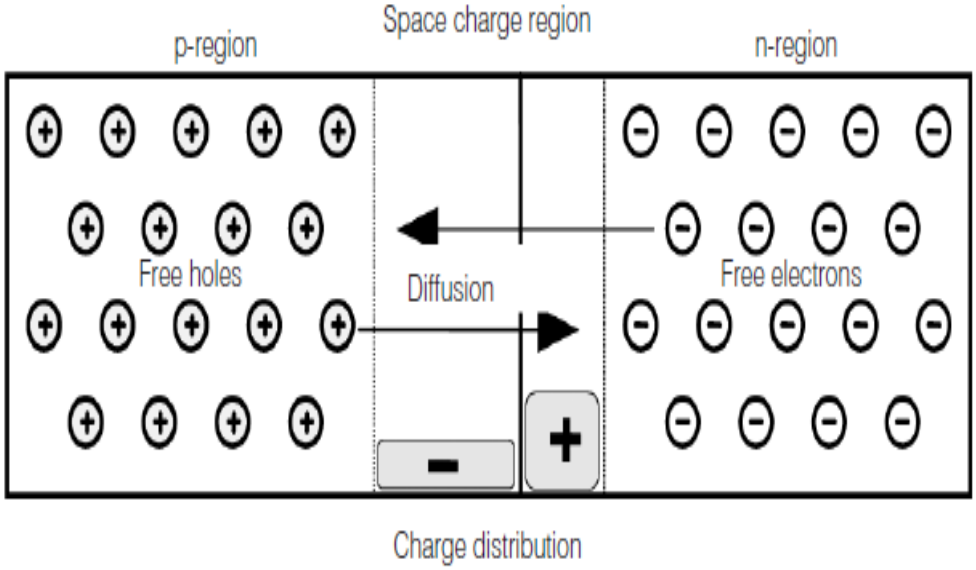

Figure 1-3 Structure of the *p-n* junction and format of space region through diffusion of electrons [23].

1.3.2 Ideal Solar Cell Characteristics

The performance characteristic of any given PV solar cell is given by it is *J-V* curve; the curve contains the essential electrical parameters of the solar cell. Figure-1-4 illustrates a typical photovoltaic solar cell *J-V* curve characteristic. For an ideal diode *J-V* characteristic is given in equation (1), where J_o is the dark saturation current.

$$J = J_o\left(e^{q.V/K.T} - 1\right) \tag{1}$$

The light characteristics of superposition of dark characteristics and the photocurrent J_{ph} is given by (2), hence this represents radiation absorbed from the Sun. The combination of photocurrent with the ideal diode is known as forwarding bias voltage.

$$J = J_o\left(e^{q.V/K.T} - 1\right) - J_{ph} \tag{2}$$

The other key output parameters of a solar cell are open-circuit voltage V_{oc}, which measures the maximum potential voltage generated by the cell when J is zero. Furthermore, the short-circuit current J_{sc} is the maximum current generated by the cell when V is zero. The relationship between the two is given by equation (3):

$$V_{oc} = \frac{K.T}{q}\ln\left(\frac{J_{sc}}{J_o} + 1\right) \tag{3}$$

The Fill Factor FF is known as the ratio of the maximum power output from the solar cell to the product of its open circuit voltage and short circuit current. It depends on the parasitic resistances of the device, as given in equation (4).

$$FF = \frac{J_m.V_m}{J_{sc}.V_{oc}} \tag{4}$$

The conversion efficiency is the percentage ratio of power output divided by power (5):

$$\eta = \frac{P_{\max}}{P_{in}} = \frac{J_m.V_m}{P_{in}} = \frac{J_{sc}.V_{oc}.FF}{P_{in}} \tag{5}$$

Where V_{oc} is the open circuit voltage, J_{sc} is the short circuit current, J_m is the current at maximum power, V_m is the voltage at maximum power, P_m is the maximum power and FF is the Fill Factor. These electrical parameters are the key to understanding the performance of the cell.

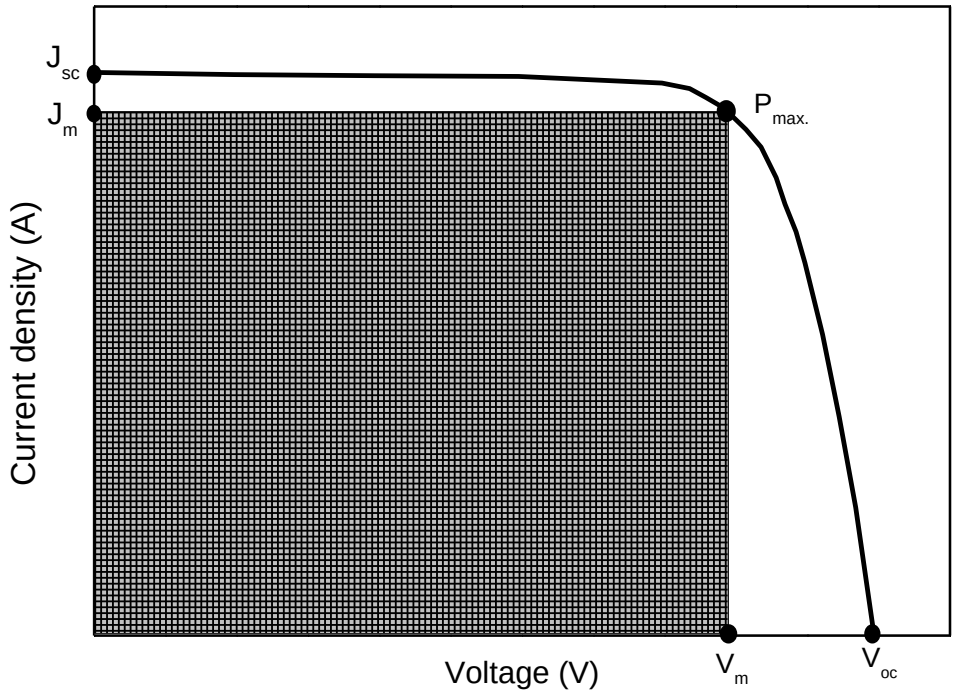

Figure 1-4 Typical *J-V* curve characteristic of an ideal solar cell.

1.4 Research Aims and Objectives

This research project aims to evaluate the performance of high-efficiency "triple-junction" solar cells and analyse its performance at different environmental conditions. Consequently, this will lead to greater understanding of the performance behaviour in order to optimise and improve the design of the CPV receiver assembly. To achieve the aims of this study, five key objectives of this research project are summarised as follows:

- To understand the operating performance of high-efficiency III–V triple-junction solar cells and the context of implementing different concentration ratios.
- To analyse and describe the performance behaviour of the solar cell's parameters at a range of cell temperatures.
- To investigate the heat generated, induced by the light concentration on photovoltaic solar cells, and the thermal response to the changes of the incident solar spectrum with *AM* and *DNI* variations.
- To develop a transient thermal-electrical model by implementing a time-dependent study model on the solar receiver.
- To characterise the dynamic performance of the thermal-electrical model by coupling it with climatic conditions.

1.5 Thesis outline

This research thesis is divided into eight chapters, the contents of each particular chapter will be briefly summarise hereunder as follows:

Chapter-1: Presenting the general introduction of the thesis, the summary of the background of energy sources, the aims listed, and the objectives of this research. Finally, a brief summary of the thesis is outlined.

Chapter-2: Summary of the theory and a literature review of previous and rational research works. Also, to present a review of important aspects of operating performance for solar CPV receivers.

Chapter-3: This chapter presents an electrical model by using the mathematical equation, in order to assess the triple-junction solar cell's performance. The model will be compared with solar cell manufacturers indoor experimental data. Moreover, it describes the electrical performance model parameters at standard conditions.

Chapter-4: This chapter presents an investigation into the effect of temperature rises (from 25 – 125^{o}C) on the triple-junction solar cell at 1x concentrating ratio. In addition, performance characterises of the *J-V* and *P-V* curves will be undertaken. The performance parameters of short-current density, the open circuit voltage, energy band gap, external quantum efficiency, fill factor, maximum power and cell efficiency will all be studied.

Chapter-5: This model describes the thermal modelling of the HCPV receiver assembly at 1000x. It discusses also the thermal performance response of the receiver, so the thermal model can be used to find the optimum cell temperature. Furthermore, to consider a developed model, of the variable environment condition of T_{amb}, *AM* and corresponding *DNI*.

Chapter-6: This chapter presents modelling of the transient nature of the solar cell of the thermal-electrical behaviour with regard to steady-state conditions. The influence of changes in incident light *DNI* and corresponding *AM* in steady state is also considered. Afterwards, to look at the effects of variable ambient temperatures on stagnated cell

temperature, and the thermal response to keep operating safely through defining the values of the convection heat transfer coefficient.

Chapter-7: This chapter analyses the performance of the solar cell receiver in a dynamic way, so weather metrological data is coupled with thermal and electrical models, to characterise performance. The daily/annual atmospheric parameters of *DNI*, *AM*, T_{amb} are considered and aspects for when the sky is both clear and cloudy. In addition, this chapter ends by giving an approximation of cell energy production.

Chapter-8: Summary of the conclusions drawn from the research work and listed proposed future search work.

Chapter 2: Background and Literature Review

2.1 Introduction

This chapter presents a detailed review of rational research work regarding general concentrating Photovoltaic systems. A brief overview is presented to give the reader a view to navigate the various points relating to CPV applications. Much research has been conducted in the past on concentrating photovoltaics on triple-junction solar cells. Despite that, the technology is still under continuous development. Furthermore, hereunder the relevant literature is reviewed.

2.2 Energy development

The availability, cleanliness and plentiful supply of solar energy makes it an attractive proposition for energy generation in the future. Solar energy is a natural energy source; it is carbon-free, environmentally friendly and has great capabilities for energy production. The efficient generation and energy storage of solar energy are economically important, in achieving the maximum power of solar energy to meet long-term energy needs [3, 25]. Recently, there has been a rapid increase in worldwide energy needs, which has given the sector added motivation and has increased the attraction, for the study and development of sustainable energy resources [25]. Nowadays, solar energy is considered as one of the common utilised renewable energy sources. According to the annual energy outlook 2019 report [26], the solar electricity generation is projected to increase from 13% in 2018 to 48% in 2050. This new, emerging technology, can participate greatly in future energy generation [25].

Due to an increase in the need for sustainable energy generation in recent years, solar cell manufacture has developed significantly. The components of semiconductor materials are the best application for extra-terrestrial and earth energy sources, due to the greater performance in contrast to another established solar cell techniques [27]. The demand for other energy sources has risen due to the increased need for clean energy. As a national program in the USA, for example, one of developed ideas was suggested for a so-called “Concentration Photovoltaic”, which was muted after the oil crisis in 1973, to overcome energy shortage demands [28].

2.2.1 Historical development of CPV technology

In Sandia National Laboratories, USA, the first CPV System project was developed in 1976. The system, which had a 1000W peak power array, was fabricated to help our understanding, and solve the problems, related to concentrating photovoltaic technology. Numerous things were learned from that project, which resulted in an acceleration in the development of CPV systems [15, 29]. Concurrently, the Institute for Solar Energy, in the Polytechnic University of Madrid, also developed the so-called 'Ramón Aceres panel': it has a silicon-on-glass focus point Fresnel lens, with a passive heat sink cooling system. During this period, the solar cells commonly used for both flat-plate and concentrated photovoltaic were both made from silicon. However, the evolution of research on multi-junction or "tandem" solar cells took a great leap forward with some good news in 1978: a dedicated group in the University of North Carolina introduced the first double-junction solar cell [15, 30].

The early 1990s was a good era for solid state physics, where develops of a high efficiency for dual-junction solar cells was attained [31]. The research development on the subject of CPV began in 1990, where the US Department of Energy made the 'Concentrator Initiative Program'. The agents participating in that initiative included four solar cell manufacturer companies (Spectrolab, Solarex, Sunpower and ASEC): each of these manufacturers produced their own module; that program ended in 1993 however, but nonetheless, the evolution in CPVs attained through this research was pertinent [32].

Significant progress in this field was achieved in the early 2000s, with the successful accomplishment of the first three-junction solar cells, based on a germanium substrate [33]. The concentration of sunlight onto the focal point upon the aperture of the high-efficient multi-junction PV solar cell, yielded to much higher power densities, in contrast to the conventional PV solar cells. Hence, the idea can be achieved by concentrating solar rays on a small cell area by using optical equipment, such as lenses and mirrors. Therefore, the concept of sunlight concentration is usually attributed to Concentrator Photovoltaic (CPV) technology. This decreases the PV cell area required as the device's light intensity rises via the corresponding factor of the concentration ratio. The CPV system includes the optical concentration, heat dissipation and the tracking systems designed to track the Sun's rays [15, 34].

The technology of concentrating PVs can produce high energy generation rates, so, based on that reasoning, it is encouraging for future generations to try to adopt higher energy plants to rival conventional fossil fuel energy generation [35].

The concept of concentrating PVs is not new, however, due to issues of reliability, matters such as the high costs of installation, the shortage of data and field skills, and information on maintenance and operation costs. The technologies of CPVs ought to, in the long run, become more economically attractive, and should attain long-term reliability for the project's designers and investors to allow the market to continue to grow. As a result, with numerous CPV industrialists entering the industry, greater operating efficiencies have become possible [27].

As shown below in figure 2-1, progress represents the top line of CPV system efficiencies; the dots show measured efficiencies of a cell, module and system. The trend lines illustrate anticipated efficiencies from different references [13, 36]. Hence, it has become commercially achievable to attain an efficiency of over 40%, by stacking different semiconductor materials on top of each other [37]. Based on that, the technology of triple junction cells is anticipated to move toward efficiency of 50% in the near future with the development of enhanced manufacturing processes.

It is worth mentioning that the concentration level has a significant effect on the system's cost. The solar cell cost vastly decreases when applying the technology of highly concentrating photovoltaic; despite that, the technology is still deemed new. The market for CPVs did not exist beforehand, because of its high cost and low concentration ratios. In turn, this leads to higher cell efficiency and lower cost [27]. For the modern CPV systems, by raising the concentration ratios from an initial level of 100x to 2000x, the cost can be decreased from approximately 2.5€/W_p to 0.9 €/W_p [38].

Despite ongoing research on CPV solar cells, modules and systems over decades, the CPV system only gained access to the market in the mid-2000s. Nevertheless, it is still a young technology, in contrast to the conventional PV, and is still a small player in the market [13, 36].

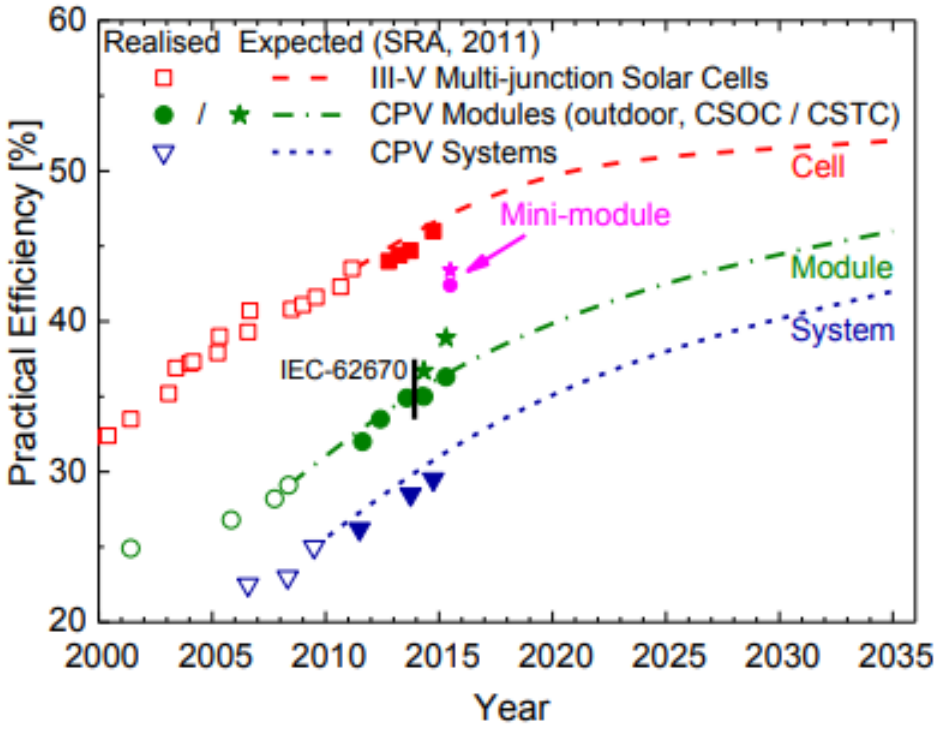

Figure 2-1 Anticipation of the development of III-V multijunction solar cells under CPV application[13, 36].

The main motivation, beyond the research and technology which concentrates on photovoltaic cells, is to boost CPV research towards a marketable level of cost in electricity; in part this will be achieved by greater efficiency. Hence, the majority of attempts by researchers aim to increase the solar cells/module efficiency. Figure 2-1 illustrates the rise in the efficiencies of the multijunction (MJ) cell's/module/system since the year 2000. Moreover, it shows the evolution achieved by research and the development of CPV modules with forecasts for the next decade [13, 36].

The technology of concentrating photovoltaics has proven its merit in the solar PV industry over numerous years. The first commissioned large-scale CPV power plant was in Spain in 2006, and the power generation was more than 1MW. By the end of 2015, there were a number of CPV power plants around the world connected to the grid. Thus, estimated total installed worldwide capacity has reached about 350MW [36].

The technology of CPV has the second lowest "energy payback time", which represents the time required to produce the same quantity of energy used through the device's installation, production and lifespan [39]. Moreover, this technology of CPV displays a greater efficiency for large scale power production than technologies of silicon PV in sunbelt countries and the estimated annual yield is > 1800 (kWh/kWp) [40]. The

technology of CPV systems has a number of applications which including desalination, BICPV Building Integrated Concentrating Photovoltaics and power electricity generation. There was a rapid development in the technology of photovoltaic (PV) systems throughout the last twenty years, which has resulted in more installations of many systems worldwide [36] and this continues to motivate the researchers to develop such enhanced renewable energy solutions.

2.2.2 Development of CPV Solar cells

2.2.2.1 Triple-junction solar cells

Before commencing presenting the triple-junction solar cells in details is important to summaries the limits of the single-junction cell. The single solar cell theoretical efficiency is limited by the material's energy band gap. The key loss mechanisms to be considered is the Shockley-Queisser efficiency limit, where efficiency of the single cell is limited to 31% [41]. As depicted in figure 2-2, it shows single cell efficiency under a temperature standard condition of 25ºC, *AM*1.5D, also the efficiency of different semiconductor materials with different band gap values. Therefore, that is the reason for utilising multi-junction solar cells, to overcome single-junction solar cell's thermodynamic limit [42, 43].

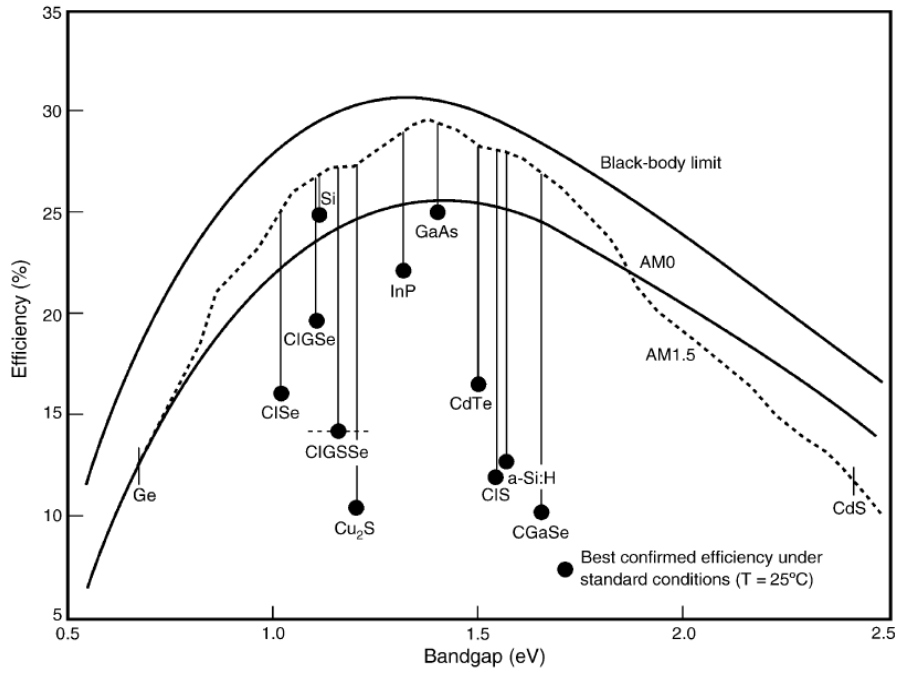

Figure 2-2 Performance efficiency of some semiconductors materials as a function of band gap [44].

A multi-junction solar cell is designed to exploit the entire solar spectrum; monolithic cascade stacks of three layers, consisting of GaInP/GaInAs/Ge, results in a combined high conversion efficiency. High-efficiency solar cells rely on high optical concentration ratios, the corresponding heat flux results in high device temperatures. The high efficiency multi-junction solar cells initially were made in applications for space technology, however, recently they have become more efficient on the Earth due to developments in concentration technology [16].

Despite of high conversion efficiencies, monolithically CPVs connected in series can lead to current mismatching, which is considered one of the constraints facing high-efficiency solar cell power production. On the other hand, that assembly has two advantages: firstly, improving the internal electric field through the different layers of junctions can be achieved by reducing the thickness of the single cell junction; secondly, usage of different semiconductor materials with different band gaps can lead to more efficient use of the whole solar spectrum [45].

Triple-junction solar (tandem III–V cells) consist of layers of GaInP/GaInAs/Ge. Series connection of three different layers allows for high conversion efficiencies. Concentrating photovoltaics usually use triple junction solar cells, made from semiconductor materials with different band gaps. The purpose of using different materials in the multi-junction solar cell is to increase the efficiency, through the capture of a large number of photon energies from the solar spectrum. Triple cells are a combination of Gallium Indium Phosphide (GaInP) in the top layer, Gallium Indium Arsenide (GaInAs) in the middle layer and geranium (Ge) as the bottom layer; currently, there are up to six layers of junction cells.

There are two configurations for the subcell connection of different semiconductors materials in the multi-junction cell: mechanically stacked and monolithically stacked. These are summarised as follows:

- Mechanically stacked multi-junction solar cells consist of many single-junctions of different materials, usually manufactured on separate substrates, and subsequently stacked on top of each other. This configuration has high series resistance, complex process and high cost. At the end, sets with six terminals are produced, as shown in figure 2-3 (a).
- Monolithically stacked multi-junction also consist of many single-junctions of different materials, connected in series; the junctions are directly grown on one

substrate and interconnected by tunnel junctions and ended by two terminals. This configuration has a simple cell process, lower series resistance and lower cost. It can distribute sunlight into subcells with different band gaps as shown in figure 2-3 (b).

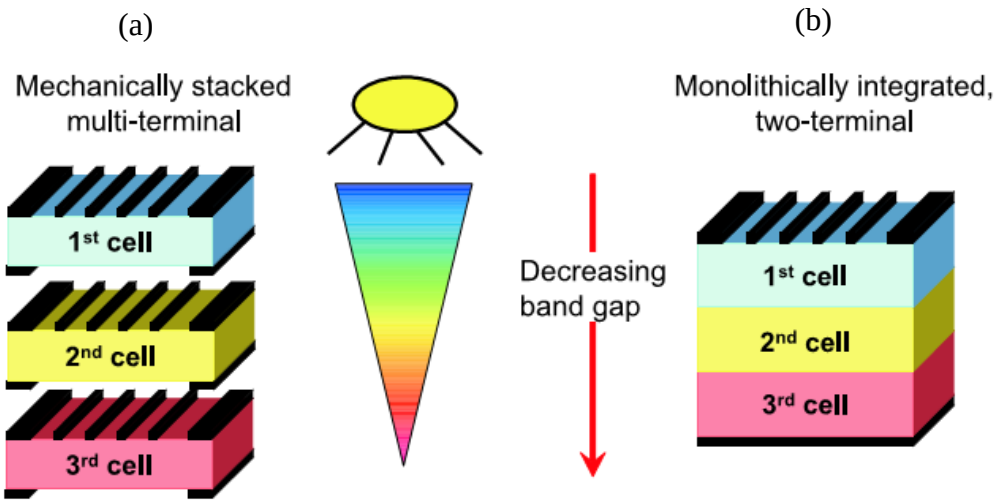

Figure 2-3 Two configurations of the triple-junction cell, (a) Cells mechanically stacked, (b) Cells integrated monolithically stacked [46].

In the technology of HCPV normally used, high-efficiency solar cells, a number of semiconductor materials are stacked differently to increase assembly efficiency. The developed design of photovoltaic layers utilises different bandgap semiconductor material (combination of elements in-group "III" with group "V") to accomplish a wide bandgap. State-of-the-art monolithic multi-junction solar cells have an efficiency record over 40% under high optical sunlight concentration [47, 48]. The main advantages of high-efficiency photovoltaic cells are [49]:

- Absorption of a larger magnitude of solar spectrum compounds.
- Reduction in the cell area of semiconductor materials.
- High conversion efficiency.

The advantages of using high concentrating photovoltaics HCPV gives us the following features [49]:

- Because of the lower entropy losses, which results in increased values of cell efficiency.
- The area of semiconductor materials required to convert the sunlight is reduced.

- Cost of concentrating materials is cheap.

The roadmap for developing solar cells with increased efficiency, by increasing the number of junctions through adding materials on top of each other with different bandgap, is shown in figure 2-4. Cell assemblies with five junctions can be achieved with an efficiency of 55% and six junctions can have an efficiency as high as 58%.

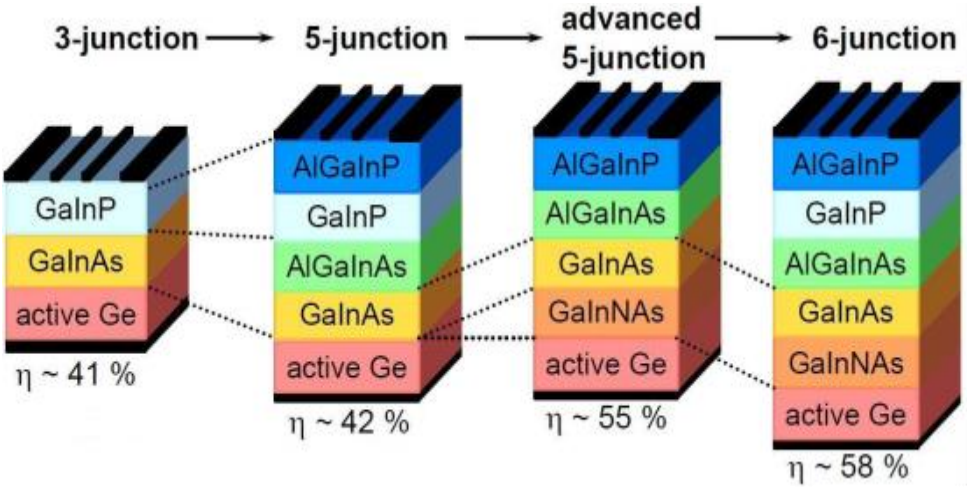

Figure 2-4 Development of solar cells, the given theoretical efficiencies values calculated and a number of junction [50].

The main goal of stacked different semiconductor materials in top of each other is to increase the cells efficiency by absorbs a large number of photon energies from the solar spectrum [37]. Usually, the direct component of the spectrum at *AM*1.5 is used to characterise of the solar cell in ideal status.

The lattice constant is defined as a measure of distance between atom locations in a crystal pattern. The lattice matching and band gap are cornerstones in design and maximize the efficiency of multi-junction solar cells. Typically, in semiconductor materials, the lattice-matched conditions are required for the epitaxial growth of high-quality materials. As shown below, the lattice-matches of the Gallium Indium Phosphide, Gallium Arsenide and Germanium are roughly equal; if Indium Phosphide in incorporate the lattice constant will increase significantly. Therefore, the lattice constant of the materials at 5.65Å, corresponding to 1.8 eV[i] band gaps of GaInP, 1.4eV of GaInAs bandgap and the Germanium is about 0.7 eV band gaps.

[i] $1eV \approx 1.6 \times 10^{-19}J$

Figure 2-5 shows the lattice constants for several semiconductors. An example is given of growing of materials with a different lattice constant, therefore if we replace the Ge bottom cell with Si one, the difference of lattice constant between them Δa=4.1%. The results are improved in efficiency by 3%, less cost, the drawback is smaller thermal expansion coefficient of the Si than that of III-V materials, which leads to cracking of the III-V epilayer while cooling down from growth temperature [51, 52]. "Growing layers on top of each other with a different lattice constant will result in a formation of dislocations which are needed to ensure high material quality" [53].

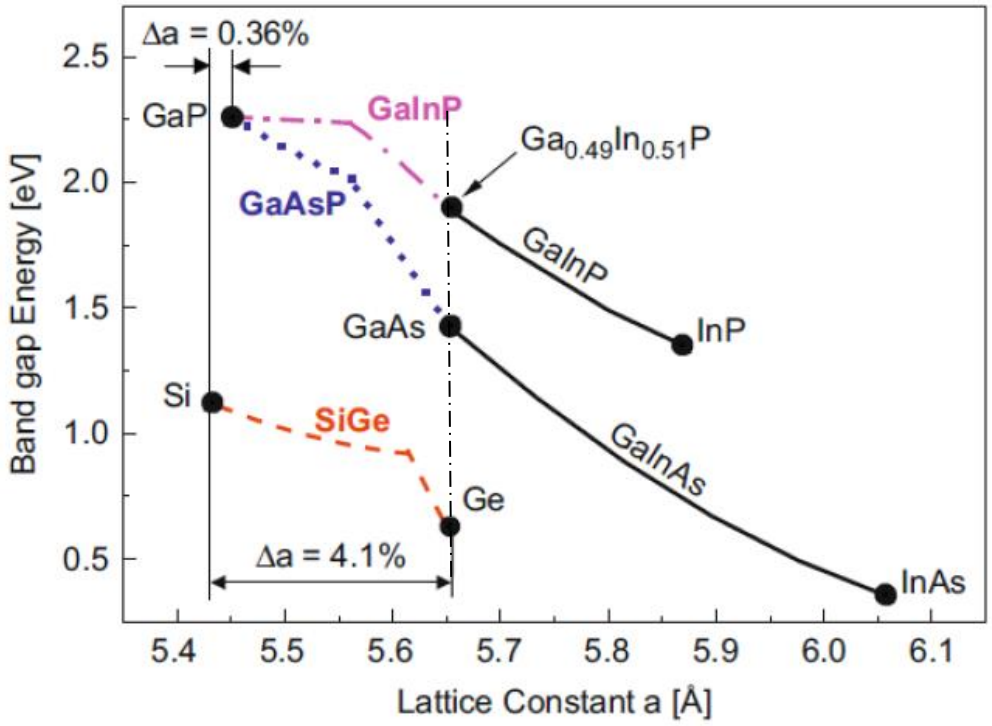

Figure 2-5 Relations between the lattice constant and semiconductors materials band gap [53].

The Lattice mismatches semiconductor materials lead to defects and dislocations, which increase the PV conversion losses. Therefore, for this reason, the most common use of multi-junction cells is manufactured using Lattice-Matched (LM) semiconductors materials [54]. However, the most important considerations in designing the high-efficiency multi-junction solar cell are the lattice constant and the energy bandgap: the energy bandgap corresponds to "the energy that is necessary to free a bound electron in the crystal, thereby creating a hole in the valance band and an electron in the conduction band". Therefore, in this state, it matches the lowest energy photon to be absorbed by the semiconductor material [54].

The technology of a HCPV (High Concentrating Photovoltaic) system mainly utilises inexpensive materials of refraction or reflection to illuminate a small area; consequently, there is an increase in the cell's conversion efficiency [47, 54]. Solar cell conversion efficiency relies on three factors: the intensity of incidence of solar radiation; the materials in the solar cell, and the cell operating temperature [55].

State-of-the-art III–V semiconductors compound technology and cell designs to growth can be split into two categories: bulk growth methods and epitaxial growth methods. The latter can grow as liquid phase epitaxy (LPE), chemical vapour deposition (CVD), molecular organic chemical vapour deposition (MOCVD), also known as metal organic vapour phase epitaxy (MOVPE) and molecular beam epitaxy (MBE) [34]. The commonly used technique of materials growth is MOCVD and MBE [56].

Figure 2-6 shows the best efficiencies found for various materials over the years; multi-junction solar cells have the highest efficiencies overall. Also shown a comparison between the three generations of developed PV cells, which plotted by the National Renewable Energy Laboratory (NREL). As results of continues development in the technology of solar cells materials the cell conversion efficiency improves. Hence, the progress from 1976–2019 the solar cells efficiency increases of the three generations. The efficiency of triple-junction solar cells has progressed remarkably to exceed 40% [57].

The applications of CPV can be harnessed in the power plant to generate electricity. In particular, large-scale, where there is abundant solar *DNI* (Direct Normal Irradiance) throughout the year. Figure 2-7 shows the application of CPV in power generation, hence (a) and (b) are represents a commercial CPV power plant. Part (c) represents a refractive Fresnel lenses array, and (d) is illustrate a FALTCON technology of single receiver assembly with the concentrator.

In spite of its drawback on the solar cell efficiency, the heat generated by the solar cell can give chances on rising the total system efficiency by incorporating the thermal and electrical technologies [58, 59]. So, this technology so-called the PV/T, which applied the photovoltaic thermal system or CPVT used for the concentrated photovoltaic thermal system. The heat removed can be re-used in the form of hot water, hot air, dual-stage refrigerant or utilised the heat in electricity generation in the form of the thermoelectric devices [58, 60].

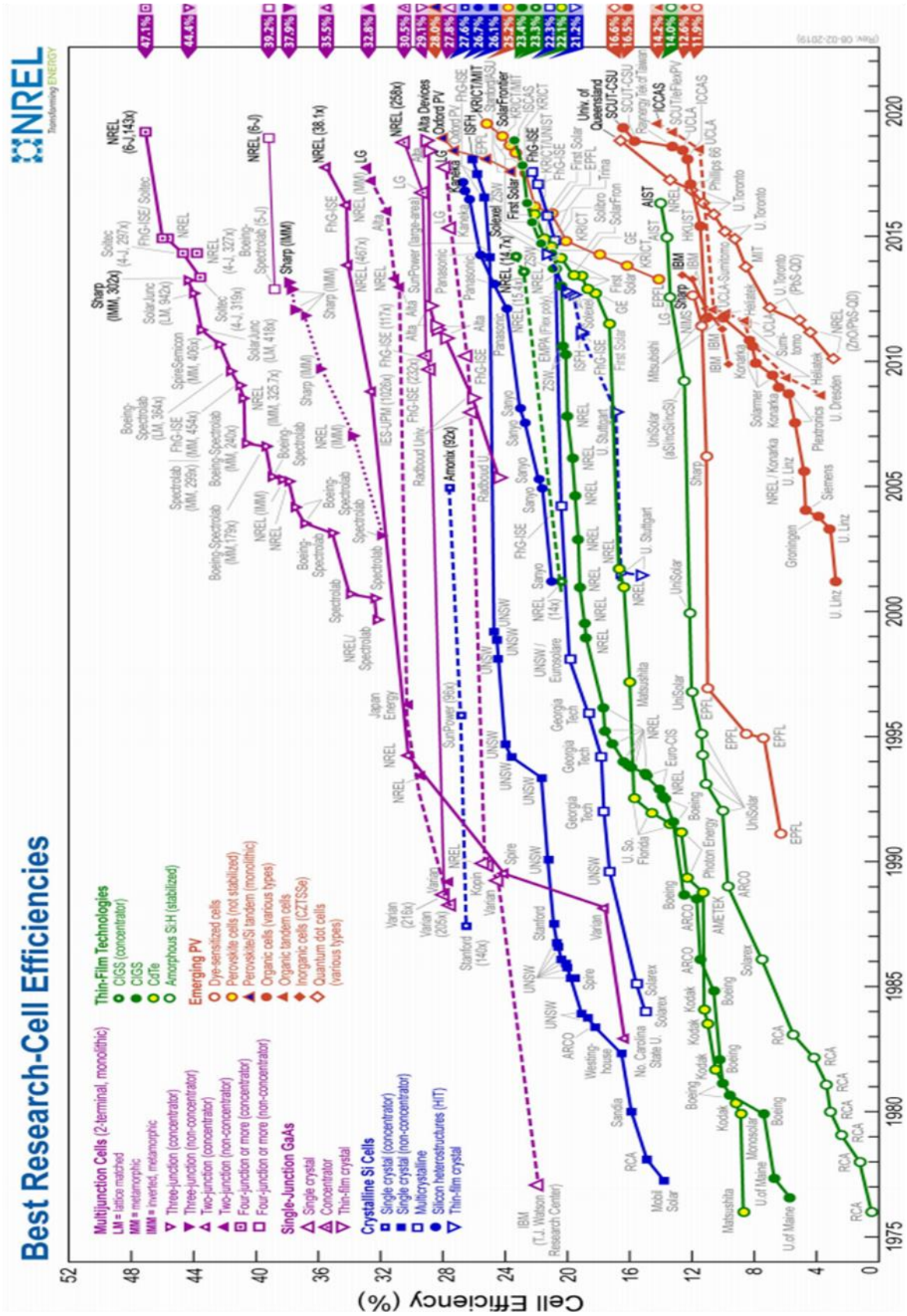

Figure 2-6 Developments in solar cell efficiencies over a period and comparison of the three generations of solar photovoltaics, solar cell energy conversion efficiencies since 1976 [57].

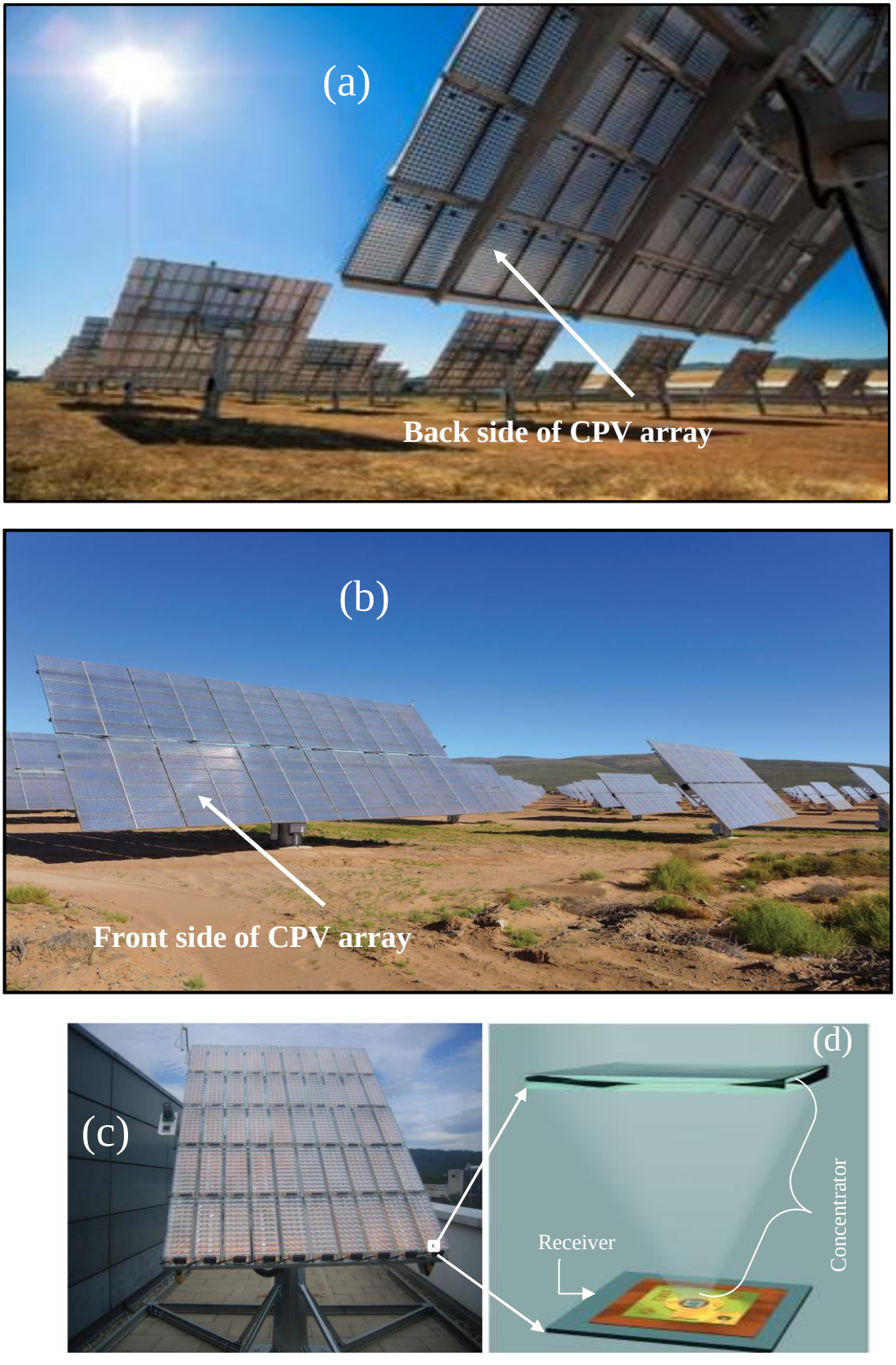

Figure 2-7 (a) CPV plant, the back side of the modules (b) concentrating photovoltaic system to generate electricity in South Africa the front side ;(c) CPV solar plant, using an array of refractive Fresnel lenses to focus sunlight; (d) single cell concentration, using Fresnel lens optics. Image: FLATCON® technology [13, 36, 49].

2.3 Solar spectrum

Solar radiation is emitted from the Sun and is incident on the Earth, despite the distance from the Sun to the Earth being approximately ninety-three million miles. This means only those photons emitted directly at the Earth contribute to the solar spectrum observed [56]. Solar spectrum quantifies the number of photons, which can contribute to photocurrent in a solar cell. The wavelength dependent spectrum can be converted into photon energy [19]. A solar spectrum is an electromagnetic form of energy; it has three regions: ultraviolet; visible light, and infrared, where a wavelength's light ranges from 280nm to 4000nm.

The solar radiation defined as the "solar energy received on the Earth's surface is the sum of *DNI* and diffused radiation after scattering in the atmosphere" [61]. While the rays travel longer through the atmosphere, the solar radiation attenuates further because of the rising atmospheric absorption and probability of scattering [61]. The performance of photovoltaic solar cells depends on the radiation and solar spectrum distribution. Because of the continuous nuclear reaction, the Sun emits electromagnetic radiation with a continuous spectrum, which matches that of a blackbody radiation at a temperature of approximately 5250^{o}C. The Air Mass (*AM*[i]) is known as a measure of how absorption in the atmosphere affects the spectral content and intensity of the solar radiation reaching the Earth's surface; this relation (6) gives the air mass value:

$$AM = \frac{1}{\cos(\theta)} \tag{6}$$

Where θ is the incidence angle (zenith angle) and is known as the angle between the sun's position and the zenith. Higher *AM* is characterised by more attenuation of the irradiance, particularly on the Ultraviolet (UV) region of the spectrum. The air mass values are always greater than or equal to one on the Earth's surface. The terrestrial spectrum represents the light that reaches the surface of the Earth after passing through the atmosphere. Air mass zero (*AM* = 0) means the spectrum of the Sun is outside the Earth's atmosphere. Air mass Global represents a direct incident irradiance compound to Earth and diffusion compounds. Figure 2-8 illustrates the different *AM* of solar radiation.

[i] *AM* =1.5D represents the light on a straight path from the Sun to the device. Although, *AM* 1.5G, is globule contains the light scattered by the atmosphere or diffused light.

There are two forms of solar radiation which are received by the Earth: the direct (beam) and the diffusion. Hence, the sum of two forms on the planet is known by global radiation:

$$Global\ radiation = Diffuse\ radiation + Direct\ radiation \quad (7)$$

The irradiance contained in the Sun's spectrum is a function of wavelength. For solar cell characterisation, the standard reference spectra are used, so the sunlight spectral distribution is observed on Earth. Figure 2-9 shows a plot of ASTM G-173-03 international standard spectral distribution. While at Air Mass = 0, the atmosphere's solar spectrum has an ultraviolet region which is in part absorbed by the ozone layer, and when reaching the Earth, also, the irradiance decreases of the visible light region. It is important to mention that the CPV systems do not effectively capture diffuse sunlight.

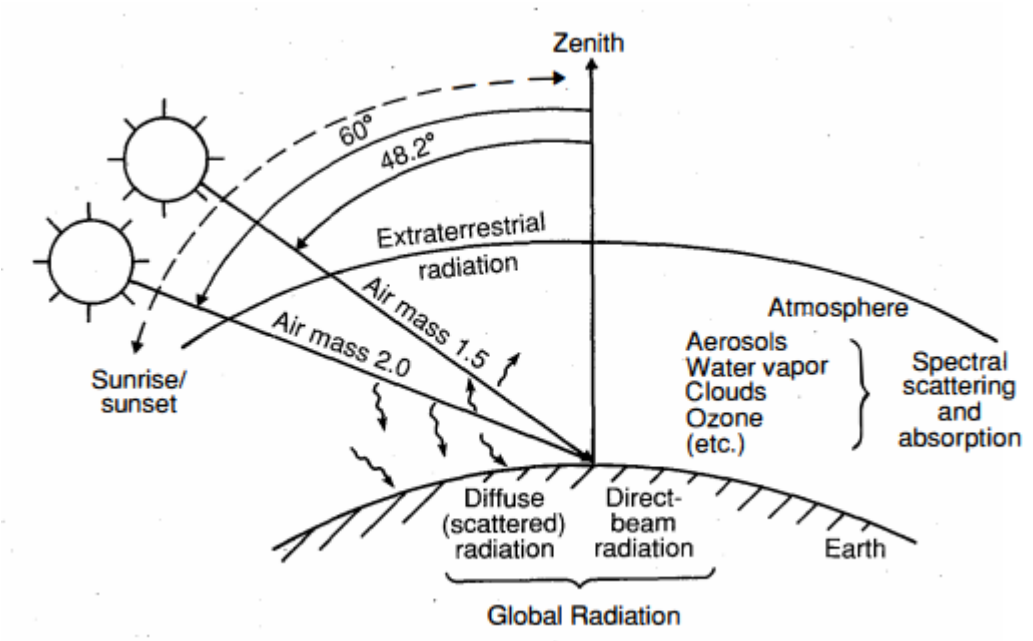

Figure 2-8 Schematic illustrates (*AM*) air mass as a function of zenith angle and spectral scattering and absorption [62].

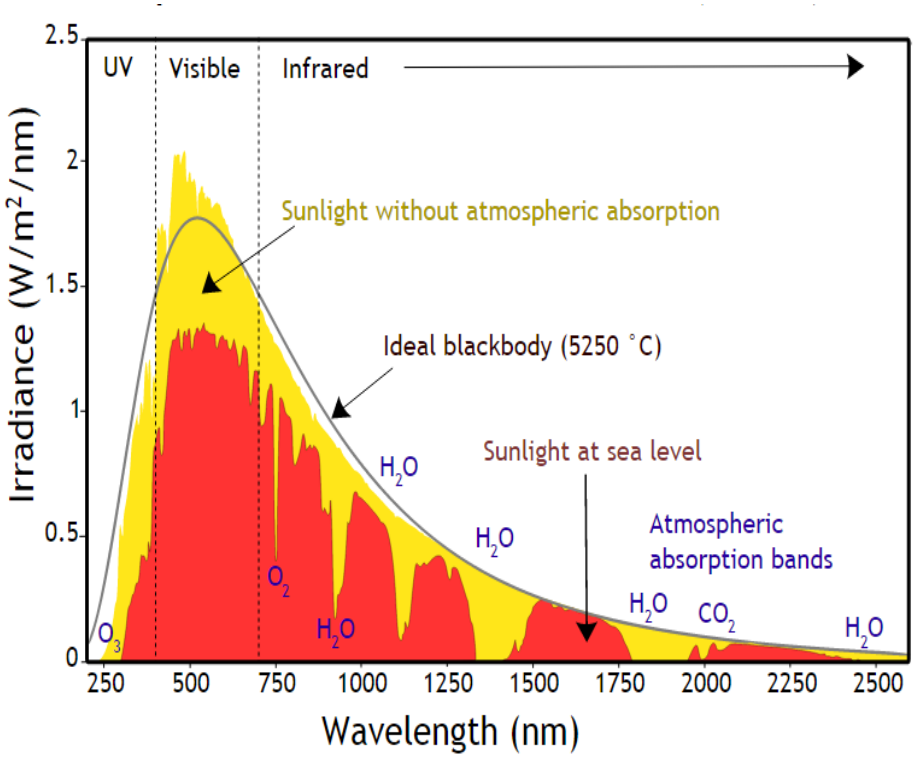

Figure 2-9 Sunlight spectral distribution solar spectrum ASTM G-173-03 International Standard extraterrestrial (*AM* 0) and terrestrial Global and direct (*AM*1.5) [63, 64].

2.3.1 Triple-junction solar cells spectral distribution

The spectral distribution of the sunlight is significant for the power generation of photovoltaic solar cells. The solar absorbers depend on the quantum efficiency of the solar cells, and the distribution of spectral irradiance of incident solar radiation.
Knowledge of the solar spectrum gives solar cell designers the ability to quantify the amount of current produced by each junction of the solar cell, and a better understanding of the solar spectrum is important, while bearing in mind cell design.

Accordingly, by stacking these cells of III-V semiconductor materials on top of each other, the bandgap decreases from the top to the bottom sub-cell. It is important to consider the effects of spectral mismatch, the non-absorption losses and efficiency losses in performance characterisation for such solar cells.

Typically, the Si Silicon solar cell utilises a relatively limited range of the solar spectrum array because of bandgap limits. Triple-junction cells can capture a larger range of the solar spectrum. This has led to the development of high-efficiency photovoltaic cells

fabricated from III-V semiconductor materials, with different energy band gaps, as displayed in figure 2-10.

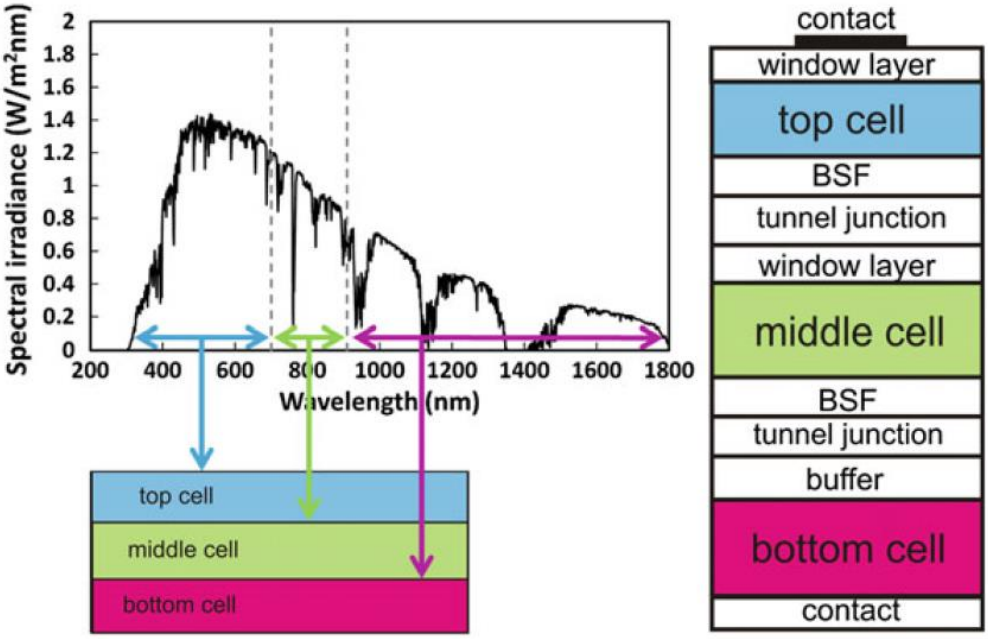

Figure 2-10 Triple junction GaInP/GaInAs/Ge solar cells as a function of wavelength [54].

To explain how the incident solar energy is partially converted into electricity and partly to the heat in multi-junction solar cells, consider a three-layer solar cell in tandem and monolithically stacked as illustrated in Figure 2-11.

If the top layer energy band gap is $E_{g,1}$, and the middle layer $E_{g,2}$, and for the bottom layer, $E_{g,3}$, the incident photons within the energy range $E_{ph} > E_{g,1}$ will be absorbed by the top layer cell. Although incident photons with energies $< E_{g,1}$ will not be absorbed, they consequently will be transparent and pass to the middle layer. The photons within energies $E_{g,1} > E_{ph} > E_{g,2}$ will be absorbed by the middle layer and lastly $E_{g,2} > E_{ph} > E_{g,3}$ will be absorbed by the bottom layer. Thus, the photons that are not absorbed by the three-layer solar cell will be transformed into heat energy [65].

It is estimated that on a clear day approximately 4.4×10^{17} photons are received every second, by each square centimetre on the Earth's surface [66]. The incident solar flux density at the Earth's surface is variable throughout the daily base hours.

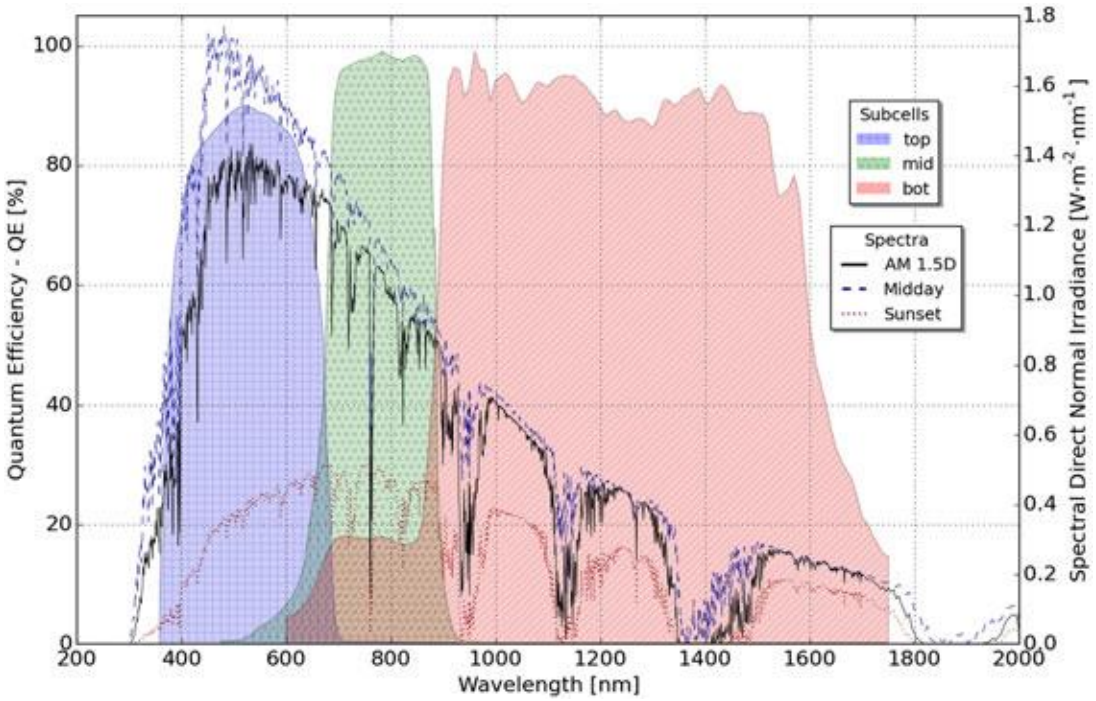

Figure 2-11 External Quantum Efficiency (EQE) for the component of the triple-junction cell as a function of wavelength [67].

Spectral distribution evaluation over the wavelength is the key step to predicting and characterising the CPV cell/module's performance. The External Quantum Efficiency (EQE) of each subcell of photovoltaic triple-junction solar cell can be seen as a function of wavelength when illuminated. The reference spectrum *AM* 1.5D G173-03 is also represented as both two other spectra: the lower values of *AM* represents condition of air mass at midday, and the large *AM* values represent air mass at sunset, this discussed in **Chapter 7**. It is essential to indicate that the distribution of the spectral irradiance on the solar cell changes throughout the day, month or year [38].

The description of the solar spectrum is for the incident irradiance on the multi-junction solar cell. There is a substantial difference of spectra between the corresponding *AM* at midday and *AM* at sunset/sunrise of the same day. Figure 2-11 shows both the reference spectrum at *AM* 1.5D-G173-03 and the (EQE) External Quantum Efficiency of the three-layer assembly cells of an LM lattice-matched, GaInP/GaInAs/ Ge solar cell [67].

It should be noted that as far as the multi-junction solar cells are concerned, the level of concentration or irradiance ought to be assessed separately for each subcell [68]. To ascertain concentration levels, component cells (which are single-junction), and which

display a similar ‘spectral response’ to that used to estimate the photocurrent in each sub-cell of a MJ cell. Component cells are built up using semiconductors, but with a diode at a single junction. The other junctions, known as ‘isotope cells’ (having growing isotype junctions), are made inactive electrically; however, they are still capable of absorbing photons, which allows the one active diode to display the same features as an MJ’s subcell [68, 69].

Therefore, the top cell responds to a light wavelength of approximately 300 – 700nm, cell tested by a solar light simulator concurrently at one sun bias, and the second, filtered, simulator with a red long-pass filter. Besides this, the spectral response is measured over an extended range of 300 – 800nm. The middle subcell responds to approximately 500 – 900nm, cell tested by solar light simulator concurrently at one sun bias, and the second, filtered, simulator with blue band pass filter, also transmitting in the infra-red. Furthermore, the spectral response is measured over an extended range of 300 – 1100nm. The bottom subcell responds to approximately 900 – 1800nm, cell tested by solar light simulator concurrently at one sun bias and the second, filtered, simulator with an infra-red rejection filter, Also, the spectral response is measured over an extended range of 800 – 1800nm [70].

2.4 Concentration ratio

The concentration ratio is defined as the amount of solar flux received by the absorber compared to the incident flux. The sunlight concentration is the maximum amount of light reflected or refracted, as efficiently as possible, onto a smaller area on the exit aperture of the concentrator. The concentration ratio is dimension less unit and normally referred to as ‘suns or x ’.There are two definitions of concentration ratio: (i) Geometrical concentration ratio (ii) Optical concentration ratio, the latter is most commonly used [56].

2.4.1 Geometric concentration ratio

Typically, the geometric concentration is defined as the ratio of entry aperture area against the exit aperture area, as expressed in equation (8), where A_1 is the aperture area of the concentrator and A_2 is the absorber area [71]. Optical solar concentrators are always characterised by their capability to concentrate rays of sunlight, which can be expressed as a geometric concentration ratio:

$$CR_g = \frac{A_1}{A_2} \tag{8}$$

The basic geometry shows the $r/R = \sin\theta_{Sun}$, where R is the distance between the centre of the Sun and the entry aperture of the concentrator and r is the radius of the Sun, as shown in figure 2-12.

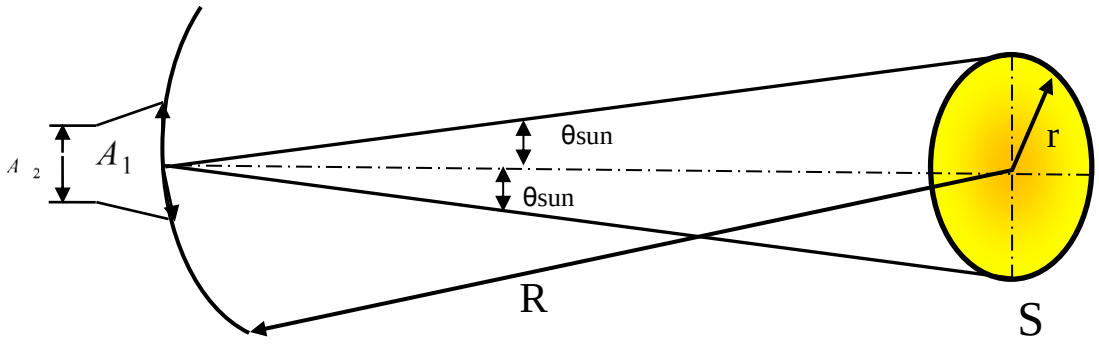

θsun is the semi-angle subtended by the source S

Figure 2-12 Solar radiation transfer through a receiver aperture A_1 on absorber A_2 [71].

2.4.2 Optical concentration ratio

An optical concentration ratio is known as "flux concentration ratio" or "intensity concentration ratio". It is defined as "ratio average energy flux on the absorber to the aperture of the concentrator" [71], as expressed in equation (9). As the energy flux on the receiver surface is not homogeneous, the average of the flux on the receiver is taken into account. Moreover, in another approach, the local concentration ratio on the absorber can be defined as the ratio of the flux at any point of the receiver to the aperture. For instance, if the flux on the absorber is 20 times, so the flux on the aperture, the concentration ratio is termed to be 20 suns [71, 72].

$$CR_{opt} = \frac{flux.receiver}{flux.incident} \tag{9}$$

2.5 Photovoltaic Concentrating Technique

The optical concentration of sunlight can be either refractive or reflective, dependent on the concentrator device used, such as lenses or mirrors. The system can reduce the area of expensive solar cells, modules, which will result in increases in efficiency [37]. The concentrating techniques are dividing into four categories depending on the concentrating ratio:

- Low Concentration [1 – 10 suns].
- Medium Concentration [10 – 100 suns].
- High Concentration [100 – 2000 suns].
- Ultra-high concentration [>2000 suns].

2.5.1 Ultra-high concentration (CR > 2000 suns)

Where the concentrating ratio is >2000 suns; one beneficial feature of using UHCPV is the rise cell efficiency [73]. This range of concentrations has currently attracted the attention of research scholars, who have indicated that the systems will have great possibilities for decreasing the CPV system cost. However, the maximum cell efficiency in these concentration ratios is limited by series resistance losses [74]. The thermal management has to be carefully considered while utilising solar cells operating at UHCPV [74, 75].

2.5.2 High concentration (CR > 100 < 2000 suns)

This system has a high concentration ratio of between 100 – 2000 suns; such systems use either refractive or reflective technologies. Linear concentration systems are used in a parabolic trough, or with linear Fresnel devices, such as lenses or mirrors. These systems are usually required for two-axis tracking. Developed HCPV systems are used with high-efficiency III-V tandem solar cells. The cells have a very high conversion efficiency; under the concentrated light, the efficiency increases [49].

2.5.3 Medium concentration (10 suns > CR < 100 suns)

Here, the systems have medium concentration ratios of between 10 and 100 suns, and generally use linear focus systems, such as a parabolic trough or linear Fresnel lenses. These systems need to function on a single or dual axis tracking. The main challenge facing these systems is the heat generated by the cell. Due to the concentration ratio, the heat generated, and the temperature of the solar cell, increases quickly. Many cooling

methods are used in order to overcome the issues of heat dissipation; it is important to consider those efforts that increase the overall system cost.

2.5.4 Low concentration (CR < 10 suns)

These systems have low concentration ratios of between one and ten suns, and utilise a linear focus system, such as holographic or luminescent. Typically, these have more flexibility in tracking requirements and can work without trackers and cooling. Their concentration ratio is quite low so that the solar cell cost is to be bear in mind.

There are numerous different configurations type of CPV system. They can be categorised based on the level of light concentration e.g. a low, medium or high concentration ratio. As illustrated in figure 2-13, the CPV systems can be classified based on optics, solar cells, a method of cooling and tracking system utilised. The tracker's system of CPV is classified into two types based on the sun trackers from a mechanical point of view [38]:

i. One-axis: this tracker is not capable to keep the CPV modules perpendicular to the sun's rays in every instant, nonetheless it allows the incident irradiation to be increased with respect to a fixed assembly.
ii. Two-axes: this tracker work on two degrees of freedom in order to retain the CPV modules perpendicular to the sun's rays, thus that it can get the maximum incident irradiation [38].

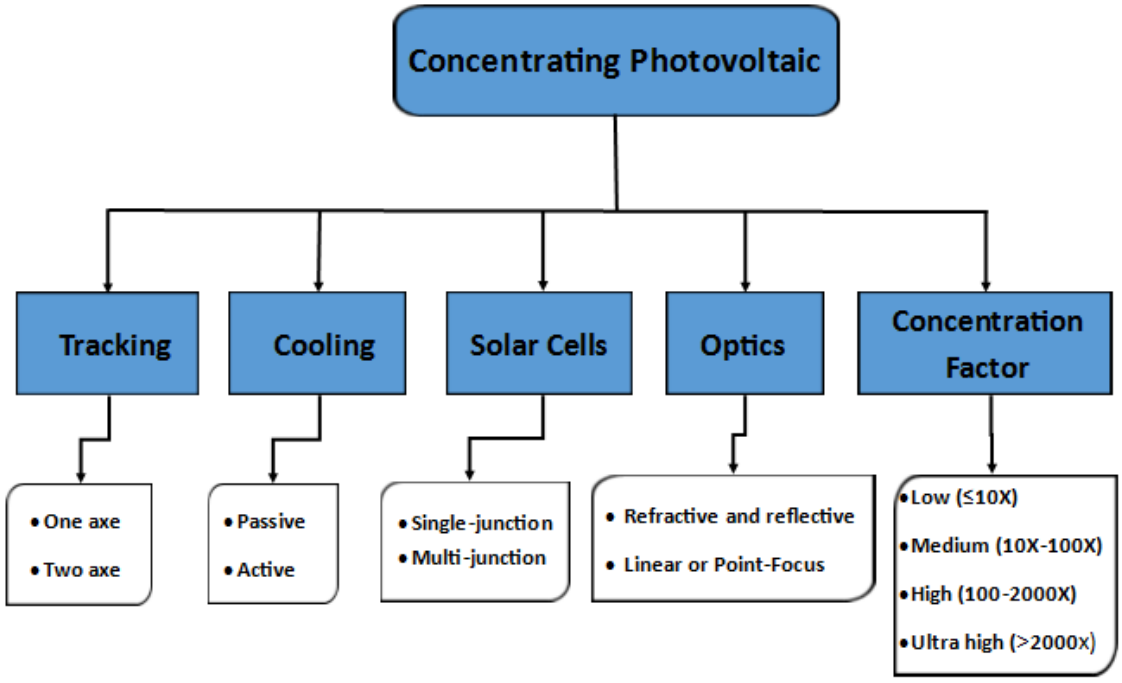

Figure 2-13 Block diagram of criteria of CPV classification.

2.6 Thermal management requirement of CPV receiver

The key aim of thermal management in a CPV system is to guarantee the reliability of the system. Thermal management is an essential part in CPV systems, hence the temperature significantly influences the solar cell's performance. The cooling can be done either passively (by using air convection) or actively by conduction and a cooling fluid through a heat exchanger [76]. In medium and high concentrating CPV systems (10suns > CR < 100 suns and CR >2000 suns respectively), cooling is very important, because of the significant decrease in the area on the receiver surface and growth in the energy flux of the concentrated sunlight [77]. Cooling mechanisms have been divided into the two categories, which are active and passive.

2.6.1 Passive heat dissipation

There are several techniques for heat removal in solar cells, such as heat sinks and heat spreaders. The latter is commonly used on medium concentration photovoltaic [77]. The passive methods by conduction to the large area than convection and radiation. Also, it is more desirable due to their low complexity compared to active cooling. Furthermore, these require relatively large areas to dissipate the heat [76]. In addition, in passive cooling, there is no need for a supplement of electrical or mechanical power [77], because of the lack of moving portions and no external sources; passive cooling might raise the CPV systems reliability and decreases the costs. Valera *et al*.[78] have performed a feasibility study by using 3D modelling of flat heat-sinks with microscale solar cells at ultra-high concentrating ratio 2000–10,000 suns, the results gives useful design for future UHCPV thermal management.

2.6.2 Active heat dissipation

The active heat dissipation refers to photovoltaic/thermal collector (PV/T) technology, where the amount of heat produced by the PV is dissipated from the cell, so it can be re-used in other purposes. Active cooling is required from exterior energy sources to cool the cell [77]. Techniques such as micro-channels heat sink or impinging jets are considered as the most promising technologies for active cooling of a CPV, as reported in references [47, 77].

In the simple model, it is assumed the incident solar radiation is transmitted through the cell encapsulation and absorbed at the solar cell junction, partly determined by the cell temperature, and is converted to electricity; the rest is converted to heat. Part assumed

that part of the heat is lost through radiation and convection from the cover glass surface. Eventually, the remaining heat must be removed by the cooling system on the surface of the substrate [47].

2.7 Concentrating Photovoltaic Receivers

A concentrating system consists of the three segments, which comprise of receiver, focusing optics and tracker. The receiver in the assembly contains the solar cell and a system for heat dissipation. The purpose of the focusing optics is to concentrate the illumination on the receiver. Meanwhile, the concentrating system works with the direct sunlight component, the receiver and focusing optics. However, the latter needs to use a single/dual axis tracker to attain optimum incident radiation [79].

The CPV receiver is defines as "an assembly of one or more PV cells that accept concentrated sunlight and incorporate the means for thermal and electric energy removal" [80]. Based on the IEC 62108 [81], the Concentrating Photovoltaics CPV receiver is manufactured using a compound of one or more solar cells, optical material, methods for current extraction, bypassing diode in shading situations, and heat dissipation. The cells are assigned to an electrical substrate, which is called a cell assembly.

The receivers of High Concentrating Photovoltaic HCPV are designed to raise production of electrical energy, in order to improve the transportation of the thermal energy and to ensure appropriate mechanical support. The option of the geometry and the materials selected rely on several factors, such as the cost, the concentration ratio, and moreover, thermal management [82].

2.7.1 Substrate

The assemblies of solar concentrating photovoltaics are normally made with three layers. Those layers are the conductive, the heat spreader and the heat sink layer. Since the conductive layer is essential to transfer the current, photo-generated energy by the cell uses removal mechanisms in order to minimise the electrical losses. The heat spreader has to efficiently transport the waste heat from the solar cell to the heat sink which, in turn, has to dissipate it to the surrounding media [83].

2.8 Heat remover module

Example of a "Diode Steal" module has specification dimensions of 200x200*mm* of lens size for CR= 820x and 550x dimension of 165x165*mm*, as illustrated in Figure 2-14 (b). The aperture sizes of the cell are 7x7*mm*, therefore this receiver is broadly used in the concentration ratio of 820 and 550x. Choice of lens size is essential due to its close relevance to heat dissipation from the cell. In the "Diode Steal" module, the heat of the concentrator cell is exchanged via the enclosure, without utilising the heat sinks or another heat removal technique [84, 85].

When the cell is subjected to significant optical concentration, heat will be generated in each subcell. However, in many applications, it will be efficiently released to the environment as happens for standard PV flat-plate panel, as shown in figure 2-14 (a). In case of concentration to a small area, there are two situations to attain this: firstly, that the heat resistance between the cell and the enclosure is adequately small. Secondly, that heat can be effectively diffused into the enclosure. Hence, the second situation relies on the heat conductivity of the enclosure (made from aluminium), also the values of concentrated heat on the cell in which proportional to the size of the lens [86].

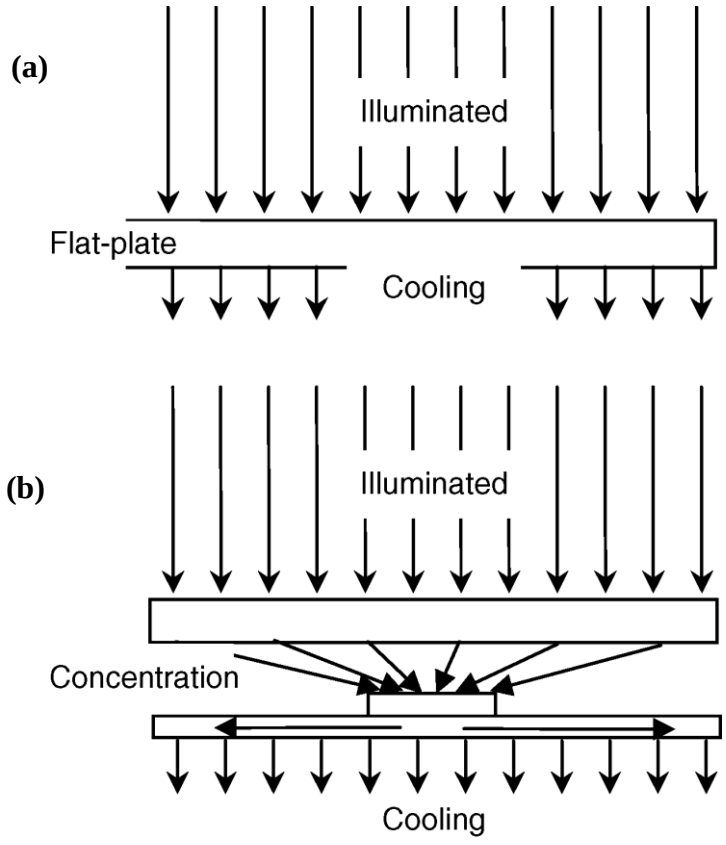

Figure 2-14 (a) PV flat-plate, (b) Design module of the heat removal design of CPV Daido Steel and compared with flat-plate PV modules [85, 86].

The thermal performance of the CPV concentrating photovoltaic module can be represented and modelled via a thermal resistive equivalent circuit. Thus, the temperature and heat flow acts using the same equivalent as voltage and current preforming in an electrical circuit. In addition, the thermal resistors correspond to ohmic resistors. The simple equivalent scheme of the main mechanism of heat extraction in the CPV module [84, 87], is presented in figure 2-15 (b).

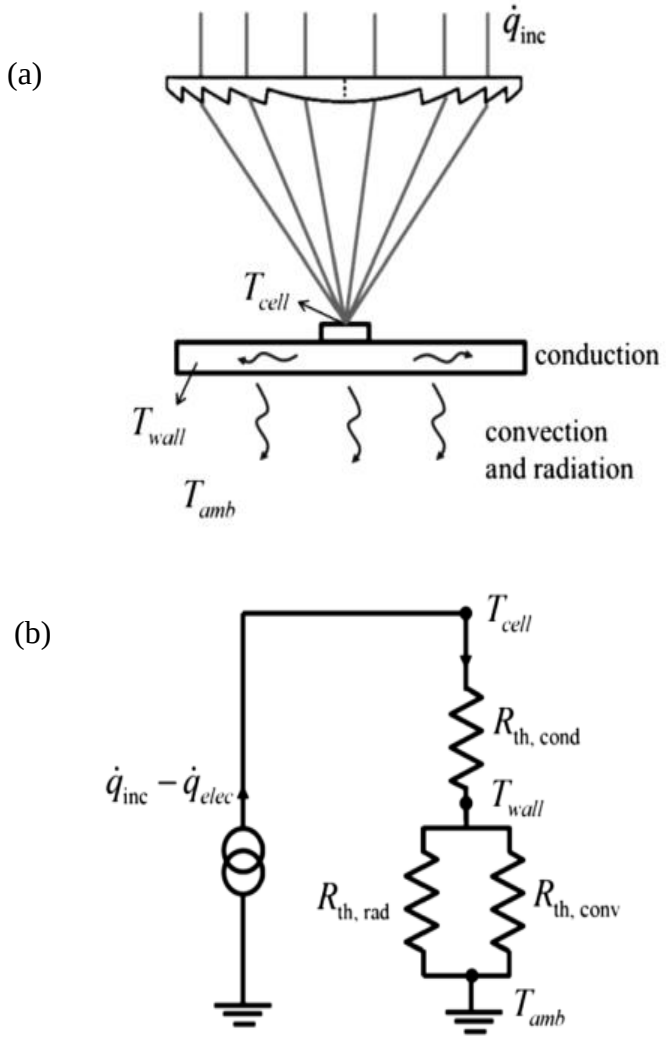

Figure 2-15 (a) thermal transfer model, (b) Simple equivalent circuit of the thermal behaviour of a CPV module [84].

The only portion of the entire incident energy flux $\dot{q}_{inc}$, which is concentrated on the surface of the solar cell, is converted to the electricity $\dot{q}_{ele}$. Although, the rest of the energy $\dot{q}_{inc} - \dot{q}_{ele}$ should be dissipated to the environment as heat. The heat flow is transferred initially by conduction, then by convection and lastly by radiation, subsequently leading to the steady-state condition [84]:

$$\dot{q}_{inc} - \dot{q}_{ele} = \dot{q}_{cond} = \dot{q}_{conv} + \dot{q}_{rad} \quad (10)$$

In order to enable the heat to be dissipated to the environment, the heat flow moves from the solar cell at a particular temperature, T_{cell}, to the module back wall at temperature T_{wall}. The heat transfer mechanism (conduction), and its efficiency, can be quantified by the thermal conductivity of the materials under the solar cell and the thickness of the cell. While further specific details of different assemblies proposed for the thermal stack is undertaken, based on heat flow q_{cond} [87, 88], as presented in figure 2-15 (a).

The operating temperature in the CPV module was predicted by considering the thermal resistance and the heat transfer coefficient. A low thermal resistance between the solar cell and the back-surface, and a high, heat transfer coefficient of the back-surface, were found to be effective for reducing the operating temperature [89].

2.9 Prediction and measuring of cell temperature

The assessment of cell temperature is essential to quantifying energy production of CPV systems [90]. Triple-junction cells are very sensitive to changes in temperature, and hence this is considered to be one of the challenges affecting a cell's conversion efficiency. Therefore, a cell's lifetime under light concentration is a matter which will always need to be taken into account.

Considering the performance behaviour under a concentration ratio of 500x, if the PV module is insulated, then the temperature can spike up and reach a value higher than 1400^{o}C. However, it is important to understand and investigate the effects of cell temperature (T_{cell}) on triple-junction electrical performance parameters [86, 91].

The maximum operating temperature of the solar cell is 125^{o}C [92]. Publication of experimental data given by Sharp solar cell manufacturing company has shown that multi-junction cell can operate up to 120^{o}C [22]. It is worth mentioning that HCPV systems are designed to operate at a temperature usually below 80°C, for safe and long-time operating and to ensure adequate cell lifetime [93]. The risk associated with higher cell temperature is cell performance degradation, which will also result in failure or deformation.

The temperature rise has a big influence on the electrical parameters of (J_{sc}), the short circuit current density, (V_{oc}) open circuit voltage, (FF) fill factor and (η), the efficiency of single and multijunction solar cells. From the experimental and theoretical analysis

already published, the temperature rise affects the energy bandgap of the cell, which can cause sensitivity to all these parameters. For this reason, the temperature assessment is a complicated problem.

The effects of temperature happen at all levels of the CPV system: optics; solar cell; receiver; module, etc. and must be predicted in order to decrease, as much as possible, their negative influence on the energy output of the system [84]. The high concentrations attained in the HCPV lead to the production of high quantities of waste heat, which requires extraction from the cell's assembly. This high temperature, in turn, will have a negative impact on the performance of photovoltaic cells and the receiver. Therefore, for this reason, it is always recommended to keep the CPV cells in a range of operating temperature between 50°C and 80°C [83].

A cell's material structure and design create limitations, which will affect heat transfer capabilities, and therefore the performance in the receiver. T_{max} can be further reduced by using a system with frequent thermal cycling, thereby increasing the longevity of the system, assuming T_{max} is maintained below 80°C [94].

Muller *et al.* [95] presented thermal transient measurements, where the module is tested when covered and uncovered, based on the temperature coefficient according to the heating and natural cooling of the CPV module. The measurement the V_{oc} of the cells was used to determine the cell operating temperature, so the advantage of this measurement technique has a very quick response.

Figure 2-16 shows an example of a module, which is tracking the sun, before and after uncovering. However, this method had disadvantages: measurements have to be very quick and it has to be applied independently to every concentrating photovoltaic module's technology [95, 96].

Moreover, it recommends repeating the experiment many times in order to decrease the uncertainty when assessing the temperature coefficients. However, the above-mentioned approaches for the solar cell's operating temperature predictions need some measurement of electrical parameters or temperature. The approaches to estimate the T_{cell}, is based on the atmospheric parameters.

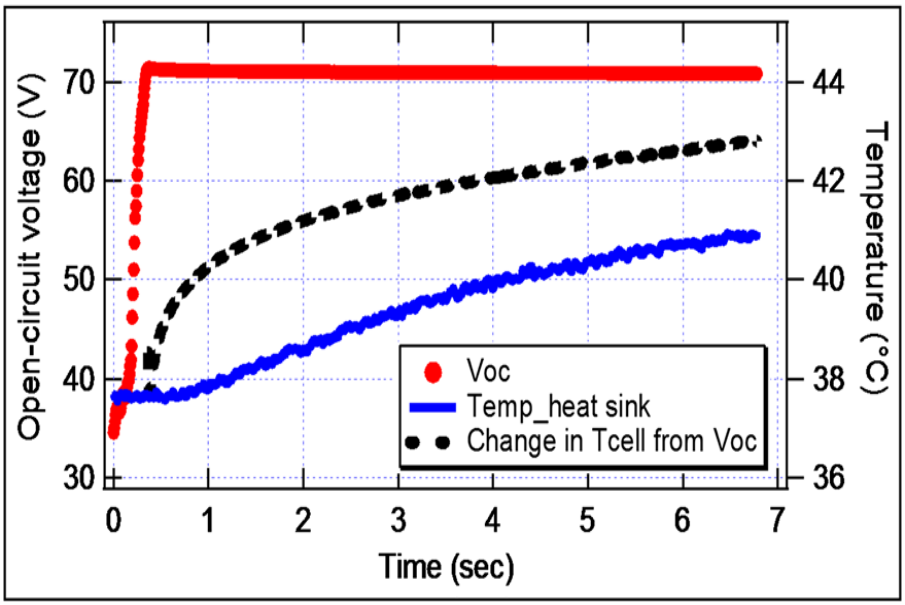

Figure 2-2 Thermal transient measuring data and the calculated cell temperature are showing the CPV module [95].

Fernández *et al.*[97] presented an Artificial Neural Networks (*ANN*) technique to estimate the cell temperature by utilising atmospheric parameters. The Artificial Neural Networks utilised the Levenberg-Markquard algorithm thus, like another approaches, the cell temperature was calculated as a function of T_{amb} and *DNI*.

Fernández *et al.*[97, 98] deduced that the methods based on the measurements of the HCPV module (such as open circuit voltage or heat sink temperature), gives better results. This approach enables scientists to estimate the cell temperature under real conditions, and electrical energy yield.

Fernández *et al.*[99] have proposed another method for estimating cell temperature of an HCPV module at the maximum power point and under real operating conditions. The suggested method determines the cell temperature of an HCPV module from its generated power, using the thermal resistance of the module. The predicted results are compared with measured and the correlation coefficient is 0.99.

Renno and Petito [90] have proposed a model called a "Random Forest" (RF), a technique which is used for the temperature analysis of triple-junction solar cell performance. The *RF* is a comprehensive learning model commonly used, which attempts to establish a general model from the database are established [100]. Normally, the ensemble-learning model attempts to create a group of models and afterwards merge them together.

Consequently, they have better performance, especially when dealing with difficult non-linear problems. Specifically, the (RF) model merges several decision trees by using an algorithm called bagging. Many ensemble strategies attempt to attain the variety of bases to have better estimated results [101].

Experimental studies of CPV systems has been performed on two sizes of solar cells, 5.5x5.5mm^2 and 1x1cm^2. Therefore, the cell temperature of the two cells has been determined in different operating conditions, and the higher temperatures gained was with the larger cell (reaching about 90°C) [90].

Figure 2-17 shows results of a good fit between predicted RF model and measured values, particularly taking into account the high number of measurements in different conditions. A regression fit between the measured and RF model was (R^2 = 0.95). Figure 2-18 shows a predicted *ANN* model and measured cell temperature of the triple-junction cell, as plotted by the scatter. Observing the means of the illustrated scatter plots, it has been noted that there is a high difference between the estimates as highlighted. There was a dispersion between measured points and the predicted model, the regression was R^2 = 0.75. The RF technique, statistically, shows the higher accuracy in the prediction as the different error measurements have been estimated [90].

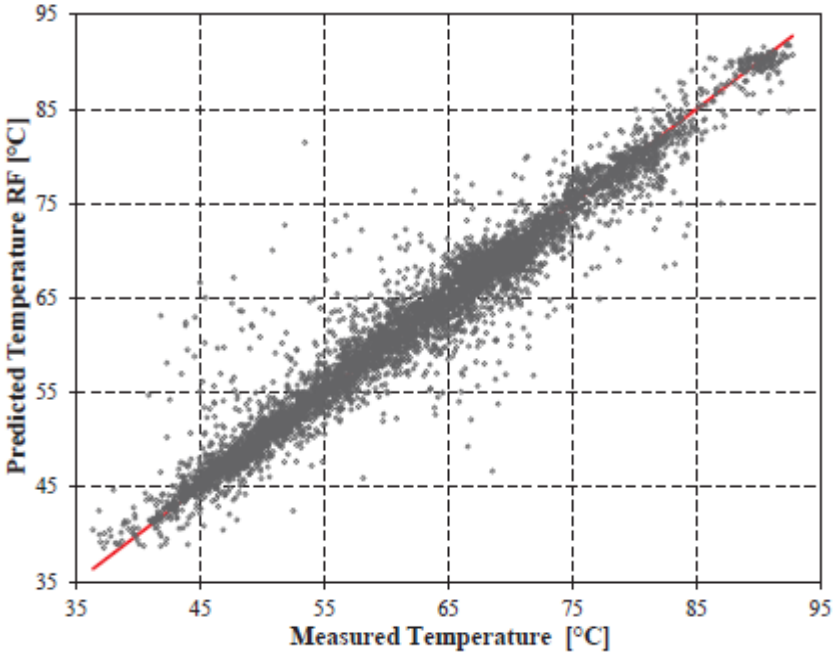

Figure 2-3 Predicted and measured cell temperature for triple-junction by using the RF models of cell 1 x1cm^2 [90].

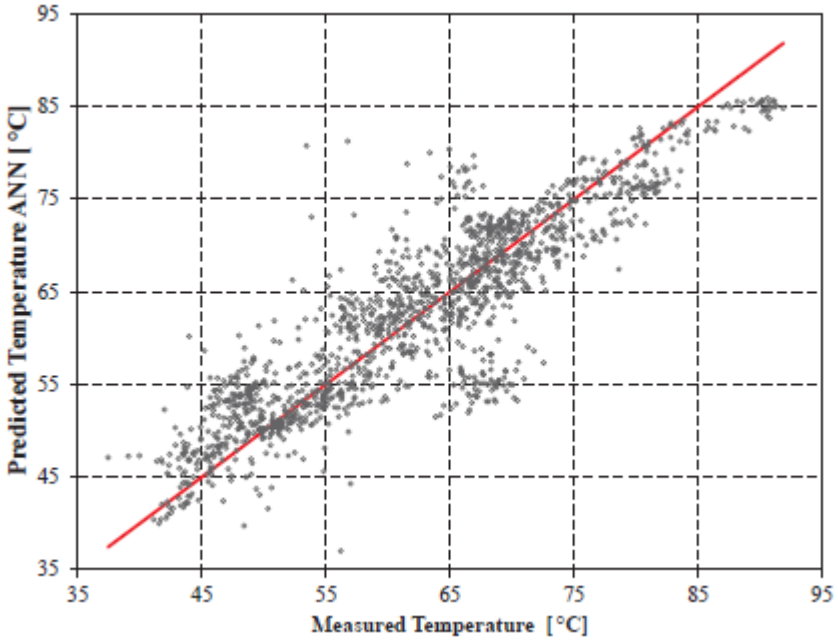

Figure 2-4 Predicted and measured cell temperature for the triple-junction by using the cell model, *ANN* model of cell 1x1cm^2 [90].

2.10 Reliability Requirements

Reliability can be known as a probability measurement of suitable system performance, where the system's necessity to work without malfunction when exposed to specific operating conditions is met.

Based on the risk of what might occur when the cell operates at high temperature, it is important to consider the reliability aspect in any further study. Performance degradation for long-term use of PV usually happens when solar cell temperatures increase over the limited level. Therefore, the temperature rise can moreover lead to mechanical failures like deformation on the surface of the cell and micro-cracks on the cell [83].

Espinet-Gonzlez1 *et al.*[102] have performed experimental measurement of the Accelerated Life Tests (ALT) transformed from accelerated stress level to nominal stress level. Additionally, the failure rate of the triple-junction solar cells for a nominal operational temperature was also ascertained. Figure 2-19 illustrates the instantaneous failure rate of cell temperature at 80^{o}C presented by the solid line, and at 100^{o}C presented by the dashed line, versus time. Therefore, "the instantaneous failure rate functions monotonically", and equivalently, with "the wear-out failure segment of the well-known bathtube curve" [102].

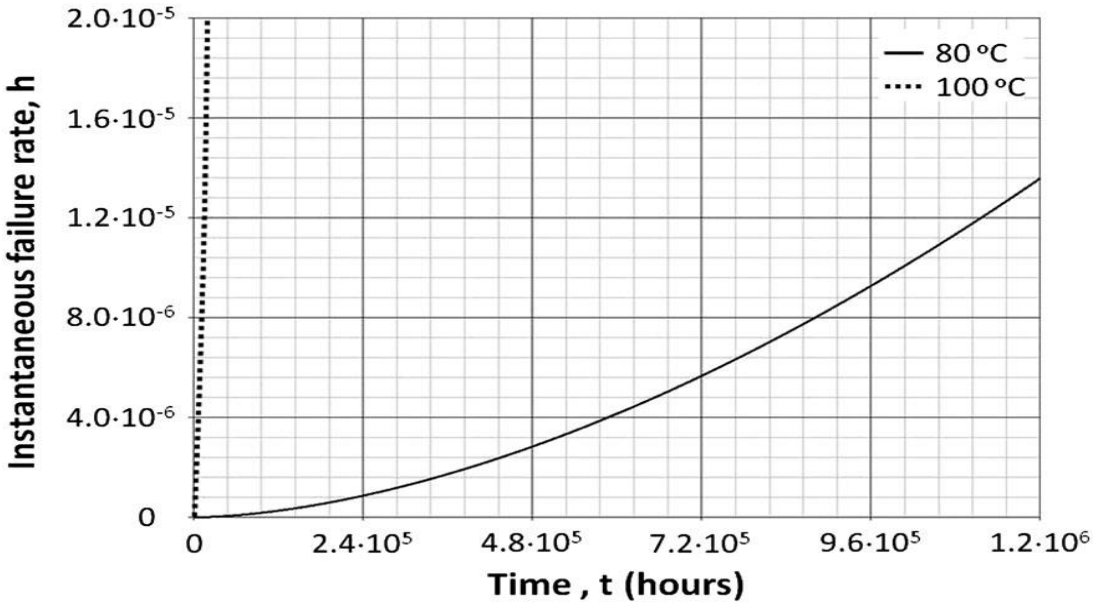

Figure 2-5 Experimental data of failure rate function of the triple-junction solar cells for a nominal operating temperature of 80ºC and 100ºC [102].

Figure 2-20 presents the reliability function (R(t)) at a nominal operating temperature of 80ºC, in the solid line, and 100ºC in the dashed line over time. Furthermore, it shows the empirical data of "the ALT transformed from the accelerated stress level to the nominal stress level" [102]. Therefore, the purple points represent the temperature at 80ºC and orange points at a temperature of 100ºC via "the corresponding Acceleration Factor (AF) attained". There was a good fit between "the reliability function extrapolated to nominal operating conditions and the transformation of the empirical points" [94, 102].

It has shown by reliability analysis, that on triple-junction solar cells at operating conditions of 820x and 80°C, the warranty time was about 113 years; while, at the operating temperature of 100°C, the warranty time was reduced to 7 years [102, 103].

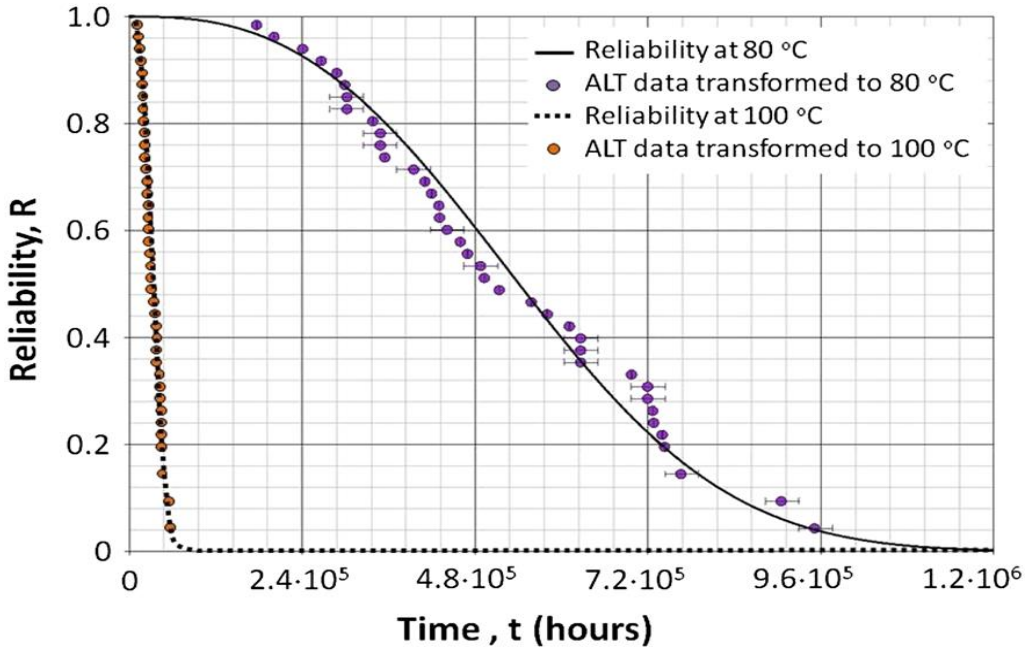

Figure 2-20 The reliability over time for a nominal operating temperature of 80ºC and 100ºC [102].

Renno *et al.*[104] performed measurement analysis of triple-junction solar cells at 310x, where the cell has been stressed via the accelerated aging method of approximately 500hours operating hours without applying any cooling. Thus, the adverse effect of overheating on the cell began to degrade the performance parameters. Consequently, it deduced that the cooling process is mandatory for the cells integrity, and to improve cost-effectiveness.

A study by García *et al.* [84] Finite Element Modelling (FEM) to estimate the maximum solar cell temperature for CR=1000X as a function of cell size; also, the thicknesses, and the materials thermal conductivities, are also considered. The area of the substrate is proportional to the area of the solar cell. The surface of the back substrate is supposed to be thermally connected to the dissipator that releases the heat to the atmosphere by convection [84]. Figure 2-21 depicts a simulation of two equivalent cases of a 1x1mm solar cell. A case layer, 75µm thick, of alumina-filled epoxy was added underneath the solar cell. This case cell is directly soldered to the copper plate [84].

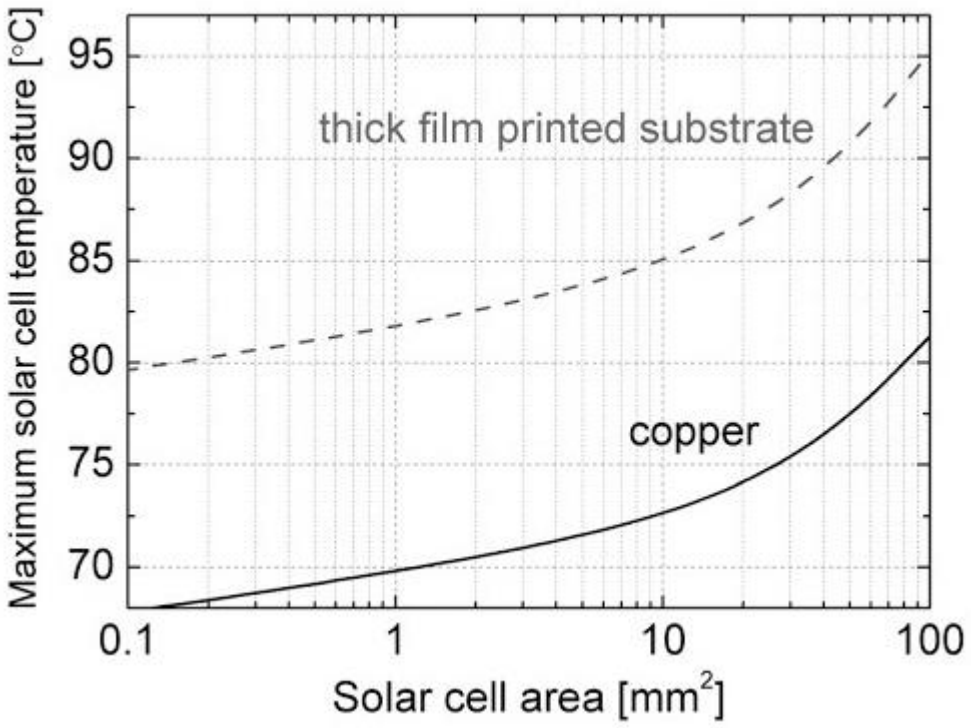

Figure 2-21 Estimations of maximum cell temperature at 1000x, as a function of cell size [84].

When the copper thickness reduces on the receiver before the ideal design point the thermal dissipator capability of the receiver decreases hence, the cell temperature rises. While, the thickness of copper in the receiver increases beyond the ideal design point, the thermal resistance of the receiver increases and subsequently, the cell temperature rises [105].

For high concentration ratios, and corresponding decrease in cell size requires significant thermal management of the whole system. Hence, oversizing the heat sinks will lead to a rise in the system's cost which might not be economically viable as a ratios with the extra energy produced [38, 106].

An example, as illustrated in figure 2-22, explains how the cell temperature also depends on the size of the cell; thus, the larger the cell size, the greater the heat produced. Consequently, CPV systems are typically coupled to a thermal management mechanism to maintain the cell operating temperature in the safe region, in order to avoid damage to the solar cell, and additionally, to decrease the temperature differences between the cells in module and across single cells [38, 102].

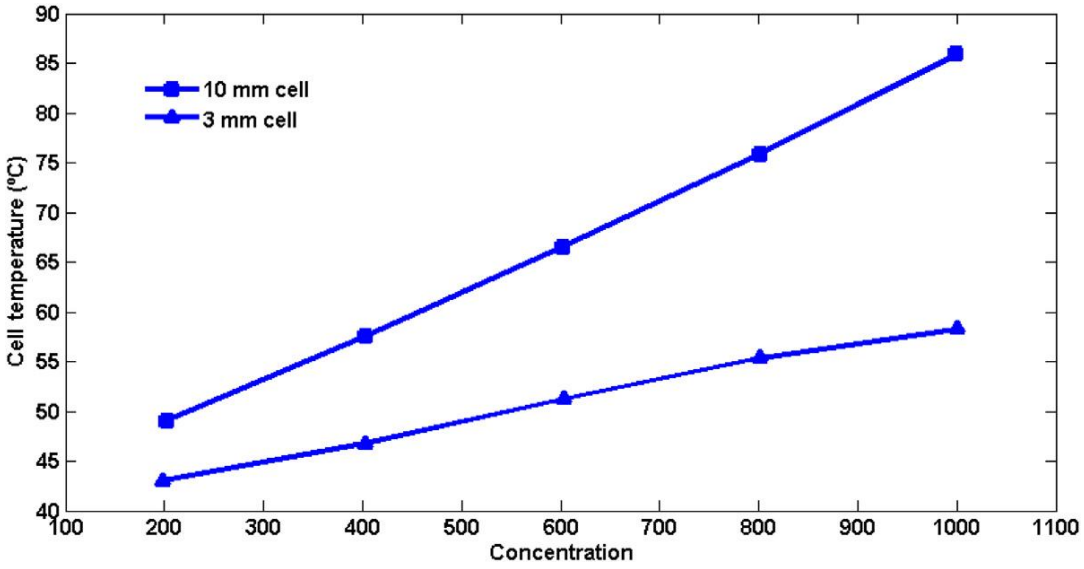

Figure 2-22 Cell temperature of the two different cell sizes, based on different values of concentration ratio [38].

Based on the aforementioned narrative of concerns, which make a concentrating photovoltaic system more complex, there are many opportunities and prospects for the development for CPV technologies, in particular with respect to the performance analysis and estimation of energy yield. Therefore, for better understanding, this potential ought to use precise modelling tools, to analyse and decreases uncertainty in the modelling results. The significance of critical analysis of a CPV receiver is to draw insight into this work modelling framework. Table 2-1 listed details reviews of CPV performance characterisation from the literature.

The performance characterisation is also an important development of any CPV plant operation. Knowledge of the matters associated with the CPV technology, and which are highlighted through the characterisation manner, leads the development of appropriate management plans, and hence one can develop models which guarantee a high quality, reliable, electrical power system.

Table 2-1 Summary of performance characterisation of CPV.

Authors	Methods	Concentration ratio	Results and remarks	Solar cells architectures
Ghani *et al.*[107].	Numerical prediction of lumped parameters by using Newton-Raphson methods. This method presented predictions of five parameter characterisations of triple-junction solar cells.	700x	• Outdoor experimental data of environmental conditions are used for characterising the parameters of the proposed method and to generate *J-V* curves by use of a single diode. • It deduced that a suggested method accurately modelled the behaviour of the photovoltaic triple-junction device and characterised the values of produced parameters. • The suggested work limitation is the need for a good start approximations to initiate the numerical solution result process. So, this matter was alleviated by utilising simple analytical equations in order to estimate the five characterisation parameters.	GaInP/GaInAs/Ge
Rodrigo *et al*. [108].	Two months of the outdoor experimental campaign.	700x.	• It estimated the temperature coefficient of an open-circuit voltage and the internal thermal resistance of HCPV models. • The proposed procedure can help the electrical and thermal characterisation of HCPV modules by outdoor measurements without the necessity of stripping the module. • The estimated values have been analysed and show a high acceptance level of accuracy while characterising the inside cell temperature of the HCPV module.	GaInP/GaInAs/Ge
Almonacid *et al.* [109].	Modelling using an artificial neural network (ANN).	1x	• Atmospheric parameters are undertaken for the electrical characterisation of triple-junction cells. • The model results in illustrations of a high quality of the assessment of spectral performance on the MJ solar cells by the approximation of the Spectral Mismatch Ratio SMR indexes. • The limitation of the models is dedicated to approximating the SMR which is associated with the difficulty of gaining a high-quality data of water vapour and aerosols.	GaInP/GaInAs/Ge

Continued on next page ⇩

Theristis *et al.* [110].	Outdoor test of CPV monomodule solar cell for the three selected days.	1090×	• Based on the spectral changes monomodule cell is electrically characterised. • Analysed the diurnal performance of electrical characteristics and monomodule temperature as a function of spectral, irradiance and ambient temperatures. • It highlighted on the influence of the atmospheric parameters on the cell performance of concentrating photovoltaics.	–
Renno *et al.* [111].	Experimentally evaluation of a triple-Junction solar cell by using a point-focus.	310 x.	• It reported the energy production with different concentration ratios, by considering eight hours a day with different irradiance conditions and electrical energy. • Measured both the solar cell and environment temperatures in order to evaluate the possible.	InGaP/ GaAs/Ge
Wanga *el al.* [112].	Both outdoor experimental test and a mathematical model of triple-junction solar cell electrical characteristics.	100 – 200x	• Characterised the performance of a triple-junction solar cell; also proposed to apply a secondary concentrator to enhance the performance of the photovoltaic system. • The outdoor experiments show that the two main influencing factors on the performance of the solar cell are the solar cell temperature and the direct solar radiation.	InGaP/ GaAs/Ge
Xu a et.al. [113].	The outdoor test carried out to investigate real performance, based on the point-focus Fresnel lens.	1090x	• The analysis displays that direct irradiance is the prevailing atmospheric parameter, which had an effect on electrical performance. • The study is performed for both thermal and electrical performance, also a model made to estimate the cell temperature at operating conditions.	InGaP/GaAs/Ge
Gupta, *et al.* [114].	Numerical modelling by using a finite element method.	12x	• The numerical model used for a topology optimisation strategy; it is suggested to design an efficient metallization manner for solar cells under non-uniform illumination and temperature conditions. • The study showed that a contact resistance can substantially affect the cell the performance.	–
Sweet *et al.* [115].	Numerical modelling of hybrid CPV cell-thermoelectric module and experimental of electrical *J–V* characteristics.	300 – 500x	• The hybrid receivers of III-V concentrator photovoltaic cells been theoretically investigated the electrical and thermal behaviour. • By combining the primary and secondary optical intensity, to obtain a coefficient as high as 0.92.	GaInP/GaInAs/Ge

In addition, the performance characterisation of the multijunction solar cells, operating for long-term reliability at high levels of concentration, ought to be characterised likewise. Figure 2-23 show an overview of performance analysis of HCPV receivers. This work fundamentally has focused on the receiver assembly, where the final component of the CPV system which converts the concentrated solar light into electricity.

A deeper knowledge of this predicted behaviour of a CPV cell, and the impact of surrounding weather parameters on its energy performance, will be highlighted via the characterisation. Nonetheless, this procedure is very complex as it's affected by a variety of environmental conditions.

The significance of a detailed analysis and precise thermal and electrical characterisation is an essential tool for improvement, optimisation and design of a CPV device. Hence, it will lead to the identification of system design issues, and in the assessment of an evaluation of the applied solutions.

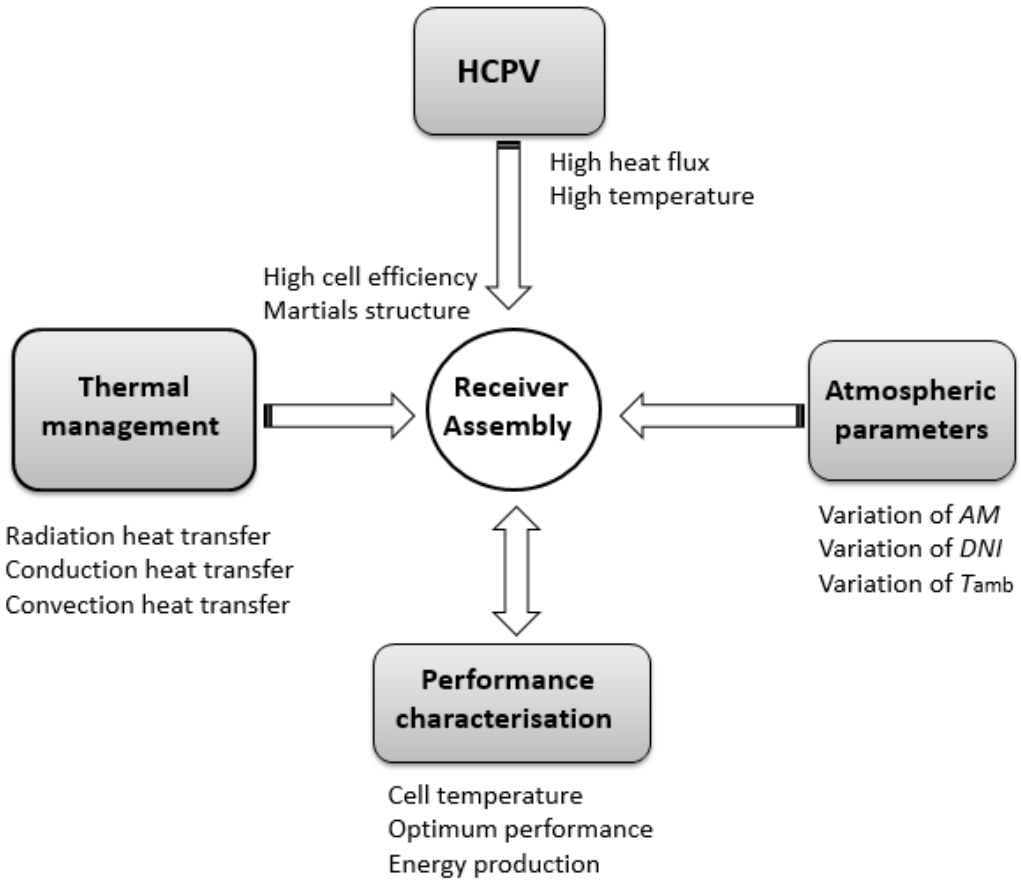

Figure 2-6 An overview of performance analysis of HCPV receiver.

Summary

The literature review gives an overview of relevant studies which have been reported in published literature. This chapter presented the motivation and the background of the present research work, which have been discussed. The main aspects of CPV receiver performance have been presented.

The aforementioned literature has recognised the importance of developing a model, which incorporates the thermal and electrical performance behaviour. In addition, it has been noted these works do not cover the aspect between the ideal performance situation and environment experimental. Therefore, the significance of this modelling work is to link between ideal performance situation and environmental applications.

The receiver CPV is simply equipped as the compound series of PV cells in order to receive sunlight concentration. It is designed to maximise the electrical energy generated and to improve the transfer of thermal energy. Thus, the high thermal capacitance of the cell will keep cell temperature higher. An adequate thermal management system provides a mechanical support of the CPV receivers. The amalgamation of electrical and thermal models is the remit of this research work.

This thesis's aim is to investigate the performance of HCPV receiver with an overview of the performance behaviour aspect, and the need for high concentrating PV cells, to make MJ solar cells, which operate at a very effective way and which are cost feasible.

The issue is the heat removal from the back of the cell in the most efficient, cheap and reliable way. The next chapters will describe the numerical model's procedures and methods used in order to investigate performance behaviour, so a theoretical simulation is important to emphasise the development of the design and system performance characterisation. In the next chapter, the electrical performance modelling of high-efficiency single and triple-junction solar cells is presented.

Chapter 3: Triple-Junction Solar Cell Performance Modelling and Characterisation

3.1 Introduction

This chapter focuses on the performance characterisation of the high-efficiency solar cell, the mathematical modelling approach is described. This model described the electrical performance of a single/triple junction cell (GaInP/GaInAs/Ge). This electrical model is deemed the cornerstone of the next chapters.

A solar photovoltaic (PV) cell is typically made from semiconductor materials, based on *p-n* junction; it is designed to generate an electric current from the absorption of photons. Triple-junction solar cells are III–V semiconductor materials with different bandgaps, used is to reduce thermalisation losses and increase the efficiency [116].

The photons have energy lower than the band gap, they are not absorbed and passes through the cell. The photons have energy more than band gap, the extra energy is lost as heat. The photons have the same energy of the band gap, the energy conversion works at the maximum efficiency [19].

3.2 Electrical model

Solar cells are the key components in determining the electrical behaviour of the HCPV receiver. The cell's physical design mainly depends on the energy bandgap to raise conversion efficiency. In the solar cell's systems, the *J-V* curves are used to characterise the cells performance parameters.

MATLAB® is a powerful tool for solar cell research modelling; it gives good simulation and prediction of assembly behaviour. The modelling is used to predict the performance, which is difficult to measure experimentally. Nevertheless, the simulation and modelling of such as state-of-the-art devices remain to be discovered in-depth knowledge.

The calculation of the electrical characteristics of solar cells is an important tool for the optimisation, performance analysis, device design and system integration. For the designer of the solar cell, it is most important for correlate the properties of device structures with electrical characteristics. Also, for system integration, it is significant to have a mathematical explanation of the solar cell to combine with larger-scale system models [117].

3.2.1 Modelling of single/triple junction cells at 1x

In this study, an electrical model of three different semiconductors materials (subcells) will be modelled together as one cell, which represents a triple junction solar cell. The aims is to increase our understanding of the performance for each materials layer.

The cell layers are composed of GaInP/GaInAs/Ge, and are electrically connected in series they have been shown to achieve an electrical conversion efficiency of over 40% [54, 118]. A simple electrical model was built in MATLAB® of the three layers, with model set up in reference condition DNI =1000W/m^2, AM=1.5D and at a temperature of 25^{o}C. The *J-V* curves represent the relationship between the voltage and current produced by the cell. This method to characterise and evaluate cell performance.

In this model, a single cell and diode equivalent circuit for electrical characteristics is considered. A monolithically stacked multi-junction cell consisted of multiple single-junctions of different III–V materials. The solar sub-cells are connected in series with the junctions directly grown on one substrate and interconnected by tunnel junctions and ended by two terminals. Figure 3-1 shows the equivalent circuit of a one-diode multi-junction solar cell, which also known as a single exponential model (SEM).

The one-diode model is deemed to be an optimum way to describe triple-junction solar cells. The difference between two diodes is a number of diodes that specify the saturation current; in the case of a single diode, this represents recombination in the depletion and quasi-neutral zones [103, 119].

For a CPV application, the Schottky by-pass diodes are utilised to reduce the electrical losses and risk of damages related to shading etc. In addition, connecting one diode per cell is considered to be the most suitable structure [83].

The *p-n* layers of multi-junction solar cells are connected in series by highly doped diodes with low series resistance and thickness, in order to reduce absorption and ohmic losses [38]. The subcell with the higher bandgap is stacked on top, to absorb the higher energy photons; the other subcells, with low band gaps are stacked respectively, in order to capture photons with lower energy [54]. Moreover, another reason for decease the band gap from top to bottom layer, it's to avoid the necessity for optical separate elements such as Prism to distribute the solar spectrum [117].

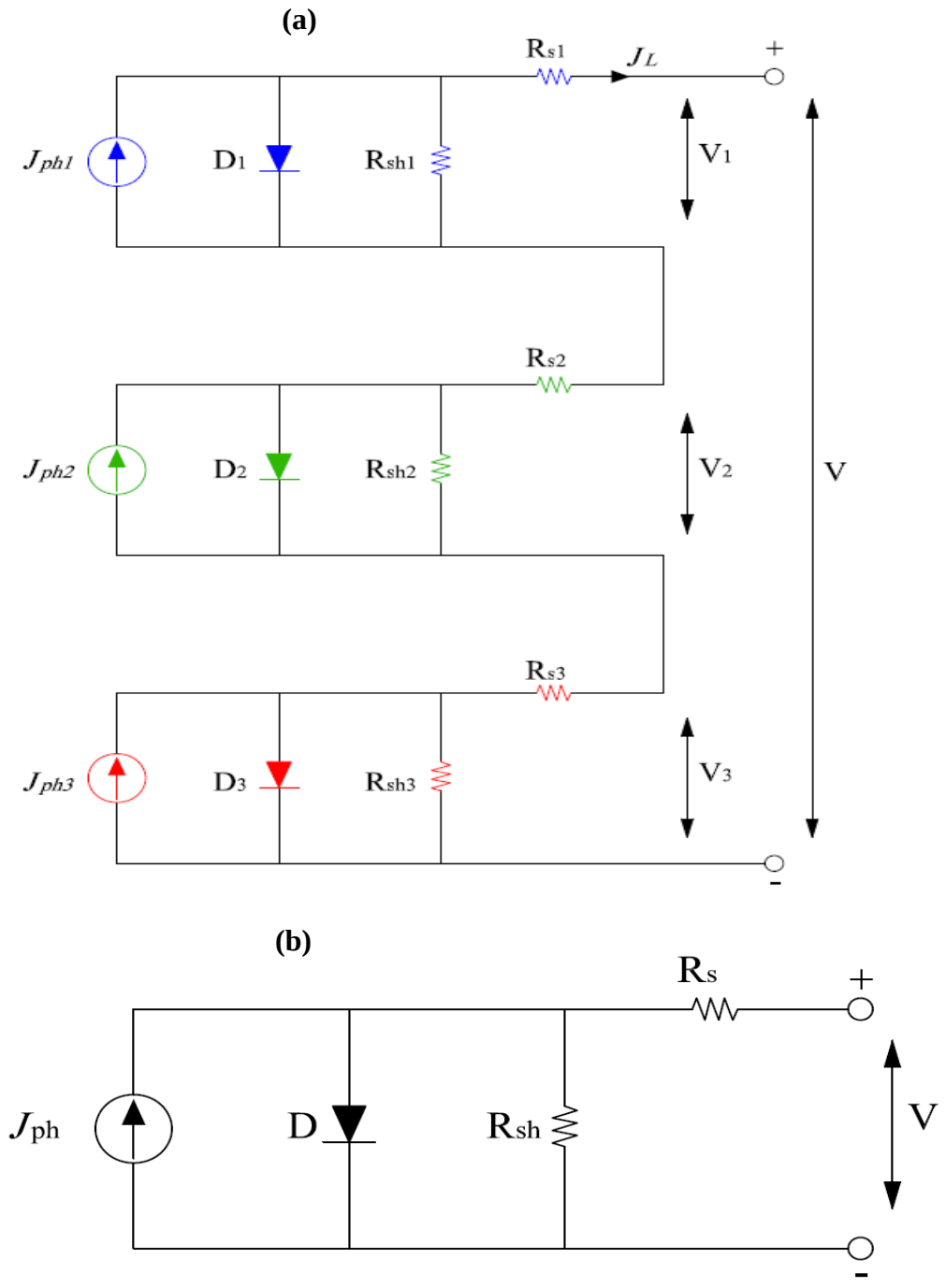

Figure 3-1 (a) The equivalent circuit of one-diode of three layers in series connection solar cell model, (b) represent equivalent circuit model for triple-junction cell.

The estimation of the maximum current density, created by semiconductor junctions relies on many factors, such as a number of incident photons, material absorption and band gap [56]. In the multi-junction solar cell, the blue-rich portions of the spectrum are absorbed by the top layer, the green-rich portion penetrated and absorbs by middle layer and the red-rich portion are absorbs by the bottom layer.

It is assumed that the spectral irradiance distribution over the cell area is uniform, a short-circuit current density will be generated in each cell; it is determined by the spectrum of incident light. Hence, an incident irradiance distribution onto the cell is integrated over a range of wavelengths over the subcell areas, and also considered in the concentration ratio as expressed in equation (11) [103].

$$J_{sc}(\lambda) = \int_{\lambda_{\min}}^{\lambda_{\max}} \frac{q.\lambda.EQE(\lambda).G(\lambda)}{h.c}.d\lambda \tag{11}$$

Where q is the electron charge, EQE is the External Quantum Efficiency; λ is the wavelength of photons. *CR* is the Concentration Ratio, c is the speed of light, h is Planck constant and G (λ) is the spectral direct irradiance. Reverse saturation current J_o is also affected by band gaps reduction, which will result in a decrease in the open circuit voltage for a given temperature and J_o is given by equation (12) [92].

$$J_{o,i} = K.T_c^{(3+\frac{\gamma}{2})} \exp\frac{-E_g}{n.K_b.T_c} \tag{12}$$

Where K_b is Boltzmann constant, n is the diode ideality factor, K and γ are materials constant of each layer. The energy bandgap of semiconductors materials is calculating via the Varshni equation (13). The temperature dependence of semiconductors band gaps is given by Varshni empirical relation [120].

$$E_{g,i} = E_{g,i}(0) - \frac{\alpha_i.T_c^{\,2}}{T_c + \beta_{,i}} \tag{13}$$

Where $E_g(0)$ is band gap at 0 *K*, the index i represent subcell of each layer; T_c is cell temperature, α and β materials constant. Equation (14) known as Shockley diode equation characterises the current produced by the solar cell:

$$J = J_{ph} - J_0\left(\exp\frac{q(V + J.R_s)}{n.K_b.T} - 1\right) - \frac{V + J.R_s}{R_{sh}} \tag{14}$$

Where R_s is series resistance, V is the voltage, R_{sh} is the shunt resistance, J_{ph} is the photocurrent. In the ideal case, the photocurrent is equal to short circuit density $J_{ph} = J_{sc}$. The R_{sh} is of a magnitude that can be neglected [103]. The total current is determined by subtracting the light-induced current from the diode dark current, given by equation (15):

$$J = J_o\left(\exp\frac{q(V + J.R_s}{n.K_b.T} - 1\right) - J_{sc} \tag{15}$$

Because of the series connection of each sub-cell, the overall current generated by the three layers is limited to the lowest current density as expressed in a relationship (16):

$$J_{total} = \min(J_1, J_2, J_3) \tag{16}$$

Equation (17) represents the relationship to calculate the open circuit voltage of the cell:

$$V_{oc} = \frac{n.K_b.T}{q} \ln\left(\frac{J_{sc}}{J_0} + 1\right) \tag{17}$$

Equation (18) is the relationship used to determine the voltage produced in each cell. The total voltage will be the sum of three subcells as indicated by equation (19):

$$V = \frac{n.K_b.T_c}{q} \ln\left(\frac{J_{sc} - J}{J_0} + 1\right) - J.A_c.R_s \tag{18}$$

$$V_{total} = \sum_{i=1}^{3} V, i \tag{19}$$

The Fill Factor (FF) known, as the ratio of the maximum output power from the solar cell to the product of it is open-circuit voltage and short-circuits current as given in equation (20).

$$FF = \frac{P_{\max.}}{V_{oc}.J_{sc}} \tag{20}$$

The efficiency represents the percentage ratio between power output divided by the power input as express in equation (21). Where P_{in} is the incident power and P_{out} is the output power produced by the cell:

$$\eta = \frac{P_{out}}{P_{in}A_c} \tag{21}$$

Short circuit current (I_{sc}) always depends on the area of the solar cell, as expressed in equation (22). To quantify the values of I_{sc}, usually short circuit current density J_{sc} used to define the maximum current produced by the solar cell.

$$I_{sc} = J_{sc}.A_c \tag{22}$$

Where J_{sc} is current density and A_c is an area of the cell. For the model, some parameters are assumed to be constant. The input parameters used for each subcell are summarised in the table listed below (3,4).

Table 3-1 Listed parameters used in the model [119].

subcell	K [A/cm^2 k^4]	*n*	γ
1	1.833x10^{-9}	1.89	1.81
2	2.195x10^{-8}	1.86	1.86
3	1.9187x 10^{-6}	1.44	1.43

Table-32 Listed energy gap parameters and material constant, for III-V triple-junction cell semi-conductors [92, 120].

Subcell	α(eV/K)	β(k)	E_g @ 0 K (eV)
1	4.72x10^{-4}	269	1.8
2	5.39x10^{-4}	204.7	1.49
3	4.77x10^{-4}	235	0.75

The usage of the multi-junction tandem stack layers is to attain the high efficiencies which, when limited to single-junction devices, are difficult to achieve. Therefore, their behaviour complicated. Nonetheless, it could be understood via examination of the (EQE) external quantum efficiency for each single-layer cell in the stack.

The standard external quantum efficiency (EQE) of each sub-cell layer illustrated in figure 3-2 when illuminated at *AM* 1.5D. It is obvious seen that EQE of the three layers accounts for the visible light and large part of infrared radiation ranging from (300 – 1800nm). The material in the top layer is GaInP, the middle subcell is GaInAs and lastly, the bottom subcell is Ge [121].

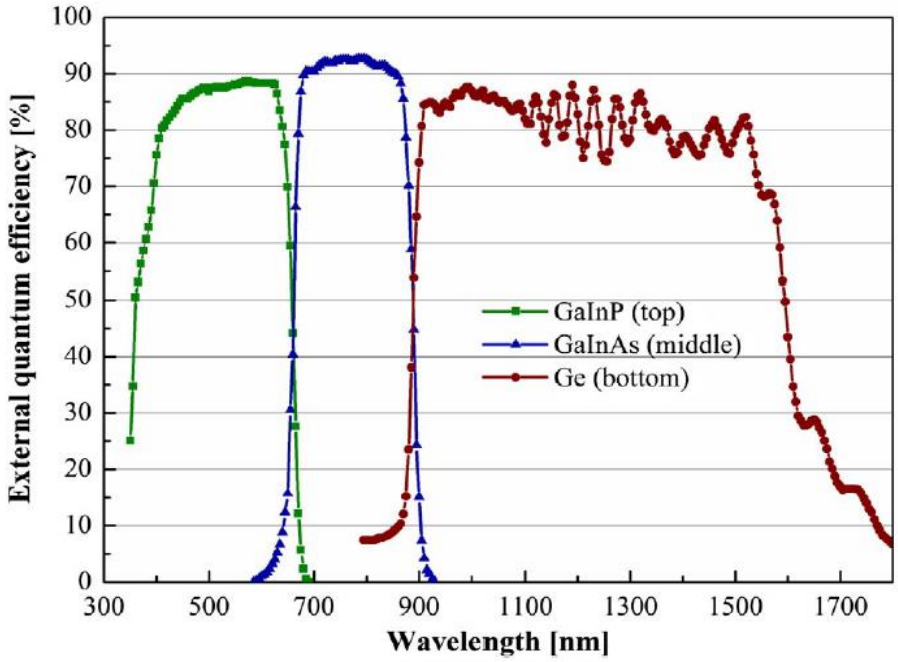

Figure 3-2 The External Quantum Efficiency (EQE) of each layer of the triple-junction solar cell as a function of wavelength [121].

3.3 Modelling results and discussions

3.3.1 Single/triple junction *J-V* curve

The electrical parameters are important in describing the performance of the solar cells. The physical design of the solar cells depends on the material's properties and the energy bandgap. The current produced in each subcell relies on the solar spectrum and selection of material band gaps. However, short-circuit current J_{sc} is the current through the solar cell when no voltage is generated, $V = 0$. The open circuit voltage V_{oc} is the maximum voltage available from a solar cell, which occurs when no current is generated $J = 0$. Figure 3-3 illustrate plots the (*J-V*) curves where (a) is the top cell GaInP, (b) is the middle subcell GaInAs and (c) is the bottom subcell (Ge).

To the understand the various components of the system is an important task, but the main part of the system is the solar cell. Hence, a detailed knowledge of (*J-V*) the current-voltage and (*P-V*) power-voltage the characteristic curves of PV cell/modules is essential to study the PV systems.

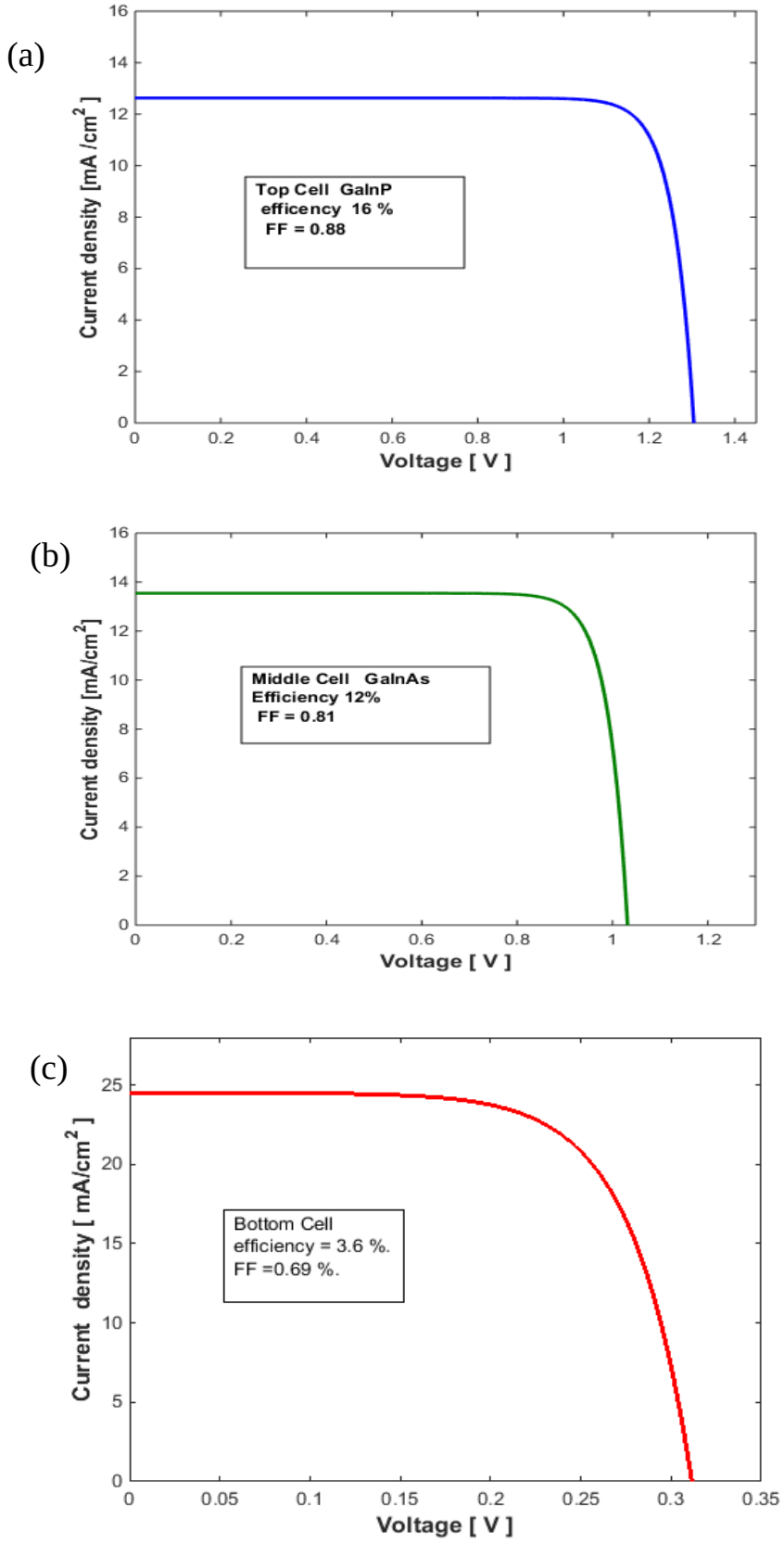

Figure 3-3 One-sun results at temperature 25ºC, (a) top cell *J-V* curve (a) middle cell *J-V* curve (c) bottom cell *J-V* curve.

The current-voltage characteristic (*J-V* curve) under one sun lighting and the spectral response are the key properties of the solar cell's performance. The *J-V* curves represent the relationship between the voltage and current generated. Figure 3-3 represents a combination of three subcells.

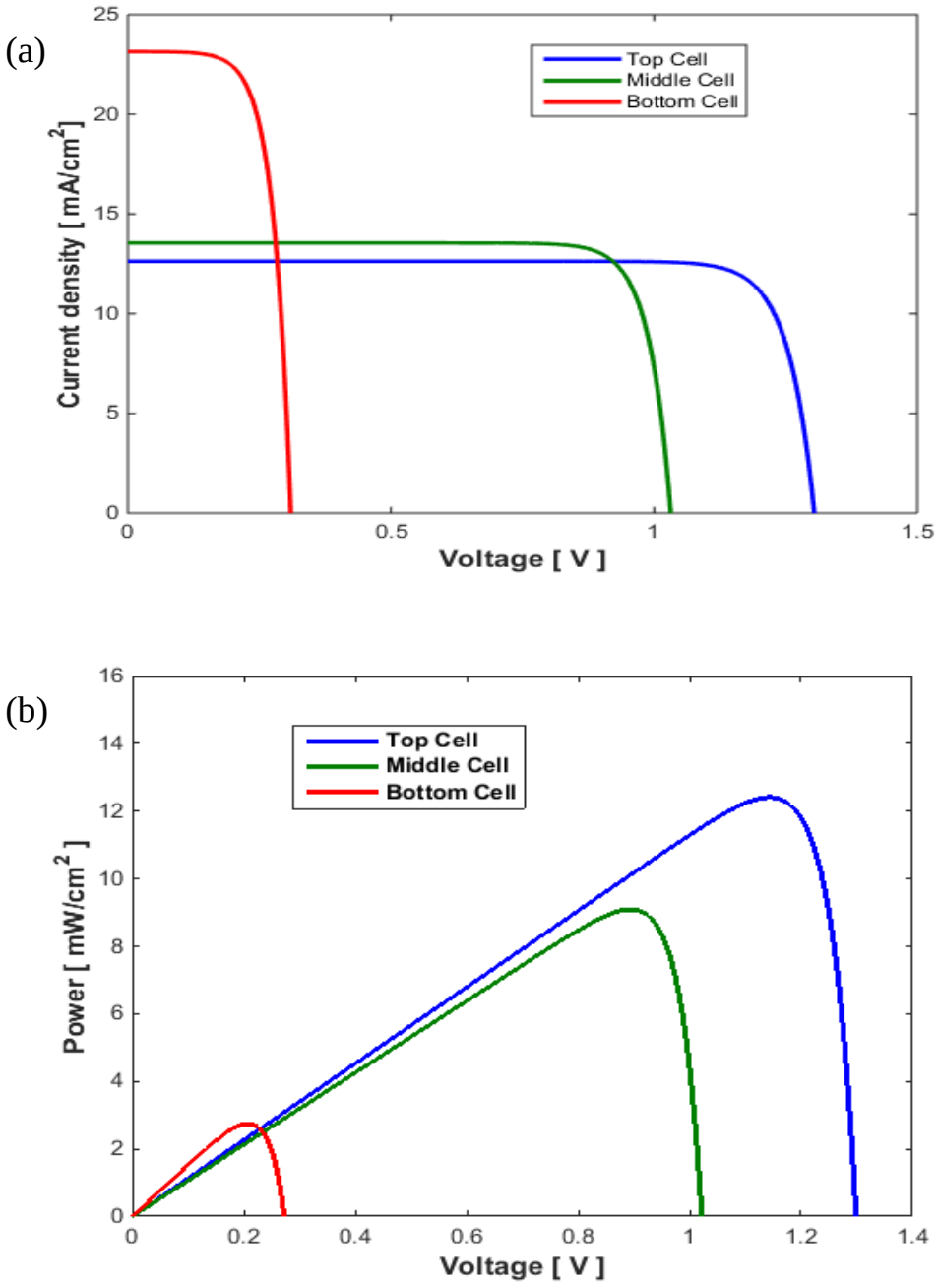

Figure 3-4 (a) *J-V* curves and (b) *P-V* curves of three layers of solar cells.

As seen in figure 3-4 (a), as results of the narrow in the band gap of the Germanium, the bottom junction cell generated less power. The photocurrent produced by this subcell is

always is higher than that produced by the top and middle subcells, even while the cell operating at standard spectral irradiance [122, 123].

Table-33 Tabulated results of a single subcell parameters model of three layers.

Subcell	J_{sc} (mA/cm^2)	V_{oc}(V)	FF	η (%)
Top layer	12.6	1.3	0.88	16
Middle layer	13.5	1.05	0.81	12
Bottom layer	23	0.31	0.69	4

3.3.2 Current limitation

In triple junction solar cells, the top and bottom cell's series connection influenced by changes in the spectrum that result in a "current mismatch" situation and reduction in current density [124]. Therefore, a subcell which has a small energy bandgap has more solar spectrum absorption, which in turn, results in lower subcell voltage and higher current. Thus, the lower open circuit voltage (V_{oc}) is directly proportional to the material bandgap. However, the *J-V* curve is used to characterise the performance of cells parameters. The changes in the solar spectrum from the reference spectrum results in one of the subcell stacks governing the overall solar cell current [125]. Optimisation for particular spectrum occurs when their current density balance of the top and middle subcell as illustrated in figure 3-5.

The optimum performance occurs for spectrum (G-173-03) *AM* 1.5D, where the top and middle cell are designed to generate equal current density "current match". The change in the solar spectrum far from *AM* 1.5D results in one of the two cells become current limiting [126]. Figure 3-6 shows the top subcell current limiting.

Also, at high operating temperatures the current limitation is by the middle subcell [38]. Figure 3-6 shows the plot of *J-V* curves of the triple junction solar cell and total limited current. Therefore, at lower values of *AM,* the top and middle junctions generate the same currents and at higher *AM* values, the top junction will govern the overall current; this is because of a decrease in the spectral factor of multi-junction cells [127].

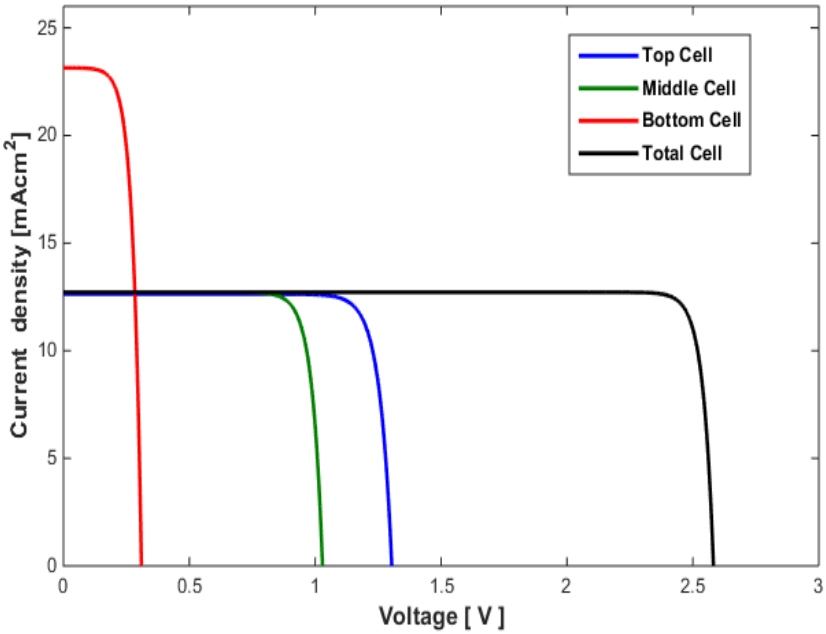

Figure 3-5 ***J-V*** **curve of a combination of the top, middle, bottom subcell of tandem three junctions the total current of solar cell limited by the top and middle cell.**

Cell temperature increases the current density J_{sc} of the junction current limitation increase, mainly because of the energy band gap decrease [127]. Current limitation means that the total current will be limited by the subcell which generates the least current, as the cells are connected in series [46]. Hence, the maximum cell efficiency will be achieved, when the current matching, which dominated by the thickness of subcell layers. Also, it should be noted that when thinning the top subcell layer, the current produced by the bottom subcell will increase at the expense of top subcell current.

For a two-junction cell, before thinning the top subcell layer $J_{sc,top} > J_{sc,bottom}$, then after thinning $J_{sc,top} = J_{sc,bottom}$. The thin of the top layer in the triple-junction solar cell to absorb a high portion of the incident light; because of the very high absorption coefficient of the top subcell. Besides, cell thinning help in decreasing the quantity of material used in manufacturing the solar cells further cost-effectiveness [128]. A small portion of the light will be transmitted at energies photon near the bandgap, and having a small absorption coefficient, also, the excessive thinner of the cell, will lead to light transmission [56]. Therefore, the current generated by a subcell, and not used in the electrical circuit, is converted to heat; this, in turn, results in a higher cell temperature. This heat supply will be taken into the account in the thermal analysis model.

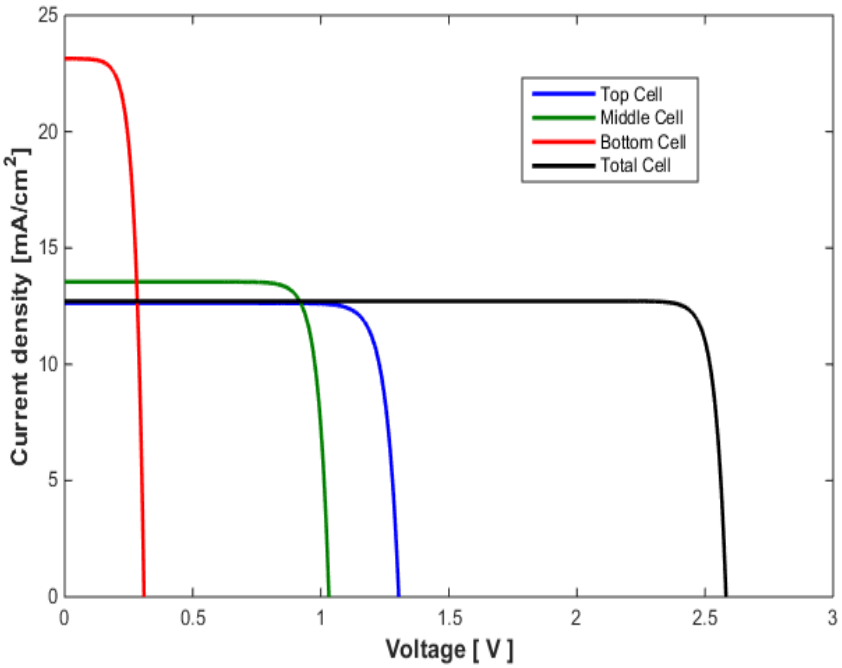

Figure 3-6 *J-V* curve of a combination the top, middle, bottom subcell of tandem 3-J; the total current of solar cell limited by top cell.

To enhance the efficiency of multi-junction solar cells, the bandgap of semiconductor materials and thickness can be altered. One possible method is to replace the bottom subcell with a higher bandgap material that will lead to less short-circuit current and higher voltage; the consequence is an improvement in the efficiency. Moreover, another technique to enhance the design is to substitute the top and middle cells with small band gap materials, subsequently having high short circuit current, and lower voltage [76, 129].

Furthermore, optimisation can be gained by equalising current densities of the two top subcells to develop a "current match". The variations in epitaxial layer growth and the *ARC* Anti-Reflective Coating results in deviations the intended balance of subcell current densities [76]. The current matching in the subcell layers is affected by the antireflective coating. Thus, if the thickness of the top subcell increases, the optimal thickness of the *ARC* also increases to compensate the losses via direct more sunlight to the bottom layer [56].

Figure 3-7 shown the *P-V* curve of the three cells of a triple junction cell. The maximum power point is limited by the lower subcell current; the bottom cells have less power due to lower voltage and higher current. Therefore, the maximum overall power yield is $30 mW/cm^2$.

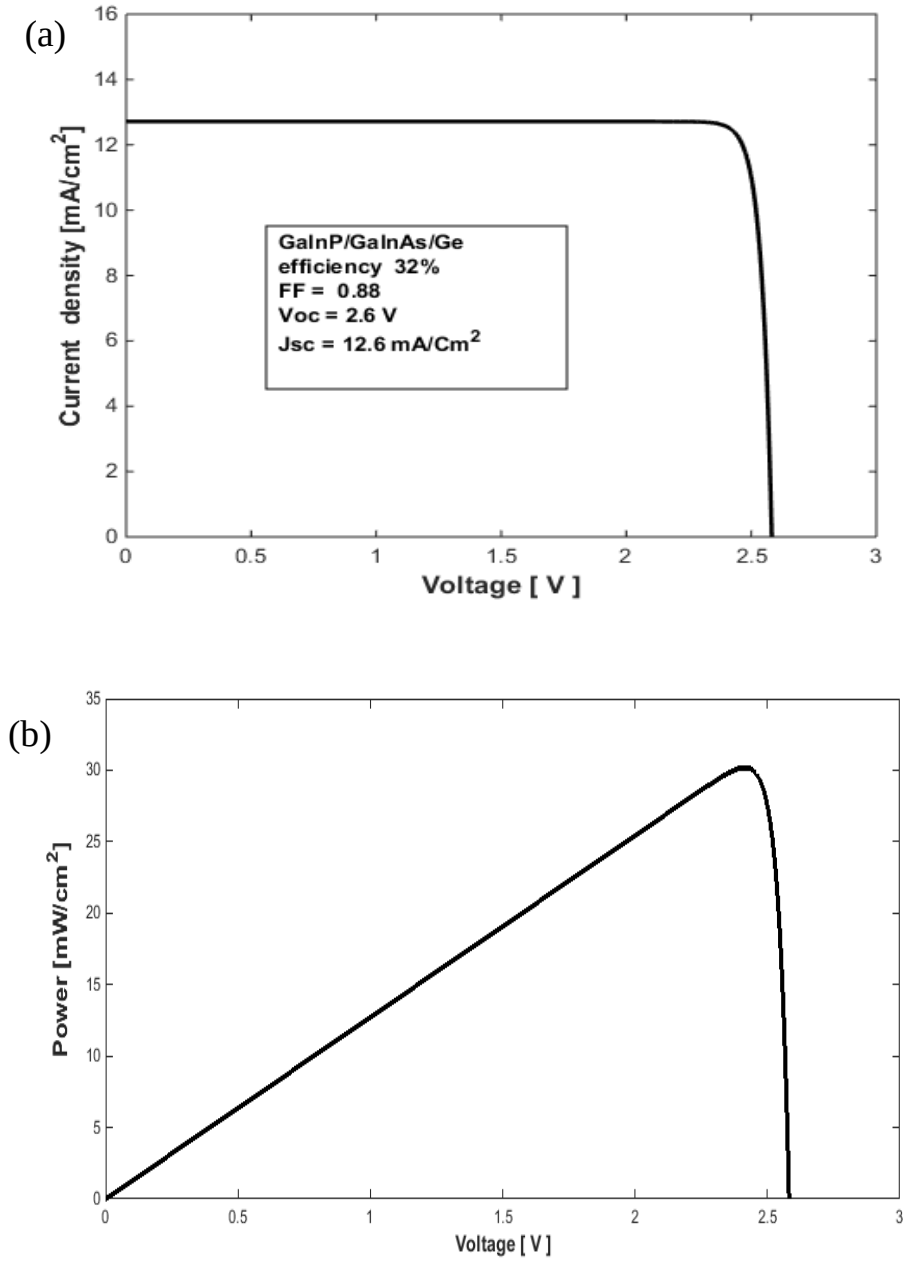

Figure 3-7 *J-V* curve of the tandem triple-junction solar cell (b) *P-V* curve of the three cells of triple junction cell.

3.3.3 Validation

Model parameter results of the current study were compared to other work; some of the parameters such as fill factor FF and efficiency are compatible with the values presented in reference [130]. The characterisation was prefromed under the following conditions: one sun concentration ratio, DNI =1000W/m^2, AM =1.5D and T_{amb} =25°C. The results are also shown compatible with parameters of efficiency and V_{oc} open circuits voltage values that presented by Green *et al.*[131]. The achieved efficiency was 32% at concentration ratio of 1x; this value in good agreement with an experimental measured

value reported in the literature [111]. Hence, the good matching results is significant for accuracy of the model prediction. Table (3-2) summarised list of four performance parameters that published in the literature and compared with the current study model.

Table 3-2 Summarised simulated *J-V* parameters compared to world record values published in the literature for a lattice-matched (LM) MJSC by Green *et al*.[131]. Walker [130] triple cell model results, the temperature at 25 °C and concentration of one – sun.

Parameters	Current study	Model by A. Walker [130]	Error (%)	World Record M. Green *et al.* [131]	Error (%)
J_{sc} ($_{m}A/cm^2$)	12.6	12.3	2.3	13.2	3
V_{oc} (V)	2.6	2.628	1	2.691	2.9
FF	0.88	0.87	0.9	0.86	2.2
η [%]	32	31.3	0.7	32.1	0.1

3.3.4 *J-V* curve verification

To verify the proposed model it is necessary to give an accurate prediction. This *J-V* curve was compared with other models in literature at concentration ratio of 1x, *AM* = 1.5D and ambient tempreture of 25ºC. A. Walker [130] and Fernández, et al. [54] had performed electrical model of triple-junction solar cells and illustrated *J-V* curves characterisation. In this comparison have been considered the four key electrical parameters: short current density, open-circuit voltage, fill factor and efficiency. Therefore as seen, there was a good match between the current study and another model's results which give confidence in the electrical model. In entirely three models the characterisatics of *J-V* curves plotted are similar in shape. The values of J_{sc}, V_{oc} are the same results, nonetheless with slight different values of fill factor FF for the three models.

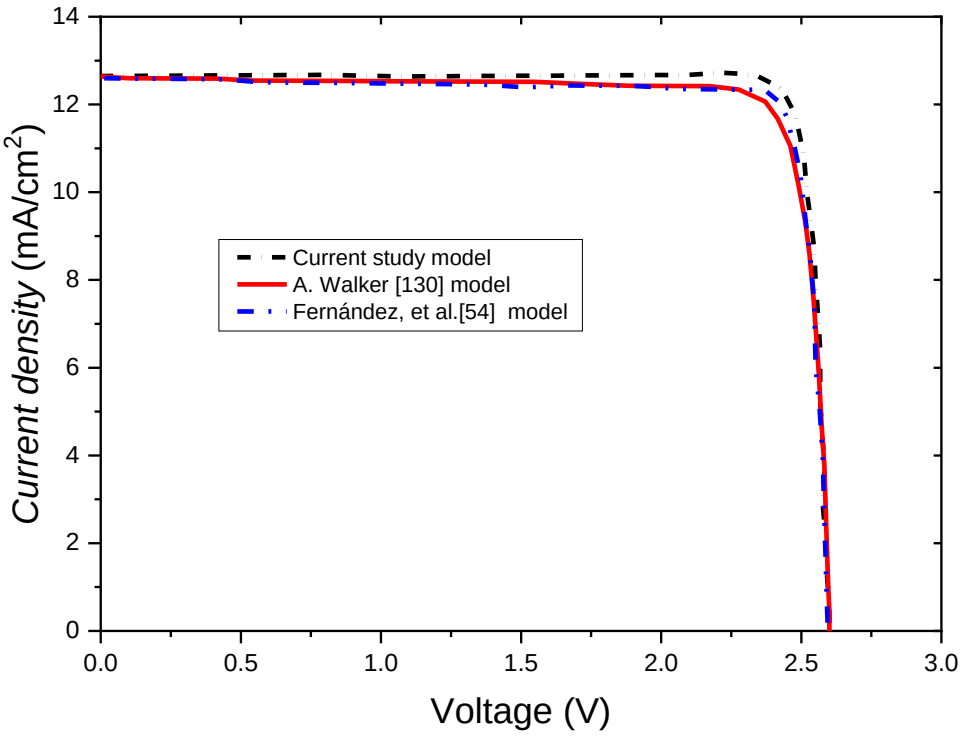

Figure 3-8 *J-V* curves of this model results in compression with A. Walker [130] model and Fernández, *et al.* model [54].

3.4 Spectrum model

Direct spectral irradiance is calculated using version2 SMARTS, the Simple Model of Atmospheric Radiative Transfer of Sunshine model for different *AM* values [132, 133]. The SMARTS2 inputs the spectrum of an ASTM 173-G and is used with the variation of air mass ranging from *AM* =1 – 10D. The results from the SMARTS2 model, the *DNI* is integrated into overall ranges of wavelength light at different *AM* values. Thus, the *AM* gave the solar irradiance *DNI* as a function of it's zenith angle. The values of *AM* can be computed as a function of Sun's zenith angle (z) as shown in Eq (23) [134].

$$AM = \frac{1}{\cos z + 0.50572.(96.07995 - z)^{-1.6364}} \tag{23}$$

The direct spectral irradiance has been generated from the SMARTS2 model. The integration of the spectral irradiance at a specific air mass gives the irradiance intensity as a function of zenith angle (z). Other parameters were kept constant at the reference conditions of the standard ASTM G173-03 (Gueymard and Myers) [135]. The design of

a multi-junction solar cell needs an accurate prediction of solar incident spectral irradiance for the model concentrator. For this application of the module, in a dry climate, the SMARTS2 model is considered as an accurate and suitable tool to predict the spectral irradiance [132, 136].

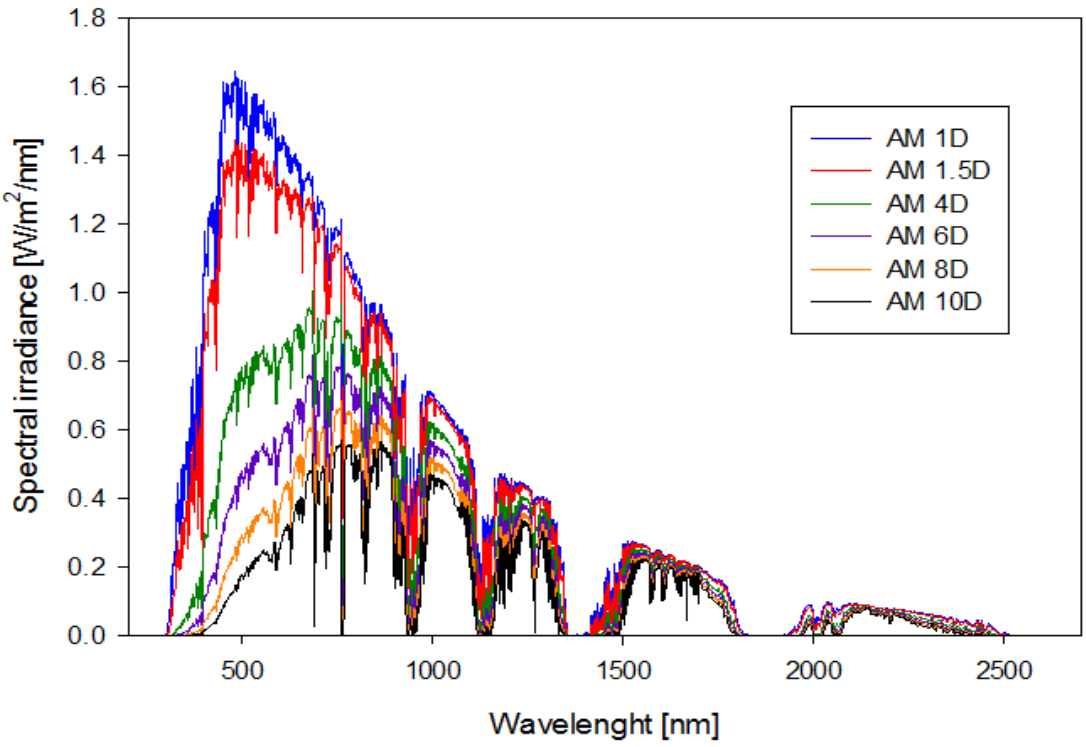

Figure 3-9 Direct spectral irradiance generated by the SMARTS2 model for different *AM* value.

3.5 Effects of increases of *AM* in the solar spectrum

Air mass is a measure of how absorption in the atmosphere affects the spectral content and intensity of the solar radiation reaching the Earth's surface. It is described as a ratio between the optical path length and the optical path length when the sun is at the zenith.

Figure 3-9 illustrates the variation of air mass over a day, which results in significant changes in the spectral distribution of direct irradiance at the surface of the Earth. When air mass increases from 1 to 10D the solar intensity decreases and the wavelengths become shorter, and that yields a shift in the direct spectrum.

In other words, at higher values of *AM* result in a shift of the photon distribution towards longer wavelengths (or lower energies), consequently, layers with high band gap are more strongly affected by such changes [117].

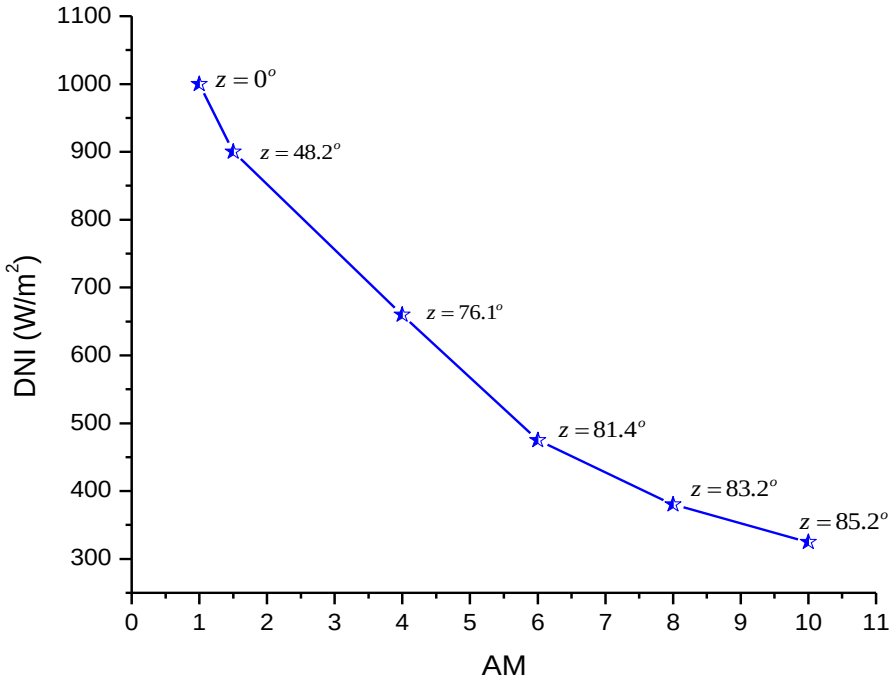

Figure 3-10 *DNI* integration versus *AM* Air Mass as a function of the zenith angle (z).

The performance of the spectral model is dependent on the air mass and the associated parameters with the length of the sunlight path through the atmosphere of the Earth. The minimum *AM* value occurs on a clear-sky day, when the Sun is on the noon-time, while the maximum occurs when the Sun is at the sunrise and sunset. The increase towards larger *AM* values is related to the red shift in the solar spectrum. Hence, a decrease in *AM* values corresponds to a rise in the blue solar spectrum component [137].

3.6 Effects of increases in the *AM* in the performance of Triple junction cell

As shown in Figure 3-6 the triple-junction solar cell assembly is very sensitive to changes in solar spectrum; that is because of the monolithic stack of the subcells. There is a significant reduction in the maximum power density as *AM* increases from 1–10D, as depicted in Figure 3-11.

Higher *AM* leads to lower maximum power; conversely higher power is achieved at lower *AM* values. Air mass has the highest influence on the performance of single/multi-junction solar cells. Based on that atmospheric parameter, always bear in mind while designing or modelling of solar cells, since the spectral effects of the incident solar irradiance cause a reduction in the electric output of the cell/module and system of the HCPV [138-140].

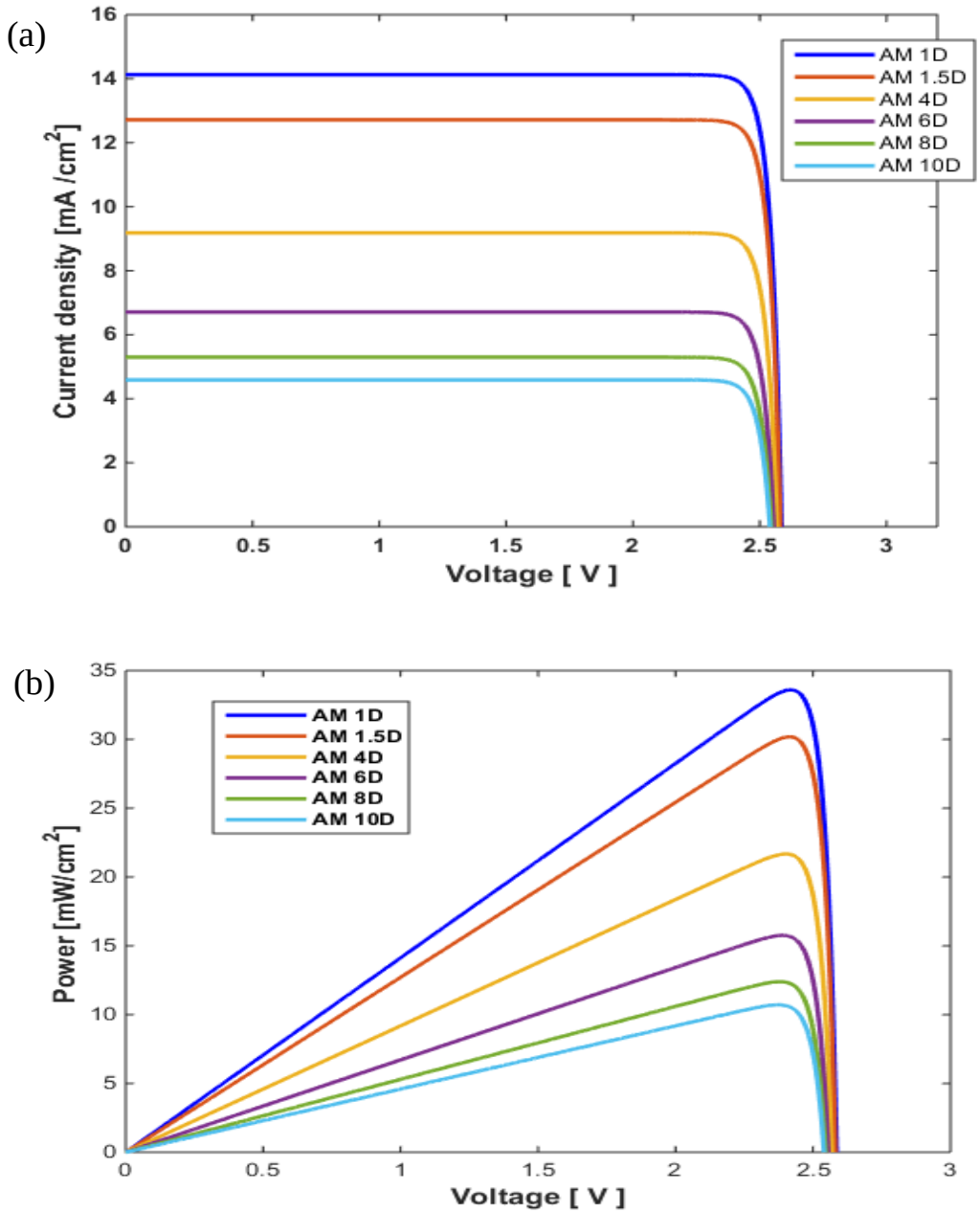

Figure 3-11 (a) *J-V* curves of triple-junction cells and the effects of a variety of air mass. (b) *P-V* curves of triple junction cells and effects of a variety of air mass.

Due to the attenuation of the wavelengths in the atmosphere, while the value of air mass increases, the current density is reduced and cell efficiency of the multi-junction solar cell decreases. Figure 3-12 illustrates the increases in *AM* which has a significant effect on the overall efficiency of a triple-junction solar cell, hence, because of this, energy photons in the solar spectrum decreases. Furthermore, the value of *DNI* decreases as *AM* values increasing. For an increase in air mass value up to *AM* =10D, the cell efficiency drops to 25%. In contrast, with the optimum value of air mass *AM* =1.5D, CR =1x, the cell achieves an efficiency of 32%.

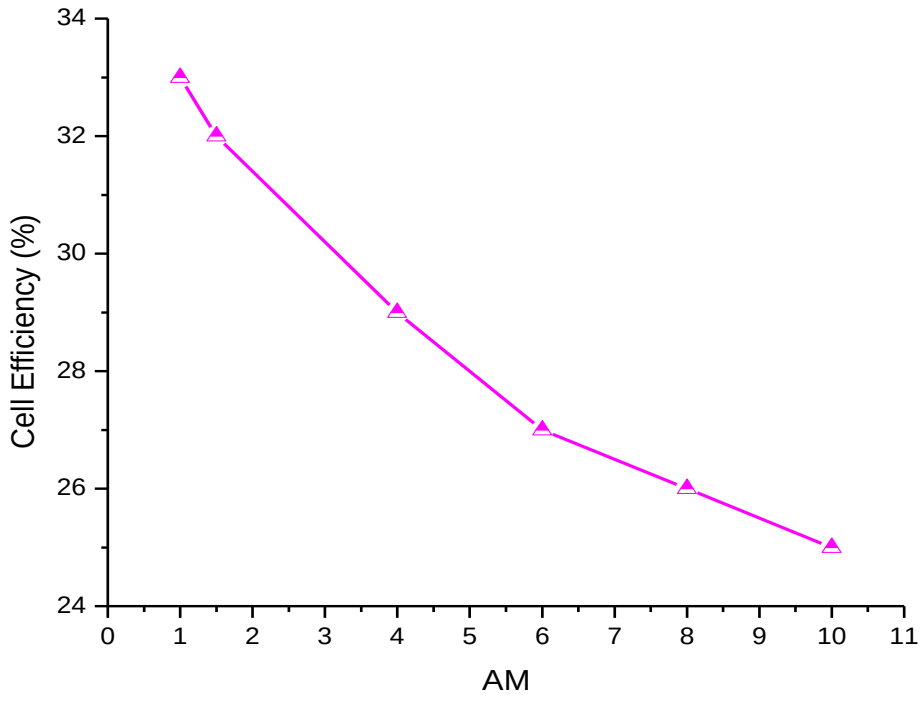

Figure 3-12 Influence of air mass variation in cell efficiency.

3.7 Different Concentration Ratio

In numerous studies, the features acquired from the concentration are assess in terms of electrical performance. As the concentration ratio increase, the energy of photons absorbed by the cell e.g. 500x or 1000x is the light is increased by 500 time or 1000 times. However, the cell temperature rises because of the incident solar flux at high concentration ratios.

The purpose of maximisation of the solar irradiance is more energy absorption and reduce as far as possible the shadow and ohmic losses that generated for the metal grid [141]. The concentration is proportional to the solar radiation that reaches the Earth, approximately equivalent to 1000 W/m^2 at 1x.

The efficiency of the solar cell generally rises as concentration increases. Therefore, this improvement in the efficiency results increases in V_{oc} and marginally, the FF. The photocurrent is just proportional to the intensity of the affecting solar radiation [117].

For high-injection current with low series resistance at a high concentration ratio, the cell photocurrent generated increases linearly [11, 142]. The high injection in semiconductor materials means “the number of generated carriers is larger compared to the background doping density of the materials” [143].

According to Ochoa *et al.*[144] who have examined the effects of high injection at different recombination techniques up to 5000x concentration ratio were discovered to be stronger in specific regions. Also, as has been analysed, the maximum current density was found in the assembly (i.e. under the edge of the metal fingers at the maximum point. The effects of high injection are predictable with a higher probability at active regions, where the majority of the photo-generation of carriers happen. The base reigns are probably to have extra of minority carriers above the doping level instead of the emitter, due to the lower base doping level. The numerical computational results presented most of the minority carrier ratio, for the top, middle and bottom cells respectively. Therefore, that study concluded that up to 5000x, the multi-junction solar cells had no signs of high injection effects.

The concentration ratio is determined by means of a proportional increase of the short-circuit current intensity J_{sc}. As results of absorbed photon flux, the generated photo-current is directly proportional to the concentration level. Hence, the concentration ratio expressed in terms of electric as follows:

$$CR = \frac{J_{sc,X}}{J_{sc}} \tag{24}$$

The open circuit voltages V_{oc} increases logarithmically with concentration ratio as given in equation (25). The power generated is linearly increase when the intensity of concentration ratio rise, consequently the solar cell efficiency increases.

$$V_{oc}(x) = \frac{n.K.T}{q} \ln \frac{J_{sc}}{J_0} = \frac{n.k.T}{q} \ln(x) \tag{25}$$

3.8 Validation of the model

In order to verify this study model, the results are compared with experimental data available in the literature. The Mean Bias Error (MBE) expressed by equation (26), Root Mean Square Error (RMSE) given by equation (27) are used to compare both results.

$$MBE = \frac{1}{N} \sum_{i=1}^{N} (i_{\exp} - i_{\mathrm{mod}}) \tag{26}$$

$$RMSE = \sqrt{\frac{1}{N} \sum_{i=1}^{N} (i_{\exp} - i_{\mathrm{mod}})^2} \tag{27}$$

Where i_{exp} is the experimental results, i_{mod} is model results and N is the number of data points matched, variety of concentration ratios for (1,10,100,500,1000) suns were applied, to open circuit voltage and current density parameters. The open circuits voltages logarithmically increase with increases in concentration. The MBE of open circuit voltage is 1.3% and the RMSE is for open circuit voltages is about 2.3%. Figure 3-13 shows a comparison of different concentration versus V_{oc}, of current study model and experimental.

Concentration ratios versus the short circuit current density (J_{sc}) linearly increases at uniform irradiance. Therefore, the current density J_{sc} , also compared at different concentrating ratio MBE = 0.9% RMSR = for J_{sc} is about 1.7%. From the compersion, is clear there is an agreement between the experimental and simulated results. Figure 3-14 shows the comparison of concentration versus J_{sc} current study model and experimental data.

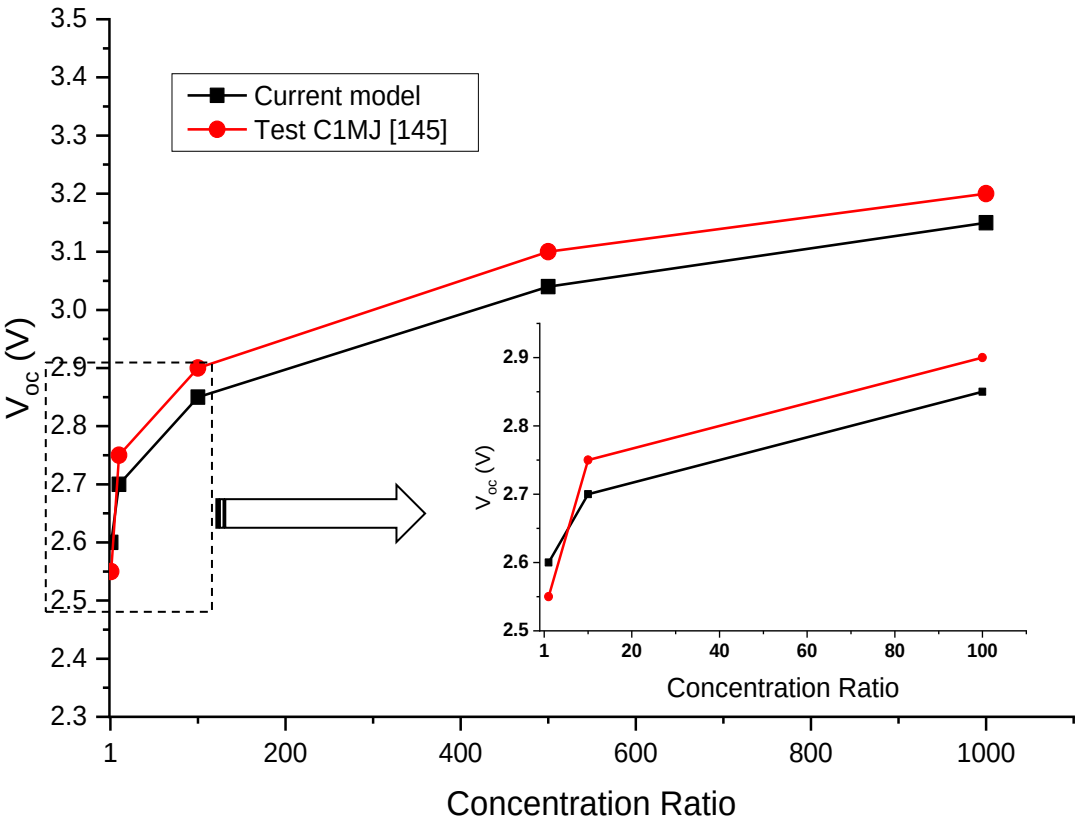

Figure 3-13 Comparisons of concentration ratio versus V_{oc}, current study model and experimental data from (Spectro Lab) C1MJ [145].

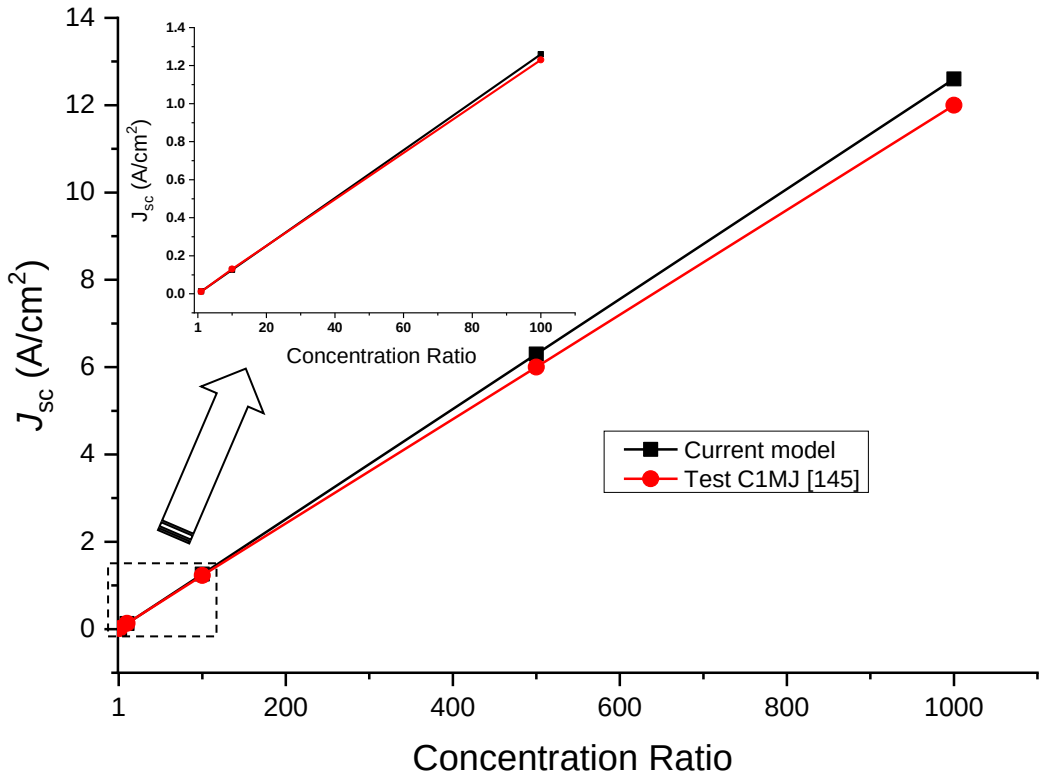

Figure 3-14 Comparison of concentration ratio versus J_{sc} current study model and experimental data from specter Lab C1MJ [145].

Summary

The performance analysis of a multi-junction solar cell, is presented it has been shown. This chapter presented a theoretical performance analysis of a multi-junction solar cell based on modelling in order to describe and understand operating behaviour. Numerical modelling is built-up to predict the performance characteristic of a solar cell. The *J-V* curves are the characterisation of solar cell performance at 1-sun, which might be utilised and enhance cell design.

The results of experimental studies and models in literature were shown to be in good agreement with this study is modelling. Performance modelling of multi-junction solar cells is a significant task for predicting energy yield from high concentrating photovoltaic modules, as the cells work at a wide extent of incident solar radiation and operating temperature.

The technology of CPV is more influenced via the spectral variations, in contrast to a conventional photovoltaic single-junction, due to the usage of multi-junction solar cells and optic components.

The electrical characterisation of the highly concentrated photovoltaic HCPV cells/ modules is an important stage for the energy prediction and performance analysis of the system or for enhancing the model designs. In addition, the electrical characterisation is highly sensitive and more complicated than traditional photovoltaic devices. That is because of the usage of multi-junction solar cells and the different materials in the receiver assembly, optical, and heat dissipation devices.

This electrical modelling and characterisation of the cells currently prevalent is necessary for optimisation of the operating PV systems. This might decrease the PV cost of systems and rise the PV generator's efficiency.

These model investigations provide a valuable knowledge, and explain how the solar cell efficiency can be augmented by the use of multiple materials with variable energy bandgaps crossing the solar spectrum. The triple-junction solar cells made of III-V assembly semiconductors attain the maximum conversion efficiencies. Thus, this model gives a better framework for the optimal performance of multi-junction cell assembly.

Ultimately, it ought to be taken into the account while designing and developing solar cell cooling mechanisms in order to improve cell efficiency. A further consideration of the behaviour of the multi-junction solar cell due to temperature augmentation will discuss in the next chapters.

The electrical model focuses on to giving the reader primary knowledge of the modelling and simulation of PV generator devices based on the fundamental mathematical equations. The modelling approaches take the electrical parameters as inputs to estimate the operating performance at specified operating conditions. Whereas, the characterisation seeks to determine the electrical performance parameters under different operating conditions.

Chapter 4: Effect of Temperature on a Triple-Junction Solar Cells Performance Parameters

4.1 Introduction

This chapter presents and assesses the effects of temperature on five performance parameters of a triple-junction solar cell under light concentration ratio of 1x. The theoretical analyses of performance parameters of short current density (J_{sc}); the open circuit voltage (V_{oc}) and in addition, looks at energy bandgaps (E_g); external quantum efficiency (EQE); fill factor (FF); maximum power (M_P) and cell efficiency (η).

Sewing *et al.*[146] concluded an investigation of the temperature dependent on the open circuit voltage and efficiency of a high concentrating photovoltaic system under one sun. They found that temperature sensitivity to efficiency is high for the open circuit voltage, while the output power was less influenced by temperature variations.

The three layers of sub-cells of triple-junction cell are (GaInP/GaInAs/Ge); the temperature vibration from 25 – 125^{o}C will be considered in this study. Accordingly, the *J-V* and *P-V* curves will plot to characterise performance under the aforementioned conditions.

The model predicts the impact of cell temperature increases on cell parameters such as fill factor, open circuit voltage, short circuit density and efficiency. The modelling gives more detailed to help understand the operating behaviours of the solar cell and will lead to enhanced performance and design. In addition, by the numerical modelling, one can develop a prediction of range operating environment conditions, for instance, temperature, solar irradiance and concentration ratio.

4.2 Temperature dependent on energy Bandgap

The bandgap of a semiconductor is "the minimum energy required to excite an electron that is stuck in its bound state into a free state where it can participate in conduction" [19]. The sensitivity to temperature of the solar cell performance is initially influence by the difference of the bandgap layers dependence on temperature. The majority of semiconductor material's bandgap decreases as temperature increase [84, 147]. In a semiconductor, a material's the energy bandgap determined by the wavelength of light.

The optimal bandgaps of three junctions are 1.8e*V*, 1.49e*V* and 0.7e*V*. The bandgap energy of semiconductor materials tends to shrinkage with temperature increase. To predict the influence of cell temperature a rise in the band gap, a model is created in MATLAB and applied in the Varshni equation (28). Therefore, this model is part interconnected to the electrical model in Chapter-3. The temperature dependence of semiconductor bandgaps is given by Varshni empirical relation [120].

$$E_{g,i}(T) = E_{g,i}(0) - \frac{\alpha_i . T^2{}_c}{T_c + \beta, i} \tag{28}$$

Where $E_g(0)$ is band gap at 0 K, the index *i* represents a subcell of each layer, T_c is the cell temperature, and α and β are materials constants. Three subcells of multi-junction cell material parameters are listed in the table (4).

Temperature variations with a band gap in each layer are quantified by how much energy is captured from the sun for cell's conduction band, and also by the amount of energy generated [19, 84]. Therefore, as temperature increases, the bandgap linearly decreases as more solar spectrum photon components are absorbed. Subsequently, a slight increase in short circuit current affects the efficiency of the cell.

The reverse saturation current also affected by bandgaps decrease, which results in a decrease in the open circuit's voltage given temperature. Although, as cell temperature decrease, the bandgap tends to increase, the open voltage as well as increase, the results efficiency enhances. The amount of current produced in each cell depending on an incident spectrum, in which set of selection for optimal bandgaps. The change in bandgap with temperature indicated by equation (29) [126, 145]:

$$\frac{dE_g}{dT} = \frac{2\alpha T}{T + \beta} + \frac{\alpha T^2}{(T + \beta)^2} \tag{29}$$

Varshni [120] believed the reasons behind the variation of the energy bandgap with a temperature arises from two mechanisms: "First the shifts in the relative position of conduction and valence bands because of the temperature dependent dilatation of the lattice. The second major contribution comes from shifts in the relative position of the conduction and valence bands owing to temperature dependent electron-lattice interaction" [120].

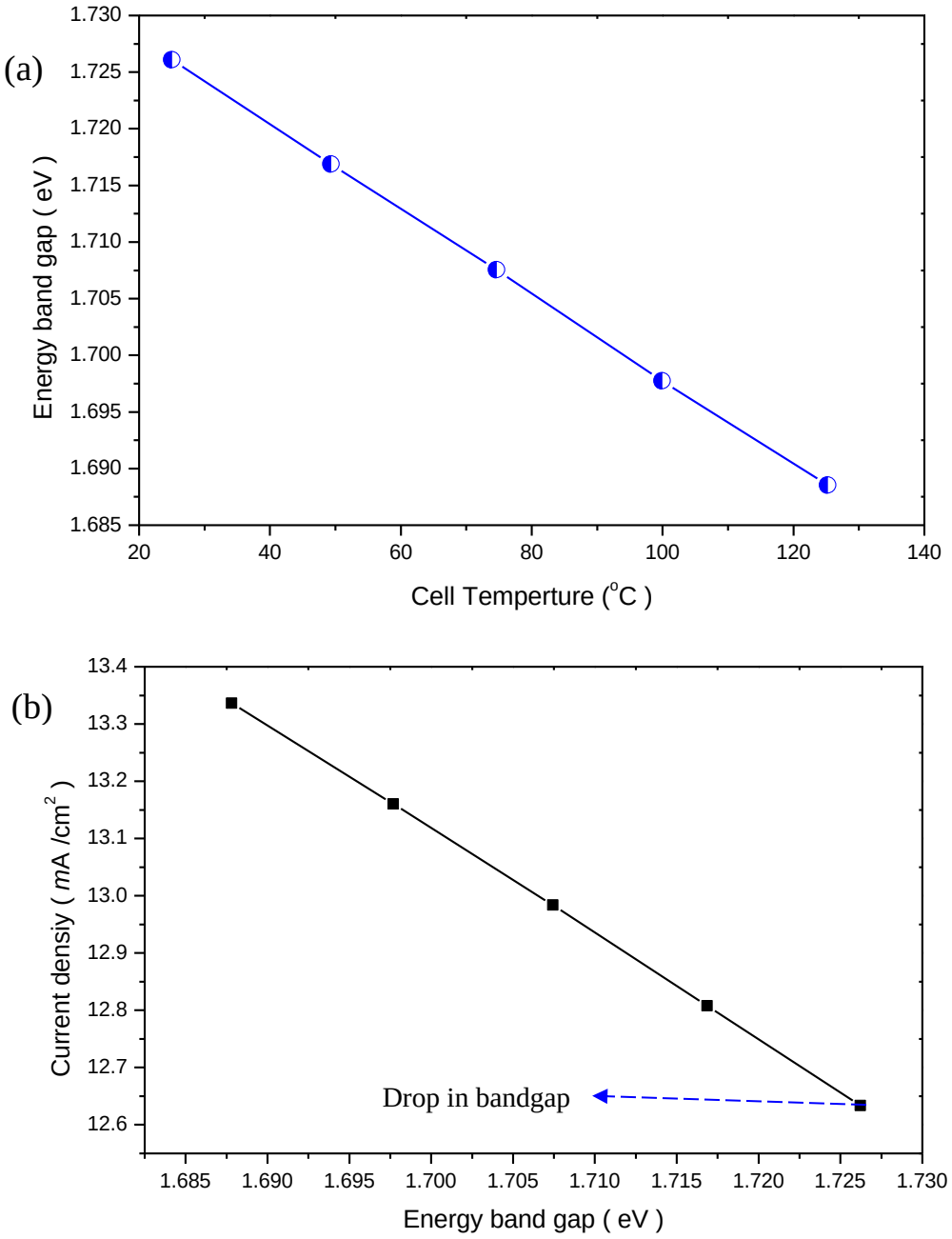

Figure 4-1 (a) top cell-cell temperature rise versus bandgap of the (GaInP) top cell, (b) bandgap versus Current density of the top cell.

For the top cell at 25°C the band gap will be 1.73eV. Once a cell operating temperature increase to 125°C the bandgap will decrease to 1.68eV. It is inversely proportional to temperature rise and bandgap as shown in figure 4-1 (a); shrinkage of bandgap results slights an increase in short circuit current density J_{sc} as shown in figure 4-1 (b).

Similarly for the middle cell, it's performance changes when operating temperature increase from 25 through to125°C. This results in a lowering in the bandgap from1.4 e*V* to 1.35e*V*, as detailed in figure 4-2 (a). As the bandgap decreases the current density gradually, increase as shown in figure 4-2 (b).

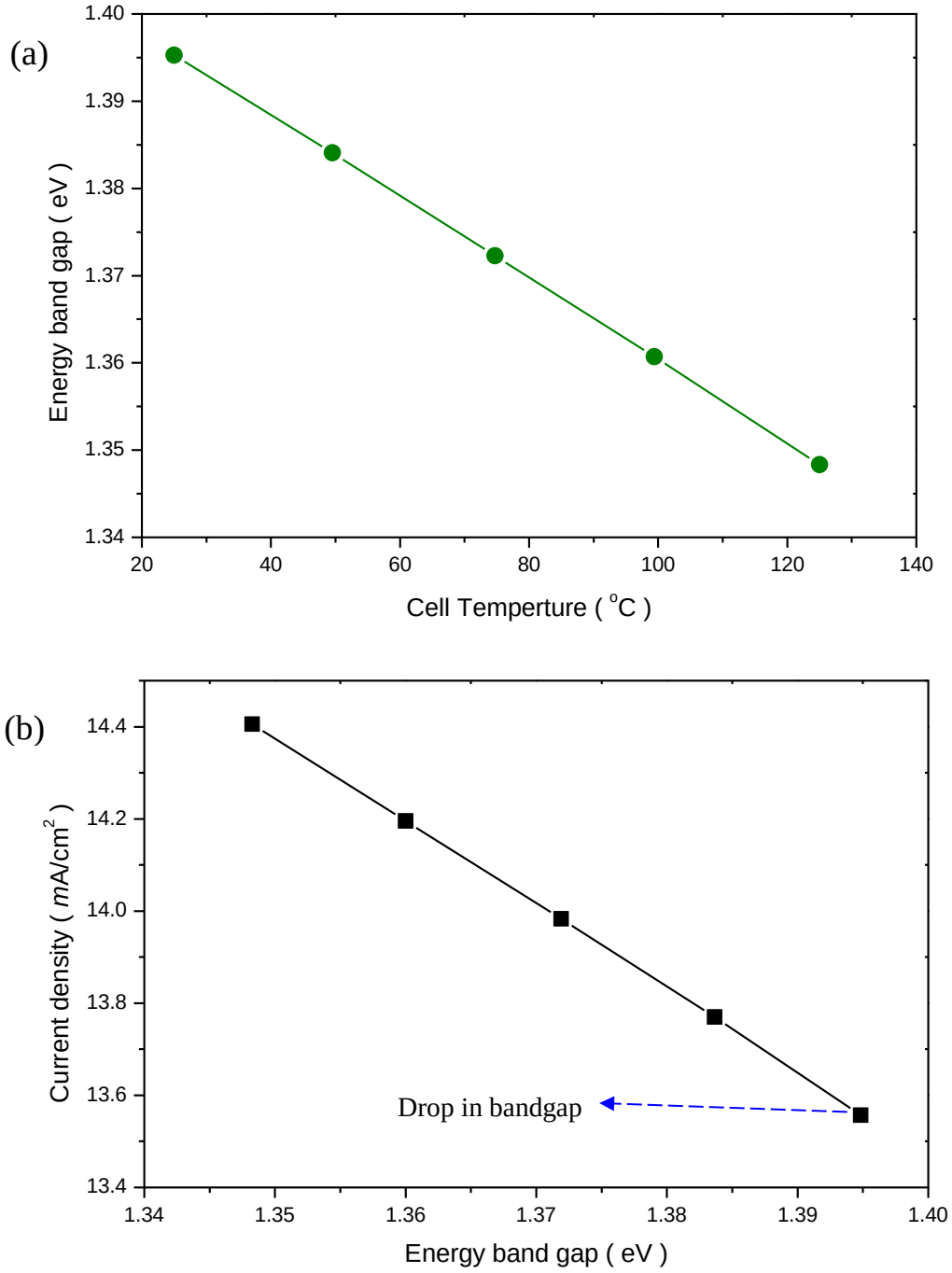

Figure 4-2 (a) cell temperature versus bandgap of (GaInAs) middle cell, (b) bandgap versus current density of middle subcell.

The bottom cell also affected by bandgap decrease; therefore, it drops from 0.67eV to 0.63eV as a function of cell temperature increase from 25 – 125°C, as illustrated in figure 4-3 (a). In addition, bandgap shrinkage in the bottom cell resulted in a small increase in the current density as illustrated in figure 4-3 (b).

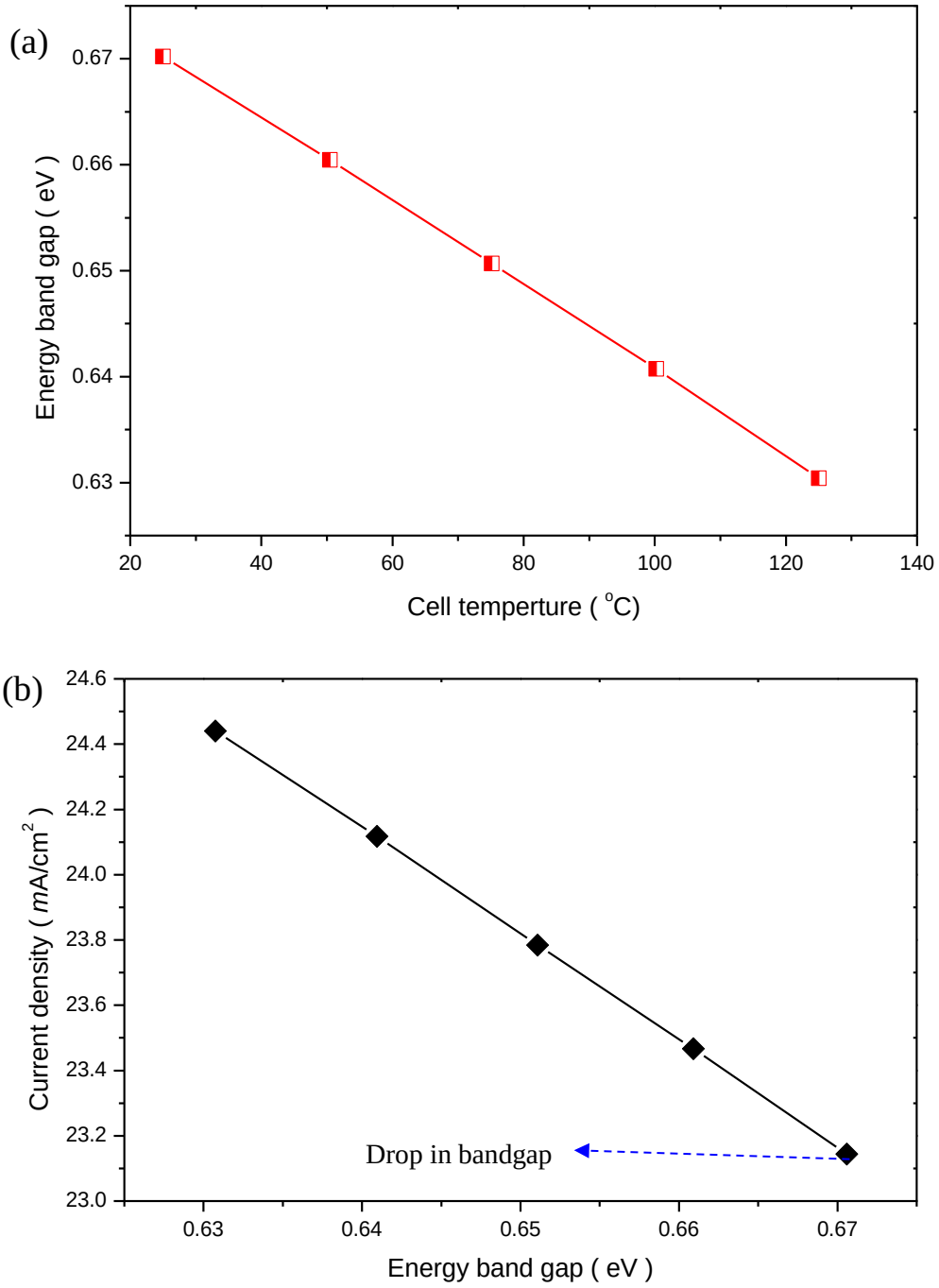

Figure 4-3 (a) cell temperature versus bandgap of (Ge) bottom subcell, (b) bandgap versus current density of bottom subcell.

For semiconductors, the bandgap decreases with an increase in the temperature due to thermal expansion of the lattice. An increase in interatomic spacing decreases the potential of the electron and consequently the bandgap decreases [148]. While, at constant illumination, the photo-generated current in a cell will change with temperature because of the temperature dependence of the energy bandgap. The thermalisation of hot carriers in multi-junction solar cell reduced by the usage of high bandgap materials for the p-n

junction. So, at the same time, transmission losses of low-energy photons are reduced by using low bandgap materials for bottom *p-n* junction [12, 148].

4.3 Temperature dependent *J-V* curves parameters

Based on the *J-V* curves been presented in chapter-3 (for T_c = 25ºC), in this chapter, the effects of variable temperature also considered. The physical perspective of the energy bandgap in the solar cell is inversely proportional to cell temperature. The higher temperatures lead to lattice expansion and attenuation of interatomic bonds. Consequently, higher cell temperatures result in shrinking of the energy bandgap, which means more photons are absorped, which in turn, leads to free charge carriers being produced. Subsequently, the energy photonic needed to liberate a free charge carrier is now lowered [129]. This is interpreted as a greater flow of electrons (i.e., more current is generated) with low energies (i.e., a drop-in voltage). Therefore, this leads to the decreases in voltage. On the other hand, however, the rise in current and the consequence is a reduction in maximum power, fill factor, as well as the conversion efficiency [129, 149].

Cell temperature rise is a matter to be optimised when designing solar cells [126]. The operation temperature of *PV* solar cell quantified by an energy balance. Solar cells absorb solar energy, which is partly converted into the electrical energy and partly into thermal energy, causing rise in the operating temperature of the cell. The electrical energy gained from the cell can exploited in the external circuit. Equation (30) used in order to predict the current density as a function of temperature rise.

$$J_{sc(T),_i} = J_{sc(\lambda)}[1+\beta_{Jsc,_i}(T_c - T_o)] \tag{30}$$

Where T_o is the reference temperature at 25ºC, T_c is the cell operating temperature and β_{Jsc} is the temperature coefficient of the short circuit current. In a multi-junction solar cell, the temperature coefficient varies between 0.005 and 1.63 *m*A/ºC^{-1}[150]. The value of short circuit current density (J_{sc}) slightly increases with an increase of temperature, as result of the increase in the base's diffusion length, and a reduction of the energy in the absorption band edge [122, 151].

The values of J_{sc} has determined the subcell current limiting of the multijunction solar cell. Hence, the whole dependency of the multi-junction solar cell J_{sc} on temperature is determined by the dominant subcell layer at each temperature [84].

Table 4-1 Temperature coefficient of J_{sc} and V_{oc} of single cells [92, 152, 153].

Subcell	$J_{sc}(dJ_{sc}/dT)$	$V_{oc}(dV_{oc}/dT)$
Top cell	0.07% K	-0.21% K
Meddle cell	0.04% K	-0.26% K
Bottom cell	0.03% K	-1.22% K

Open circuit voltage is also affected by temperature increases that significantly decrease the V_{oc} values, a temperature dependence of the V_{oc} is expressed by equation (31).

$$V_{oc(T),i} = V_{oc,i}^{*}[1+\beta_{Voc,i}(T_c - T_o)] \tag{31}$$

Where V_{oc}* is the open circuit voltage at the reference condition; β_{Voc} is open circuit voltage temperature coefficient. Figure 4-4 (b) shows relationship *J-V* curves of the top subcell (GaInP), as depicted above. As cell temperature increase, the result is a significant decrease in the open circuit voltage. On the other hand, Figure 4-4 (a) illustrated the current density slightly increases as the temperature rises, from 25 – 125ºC, and cell temperature increases the current density from 12.6 to 13.3mA/cm^2. In addition, the open circuit voltage V_{oc} drops from 1.31 to 1.09V.

Generally, the open circuit voltage (V_{oc}) of the solar cell increased with an illumination increase and decreases with temperature rise. Hence, the derivative of the open circuit voltage (V_{oc}) for triple-junction solar cells is the sum of all subcell's the derivatives. The values of V_{oc} rely on the J_{sc} in which changes with temperature. The V_{oc} derivative with temperature is given by (32) [84, 151].

$$\frac{dV_{ov}}{dT} = \frac{V_{oc}}{T} + \frac{nkT}{q}\left(\frac{1}{J_{sc}}\frac{dJ_{sc}}{dT} - \frac{1}{J_o}\frac{dJ_o}{dT}\right) \tag{32}$$

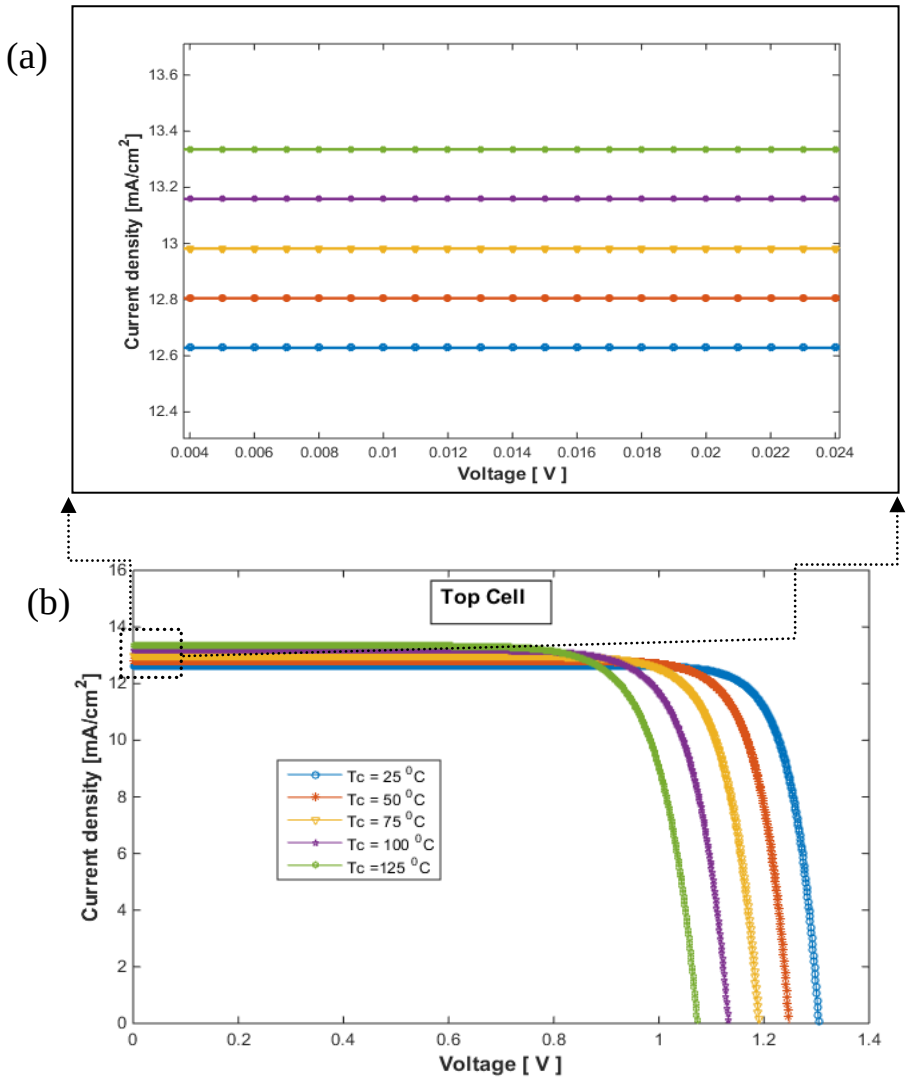

Figure 4-4 (a) current density increase due to a temperature rise of the top cell GaInP, (b) *J-V* curves of the top subcell GaInP as a function of temperature increase.

Figure 4-5 (b) shows relationship *J-V* of middle subcell (GaInP). As the cell temperature increases, the result is a significant decrease in the open circuit voltage. Additionally, Figure 4-5 (a) illustrates the current density slightly increases as temperature increases from 25 – 125^{o}C. The increase in cell temperature increase the current density variable from 13.5 to14.3 mA/cm^2. In addition, the open circuit voltage V_{oc} drops from 1.01 to 0.81V.

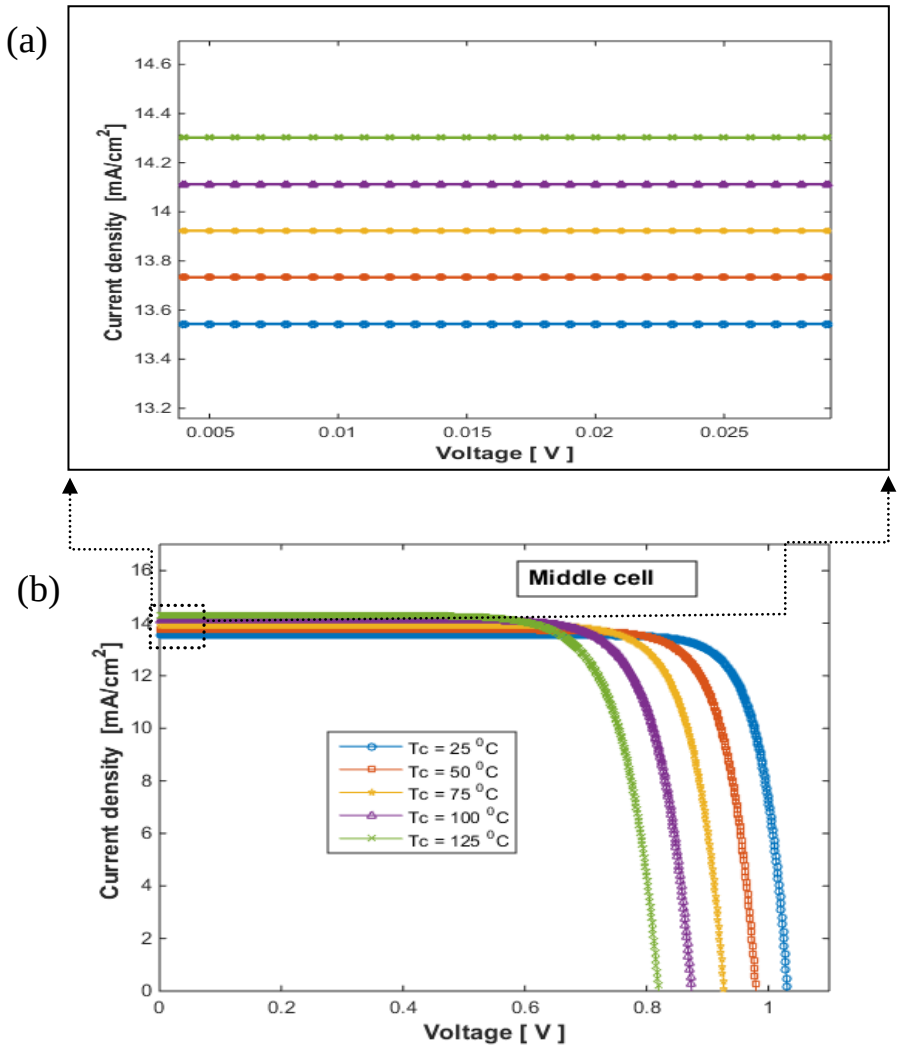

Figure 4-5 (a) current density increase because of temperature rise of middle cell GaInAs, (b) *J-V* curves of middle subcell GaInAs as a function of temperature increase.

Figure 4-6 (b) shows the relationship *J-V* of bottom subcell (GaInP). As cell temperature increases this results in a significant decrease in the open circuit voltage. On the other hand, Figure 4-6 (a) illustrates the current density slightly increases as temperature increases from 25 – 125°C. Cell temperature rises the current density variable from 23 to 24.5mA/cm^2. In addition, the open circuit voltage V_{oc} drops from 0.31 to 0.02V.

Nishioka *et al.*[152] performed experiments to determine the effects of high temperature on the behaviour of the bottom subcell (Ge). It deduced that V_{oc} decreases close to zero where the temperature exceeds 120°C under CR=1x.

Helmers *el al.* [154] performed experimental test to assess the influence of temperature on the performance of the multi-junction solar cells, and the behaviour of the (Ge) subcell when exposured to temperatures over 100°C are performed. It was found that as the V_{oc}

parameter decreased close to zero, which leads to collapse in *J-V*, curves shapes. Therefore, both experiments have similar behaviour as noted by Nishioka *et al.*[152] and Helmers *et al.*[154]. Based on that, the modelling results shown in figure 4-6 agreed with performance behaviour that has been observed in experimental similar work done published previously.

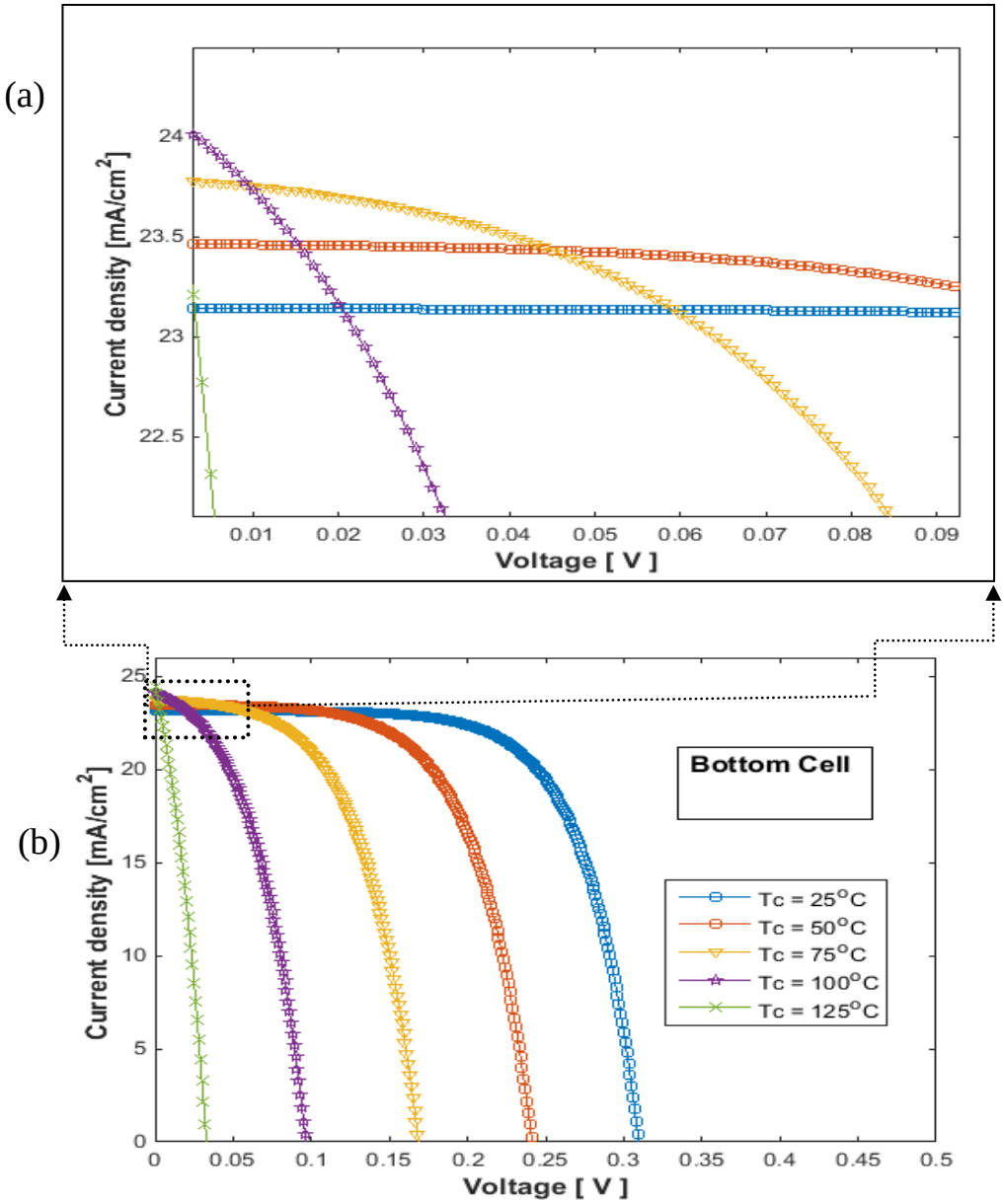

Figure 4-6 (a) current density increase as results of temperature rise of middle cell Ge, (b) *J-V* curves of middle subcell Ge as temperature increase.

Figure 4-7 (a) shown *J-V* curves of triple junction cell; the current density slightly increases as temperature rise from 25 – 125ºC. Cell temperature increases the current

density variable from 12.6 to13.35mA/cm^2. In addition, the open circuit voltage V_{oc} drops from 2.6 to 2.2V, due to the series connection of multijunction solar sub-cells being more sensitive to changes in the incident solar spectrum than a single cell. Hence, the effect temperature on III-V multijunction solar cells performance parameters relies on the incident solar spectrum [155].

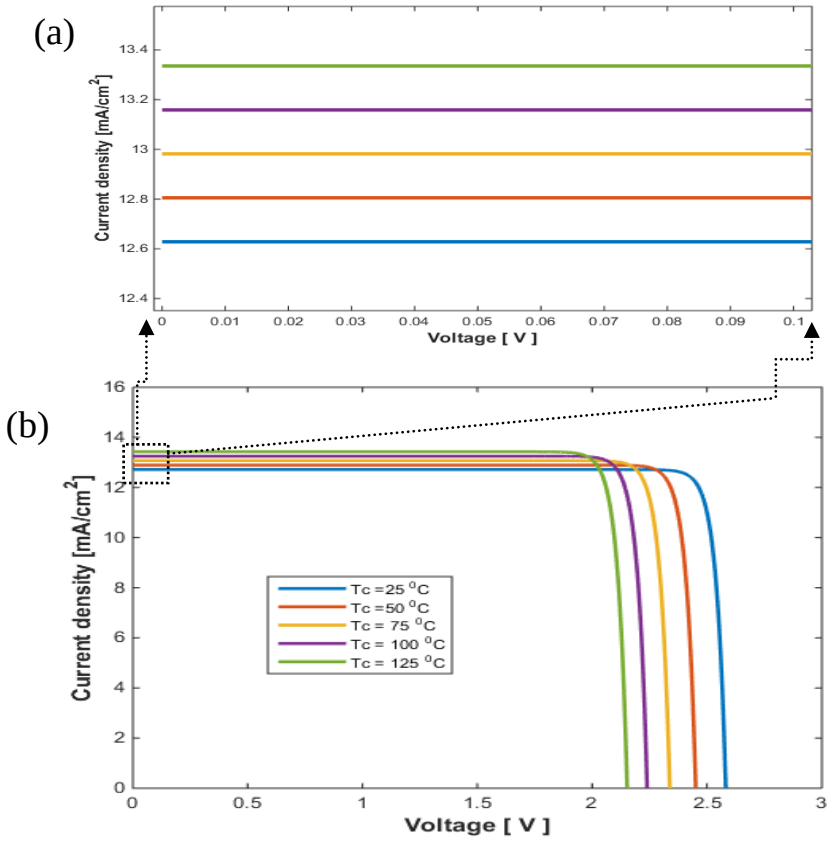

Figure 4-7 (a) current density increase due to temperature rise, (b) *J-V* curve of tandem cell in triple junction cell as a function of temperature increase.

The overall performance of a triple junction cell influenced by temperature rise is seen in figure 4-7. A high temperature dependent i.e. a temperature rise leads to a drop in open circuit voltage, where the open circuit voltage (V_{oc}) of a Triple-junction solar cell is the sum of the (V_{oc}) of all subcell layers.

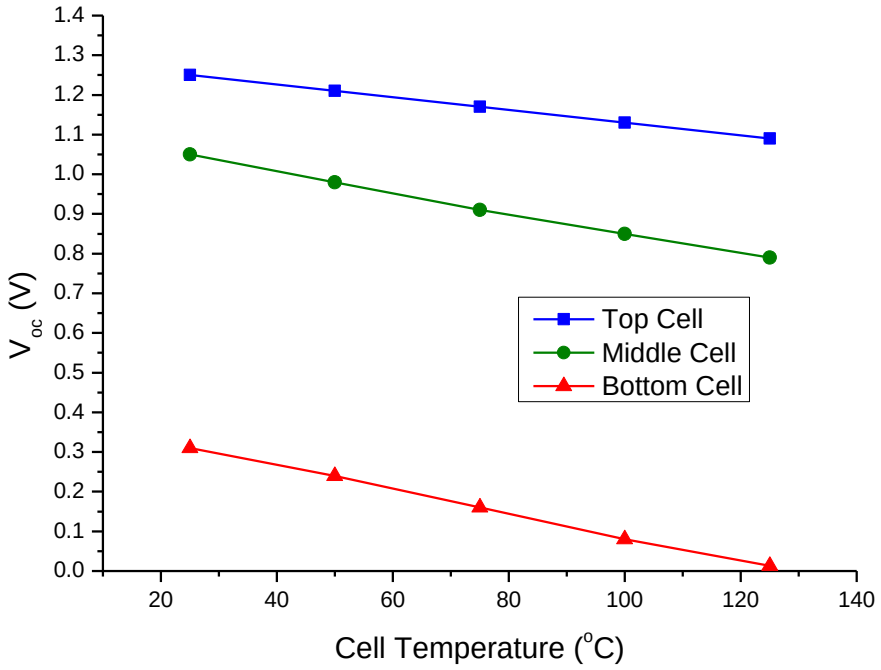

Figure 4-8 Temperature dependent on the open circuit voltage of the three layers GaInP/GaInAs/Ge.

4.4 Temperature-dependent EQE

The external quantum efficiency is one parameter of a solar cell to describe the inner performance operation and should be considered in the optimum design of the cells. The EQE defined as the ratio of the number of carriers collected at the electrons for one particular wavelength with the total number of incident photons of that wavelength. Through EQE, the behaviour of solar cells performance as express in equation (33) [54] can be described.

$$EQE(\lambda) = \frac{\text{Number of electrons}}{\text{Number of photons}} \tag{33}$$

The quantum efficiency and Spectral Response (*SR*) are properties used to describe the recombination, current generation, and solar cell diffusion mechanisms. The spectrum response is defined as "amperes generated per watt of incident light for given a wavelength" [54]. Usually, spectral response determined by the quantum efficiency as expressed in equation (34) [54, 156]:

$$SR_{(\lambda)} = \frac{q.\lambda}{h.c}.EQE_{(\lambda)} \tag{34}$$

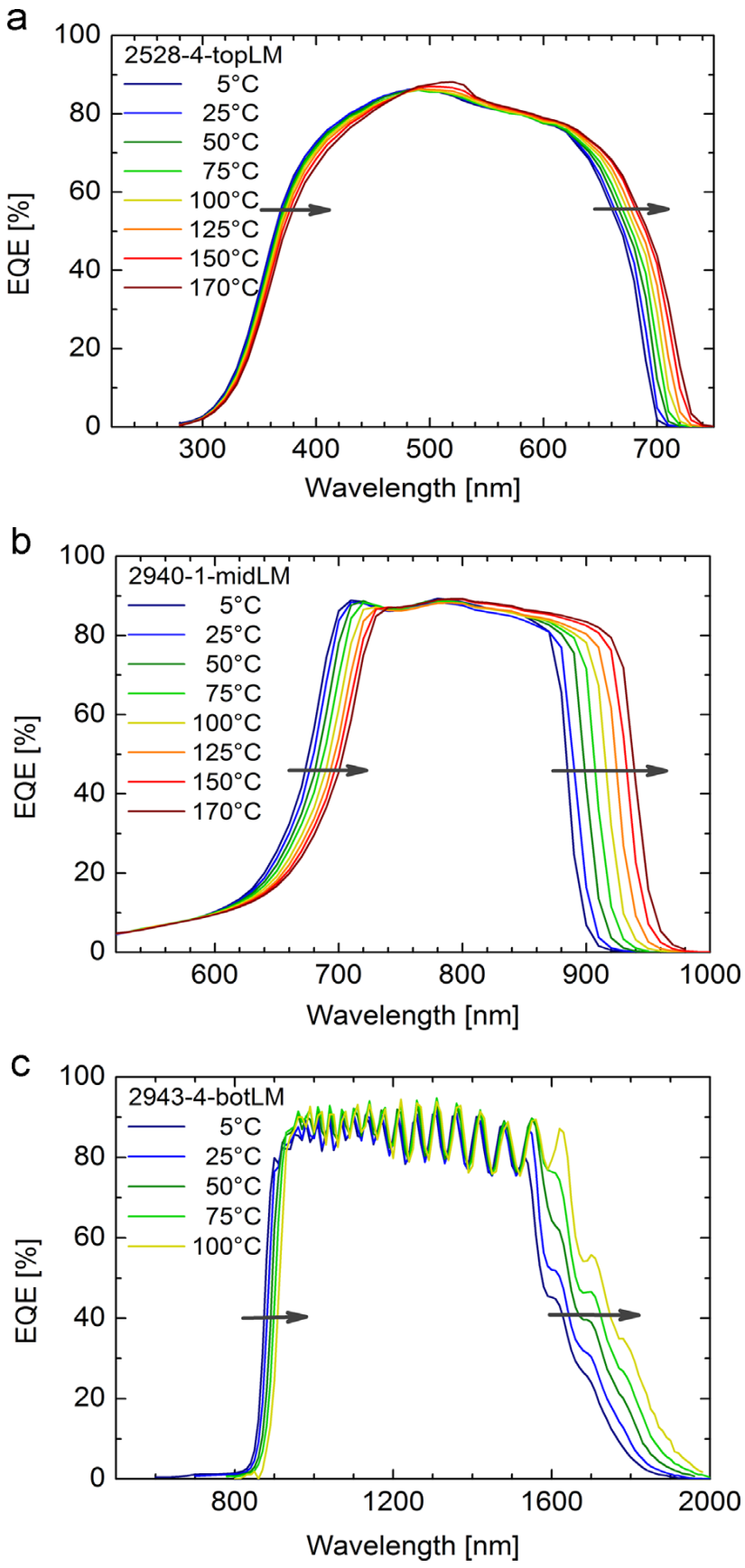

Figure 4-9 Experimental data of EQE as a function of temperature rise, (a) top subcell (b) middle subcell (c) bottom subcell [154].

Where *h* is the Planck constant *c* is the speed of light and *q* is the electron charge. Hence, through the behaviour of a solar cell's performance can be described. As the cell temperature increase, there will be a drop in material's bandgap absorbing, which typically causes an increase of J_{sc} of the solar cell and in turn, the EQE will shift to higher wavelength absorption.

Figure 4-9 (a) represents a top subcell GaInP external quantum efficiency (EQE) as a function of temperature. Hence, a cell's temperature increase significant moves the EQE toward higher wavelengths. That will cause an increase in cell photocurrent as temperature increases [126, 157].

Figure 4-9 (b) shown the impact of cell temperature of a middle subcell (GaInAs) for a range of temperature. The light intensity filtered through top subcell, thus shot wavelength is gradually shifted to a longer wavelength. As the temperature rises, the long wavelengths in the domain affects the (EQE), and this shifts to long wavelength [154, 157].

Figure 4-9 (c) illustrates the effects of temperature on EQE of the bottom subcell (Ge). This subcell responds to the range of infrared light. As the cell temperature rises the (EQE) will shifts to longer wavelength. This subcell generates higher current, but not so much that it will be current limiting of the overall cell. Figure 4-9 (a,b,c) is used only for illustrative purposes only and no quantitative measures for the EQE as a function of temperature rise is calculated.

4.5 Temperature-dependent Power

The solar characterisation with *P-V* curves represents the relationship between the current density generated, and the cell voltage. Figure 4-10 (a) shows a *P-V* curve of the top cell as a function of cell temperature increases from 25 – 125^{o}C; the power generated at 25^{o}C was 14*m*W/cm^2, at a cell temperature of 125^{o}C and the power decreases to 10*m*W/cm^2.

Figure 4-10 (b) illustrates the middle subcell. The power generated is about 12*m*W/cm^2; subsequently, as the cell temperature increase from 25 – 125^{o}C, this causes a power drop to 9*m*W/cm^2. Figure 4-10 (c) illustrates the bottom subcell, which generated less power at 25^{o}C (about 5*m*W/cm^2) and at 125^{o}C the power generated drops to around 0.03*m*W/cm^2.

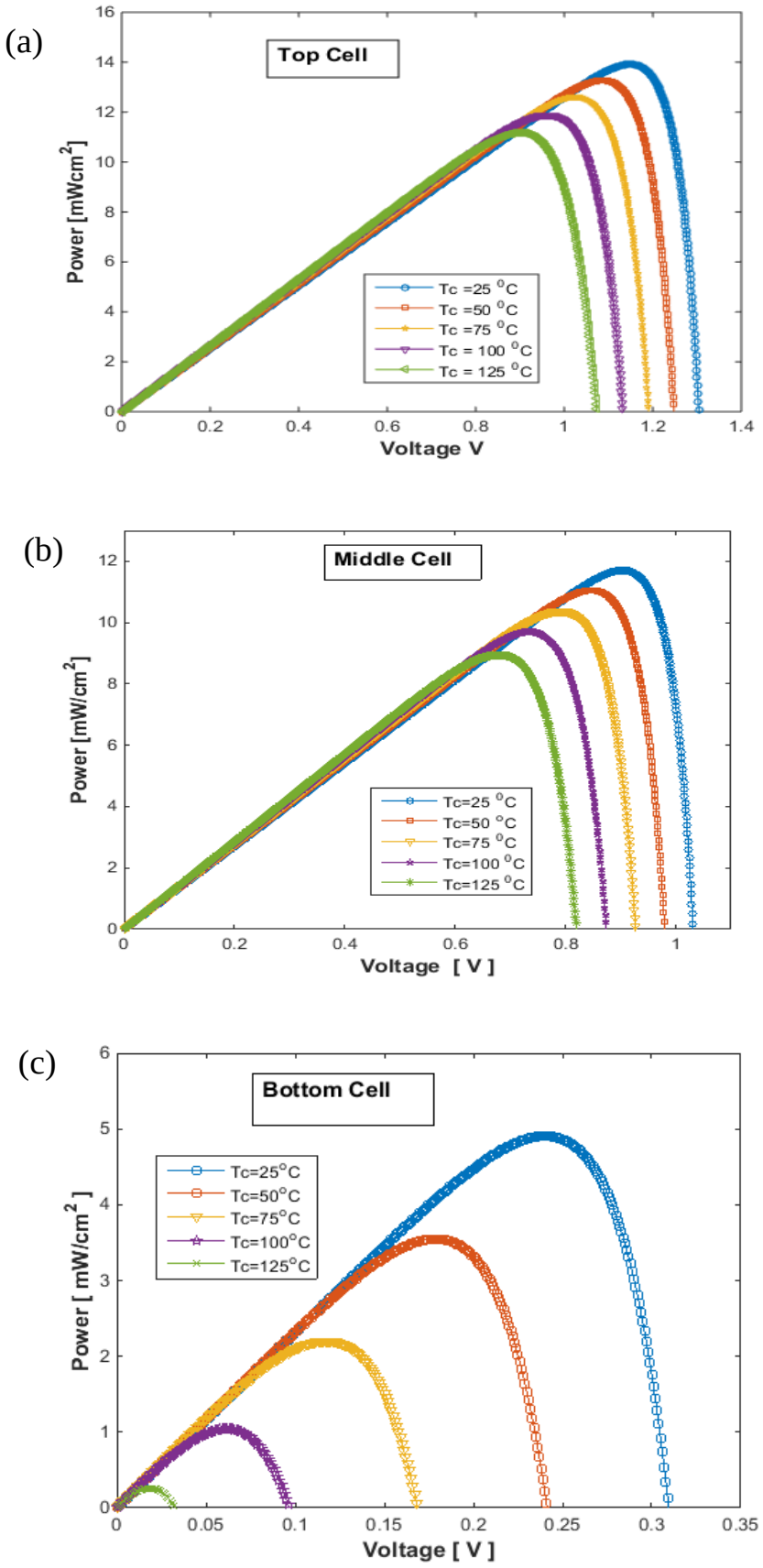

Figure 4-10 ***P-V*** **curve of a single layer for triple-junction cells respectively, (a) top subcell GaInP (b), middle subcell GaInAs and (c) bottom subcell Ge. As a function of temperature increase, where varies from 25 to 125ºC.**

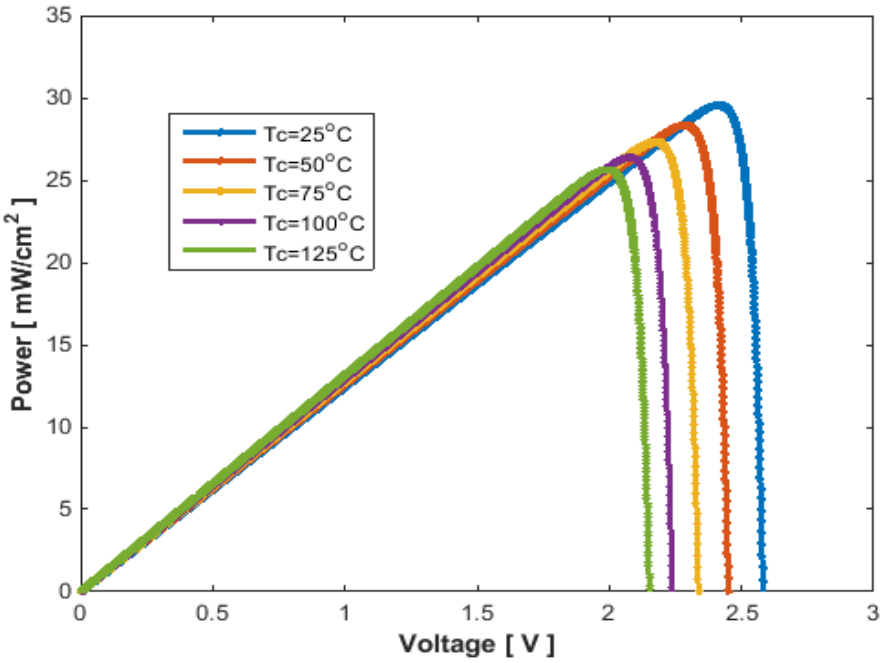

Figure 4-11 Triple junction cell *P-V* as a function of temperature from 25 – 125ºC.

The maximum power point is limited by the lower subcell current; the bottom cell has less power due to less voltage and higher current. Therefore, the power yield of the cell drops because of the drop-in voltage; the maximum power decreases from 30mW/cm^2 to 26mW/cm^2. Figure 4-11 illustrates the *P-V* curve of the triple-junction solar cell as a function of temperature.

4.6 Temperature dependent Fill Factors (FF) of a Triple-junction Cell

The FF also depends on the band gap of subcell, so a low bandgap cell will result in a lower FF. A thinning of the top cell affects the fill factor, V_{oc} and the total current of the three subcells. Figure 4-12 illustrate the fill factor of the three-layer cell at a temperature of 25 – 125ºC. The fill factor is affected by temperature increases: as cell temperature increase, the FF rapidly decreases from 88% to 84% as shown in Figure 4-13. The efficiency of the solar cell is limited by temperature increase; however, as the cell temperature increases the effect linearly decreases in cell efficiency. The efficiency temperature dependent is expressed by Eq (35) [84]:

$$\frac{1}{\eta}\frac{d\eta}{dT} = \frac{1}{V_{oc}}\frac{dV_{oc}}{dT} + \frac{1}{FF}\frac{dFF}{dT} + \frac{1}{J_{sc}}\frac{dJ_{sc}}{dT} \tag{35}$$

Where the efficiency of a solar cell is proportional to the produce of FF, J_{sc} and V_{oc}. Consequently, the sensitivity of the efficiency to temperature is determined by the sensitivity to temperature of J_{sc}, V_{oc} and FF [84].

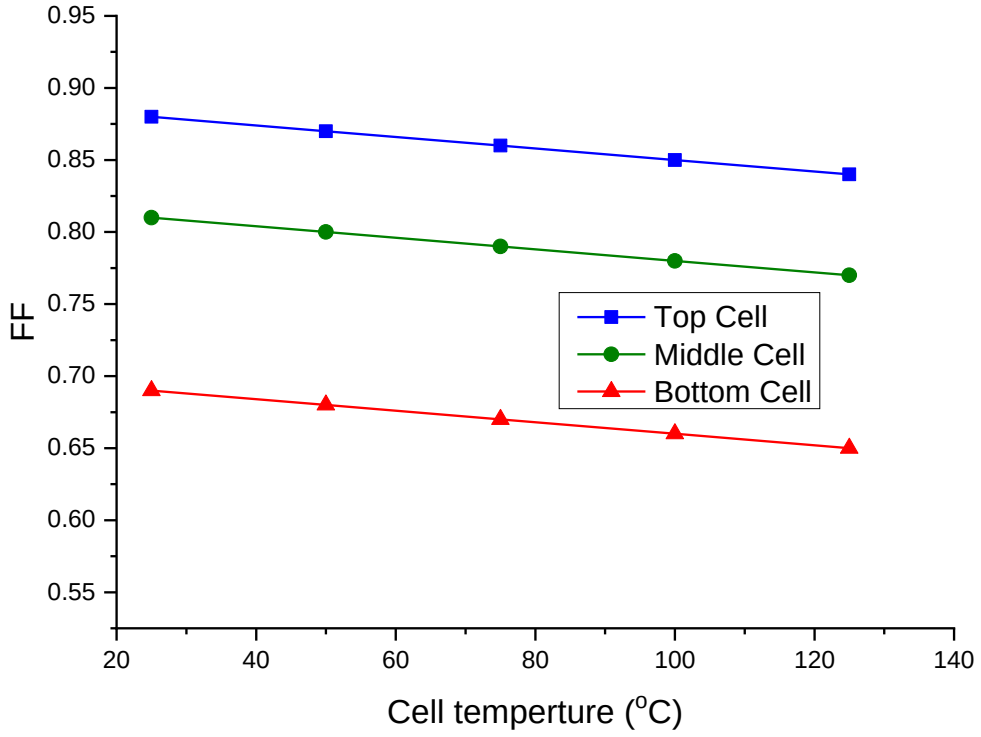

Figure 4-12 Fill factor of the three-layer cell at a temperature from 25 – 125ºC.

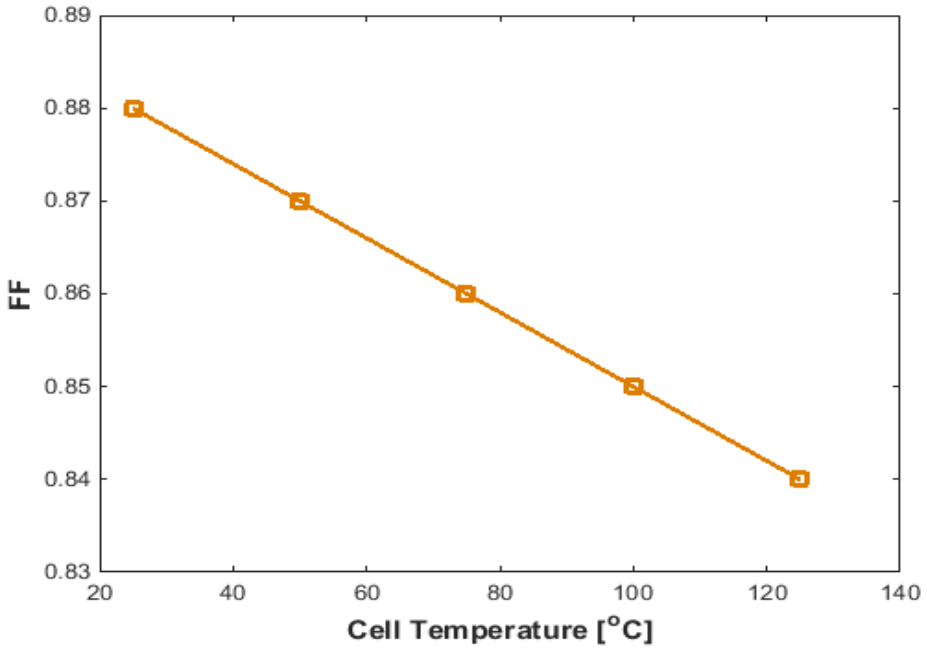

Figure 4-13 Cell temperature rise from 25 – 125ºC, versus decreases in fill factor.

4.7 Temperature dependent of Triple-junction cell efficiency

The temperature sensitivity of a single junction cell efficiency is contributed by the J_{sc}, V_{oc} and FF parameters [84]. Figure 4-14 shows individual three-layer cell of a triple-junction cell sensitivity to temperature.

In the triple-junction cell, the same parameters contributed to the single cell efficiency. As solar cell temperature increases from 25 – 125°C, the yield efficiency decreases from 32% to 26%. Figure 4-15 illustrated a cell temperature rise versus efficiency decrease.

For the series connection of PV modules, efficiency is limited as temperature increase. Once the temperature reaches a certain point, the bypass diode will override the cell, which leads to a reduction in module efficiency [154, 158].

As an effect of temperature increases, the over efficiency will decrease due to aforementioned degradation. It is therefore necessary to be consider an appropriate cooling technique in order to maintain cell lifetime under high concentration ratios. In addition, and great importance is needed to improve cell efficiency in order to reduce unit cost of energy from the system.

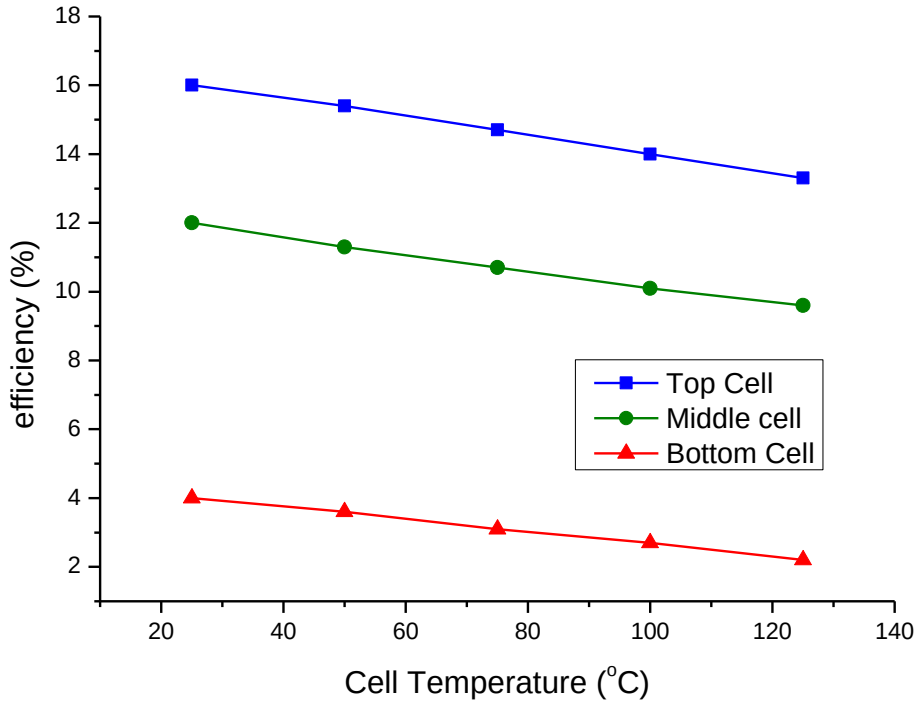

Figure 4-14 Cell temperature versus single junction cell efficiency from 25 – 125°C.

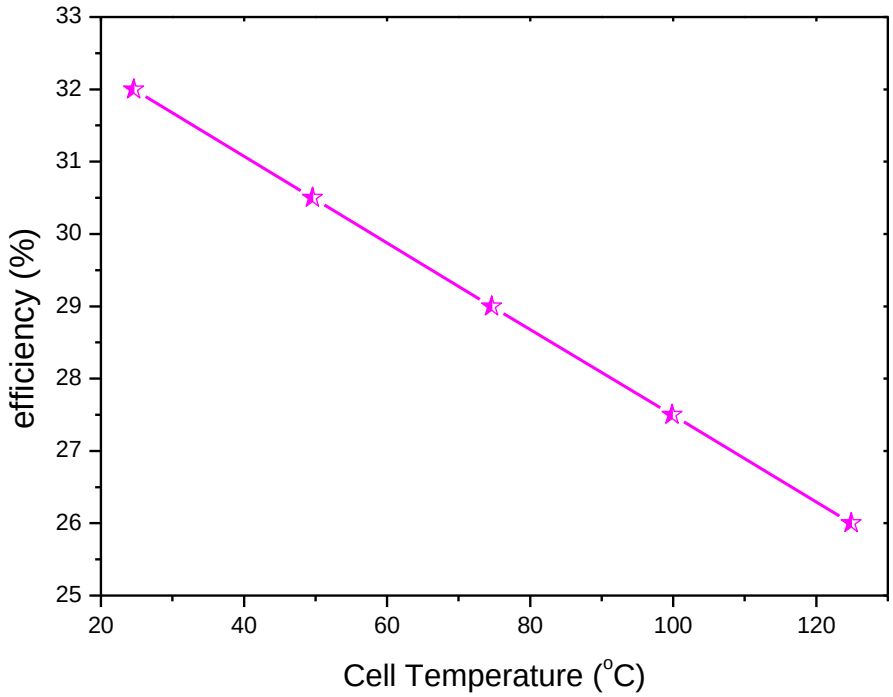

Figure 4-15 Cell temperature versus overall cell efficiency from 25 – 125°C.

4.8 Sensitivity analysis

In this model, a sensitivity analysis has been implemented for five performance parameters (shown in table 4-2). In order to investigate the sensitivity to cell temperature under CR =1x, the temperature was incremented from 25 – 125°C. The results are show that current density is increased by approximately 5.5%, the open circuit voltage is decreased by 15%, and the efficiency dropped by 17%. In addition, the fill factor also decreases by 4.5%. Lastly, the maximum power decreased by roughly 13%.

Table 4-2 Detailed performance parameters of temperature rises from 25°C to 125°C with variation±.

Parameters	**T_c = 25°C**	**T_c = 125°C**	**Variation**
J_{sc} [mA/cm^2]	12.6	13.3	+5.5%
Efficiency %	32	26	-17%
Fill factor	0.88	0.84	-4.5%
V_{oc} [V]	2.6	2.2	-15%
Maximum Power [mW]	30	26	-13%

The analysis indicated that the most sensitive parameter is the efficiency. In addition, the open circuit voltage is sensitive to temperature increases. On the other hand, the fill factor shows less sensitivity to the temperature rises. Figure 4-16 shows visually the percentage of temperature variations in electrical parameters. The temperature sensitivity of electrical parameters of the solar cell degrades, even with light concentration [84]. Therefore, thermal management is required in order to maintain efficient operation.

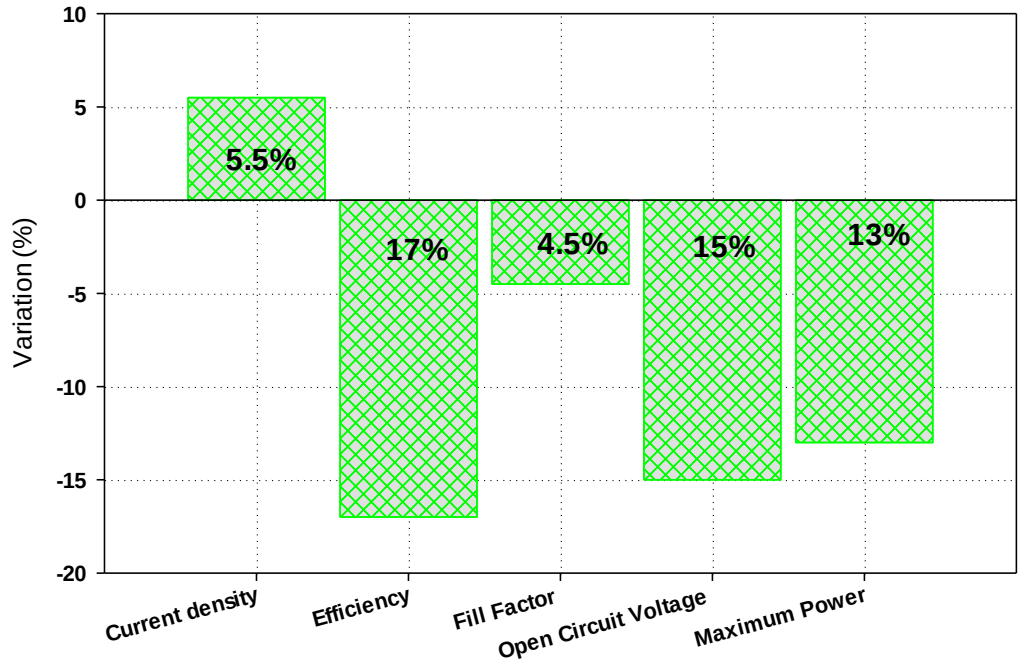

Figure 4-16 Cell parameters changes due to temperature variation from 25 – 125ºC.

Summary

Multijunction solar cell performance behaviour changes because of temperature increase. The increases in cell temperature leads to cell degradation, which results in substantial effects on cell performance parameters. Materials band gap decrease linearly with temperature increase. As short circuit current slight increases, open circuit voltage and fill factor will decrease. In addition, external quantum efficiency will shift to high wavelength absorption.

The cell temperature's increase has a negative impact on cell parameters, such as fill factor, open circuit voltage, short circuit density, power and efficiency. The predicted

model gives a detailed understanding of the operating behaviours of the solar cell, which will lead to enhanced performance and design.

The implication of cell temperature increase on the cell performance parameters has been discussed previously (section 4-3). It is noticed that, the temperatures increment above 120°C at CR =1x; the output voltage of the small energy bandgap subcell in the germanium layer is decreased to near zero volts.

The temperature sensitivity of semiconductors layer has utilising to understand devices behaviour, in order to know the temperature effect and making a clear indication. However, in most of the cases, the performance sensitivity of a semiconductor device to the temperature is typically undesired effect.

This chapter summarised the variation of temperature augmentation of three layers cells of GaInP/GaInAs/Ge. The device energy bandgap with temperature is predicted by using the Varshni empirical relationship. Therefore, due to temperature rise effects on the bandgap, it has a significantly influence on the cell's electrical parameters. From the model, the implication of cell operating temperature variation from 25 – 125^{o}C has been shown and is a consequence of a reduction in bandgap magnitude of the GaInP top cell, middle subcell and of Ge bottom cell.

Chapter 5: Thermal Modelling and Performance Analysis of a High Concentrating Photovoltaic Receiver

5.1 Introduction

This chapter focuses on the thermal performance response of the receiver; the thermal model is used to find optimum cell temperature. The chapter content is partly published in Journal of Thermal Science and Engineering Progress TSEP in references [156, 159].

In order to design an efficient HCPV system from an electrical conversion efficiency point-view, the operating range temperature of a CPV system needs to be predicted and minimised consequently. To do so a heat transfer thermal model is essential for system design to investigate the system thermal and electrical performance [160].

For high concentrating photovoltaics, thermal management is essential to maximise electric conversion efficiency, to prevent thermal damage, and to prolong the cell's lifetime. The heat generated in the solar cells can be dissipated by either active or passive cooling. Furthermore, the assembly configuration can be optimised for both heat and electrical energy as required. There are several techniques available to passively cool solar cells, such as heat sinks and heat spreaders etc. [47].

A high concentrating photovoltaic system requires appropriate thermal management to maintain an operating temperature at or below 80°C [93, 161]. Long-term exposure of solar cells to high optical concentration leads to higher temperatures which will, in turn, decreases the lifetime of the cells [94].

5.2 Methodology

The electrical model presented in chapter-3 is the cornerstone of the thermal performance model. A thermal model was built in MATLAB® and described in section 5-3. In addition, a 3D model was built in COMSOL Multiphysics, to simulate heat transfer as described in section 5-4. For a thermal steady state condition, equations (38, 39) are used through COMSOL's Live-link with MATLAB. An external MATLAB function is used to solve the model.

As drawn in the flowchart diagram in Figure 5-1, the cell temperature T_{c2}, is estimated by following the sequence steps. To solve the model, several steps are repeated in order to converge at a steady state, so the relative error is < 0.1%.

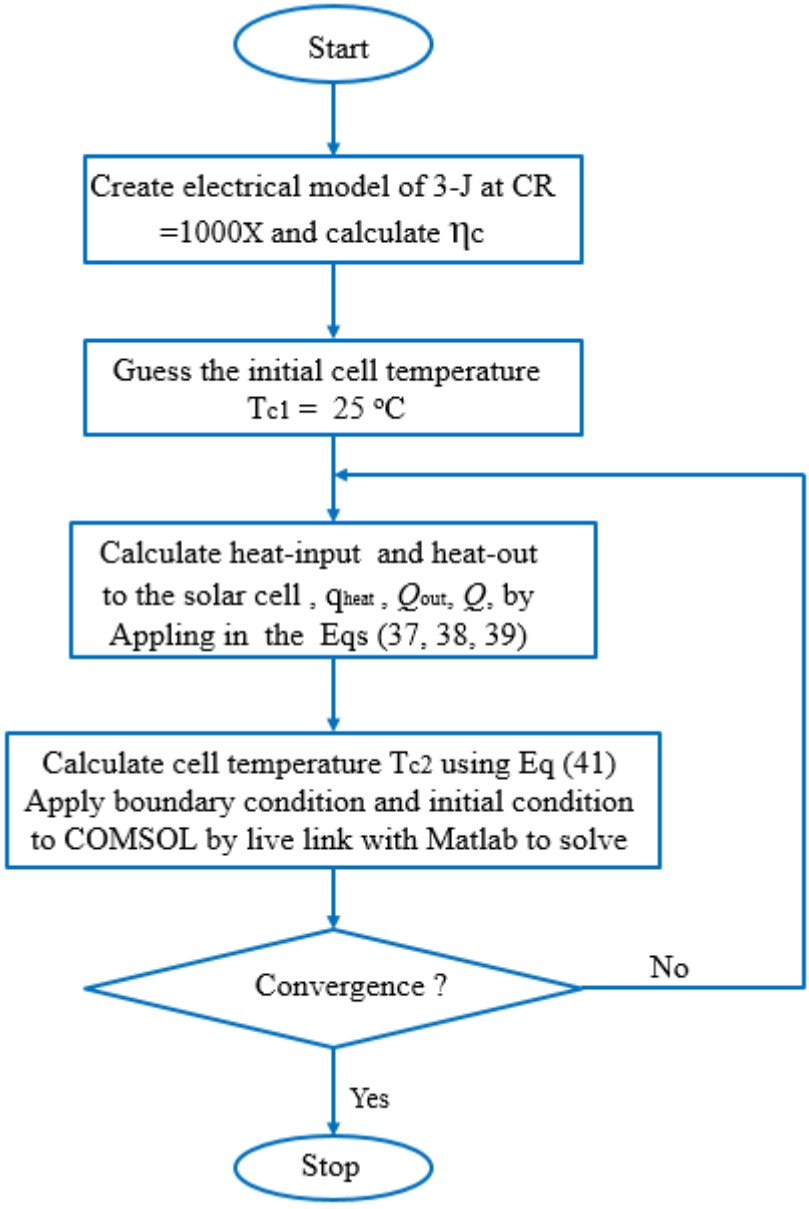

Figure 5-1 Flowchart diagram of model for cell temperature.

5.3 MATLAB Thermal Model

One of the methods of predicting the cell temperature under high concentrating photovoltaic is through the use of solar cell's electrical parameters, such as open circuit voltage and short circuit current. Hence, in theory, used the single exponential model to estimate the cell temperature [150, 162]. The temperature of the cell has a significant

influence on the reliability and the performance of the cell. Consequently, it is essential to have the adequate characterisation of HCPV solar cell [112, 163].

In order to estimate the cell temperature, a numerical model written in MATLAB script is solved iteratively, beginning with the first approximation of the cell temperature T_{c1}. The cell operating temperature is expressed by Eq.(36) [79]. It is estimated from electrical parameters, with consideration to the concentration ratio and environment temperature.

$$T_c^* = T_{amb} + \frac{V_{oc}(x) - V_{oc}}{\beta_{Voc}} \tag{36}$$

Where T_c* is the cell operating temperature, T_{amb} is the environment temperature and β_{Voc} is the open circuit temperature coefficient. Equation (37) [164, 165] is used to calculate the cell conversion efficiency η_c as a function of temperature, where η_{el} is the cell electric efficiency for the concentration ratio of a reference temperature T_o , β_η is the temperature coefficient of the efficiency.

$$\eta_c = \eta_{el}\left[1 - \beta_\eta (T_c^* - T_o)\right] \tag{37}$$

The amount of heat power generated in the solar cell from the radiant heat transfer in the solar spectrum is given by Eq (38) [99, 166]. Where q_{heat} is the heat power generated and *CR* is a concentration ratio.

$$q_{heat} = DNI_{(AM)}.(1-\eta_c).A_c.CR.\eta_{opt} \tag{38}$$

Heat is dissipated by free or forced convection by either passive or active cooling. Newton's law states that the convective loss is proportional to the difference in temperature between the surface and the fluid [167]. Convective heat transfer depends on cell mounting, wind conditions and properties of the surrounding air. The amount of heat removes by convection given in Eq (39):

$$Q_{out} = h_{conv}.A_s.\Delta T \tag{39}$$

Where Q_{out} is the heat dissipated from the cell by convection, h_{conv} is the convective heat transfer coefficient, A_s is the convective surface area and ΔT is the temperature difference between the rear surface and the ambient air. *Q* is the amount of heat added to the cell after the heat dissipation; therefore, the cell operating temperature estimation is determined as expressed in Eq (40):

$$Q = q_{heat} - Q_{out} \tag{40}$$

The steady-state cell temperature is obtained by an iterative process where the cell temperature is increased by a temperature rise equivalent to heat generated and is expressed in Eq (41); T_{c2} represents modified cell temperature, C_p is the heat capacity and m is the mass of the cell, as given in relationship (42); where x_c is the thickness of the cell, A_c is the cell area and ρ is a material density of the solar cell.

$$T_{c2} = T_{c1} + \frac{Q}{m.Cp} \tag{41}$$

$$m = x_c.A_c.\rho \tag{42}$$

5.4 (FEM) Finite Element thermal model

A thermal FEM model using COMSOL Multiphysics, together with an electrical model, iteratively solves partial differential equations [168] to determine the thermal distribution throughout the cell assembly. The receiver assembly consists of the solar cells in the top interconnection at the rear side of a carrier Direct Copper Banded (DCB). The DCB is made of copper/Al_2O_3 ceramic/copper and silver used for the electrical connection. Aluminium oxide is selected for it's good balance between thermal performance, weight, and cost [106, 169]. The insulation materials in the middle of the DCB sandwich between the bottom and top copper, hence Al_2O_3 has excellent combined properties as electrical insulator and thermal conductor [84]. These materials have the high thermal conductivity necessary to dissipate heat. Figure 5-2 illustrates the main receiver assembly configuration and boundary conditions.

Defining the operating temperature of the solar cell makes it more important to assess the energy performance of the high concentrating photovoltaic module. Nevertheless, the measurement of the cell temperature in HCPV modules is a very complicated task. Because of the specific characteristic of these kinds of modules, it is beneficial to develop indirect approaches to compute it [162].

It is important to predict the cell temperature rises in high concentration PV, because cell performance depends on the temperature. Therefore, it necessary to estimate cell temperature to improve the design or an operating performance assessment.

In this simulation, the physics used is heat transfer in the solid state. Table 5-1 lists all boundary conditions and assumptions. The heat dissipated by conduction through the receiver of the solid component is given by Fourier's law (43):

$$q_{con} = -K\nabla T \tag{43}$$

Where k is thermal conductivity and q_{con} is conductive heat flux. The heat dissipated by convection is expressed in equation (44) by Newton's law of cooling: -

$$q_{conv} = h_{conv}.A_s.\Delta T \tag{44}$$

The heat lost by radiation, which transfers heat electromagnetically to the environment is given by equation (45):

$$q_{rad} = \varepsilon.\sigma.(T_s^4 - T_{amb}^4) \tag{45}$$

Where q_{rad} is radiation heat flux, T_s is the surface temperature, ε is the surface emissivity and σ is the Stefan–Boltzmann constant.

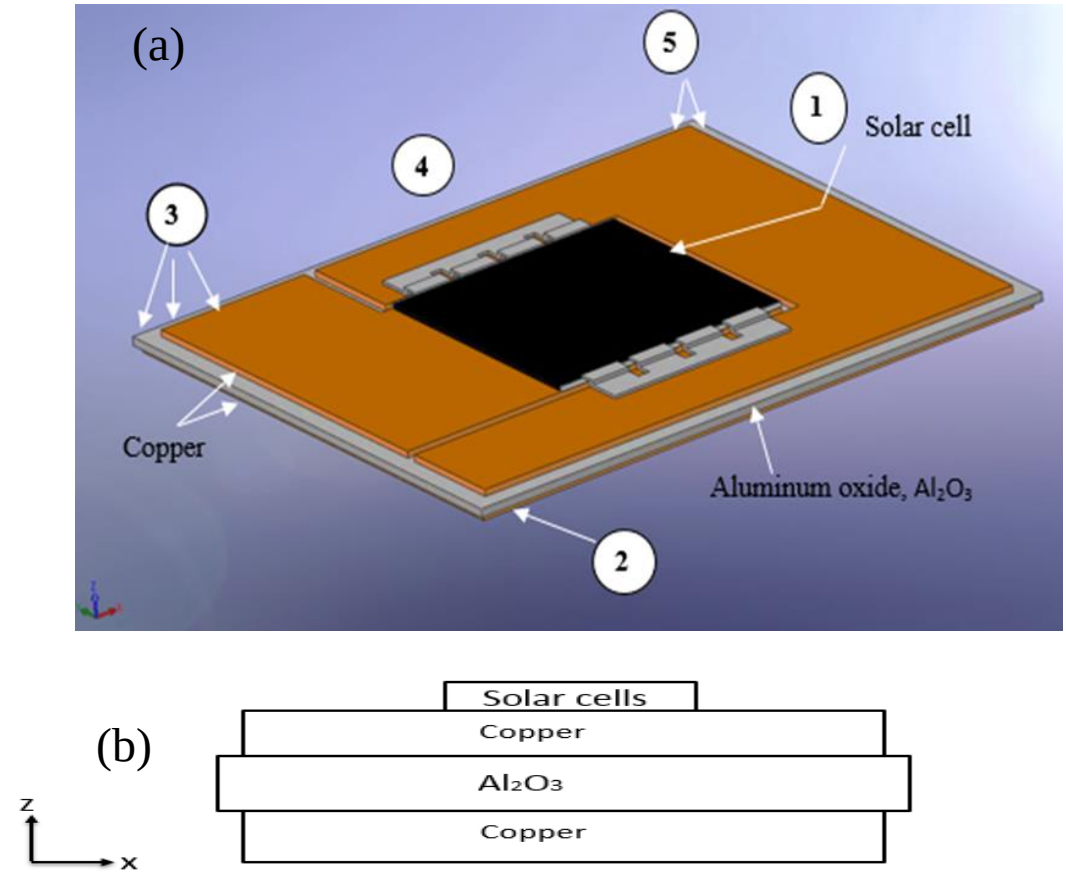

Figure 5-2 (a) Receiver assembly component structures and boundary condition, (b) schematic diagram of the receiver.

Table 5-1 Listed boundary condition.

No	The boundary conditions
1	Solar cells (the heat source).
2	Rear plate convection heat transfer = 2000 – 2400W/m^2K.
3	Natural convection of all free surface.
4	Ambient temperature = 25^{o}C.
5	Surface radiation.

Table 5-2 Materials thermophysical properties.

Material	C_p (J/(kg K))	k(W/(mK))	ε	ρ (kg/m^3)
GaInP	370	73	0.04	4470
GaInAs	550	65	0.4	5316
Ge	320	60	0.9	5325
Copper	385	400	0.05	8700
Aluminuim ceramics (Al_2O_3)	900	30	0.75	3900
Silver	325	430	0.03	10.490

Table 5-3 Dimensions of PV receiver assembly.

Receiver layer	With (mm)	Thickness (mm)	Length (mm)
Solar cell(C1MJ)	10	0.19	10
Copper	19.5	0.25	24
Al2O3	21	0.32	25.5
Copper	20.5	0.25	25
Bus-bar	0.305	0.006	10

5.5 Results and discussions

5.5.1 Thermal model

The concentration ratio used in this thermal model is 1000x, where 1x =1000W/m^2. In HCPV, a cooling system is needed to remove the generated heat from the cells, for safety and reliability reasons. It is recommended that maintain the cell operating temperature be maintained at or below 80^{o}C. The amount of heat produced must be equal to the removed heat from the cells in order to prevent the temperature from rising and to allow the system to work under steady-state conditions [169].

The temperature of a solar cell is quantified by incident power and ambient temperature and influenced by cell efficiency. The amount of heat power generated in the solar cell is given by Eq (36). As shown in the flowchart diagram in (Figure-5-1) the cell temperature T_{c2}, is estimated through a sequence steps. To solve the model, it is repeating several steps in order to converge at a steady state temperature, so the relative error is < 0.1%.

5.5.2 Meshing convergence

The simulation was carried out using (GMRES) Generalised Minimum Residual, which is an iterative solver for general linear systems. An iterative approach is different from the direct method as this solution obtained gradually, instead of one large computational step. While solving a problem with an iterative method, the error estimate in the solution decreases with the increase in the number of iterations [170]. A balance between model accuracy and computational time needs to be found, it is therefore necessary to the selection of optimum mesh sizes. When increasing the mesh density, the number of mesh elements increases, as shown in Figure 5-4, for different mesh simulation type.

The selection of a fine mesh can enhance the simulation accuracy, but that increases the time of simulation and the device memory used. Conversely, a coarse mesh can reduce the time of the simulation and shorten the memory device used. The receiver configuration set at the bottom convective area is about 5.13x10^{-4} m^2 and the solar cell area is $1cm^2$. However, it is a necessity to determine the optimum mesh size that guarantees the simulation accuracy, through a mesh convergence analysis. The optimum geometry mesh is a normal size, free triangle type as shown in Figure 5-3. The domain contains 92300 elements of normal size mesh. Table 5-4 summarises the mesh stability and the number of elements.

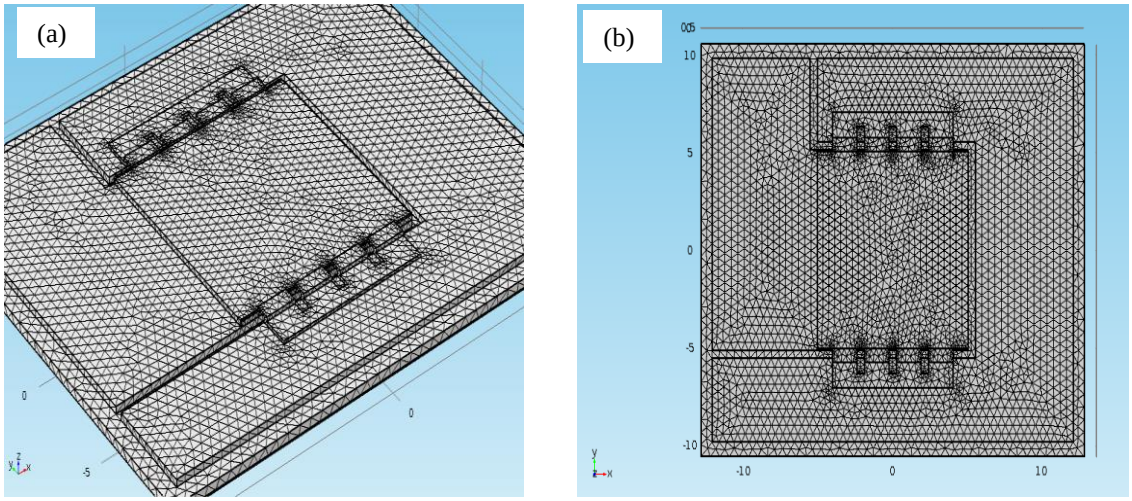

Figure 5-3 Receiver assembly of triangle normal size mesh (a) 3D mesh and (b) 2D mesh.

Table 5-4 Detailed mesh optimisation data.

Mesh type	**Exert coarse**	**Coarser**	**Coarse**	**Normal**	**Fine**	**Finer**	**Exert fine**
Number of elements	20693	30868	52068	92300	160488	307384	586036
T_{Cell} (°C)	79.1	79.45	79.7	80.1	80.1	80.1	80.1

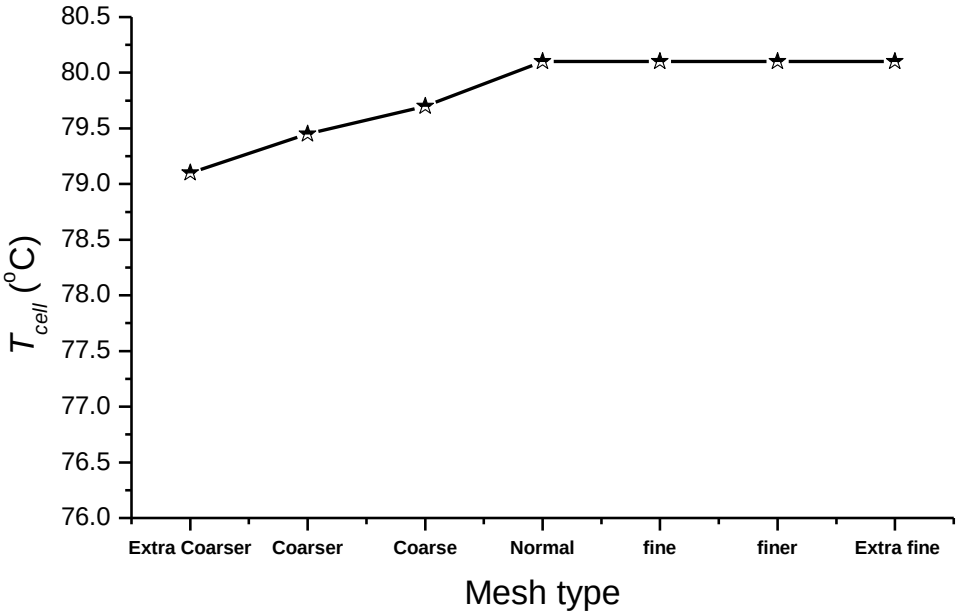

Figure 5-4 Mesh convergence verses cell temperature.

5.6 Analysis of Performance convergence

The energy balance of the solar cell per unit area is equivalent to incident solar irradiance, less the electrical power and power dissipated as heat to the atmosphere. The heat in a solar cell can be either absorbed to increase the cell temperature or released by radiation or convection. Theoretically, a low normal thermal resistance and high lateral heat spreading of the carrier is the best way for receiver thermal management [171].

A triple junction solar cell assembly is composed of multiple-layers of materials solar cells. The thermal modelling is usually considered as a single layer, and modelling the bottom, subcell (Ge) Germanium. That is because of the thickness of the top cell and the middle cell which are only is few micro-metres thick. The Ge substrate has the greatest thickness of the subcells typically 0.19*mm* in thickness [32].

The convective heat transfer coefficient thermal boundary condition was varied to investigate the effect of cooling on the oval performance of the cell. The initial cell temperature was set at 25^{o}C for all models. Cell temperature stabilises at a point where the generated heat is equivalents to the heat dissipated by the cooling mechanism. This particular condition is attained the cell operates under steady conditions.

Figure 5-5 shows temperature distribution on the receiver for the steady-state model. The model in convergence occurs after 14 iterations; the low temperature at the edge of the receiver is 61^{o}C. A heat transfer coefficient $h_{conv} \geq 2000 W/m^2K$ is required to keep the cell temperature below 100^{o}C for an T_{amb} = 25^{o}C.

Figure 5-6 illustrations the calculated cell temperature T_{c2} variation for 20 iterations to converge on a steady state. The convective heat transfer coefficient $\geq 2.4 KW/m^2K$, is needed to maintain the cell operating temperature of less than 80^{o}C and converges after approximately 11 iterations. In addition, a convective heat transfer coefficient > 2 KW/m^2K needed to keep the cell temperature below 100^{o}C and converge after roughly 15 iterations.

Figure 5-7 shows the temperature distribution on the receiver for $h_{conv} \geq 2400 W/m^2K$ and ambient temperature = 25^{o}C. To keep the cell operating temperature below 80^{o}C a convection heat transfer coefficient $\geq 2400 W/m^2K$ is needed. The highest cell temperature at the centre of the cell and decreases as moves toward the receiver's edge. The convergence occurs after 8 iterations

Figure 5-8 shown maximum cell temperature variation and convergence after 20 iterations, for different initial cell temperature scenario. A convective heat transfer coefficient of 2400W/m^{2}K, was applied for all scenarios, all these converge and comes to the same steady-state temperature as initial T_{c1} changes. The initial T_{c1} nearest to 80^{o}C is converges with the fewest number of iterations.

The solar cells are mounting on the substrate, which gives a mechanical support to the structure and is designed to gather the produced current while reducing the electrical losses. In addition, this gives an efficient transfer of the waste heat from the cell to the surrounding environment. The most commonly used substrate, for HCPV systems, is the direct bonded copper boards, nevertheless insulated metal substrates are gaining attention because of their good performance, and availability at lower costs [82, 83].

Forcing the cell's by short circuit current (J_{sc}) through the electrical circuit results ohm losses or so-called "Joule losses" which would influence the maximum temperature. Micheli *et al.*[83, 172] found there are no impacts of Joule losses in terms of maximum temperature a rise of (TJ) Triple-Junction cells. For this reason, the Joule losses are considered negligible and not taken into the account in the thermal modelling.

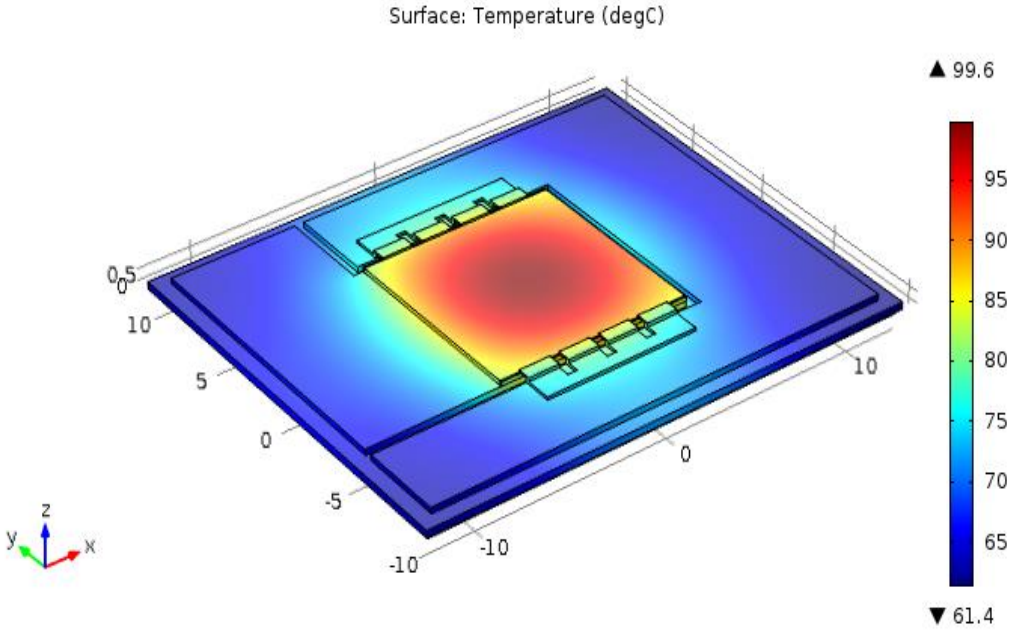

Figure 5-5 Steady-state cell temperature distribution, $h_{conv} \geq 2000$ W/m^{2}K.

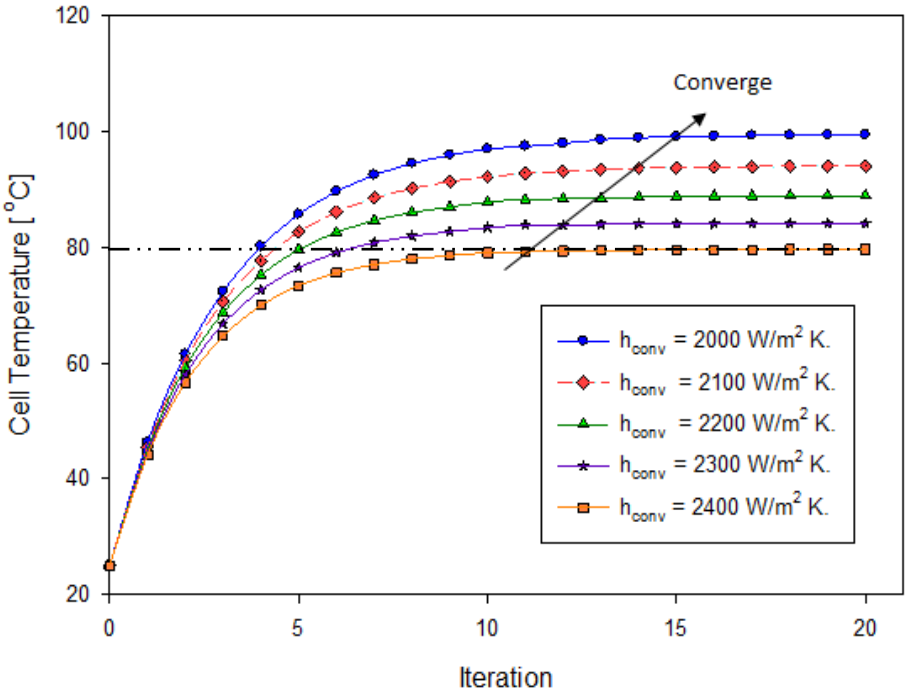

Figure 5-6 Cell temperature T_{c2} versus to iteration as a function of convection heat transfer coefficient at constant initial cell temperature h_{conv} from (2000 – 2400) W/m²K.

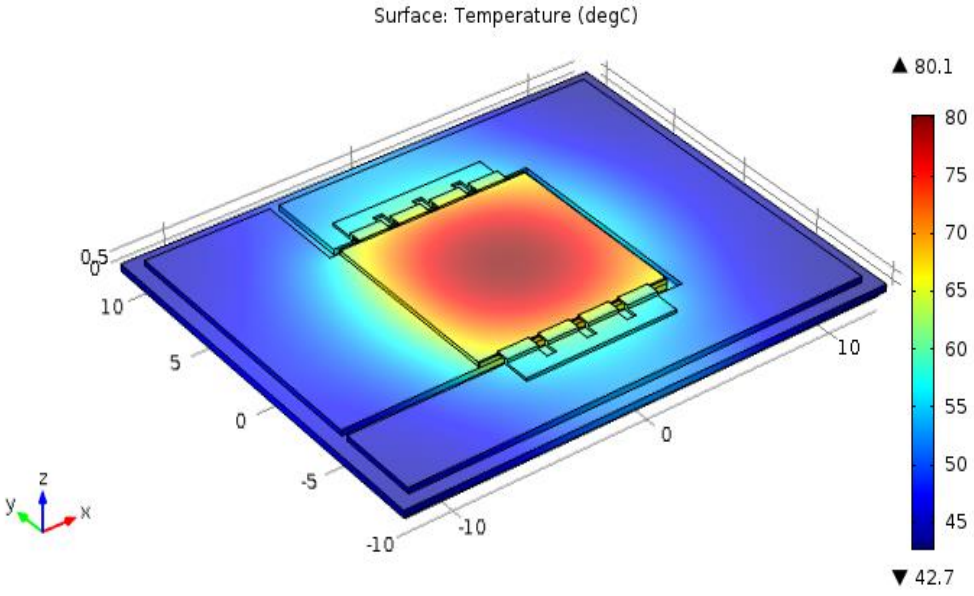

Figure 5-7 Steady state cell temperature distribution, $h_{conv} \geq 2400$W/m²K.

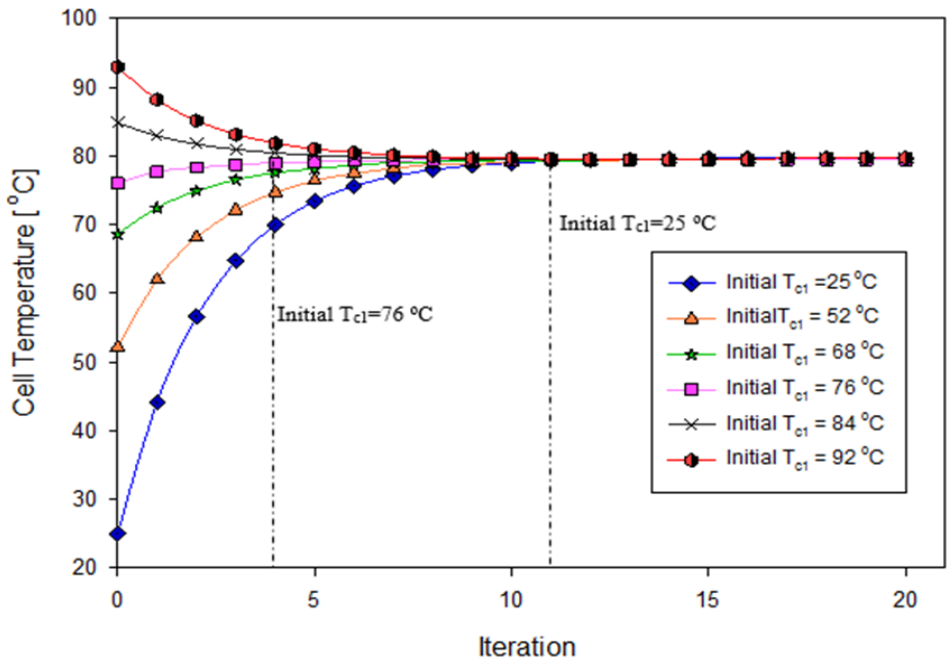

Figure 5-8 Cell temperature T_{c2} versus to cycle iteration at different initial cell temperature T_{c1} at constant h_{conv} = 2400W/m^{2}K.

5.6.1 Verification

The steady-state cell temperature has verified the numerical FEM model with another model work performed by Muron *el al.*[105], which experimental calibrated with a known design. The simulation results are compared with their numerical heat transfer model, which is in consistent and good agreement with their experimental. Figure 5-9 (b) shown the current study cell convergent temperature is 80.1^{o}C on the solar cell. Figure 5-9 (a) shown the COMSOL Multiphysics model results by Muron *el al.* the cell deviation between two models is 0.12%, also temperature pattern is dense on the cell centre for both models. The condition of ambient temperature is 25^{o}C and the concentration ratio of 1000X. The receiver structure of a triple-junction solar cell stack on the substrate DCB of copper/aluminium/copper as a sandwich. Moreover, both of these FEM models had the same solar cell area which is about 1cm^2.

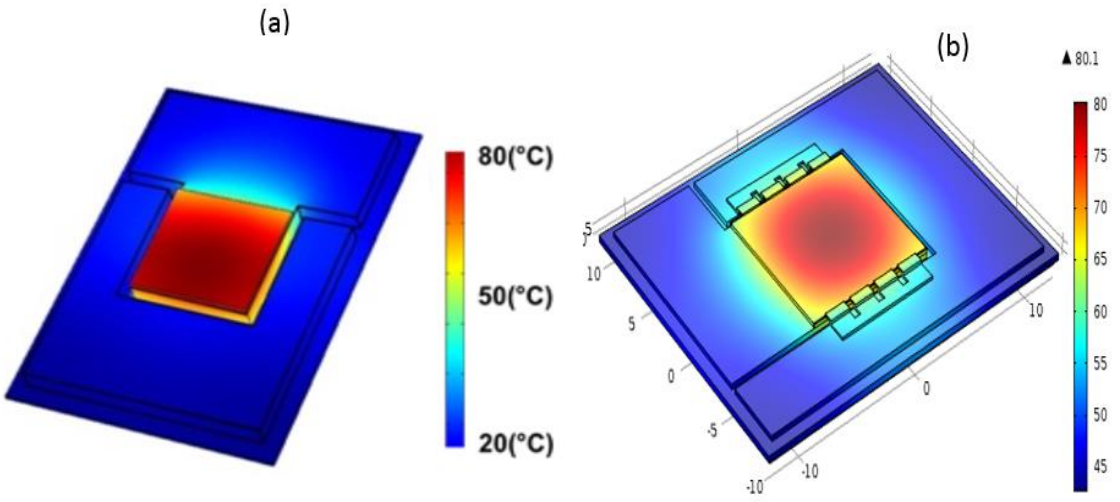

Figure 5-9 Plot of thermal receiver assembly results, (a) FEM model done by Muron *el al.* [105], (b) Current study model.

5.7 Model development for different *AM*

The modelling approach is summarised in the flow diagram in Figure 5-10. Direct spectral irradiance is calculated using version2 SMARTS, the Simple Model of Atmospheric Radiative Transfer of Sunshine for different *AM* values [132, 133].

The SMARTS2 inputs the spectrum of an ASTM 173-G and is used with vary of the air mass from *AM* =1 – 8D. The results from the SMARTS2 model show that the *DNI* is integrated into overall ranges of wavelength light at different *AM* values. Thus, the *AM* gives the solar irradiance *DNI* as a function of the zenith angle.

To predict cell temperature as a function of *AM* values, a thermal model was developed in MATLAB. The heat power is generated from the solar power, which is not converted to electricity due to current mismatch due to current limitation/mismatch, which is detailed earlier in section (3.3.2). The ambient temperature is considered in the prediction of the cell operating temperature for a variety of h_{conv}. Additionally, a steady-state thermal model was developed using a Finite Element Method (FEM) in COMSOL Multiphysics software, in order to predict cell and receiver assembly temperature distributions.

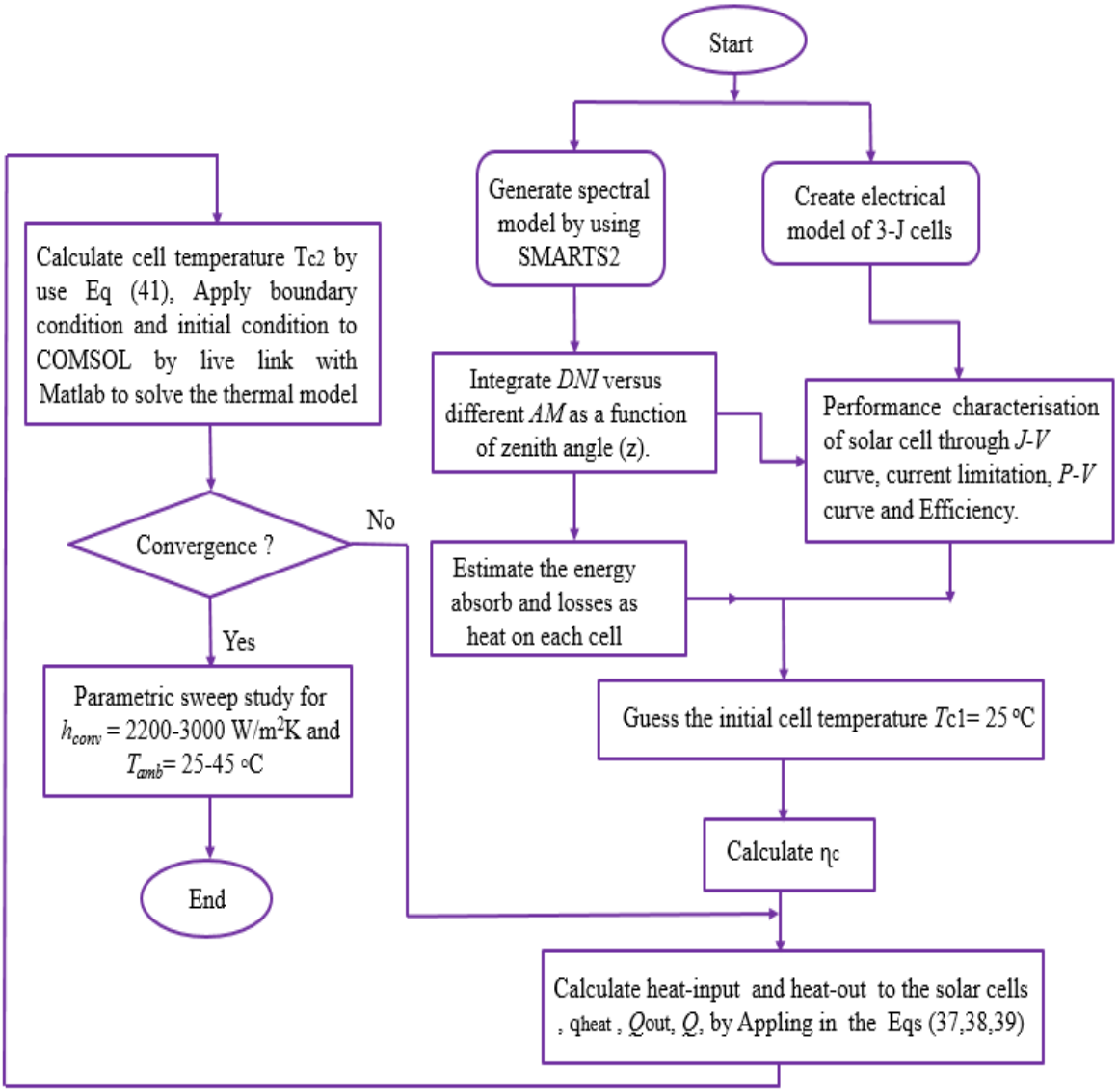

Figure 5-10 Flow diagram of a process and the steps of the proposed modelling.

Table 5-5 Listed boundary condition.

No	The boundary conditions
1	Solar cells (the heat source).
2	Rear plate convection heat transfer = 2200 – 3000W/m^{2}K.
3	Natural convection of all free surface.
4	Ambient temperature = 25 – 45^{o}C.
5	Surface radiation.

5.7.1 Estimation of energy conversion yield

The standard test condition is *DNI* = 1000W/m^2 at *AM* 1.5D, T_{amb} = 25^{o}C, while the standard operating conditions are *DNI* = 900 W/m^2, ambient temperature T_{amb} = 20^{o}C at *AM* 1.5D [123, 136]. In this study, the External Quantum Efficiency (EQE) measurement data is taken from Kinsey and Edmondson CM1 [126]. The EQE corresponds to the cell (or sub-cell) absorbing spectrum response.

The top cell (GaInP) absorbs the part of the solar spectrum which contains the ultraviolet and visible wavelength. It responds to approximately 300 – 700*nm* wavelength with E_g = 1.8(eV). The middle (GaInAs) layer absorbs the near infrared spectrum. It responds to approximately 700 – 900*nm* wavelength with E_g = 1.4(eV). The bottom (Ge) subcell absorbs the lower photon energies in the infrared spectrum between 900 and 1800*nm* with E_g = 0.7(eV). The photons absorption is quantified by the energy gap of the semiconductor material alloy and it is absorption coefficient [149]. In order to predict the energy available to be absorbed by each subcell, the *EQE* as a function of irradiance utilised as expressed in Eq. (46). Energy lost from an incident spectrum occurs, some by absorption and some by reflection.

$$G_{in(\lambda),i} = \int_{280}^{4000} G_{(\lambda)} . \int_{300}^{1800} EQE_{(\lambda),i} . d\lambda \tag{46}$$

$$DNI_{abso(AM)} = \int G_{abso(\lambda),i} - \left(Th_{losses,i} + Q_{cm,i}\right) \tag{47}$$

Where G_{abso} is the amount of an incident spectrum absorbed and converted to electricity by each subcell, Th_{losses} are the thermalisation losses. The portions of power absorbed as a function of air mass, $DNI_{abso}(AM)$ by the three junctions of the solar cells and converted to electricity is expressed by Eq. (47).

The proportion of the radiation not converted to electricity is a loss as heat and results in an increase of solar cell temperature. The thermalisation losses in the solar cell occur where the absorption of energy is greater or less than the bandgaps [49, 148]. In a triple junction cell, due to a series connection, the total current of three cells is limited by the minimum. The amount of energy not converted to electrical energy is wasted as heat, as given in equation (48) [148, 173], based on current limitation and spectrum variation effects at different *AM*.

$$Q_{cm} \leq \sum_{i=1}^{3} \left[J_{sc,i} - J_{total} \right] V_{oc,i} \tag{48}$$

Where Q_{cm} is the heat generated due to current mismatch and J_{sc} is the short circuit current in each layer. The J_{total} is the total current of the three cells; V_{oc} is the open circuit voltage of each layer. The most heat produced due to current limitation comes from the bottom subcell, which generates the highest current. The total estimated energy wasted is estimated by adding the heat generated because of current mismatch to the energy losses from the incident spectrum.

The available incident solar power that responds at each range for each subcell (GaInP/GaInAs/Ge) is shown in Figure 5-11 *AM* (1.5D) and air mass values of 4D) shown in figure 5-12. The energy greater than the bandgaps is wasted. Adding different semiconductor materials is one-way to utilise such solar spectrum losses and minimise the heat generated. High *AM* values lead to less incident power, as shown in the (5-13) figure at *AM* 8D; the Ge layer will produce less power compared with *AM* 1.5D.

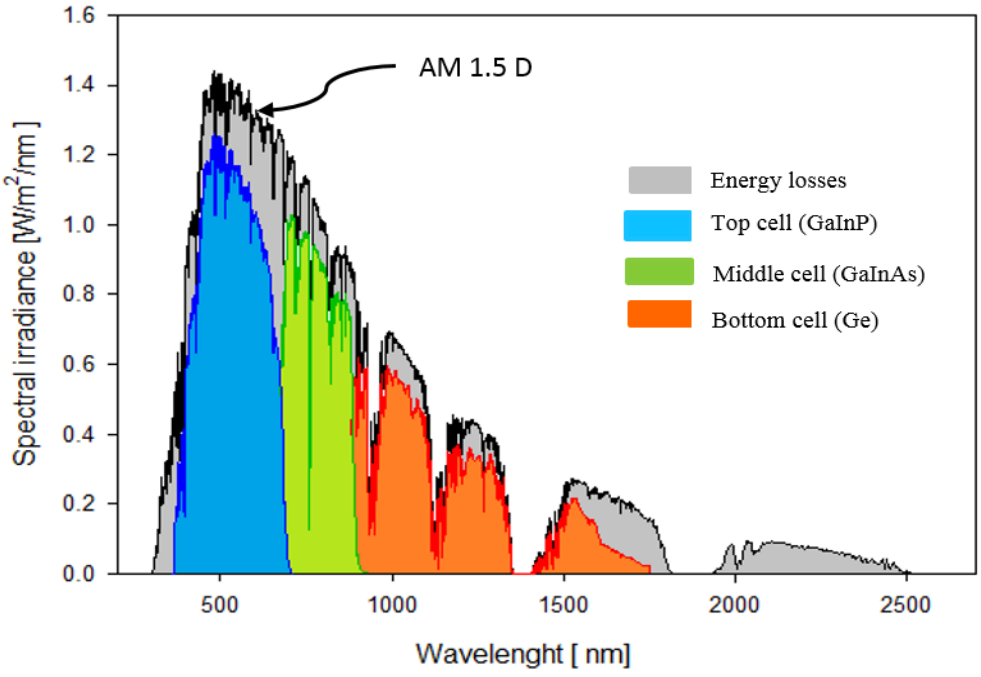

Figure 5-11 Estimation of portions energy absorbs and approximation of energy losses by each layer of triple-junction cells for *AM* 1.5D.

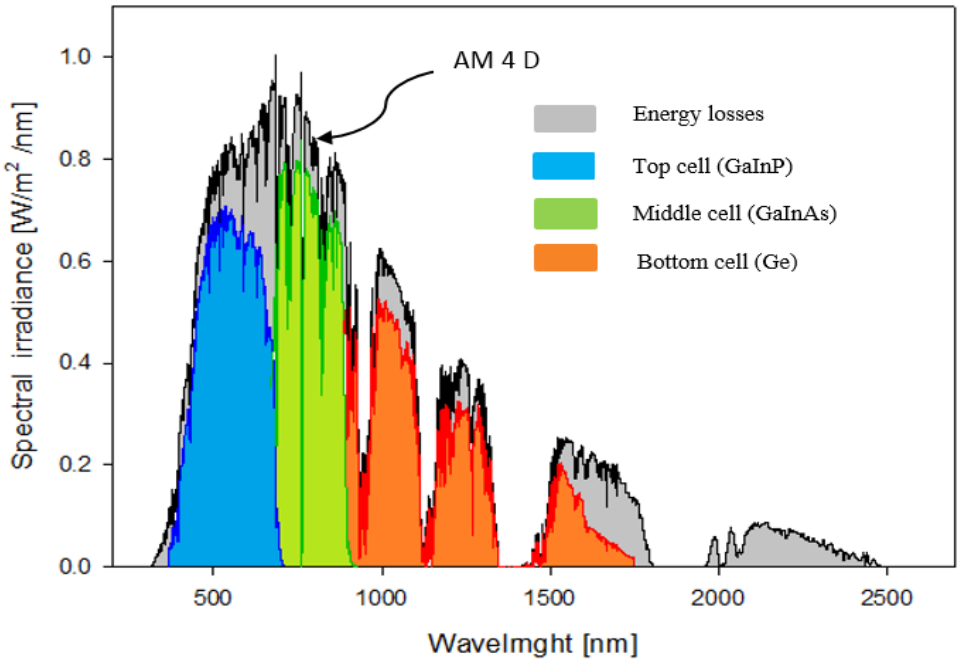

Figure 5-12 Estimation of portions energy absorbs and approximation of energy losses by each layer of triple-junction cells for *AM* 4D.

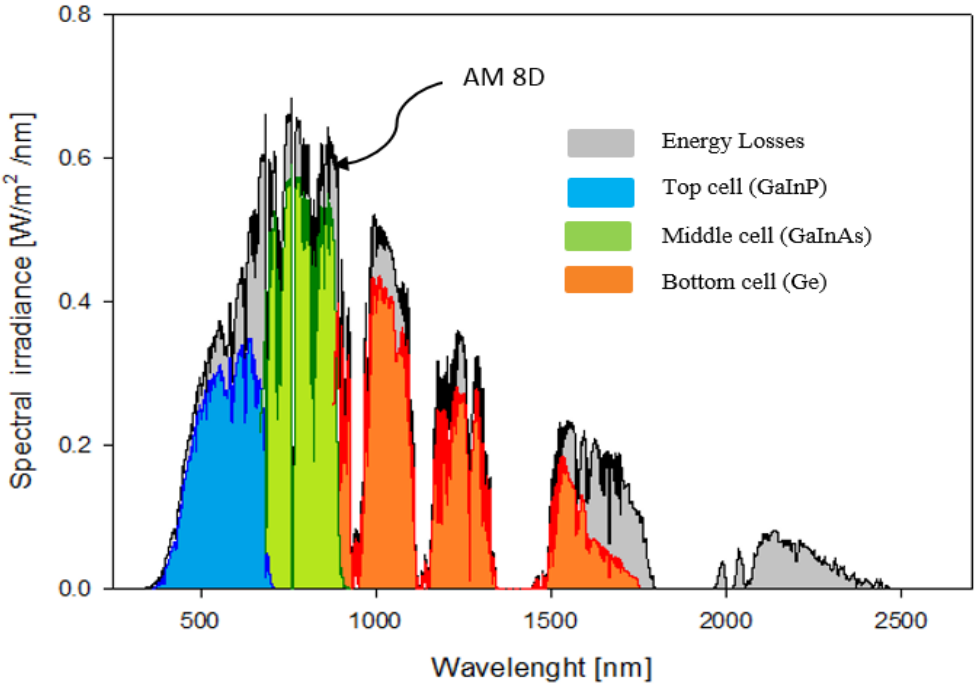

Figure 5-13 Estimation of portions energy absorbs, and an approximation of energy losses by each layer of triple-junction cells for *AM* 8D.

5.7.2 Convergence analysis

Figure 5-14 illustrations cell temperature T_c at *AM* 1.5D, T_{amb} 25°C, iterated in 20 steps to converge to a steady state. A convective heat transfer coefficient, $h_{conv} \geq 2.4$ KW/m^{2}K is required to maintain a cell operating temperature of less than 80 °C, and converges after approximately 12 iterations. The black trend line represents a cell temperature at *AM* 4D, iterated to converge to a steady state. The convective heat transfer coefficient of 2.3KW/m^{2}K is applied and converges after approximately 11 iterations. The orange trend line represents a cell temperature at *AM* 8D, iterated to converge in a steady state. The $h_{conv} \geq$ 2.2KW/m^{2}K, and converges after approximately 10 iterations. Table-5-6 summarised the details of parameters of the efficiency, h_{conv} and q_{heat} versus different *AM* values. State that each h_{conv} was chosen, so the final temperature would be the same for all air mass values.

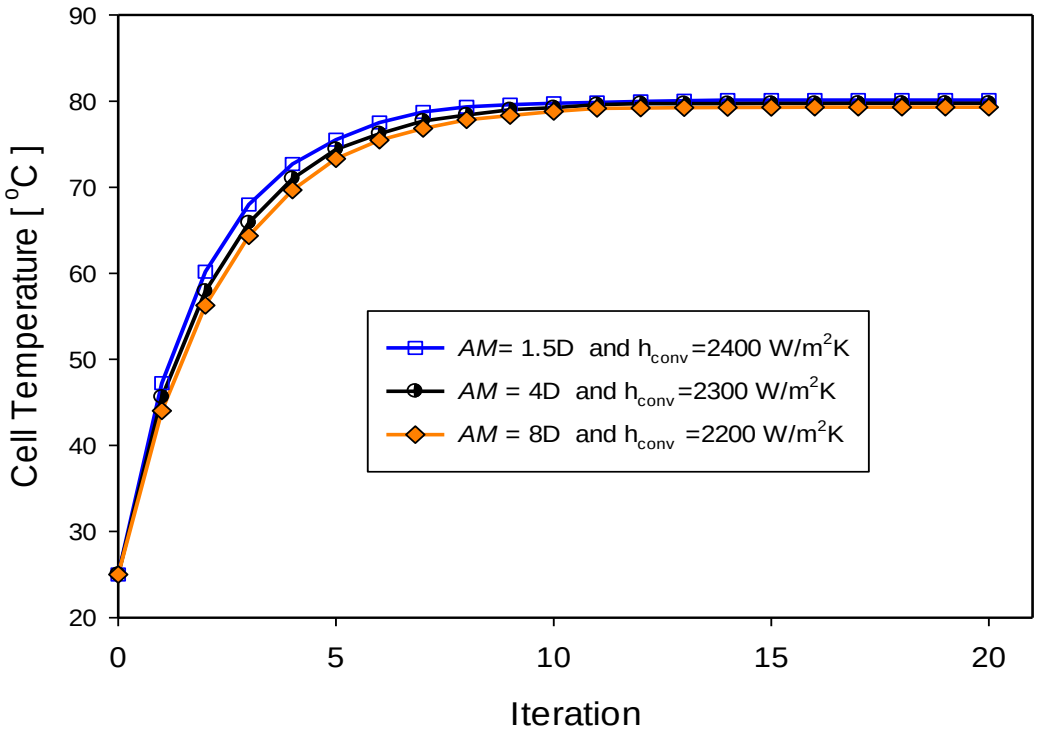

Figure 5-14 Cell temperature convergence versus iterations; this model of triple-junction cells, at the variation of h_{conv} between 2200 to 2400 W/m^{2}K to maintain a cell temperature below 80°C.

Table 5-6 Listed different *AM* versus cell temperature converges with different h_{conv} and T_{amb} = 25°C @1000x.

AM	Efficiency (%)	q_{heat} [W]	h_{conv} [W/m^{2}K]
1.5D	39	50	2400
4D	37	45	2300
8D	35.5	41	2200

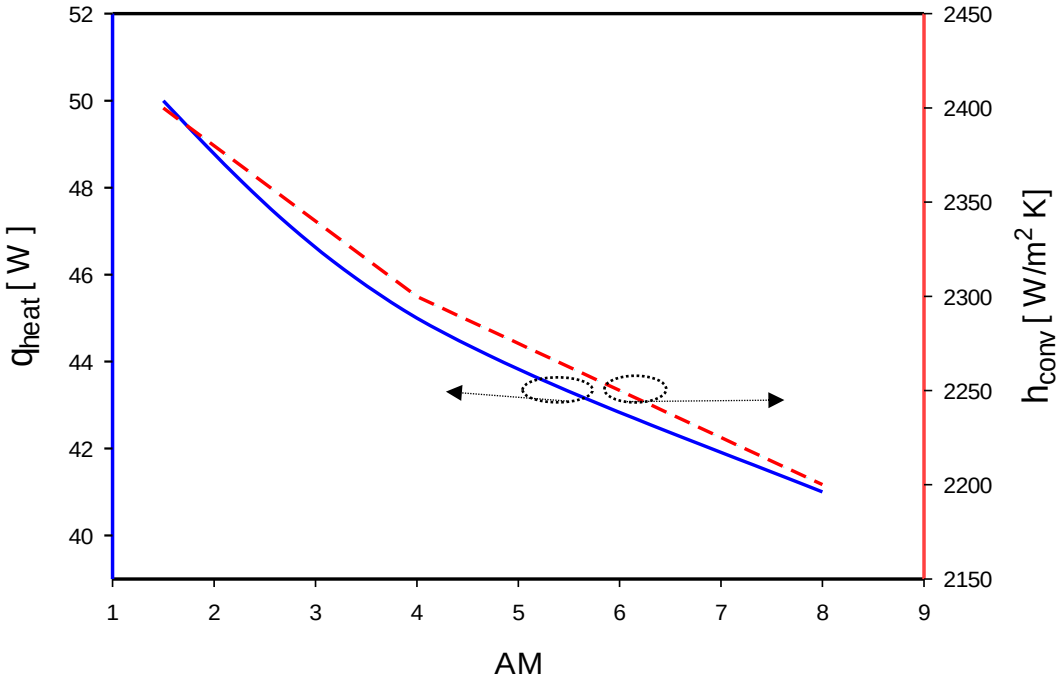

Figure 5-15 *AM* as a function of irradiance versus heat power generated on the solar cell, also *AM* versus h_{conv} required to maintain a cell temperature below 80°C.

In figure 5-15, the heat power generated and heat transfer coefficient versus increase of *AM* are presented. As *AM* increases from 1.5 to 8D, the results is directly proportional to the q_{heat} and h_{conv} which decrease significantly. To maintain a cell operating temperature below 80 °C, the value of h_{conv} remarkably decreases as *AM* increases. This is due to the increase of *AM*, which results in the cell efficiency dropping, which subsequently leads to decreases in the heat power. Also, because the incident radiation is lower for high *AM*.

A multi-junction solar cell can operate above 1000x due to its effectiveness at high temperature [112]. Passive cooling is often applied to concentrating photovoltaic systems ranging from 300 – 1000x and operating temperatures between 50 – 80°C [97, 154, 174].

The distribution of temperature on the PV cells/module relies on: the materials of the PV cell, the type of the cell, panel structure and uniformity of incident sunlight. Moreover, the attached electrical load to the PV system, the environmental conditions prevailing, and characteristic of the heat removal all need to be considered [175].

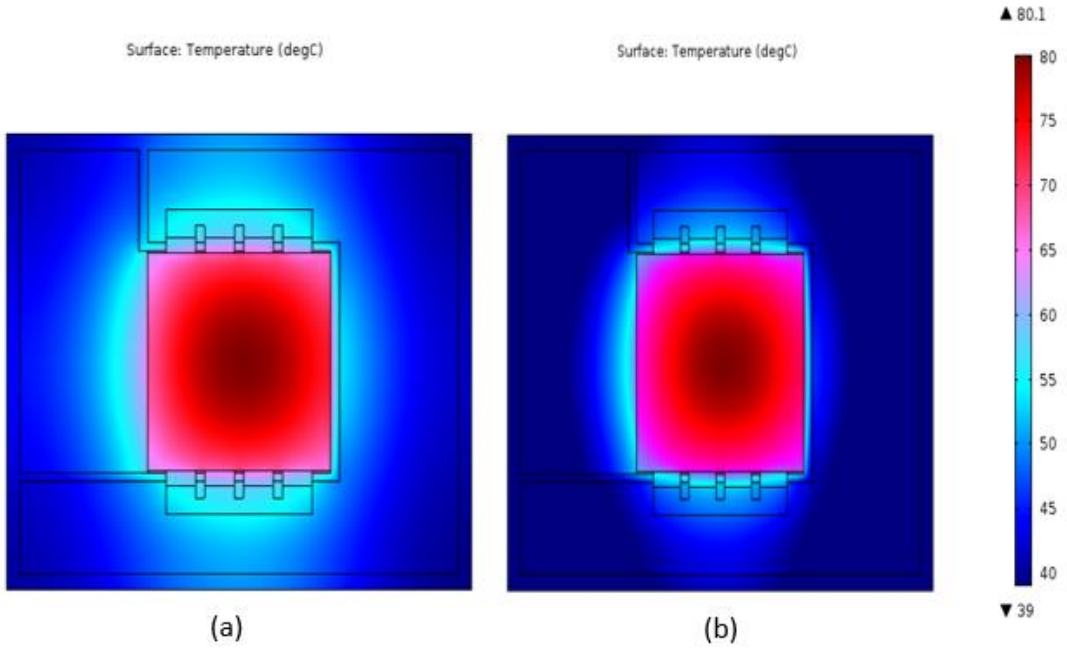

Figure 5-16 2D plot of temperature distributions on CPV receiver, (a) *AM* 1.5D and at an ambient temperature of 25°C, h_{conv} = 2400W/m^{2}K, (b) *AM* 1.5D at an ambient temperature of 45°C and h_{conv} = 3000W/m^{2}K.

In order to predict cell temperature or the thermal behaviour as a function of the ambient temperature and *AM*, a parametric sweep study was conducted for T_{amb} = 25 to 45°C and h_{conv} = 2200 to 3000W/m^{2}K. Figure 5-16(a) shows the 2D plot of temperature distribution on the receiver of h_{conv} = 2400W/m^{2}K, an ambient temperature of 25°C and *AM* 1.5D to keep the cell operating temperature below 80°C.

The highest cell temperature occurs at the centre of the cell and the temperature decreases towards the receiver edge. Figure16-(b) is the 2D plot of temperature distribution on the receiver for h_{conv} = 3000W/m^{2}K, and ambient temperature of 45°C and *AM* 1.5D.

Figure 5-17 (a) illustrates the temperature distribution on the receiver, the h_{conv} = 2300 W/m^{2}K to maintain the cell operating temperature below 80°C, at an ambient temperature of 25°C and *AM* 4D. Figure 5-17 (b) illustrates a temperature distribution at h_{conv} = 2800W/m^{2}K at an ambient temperature of 45°C and *AM* 4D.

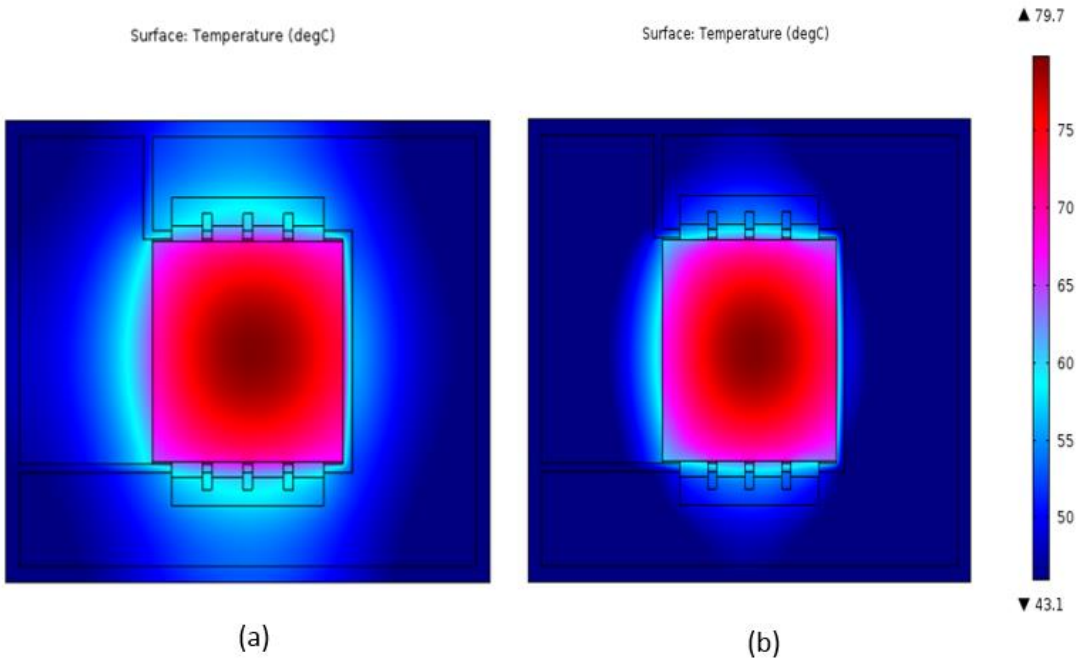

Figure 5-17, 2D plot of temperature distributions on CPV receiver, (a) *AM* 4D, h_{conv} = 2300W/m^{2}K and ambient temperature of 25^{o}C, (b) *AM* 4D and h_{conv} = 2800W/m^{2}K at ambient temperature of 45^{o}C.

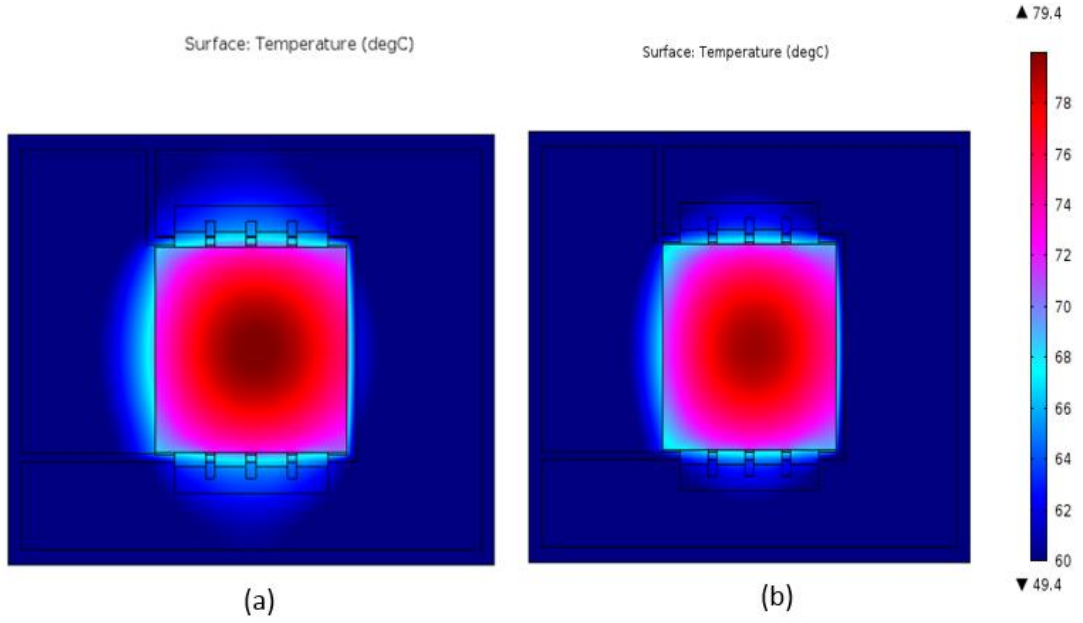

Figure 5-18, 2D plot of temperature distributions on CPV receiver, (a) *AM* 8D and ambient temperature of 25^{o}C and h_{conv} = 2200W/m^{2}K, (b) *AM* 8D for ambient temperature of 45^{o}C and h_{conv} = 2600W/m^{2}K.

Figure 5-18 (a) shows temperature distribution on the receiver, the h_{conv} = 2200W/m^{2}K, ambient temperature = 25^{o}C and *AM* 8D to keep the cell temperature below 80^{o}C. Figure 5-18 (b) illustrates the plot of temperature distribution on the receiver for h_{conv} = 2600W/m^{2}K, an ambient temperature of 45^{o}C and *AM* 8D. The main significant features in figures (5-16 to18) are summarised, hence as T_{amb} changes from 25 – 45^{o}C, the values

of h_{conv} rapidly increases in order to keep cell temperature below certain values. In contrast, increases in air mass *AM* =1.5, 4, 8D leads to a reduction in the required value of h_{conv}.

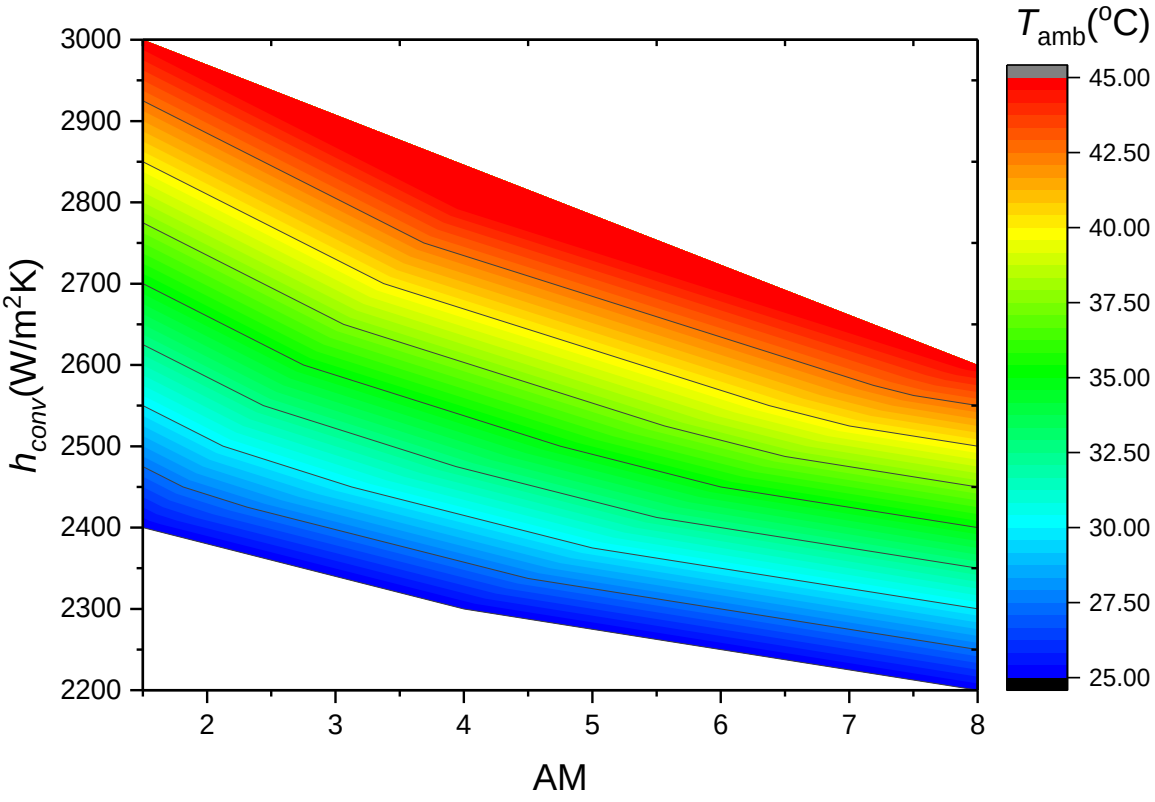

Figure 5-19 Variation values of h_{conv} as a function of variation T_{amb} for the different of *AM*.

Figure 5-19 illustrates the significant impact of a higher ambient temperature, and lower value of air mass, on the solar cell's operating temperature. Therefore, the thermal response through the values of the convective heat transfer coefficient need to be increased at the back of the receiver in order to operate below 80°C. In contrast, when the air mass values increase, the response values of the convective heat transfer coefficient decrease, and it's magnitude also depends on the environmental temperature. Therefore, it is important in further receiver design at such environments condition, when it's subjected to the condition of higher ambient temperature and lower air mass. Hence, select of adequate thermal management which lower cost and to handle with the high thermal capacitance of the solar cells. In the real operating conditions, the aforementioned parameters are variable in daily basis hours and in yearly performance is variable from month to another.

The thermal resistance 10^{-5} (Km^2/W) needed for a concentration ratio of 1000x [47]. The design of the solar receiver for high concentrating photovoltaic is developed by reducing the thermal resistance of the materials at the back of the solar cells [77, 169].

For passive heat dissipation from an HCPV system, the heat flux is conducted from the solar cell to the heat dissipator. Hence, the heat flux is distributed and transferred to the environment. The solar cell temperature is mainly dependent on the design and integration of the dissipator and the heat transfer conditions [176].

Summary

This chapter presented a thermal model of an HCPV receiver. The COMSOL Multiphysics software is used to visualise thermal performance behaviour, which gives an overview of its enhancing performance and physical understanding of changes in parameters and optimal design.

The convergence of geometry mesh is performed in order to improve the accuracy of the simulation. As described, the thermal behaviour of the solar cell shows significant sensitivity to the value of the convective heat transfer coefficient (h_{conv}). Furthermore, as the value of heat released from the solar receiver increase, the cells can operate at safer and lower temperatures.

The initial model is found by applying the mathematical formulation of electrical - thermal cells under concentrated ratios of 1000X. This technique is based on the convergent iterative simulation, in order to achieve cell operating temperature at/or less than 80^{o}C. Therefore, it was found that a value of the convective heat transfer coefficient of $\geq 2.4 KW/m^2K$ is needed.

In phase two of the developed model, the variable environment condition of T_{amb}, *AM* and corresponding *DNI* were considered. An iterative computational technique is also performed to predict the steady-state cell temperature. The cell efficiency at 1000x concentrating ratio is significantly decreased to 3.5% when the *AM* increased from 1.5 to 8D, which leads to a decrease in the thermal response of the h_{conv} and heat power generated by the solar cells, to keep cell temperature under safe operating conditions.

The effects of atmospheric radiative changes (AM = 1.5, 4 and 8D) is also considered in order to predict the cell temperature. For steady-state temperature $\leq 80^{o}$C, and T_{amb} = 25^{o}C, a h_{conv} between 2200 to 2400W/m^{2}K was required. A parametric sweep study for T_{amb} = 25 to 45^{o}C and h_{conv} = 2200 to 3000W/m^{2}K and (AM = 1.5, 4 and 8D) was also conducted to maintain the cell temperature below 80^{o}C. This thermal-electrical numerical model has been developed by using a convergent iterative technique.

The thermal analysis had significantly illustrated that CPV solar cell temperature is augmented with the growth of solar concentration flux, and also with varying ambient temperature.

Chapter 6: Transient Thermal-Electrical Behaviour of a Concentrating Solar Photovoltaic Receiver

6.1 Introduction

High-efficiency multi-junction solar cells are widely used in (CPV) Concentrating Photovoltaic systems, due to their high economic viability. In this CPV application technology, as the solar flux increases, the output power increases. Usually, CPV systems consist of dense arrays and a point focus are concentrations between (500-1000x) [177].

The efficiency of multi-junction solar has been developed and manufactured in both laboratories and factories. Therefore, the efficiencies of such solar cells have been reported at over 40% [178, 179]. In designing solar cells under high concentrations, the heat dissipation is a challenge that needs optimisation. The heat source from the power produced by the cells due to incident lights produces a high temperature [126].

As a result of CPV, the solar flux shows up as heat at the top surface of the solar cells; therefore, the accumulation of thermal energy raises the temperature of the surface of the solar cells. In turn, this leads to reducing the cell conversion efficiency, since that negative effect might cause mechanical failures in long-term operation [160].

Solar cell behaviour at high concentrations, coupled with the presence of the heat power on the surface of solar cells, leads to sharp increases in cell temperatures. Hence, higher temperatures cause a reduction in electrical conversion efficiency, and subsequently the temperature effect on maximum of power and open circuit's voltage [151]. In CPV systems, it is important to predict the solar cell's temperature, for use in performance analysis and characterisation. Moreover, to keep a high level of performance efficiency, the heat on the solar cell carrier must be dissipated [103, 105].

The majority of electronic devices operate over a long period, thus their mechanisms of cooling are designed for steady-state operation conditions. Nevertheless, in some electronic devices, applications do not ever operate long enough to achieve steady state operating. In those cases, it might be adequate to employ a restricted cooling procedure, such as thermal storage, for a short time (buffering), or not to use one at all [180].

Ning *et al.*[181] performed a study of an HCPV module based on implementing a forward voltage technique, in order to measure and monitor the transience of a junction's

temperature. A detailed analysis of the thermal characteristic of the Finite Element Model was established and compared with experimental data.

Muller *et al.*[95] had proposed thermal transient measurements based on the temperature coefficient to heating and natural cooling of the CPV module. In the measurement of the module to determine temperature, a sensor was pasted on the back plate attached to the cell. Torres-Lobera *et al.*[182] simulated dynamic in a PV module system. This model was performed on the PV module's string of six series-connected solar modules by using MATLAB Simulink software. The measurements of environmental parameters and the electricity of PV solar power plant was used for validation.

Migliorini *el al.*[183] investigated the performance thermal-electric model for the PV module, and takes into accounted for dynamic behaviour. The thermal model considered five different featured layers and the electrical model considered the behaviour of five parameters. In addition, predictions of the electric power produced with both explicit and simple relations, considering, for instance, the model of nominal operating cell temperature or the fill factor.

For a HCPV application, the peak cell efficiency is achieved at a concentration ratio of 500x. However, the temperature dependence on cell efficiency is to be taken into account in any modelling or design [141, 184]. Despite all these other valuable studies, the current study will specify performance behaviour. In this study, models for predicting the cell temperature steady state of CPV at 500x have been developed, in terms of the transient thermal performance characterisation.

Despite of many studies related with dynamic models to calculate PV solar cell temperature are introduced in the literature. However, in this research a developed model of HCPV for transient response is presented. The significance of the transient model is being the link between the ideal modelling, and environmental, operating conditions.

A thermal model based on the steady-state equation is obtained by considering the total energy balance in the PV module. This builds upon the previous model (chapter-5), so the current study looks at the transient and steady-state operations. In addition, a stationary model that is based on constant efficiency is compared with this dynamic model. The efficiency as a function of temperature has been modelled and verified with data from a commercial CPV cell. The comparison of the results for temperatures ranging

from 25 – 80ºC is reported. The deviation of efficiency approximately 0.8% is found for the initial temperature and approximately 2.5% for the high temperature within the range.

6.2 Methodology

Figure 6-1 illustrates the flowchart diagram describing the modelling approach. The proposed models are set initially by electrical modelling of GaInP/GaInAs/Ge, since the standard *DNI* = 1000W/m^2 and at CR = 500x. Temperature dependence has been predicted for cell efficiency and heat power generated from incident solar power. The modelling results are compared with commercial CPV cell at a temperature of 25 – 80ºC.

A numerical simulation of a three-dimensional FEM with thermal model is coupled with an electrical model at both transient and steady state. Hence, the stationary and transient model is performed, in order to understand thermal performance behaviour and characterisation. The model was developed by using live-link, both electrical and thermal, in order to solve the numerical 3D model and 1D plot. The steady state occurs when cell temperature remains constant i.e. no change in temperature with time.

A transient model is a model that contains a dependent variables that changes over time, such as in the heat equation or an electrical equation. In addition, this is known as a dynamic model, time-dependent model or unsteady model [168].

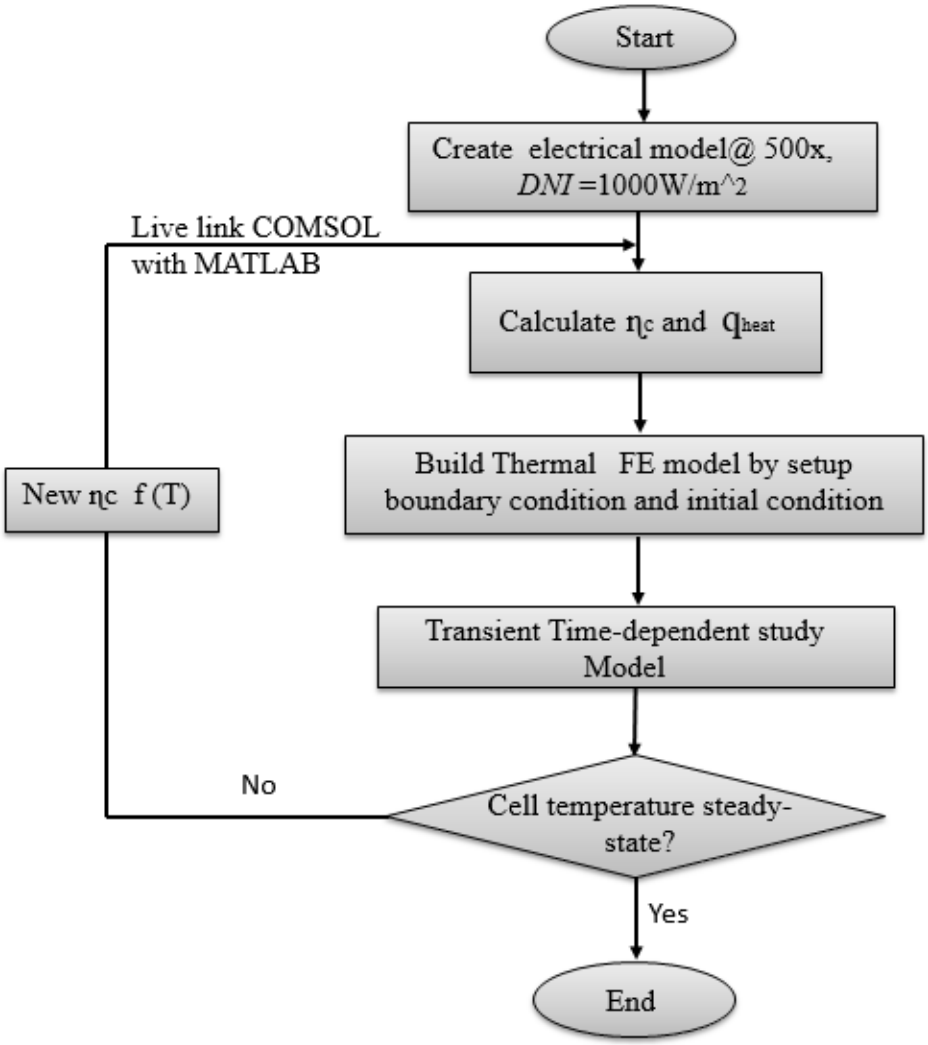

Figure 6-1 Flow chart of the transient modelling process.

6.3 Numerical modelling

6.3.1 Triple-junction cells electric model

The electrical model is the cornerstone on performance evaluation and energy generation of PV solar cells. A solar cell is a semiconductor material based on *p-n* junction designed to produce current by absorbing the light of energy photons. Performance evaluation of solar cells is dependent on parameters of voltage-current characteristics. Triple-junction solar cells are made of III–V materials, and it's consistent of three-layer cells of GaInP/GaInAs/Ge monolithically stacked. It is important to determine the current density generated by the cells, as given by Eq (49) [122].

$$J_{sc,i} = CR.\int_{\lambda 1}^{\lambda 2} SR_{i(\lambda)}.\eta_{opt(\lambda)}.G_{(\lambda)}.d\lambda \tag{49}$$

Where *CR* is a concentration ratio of 500x and *SR* is the spectral response and η_{opt} is the optic efficiency. The overall current is determined by the light-induced current from the diode dark current and is given by Eq (50). The open circuit voltage (V_{oc}) can be given by the relationship (51):

$$J = J_o\left(\exp\frac{q(V + J.R_s)}{n.K_b.T_c} - 1\right) - J_{sc} \tag{50}$$

$$V_{oc} = \frac{n.K_b.T_c}{q}\ln\left(\frac{J_{sc}}{J_0} + 1\right) \tag{51}$$

Where n is the diode ideality factor, K_b is Boltzmann constant, T_c is temperature, q is the electron charge, R_s is a series resistance and J_o is the reverse saturation current. The voltage output of the entire cell is the sum of the three layers. The total current is determined by limited the lowest photocurrent generated by three layers. The Fill Factor (*FF*) is the ratio of the maximum output power P_{max} from the solar cell divided by open circuit voltage and short-circuits current as given in Eq (52):

$$FF = \frac{P_{\max.}}{V_{oc}.J_{sc}} \tag{52}$$

The electrical efficiency of the cell (η_{el}) is quantified by dividing power output by power input, as given by equation (53). Where P_{out} is a delivered power and P_{in} is the amount of incident power in the solar cell.

$$\eta_{el} = \frac{p_{out}}{p_{in}} \tag{53}$$

Cell efficiency, η_c, as a function of temperature can be calculated by equation (54) [164, 165]. Where η_{el} is cell electrical efficiency for the concentration ratio, β_η is efficiency temperature coefficient and T_o is reference condition temperature.

$$\eta_{c(T)} = \eta_{el}\left[1 - \beta_\eta(T_c^* - T_o)\right] \tag{54}$$

6.3.2 Thermal FEM model

Thermal FEM modelling utilises COMSOL Multiphysics, which is iteratively solved by partial differential equations. In the FEM, the simulation starts by producing the geometry and divided it into finite elements. The “Heat Transfer in Solids” simulation physics is

used, in order to develop 1D and 3D dynamic thermal models. The aluminium oxide interlayer offers electrical insulation between the top and bottom sub-cell materials. To simplify the model, the electrical terminals and bypass-diodes are not considered in this model.

For optimum design of a CPV system from the perspective of conversion efficiency, the level of temperatures at a CPV system should be predicted and decreased as much as is possible. Therefore, to implement a heat transfer model it is essential to design a system, in order to investigate the variance in temperature and system performance. The thermal design is built on our understanding of the process of heat transfer, from assembly to unit level, by conduction, convection and radiation. Equation (55)[103, 161, 185], expresses the heat dissipation by conduction through the receiver of the solid component. Where (∂T/∂x) is the temperature gradient, K is thermal conductivity and q_{con} is conduction heat transfer.

$$q_{con} = -K.A_s \frac{\partial T}{\partial x} \tag{55}$$

The amount of heat that is dissipated by convection from the surface to the air is expressed in equation (56), which is known as Newton's law of cooling.

$$q_{conv} = h_{conv}.A_s.\frac{\partial T}{\partial x} \tag{56}$$

The heat loss by radiation transferred heat by electromagnetic waves to the environment is expressed by equation (57). q_{rad} is radiative heat flux, T_s is surface temperature, ε is surface emissivity and σ is Stefan-Boltzmann constant.

$$q_{rad} = \varepsilon.\sigma.(T_s^4 - T_{amb}^4) \tag{57}$$

Thermal equilibrium with the surrounding environment occurs in the electronic device, when it is not under operating conditions, and at the temperature of the surrounding media. Although when the device is active, the components' temperature and the solar cell device begin to increase due to the absorption of heat. The temperature of the device stabilises at the point when heat generated equals the heat released throughout the cooling mechanism. At that point, the device has reached steady state operating conditions. The period during the warming-up, when the component temperature rises up is called the operation transient period [180].

6.4 Results and discussions

6.4.1 Temperature-dependent on cell efficiency

The solar cells generate heat and an electrical source in CPV, because of the optical ray's concentration on a focal point. In a series connection the PV module's efficiency is limited as temperature increases. A solar receiver assembly usually contains a bypass diode, which will override the cell to avoid overheating, which leads to a reduction in module efficiency [154, 158].

The current model accounts for the temperature dependence of the solar cell's efficiency and the effects over time i.e. T =25 – 80°C, although the trends of efficiency decrease linearly as the temperature increases. The normalised temperature coefficients of the conversion efficiency ($\Delta\eta/dT$) of the triple junction solar cell is 0.047% [186]. The variation of efficiency with temperature is shown as a linear relation between temperature and efficiency, as illustrated in figure 6-2.

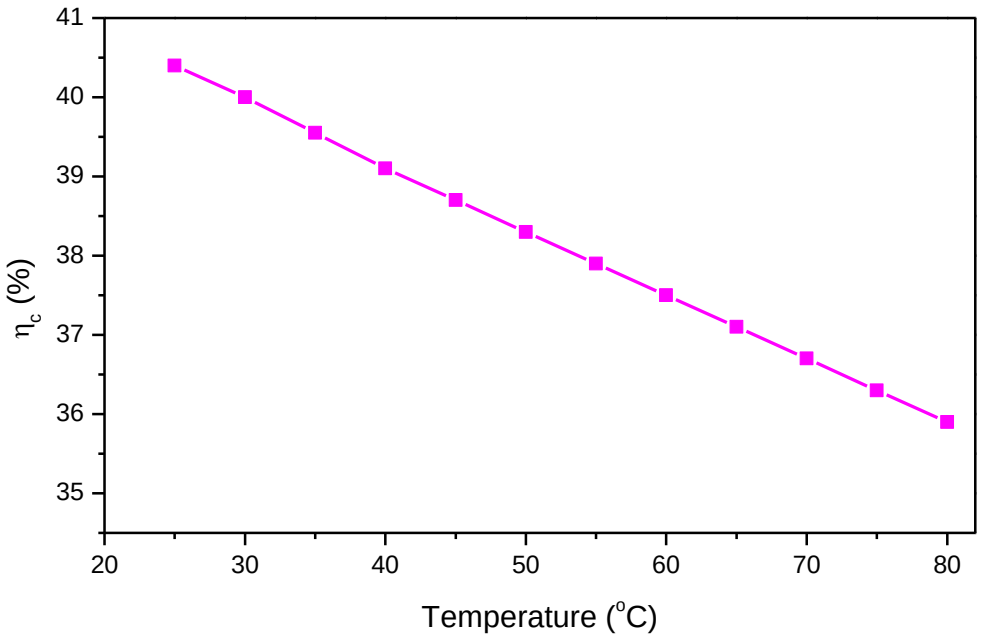

Figure 6-2 Temperature dependent on cell electrical efficiency as a function of temperature from 25 – 80°C at CR of 500x.

This study considered the transient response to a step input from unilluminanted to being subjected to concentrated (500x) sunlight. During the process of the solar concentration the uniform light of solar radiation is concentrated onto a small area. The thermal gradient is affected by the temperature difference between the edge, and centre, of the solar cell.

That is due to the difference in heat dissipation from conduction and convection heat transfer [117, 187].

Initially, as the cell temperature rises, the cell material's band gap decreases, hence a larger portion of the incident spectrum can be absorbed by the hottest region. The effect of the temperature rises are decrease the operating efficiency of the solar cells. The current mismatch can happen between several regions of a cell operating at different temperatures. The generation of thermal energy at every layer cell in GaInP/GaInAs/Ge triple-junction solar cells is higher in the bottom subcell Ge [188].

6.4.2 Validation

This proposed model is verified by using data from a commercial CPV cell. It is detailed the conversion efficiency as a function of temperature from 25 – 80^{o}C versus concentration ratio. The measured data from AZUR-SPACE Solar Power GmbH, as shown in Figure 6-3 [186]. Table 6-1 summarises a comparison between this study, modelling and measurement of efficiency at a temperature of 25^{o}C. The results show the efficiency deviation of about 0.8% found at 25^{o}C, and about 2.5% at a temperature of 80^{o}C.

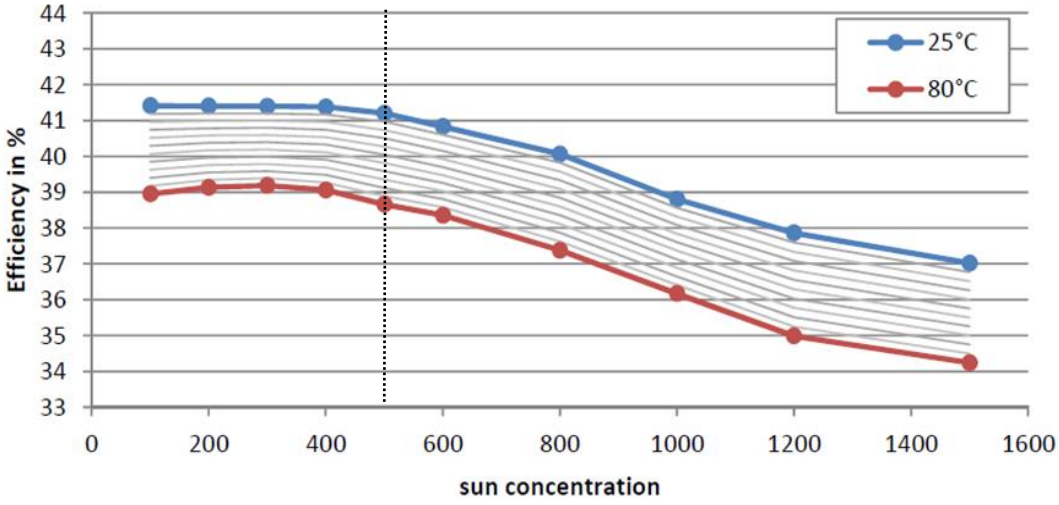

Figure 6-3 Measurement data of the performance curve of 3C42A, 2014 for different concentration ratio verses efficiency at a variable operating temperature [186].

Table 6-1 Comparison of cell efficiency resulted from this modelling and between empirical data extracted from 3C42A, AZUR–SPACE and current model at 500x.

Temperature (^{o}C)	**AZUR-SPACE η_c** [186]	**Current model η_c**	**Deviations (%)**
25^{o}C	41.2%	40.4%	0.8
80^{o}C	38.5%	36%	2.5

6.4.3 Heat power

The main reason for the decrease in cell efficiency at high concentrations is attributed to the temperature rise. The heat power (or heat flux), is the heat generated on the top of the solar cells as a result of optical concentration. The heat power as a function of temperature are considered in this study for a temperature range from 25 – 80°C. Under concentration, the heat power generated by the solar cell is quantified by the given equation (58) [99, 166].

$$q_{heat(T)} = DNI.(1-\eta_c).A_c.CR.\eta_{opt} \tag{58}$$

Temperature-dependence on heat power can be predicted (q_{heat}) based on the efficiency temperature dependence. It indicates that a decrease in the heat power due to an efficiency drop results in an increase in temperature as shown in figure 6-4, where the *DNI* is taken as a constant value of 1000W/m^2 and *AM* 1.5D, the η_c is variable with cell efficiency as a function of temperature.

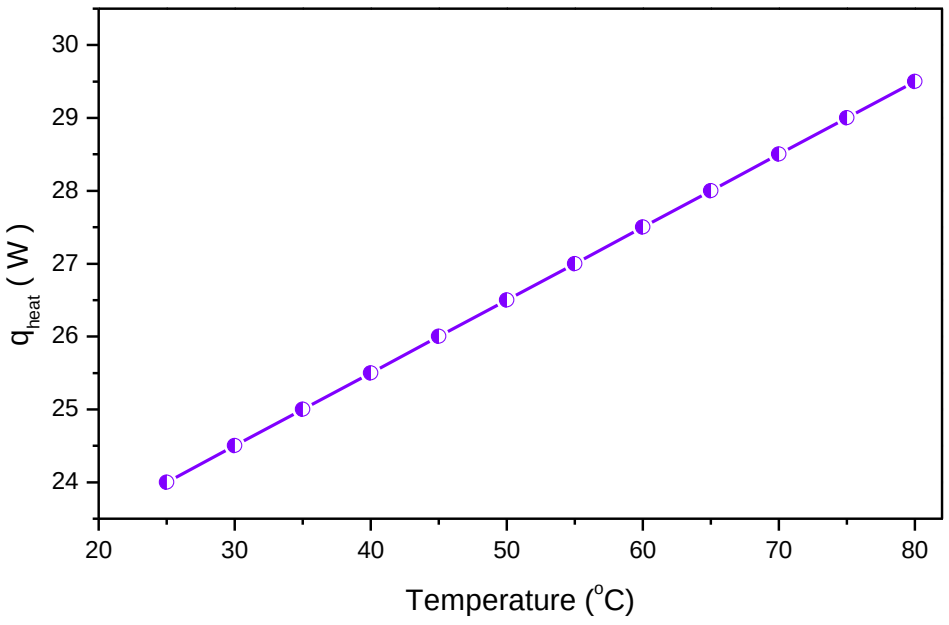

Figure 6-4 Temperature dependent on heat power generated by the temperature of the cell from 25 – 80°C.

6.4.4 Receiver geometry and boundary condition

The boundary conditions in the solid domains are applied. The model geometry of a receiver assembly is attached to a BCB carrier. Using the multi-junction solar cell's heat source at CR = 500x, the heat power is generated by the portion that is not converted to electricity. Heat transfer in the solid state is due to the material's thermal properties. A

convective heat transfer boundary condition has been applied to the backside of the plate, h_{conv} = 1400W/m^{2}K. The ambient temperature around the receiver is also considered constant at 25^{o}C. Figure 6-5 shows a 3D receiver structure and the selected point at the centre of the cell for the 1D single plot.

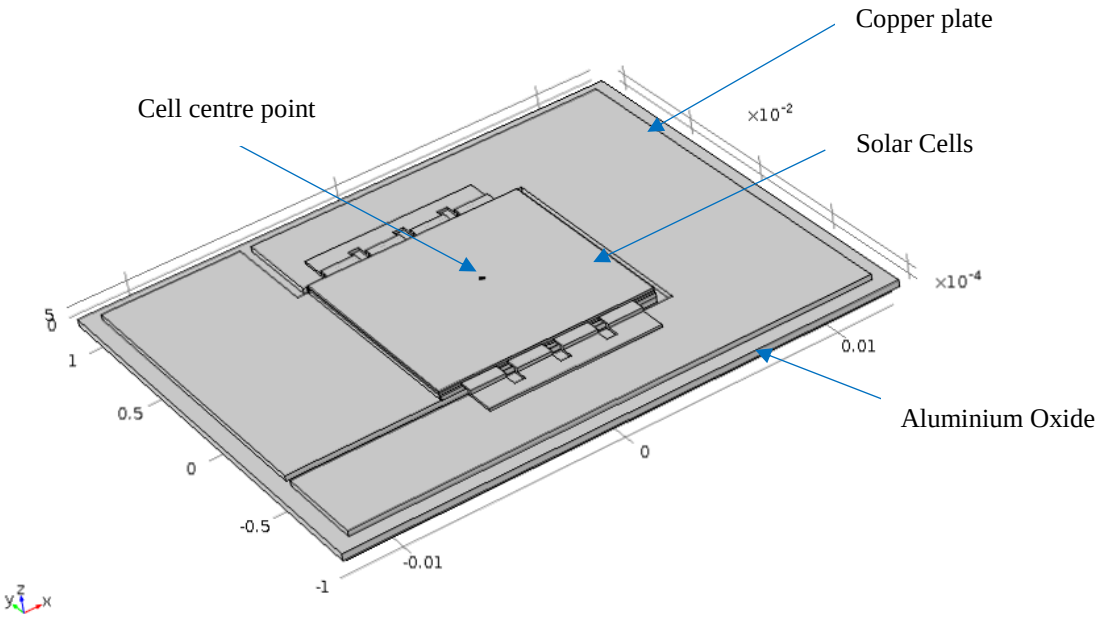

Figure 6-5, 3D structure of receiver assembly.

6.5 Thermal response analysis

In this simulation, the model is run twice, once by using a stationary cell efficiency study, and another by dynamic cell efficiency. Thus, the time-dependent model is beneficial in comprehending the heating time required by the cell to reach the steady-state condition. The dynamic model comprises of a series of steady state model, where the time step between successive steady-state models becomes a factor.

Based on the FEM model, the initial and boundary condition are set. As a result, electrical efficiency decreases as a function of temperature, which corresponds to the increase in heat power generated. Therefore, this approach gives an overview of understanding the device's transient performance. Most of the heat is densely focused in the centre of the solar cell and decreases gradually towards the receiver assembly edge. Figure 6-6 shows a graph of steady-state temperature, so Δt is optimised for different times (1,5,10s). The initial cycle is at 0s, the cell efficiency is 40.4%; whereas the last cycle, at a steady state condition, the cell efficiency is 36.5%.

In this model we consider a uniform illumination on the cell surface. The actual heat dissipation distribution is non-uniform across the receiver. Basically, the heat is transferred through the PV cell's solid layers by conduction. Thus, the heat conduction most intense at the cell's centre, although at the edge of the cell, conduction and radiation heat transfer does take place. Eventually, the heat is dissipated to the surrounding environment by convection and radiation heat transfer.

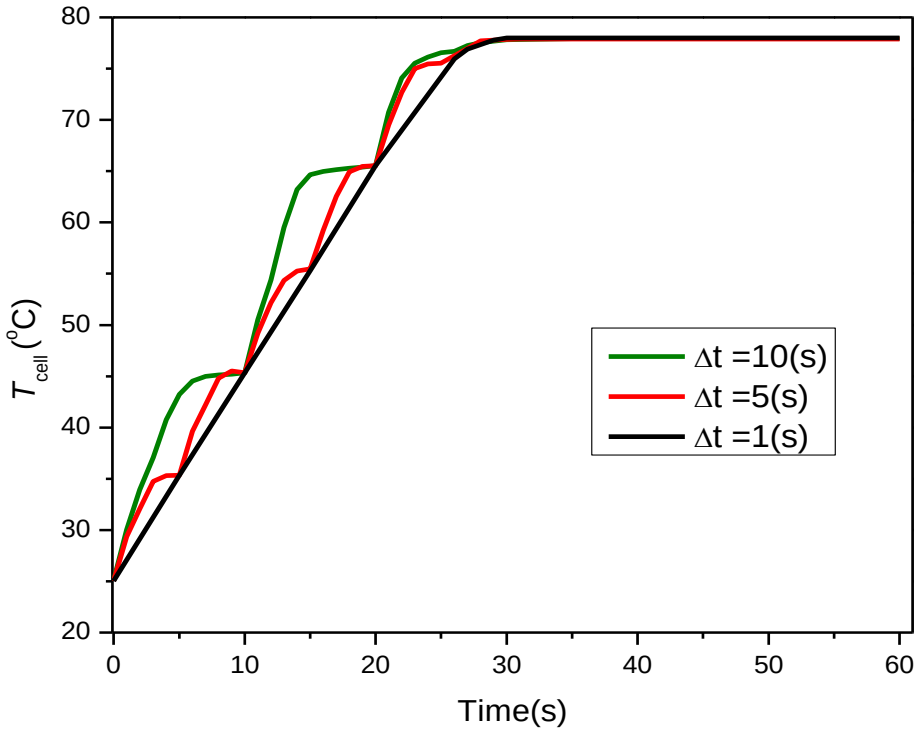

Figure 6-6 Transient model and steady state, this to determine steady-state maximum cell temperature.

Here, the time-dependent model is run at various times (Δt), the intervals were from (0 – 60s). The heat power is transient with time; thus, times stepping is optimised for three different times. When the time-dependence is long (i.e. Δt = 10s), the ΔT is large, and the transient efficiency values will be greater. While at a short transit time-dependence (i.e. Δt = 1s), the ΔT is small and the transient efficiency tends to be smaller.

The error ratio between the dynamic efficiency with constant efficiency is calculated. Integrated Error (IE) from (0 – 60s) is about 12%, from an initial temperature of 25°C, to a steady-state temperature, which occurred at around 30s; hence, maximum cell temperature is 78.4°C. The Maximum Error Point (MEP) is about 24% and occurs at 10s. In this model, cell temperature loops until reaching a steady state, although that steady state occurs when the transient cell temperature (T_{cell}) trend and adjacent cell temperature

trend = 0%, with a stationery efficiency of 36.5% and the initial temperature of 25ºC. Figure 6-7 shows the results of comparison between the steady-state temperature for both constant and dynamic efficiency.

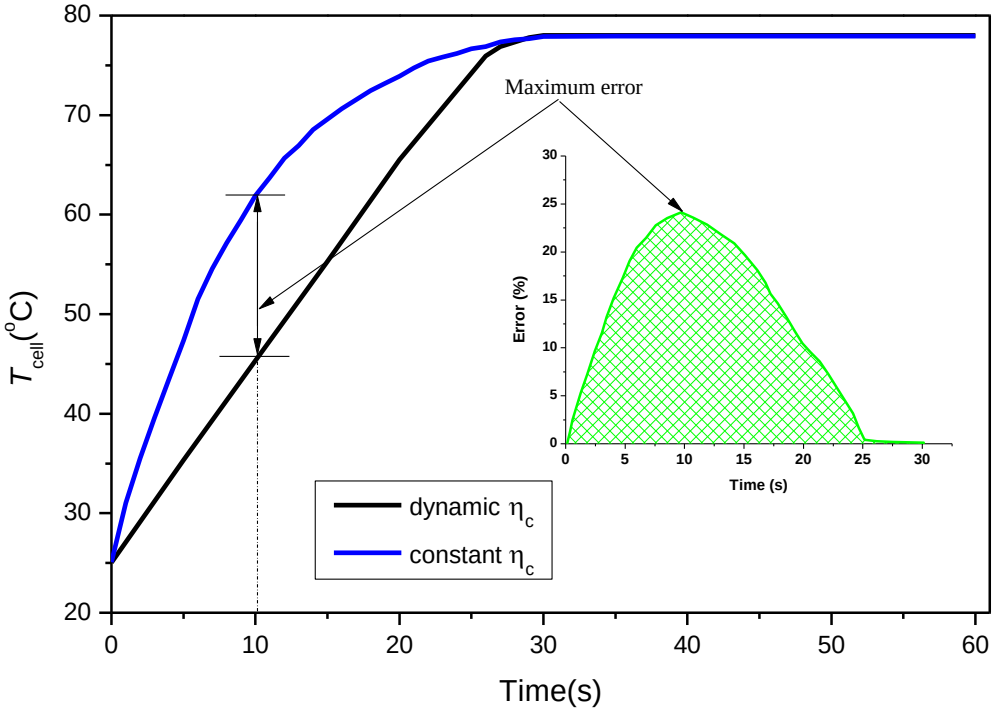

Figure 6-7 Transient model results in steady-state maximum temperature for both constant efficiency and dynamic efficiency.

The receiver assembly is simulate by considering a transient thermal model, for time intervals from 0 – 30s. From modelling, results of different intervals, of temperature and distribution patterns at 500x were obtained. Figure 6-8 illustrates a 3D of temperature distribution patterns at CR = 500x and h_{conv} = 1400 W/m^{2}K.

In this modelling simulation, it is well-known that the thermal response of the assembly is based on convection from the back of the receiver and environmental conditions. The thermal performance behaviour response is guided by the ability to dissipate heat from the back of the receiver. It is important to mention in Concentrating Photovoltaic (CPV) effective cooling system, or thermal management, can enhance the efficiency. Here, the changes of different time intervals shows the thermal response in transient and steady state.

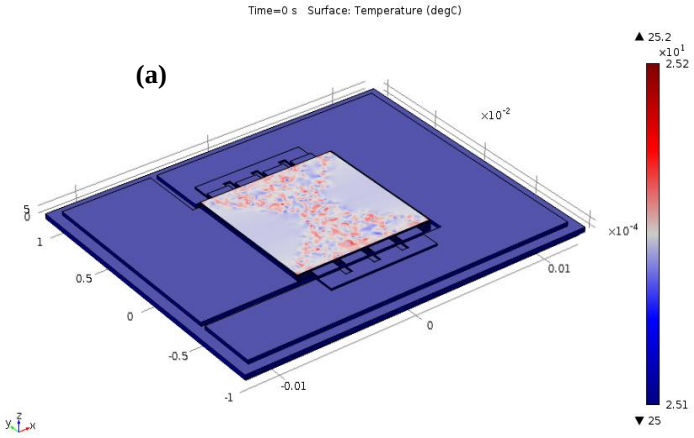
Time=0 s Surface: Temperature (degC)
(a)
▲ 25.2
×10¹
2.52
2.51
▼ 25
×10⁻²
×10⁻⁴

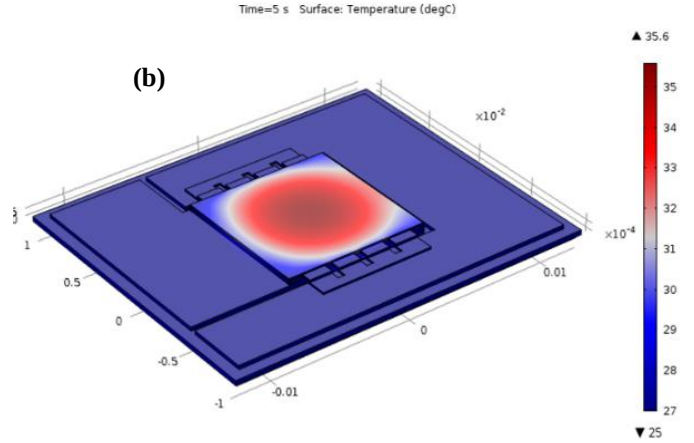
Time=5 s Surface: Temperature (degC)
(b)
▲ 35.6
35
34
33
32
31
30
29
28
27
▼ 25
×10⁻²
×10⁻⁴

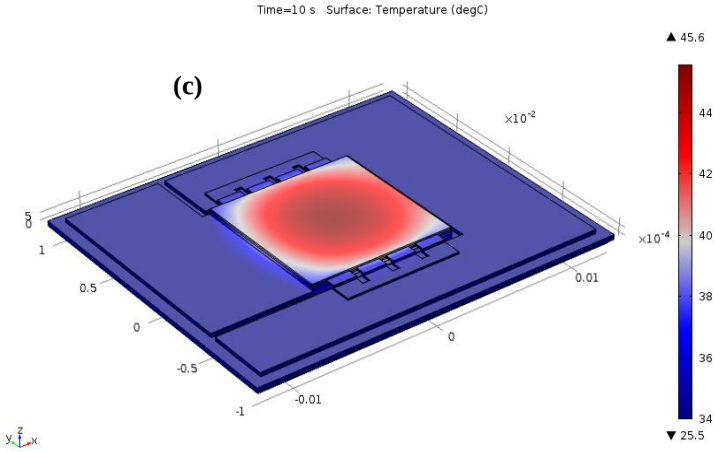
Time=10 s Surface: Temperature (degC)
(c)
▲ 45.6
44
42
40
38
36
34
▼ 25.5
×10⁻²
×10⁻⁴

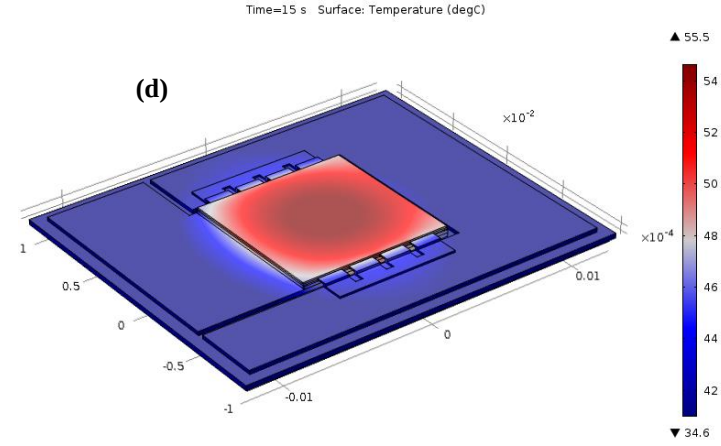
Time=15 s Surface: Temperature (degC)
(d)
▲ 55.5
54
52
50
48
46
44
42
▼ 34.6
×10⁻²
×10⁻⁴

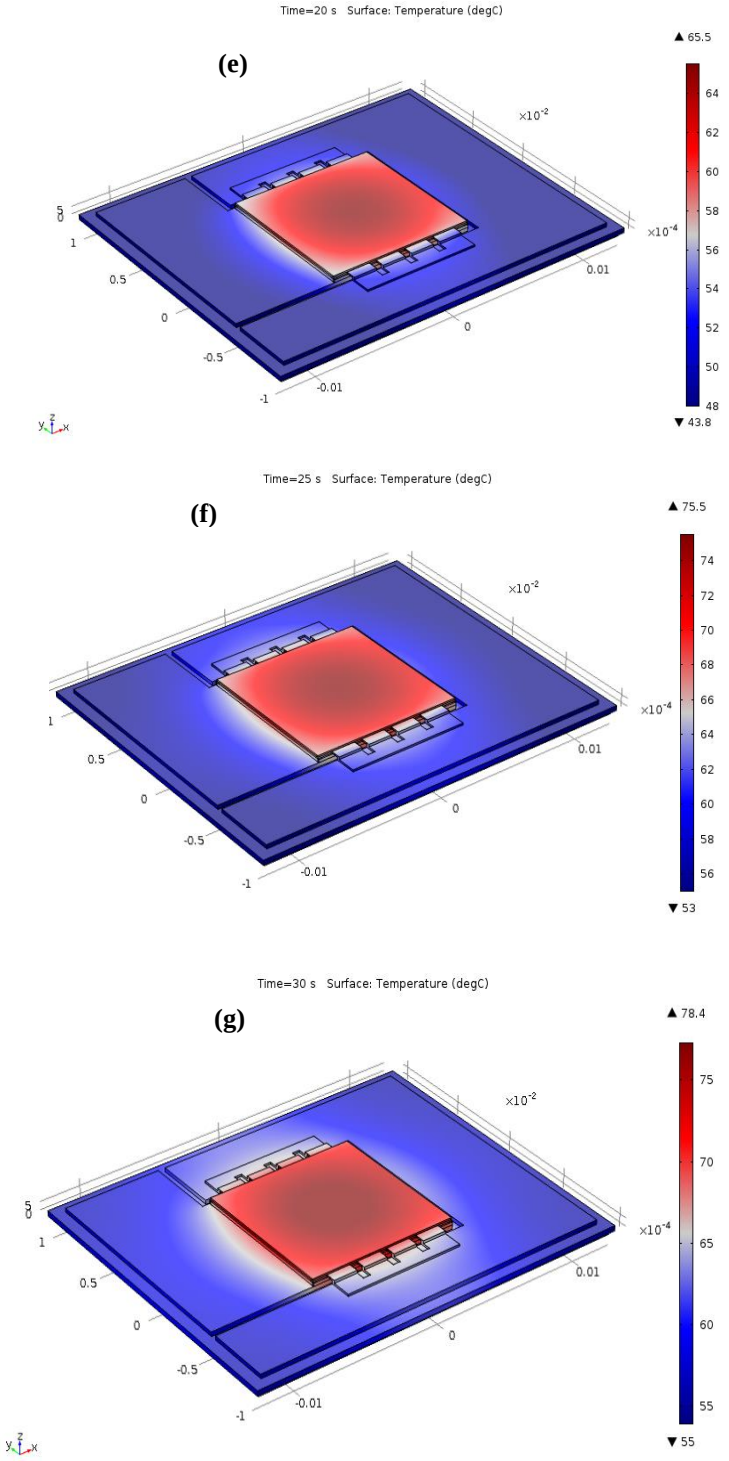

Figure 6-8, 3D Temperature profile distribution patterns of the dynamic efficiency of receiver assembly for different intervals (a, b, c, d, e, f, g) time prospectively (0, 5, 10, 15, 20, 25, 30 seconds).

The utilising of the thermal dynamical model for the photovoltaic systems is justified, due to the significance of unsteady state system differences on time scales in order of

seconds. It is important for the behaviour of control strategy and the efficiency that in turn directly affects the quality of posted energy [183].

In order to determine the cell temperature, a three-dimensional model (3D) of temperature profile distribution on multijunction solar cells receiver is visualised. Figure 6-9 shows a temperature profile distribution model at constant efficiency, the steady-state at constant cell efficiency. For a time period of 0 – 60s, the constant efficiency used in this model is approximately 36%, the stagnation cell temperature is 78.4 ^{o}C, and occurs at 30s. The final maximum cell temperature at dynamic efficiency was similar to that reached in constant efficiency with dynamic efficiency.

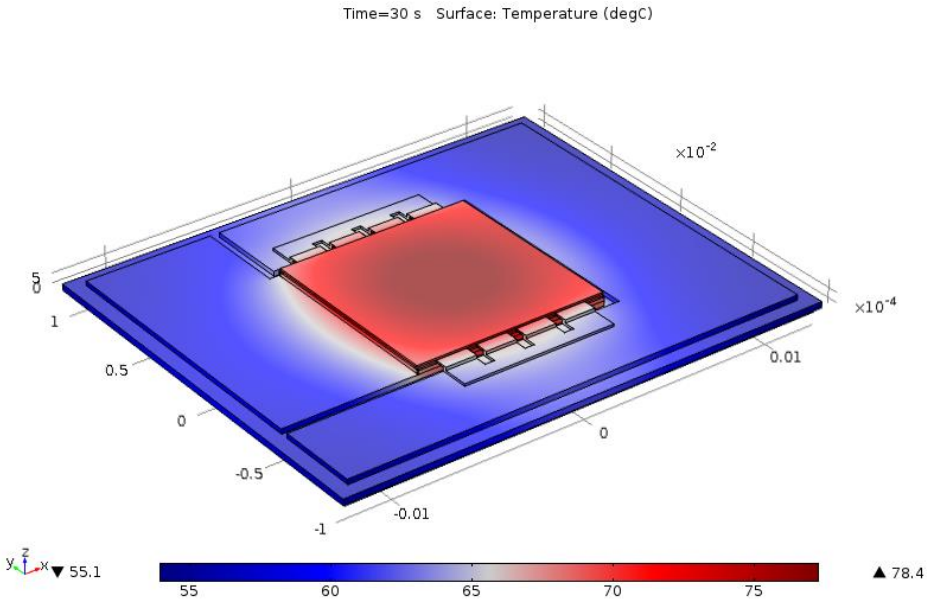

Figure 6-9, 3D temperature profile distribution, steady-state model at constant efficiency.

In the three-dimensional model, the temperature distribution of the triple-junction cell needs an accurate light profile, since overall input with comprehensive information on a material temperature is dependent on parameters such as energy band gap, absorption, etc. for semiconductor materials with a stack of multi-junctions. Hence, the presence of the 3–D model will help in predicting regions of the solar cell which have malfunctions as the effect of high temperatures [117].

6.6 Analysis of electrical parameters response

In steady-state conditions, the entire heat generated by the assembly is transferred to the ambient environment. Thus, the optimum thermal management mechanisms reported for CPV application at 500x, might include a heat spreader, heat sink, micro-channel, jet impingement and liquid immersion. Therefore, the predicted cell temperature is approximately 78.92^{o}C, which was achieved on solar cell [189].

The cell performance is very sensitive to temperature increases, which are simulated in transient methods. In figure 6-10 when the solar cell's performance parameters are decreased as temperatures increase, the temperature dependence on the short-circuit current density (J_{sc}) slightly increases over time until the temperature reaches a steady state, at 30s, as shown figure 6-10 (a).

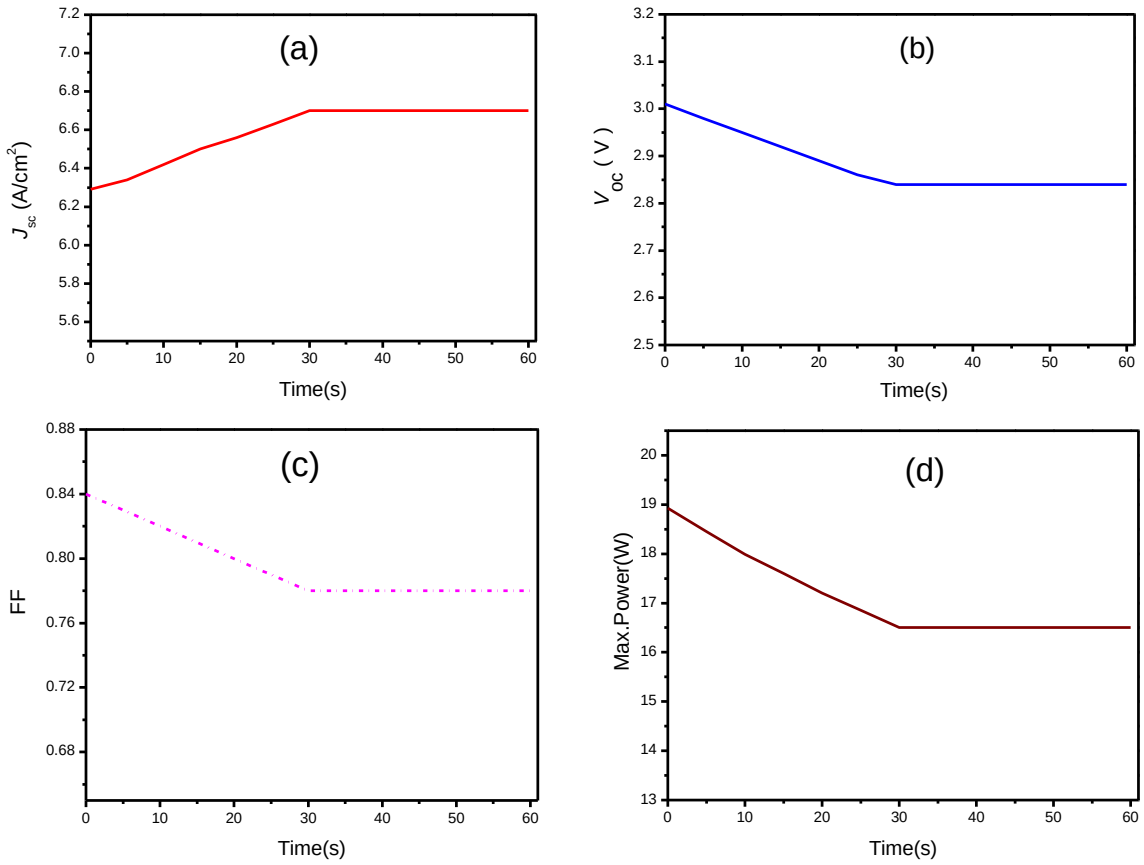

Figure 6-10 Electrical parameters versus to cell steady state condition at 500x, (a) Current density versus time (b) open circuit voltage versus time (c) fill factor verses to time (d) maximum power point verses to time intervals.

The temperature dependence on the open circuit's voltage (V_{oc}) decreases over time as shown in figure 6 -10 (b). The fill factor, also, decreases as cell temperature increases (figure 6-10 (c)). The maximum power point also drops as temperature increases with time until stagnation temperature stabilises (figure 6-10 (d)).

Figure 6-11 illustrates the overall solar cell's conversion efficiency using the time-dependent temperature, where it tends to decreases to a steady state. The efficiency in a time-dependent pattern drops from 40.4% (at 0s) to steady-state efficiency of about 36.4%, which occurs at 30s. Accordingly, the high temperature proven is a reason leads to decreases on the conversion efficiency and details of that observed on the process of dynamic losses.

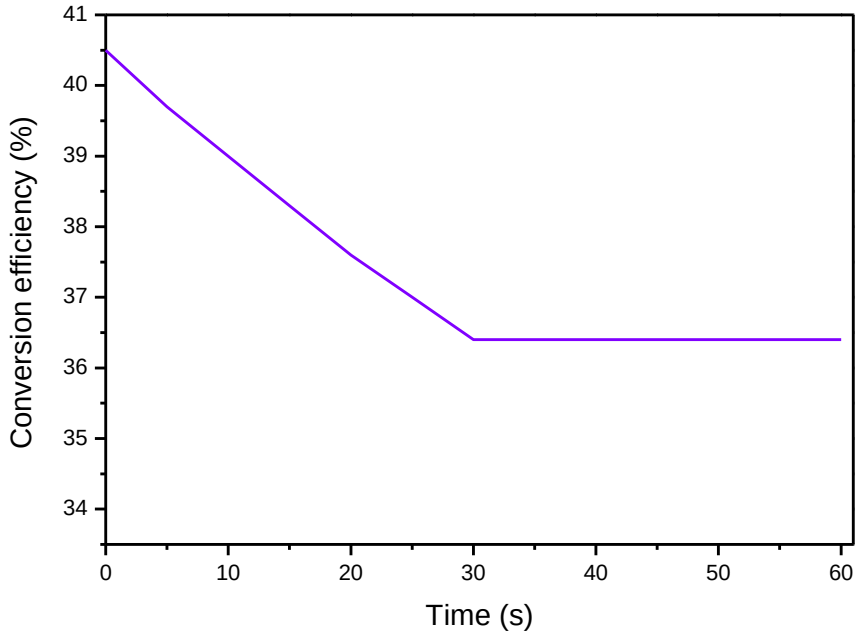

Figure 6-11 Conversion efficiency versus cell steady-state condition.

6.7 Effects of varying irradiance intensity on steady-state temperature

Knowing the temperature behaviour of multi-junction solar cells for various irradiations is essential for both the Earth concentrator applications and space applications [154]. Despite the impact of temperature on HCPV operating performance and system integrity, the modelling technique used predicts the range of operating temperature for various environment conditions, including, irradiance and environment temperature etc.

The performance of the solar cell is influenced by incident illumination and its operating temperature. Figure 6-12 depicts the solar cell steady-state temperature versus different values of *DNI*, the optimum time-dependent, selected at Δt =1(s). The high irradiance intensity of 1000 W/m^2 the steady state cell temperature was 78.4^{o}C at the time of 30s.

Hence, at an irradiance intensity of 700W/m^2, the steady-state temperature was about 67.5^{o}C at the time of 25s. Although at low values of irradiance intensity of 400W/m^2, cell steady-state temperature were 56.1^{o}C at approximately 20s.

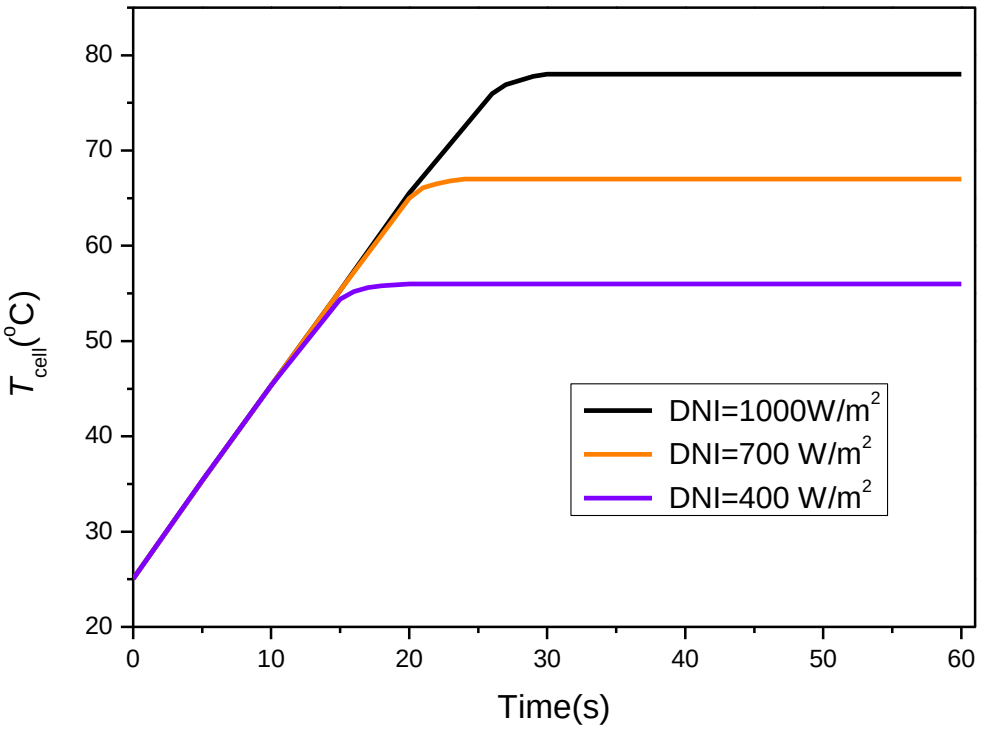

Figure 6-12 Effects of changes *DNI* in the maximum cell temperature at the dynamic efficiency of time for steady-state temperature.

The irradiance intensity has a significant influence on steady-state cell temperature. As the values of *DNI* changes (1000W/m^2, 700 W/m^2, 400W/m^2) the slope linearly increases; the regression was R^2 = 0.9996. The predicted cell temperature was variable (between 78.4 – 56.1^{o}C), the cell efficiency decrease sharply from 36.4% to 32.3%, as illustrated in figure 6-13.

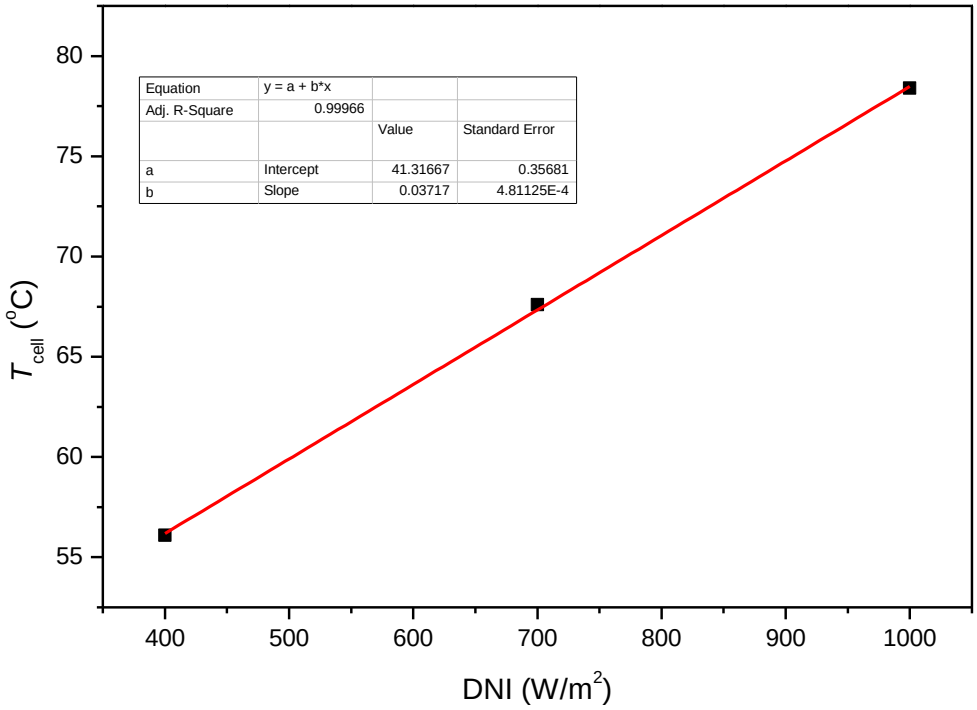

Figure 6-13 Different *DNI* versus to maximum cell temperature at steady-state temperature.

In summary, as shown, the increase of *DNI* leads to an increase in cell temperature as a result of increased heat flux and a reduction in conversion efficiency. Table 6-2 also summarises a comparison of different *DNI* steady states values. Nonetheless, to be taken into the account on the daily basis, the *DNI* values are variable between sunrise, midday and sunset. The cell's operating performance behaviour will change accordingly.

Table 6-2 Detailed variations of *DNI* for maximum cell temperature, steady-state conversion efficiency and time.

Parameters	***DNI* =1000 (W/m^2)**	***DNI* =700 (W/m^2)**	***DNI* = 400 (W/m^2)**
Steady state T_{cell} (^{o} C)	78.4	67.5	56.1
Steady state (η_c)	36.4	34.5	32
Steady state time (s)	30	25	20

Figure 6-14 illustrates the different values of *DNI* and their corresponding values of *AM*. As is significantly shown in the figure, there is a directly proportional relationship between these two parameters. In the real operating conditions on a daily basis, the values of *AM* and *DNI* are variable, from sunshine to sunset, and will be presented in the next chapter.

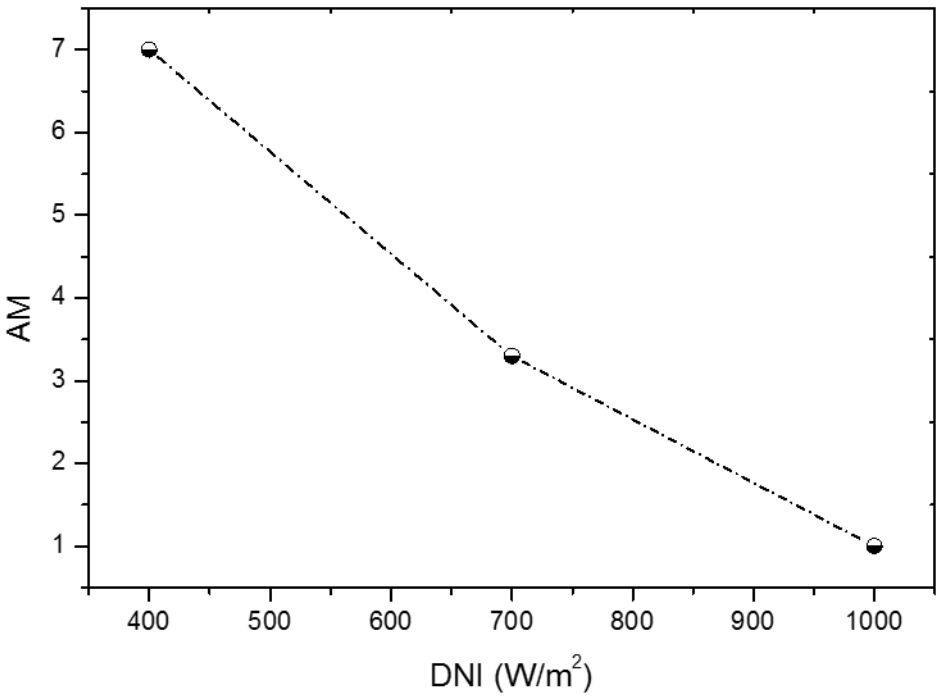

Figure 6-14 Represents the values of various *DNI* and corresponding *AM*.

6.8 Effects of varying ambient temperature in the steady-state temperature

The factor which is essential when considering the PV cell temperature is the ambient temperature, with regards to the variability of ambient temperature and its effect on the solar cells steady state temperature. In this scenario, when the DNI = 1000W/m^2 and the ambient temperature T_{amb} = 25^{o}C the steady state cell temperature is 78.4^{o}C for h_{conv} =1400W/m^{2}K. Furthermore, for T_{amb} = 35^{o}C, the steady-state cell temperature is 78.8^{o}C for h_{conv} = 1500W/m^2. For T_{amb} = 45^{o}C, the steady-state cell temperature is 79.2^{o}C and h_{conv} = 1600W/m^{2}K. Figure 6-15 illustrates the steady states cell temperature at a variety of ambient temperatures.

However, the predicated model can provide monitoring of the devices in order to have a better understanding of performance behaviour, which will enable proper selection of appropriate solutions for heat dissipation. The techniques to limit the influence of the operating temperature of the internal device are not assessed.

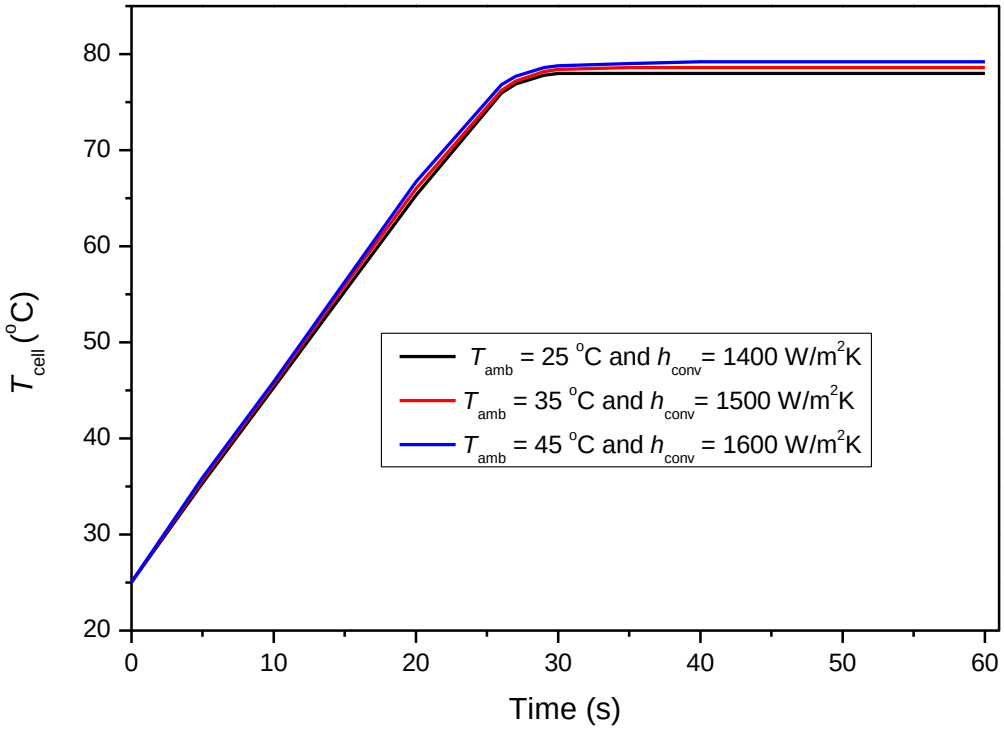

Figure 6-15 Steady states cell temperature at a variety of h_{conv} and ambient temperature.

Summary

This work has been simulated for both transient and steady-state temperatures, based on efficiency temperature dependence, in order to predict a cell's stagnation temperature. The final cycle of steady-state temperature occurs at a maximum cell temperature of 78.4ºC (within 30s) for 1000W/m^2, T_{amb} and h_{conv}. Through the dynamic model, it can estimate the impact of different incident powers on the power output of the photovoltaic device.

Performance of a solar cell are influenced via the incident light and cell operating temperature. The cell efficiency of a CPV system can be improved by introducing effective thermal management, or a cooling system. The multi-junction solar cells under Concentration Ratio (CR) of 500x used and the cell efficiency were variable with temperature dependent from 25 – 80ºC.

For a CPV module, the cell operating temperature is a main factor effecting cell efficiency, therefore, it is necessary to decrease the operating temperature in order to generate a higher output power of a CPV module in field operations. The consequence of a higher heat transfer coefficient leads to lower thermal resistance, which in turn lowers the operating temperature of the CPV cell/module.

This chapter also presents a summary of the developed multiphysics model, for PV performance prediction, which was used to simulate the thermal aspect. The heat transfer thermal physics is used on the Finite Element Method FEM of COMSOL Multiphysics model. Hence, transient analysis of the thermal and electrical is performed, and these collected notifications will be used to provide improved knowledge of CPV performance behaviour, in order to save the time of the simulation.

The developed transient model of a time-dependent study is used to characterise the behaviour of an HCPV receiver. A live-link technique of COMSOL with MATLAB was used to examine the thermal and electrical models for the steady-state. The performance behaviour of electrical parameters of the J_{sc}, the V_{oc}, the FF and conversion efficiency are studied. Also, in the proposed model, a dynamical efficiency compared with constant efficiency and Integrated Error (IE) is approximately 12%.

Chapter 7: Dynamic Characterisation of Thermal-Electrical Model and Coupling with Climatic Conditions

7.1 Introduction

This chapter presents and describes the performance simulation of the cell with the dynamic weather for daylight hours. In this case, we will exploit the weather data of Albuquerque, New Mexico, USA, to estimate the dynamic performance of the solar cell.

In previous chapters, we used *DNI* equal to 1000W/m^2 however this value is the peak flux. Therefore, in real operating conditions, on a daily basis, this value is varies with time from sunrise to sunset, where the maximum value is reached at solar noon, at the Sun's zenith.

The incident power has a big effect on cell temperature and energy produced by the cell. The yearly energy generation at real operating status is the more accurate norm for solar cell performance. Therefore, optimisation of cell performance for a particular standard solar spectrum is different from the optimum for yearly electricity generation.

Theristis *et al*.[190] investigated a concentrating triple-junction solar cells in real solar conditions. In their numerical study, the effects of solar spectrum distribution change, due to atmospheric parameters such as aerosol optical depth, perceptible water and air mass were reported. In addition, case studies were performed in four locations in the US; the typical meteorological year was used to estimate the thermal and electrical performance of III-V cell at 500x.

García-Domingo *et al*.[123] analysed the influence of atmospheric conditions on the electrical behaviour of the CPV module. The measurement of outdoor parameters were considered (*DNI* spectral distribution, T_{amb} and W_S). Consequently, this model allows for a prediction of the maximum power produced by the module under specific working atmospheric conditions. Further to these studies, the current research will predict the cell temperature variations daily, and over the year, for dynamic values of *AM*, T_{amb} and *DNI*. Also, based on that, the dynamic electrical performance response is characterised to predict the magnitude of a device's energy yield.

7.2 Model approach

Meteorological data collected from Albuquerque will be used in this study *DNI, AM,* T_{amb} for three days at the unclouded and cloudy sky are considered to evaluate the performance of a triple-junction solar cell under such conditions. Based on the transient model in chapter-6, the electrical model promoters of CR = 500x are used. The convergent efficiency is considered for predicting the amount of heat power generated as a function of *AM, DNI* on daily basis hours.

To predict cell temperature, as a function of *AM*, *DNI*, T_{amb} values, a thermal model was developed in MATLAB. The ambient temperature is taken into account in the prediction of the cell operating temperature for a range of h_{conv}. Additionally, a steady state thermal model was developed using a Finite Element Method (FEM) in COMSOL Multiphysics. The boundary conditions are the same as in the transient model.

7.3 Daily variation of Atmospheric Parameters

In this part, metrological weather data is considered (*DNI, AM,* T_{amb}) for cloudy and clear skys. This data was taken by measuring every 60 seconds for diurnal hours of Albuquerque, New Mexico, USA. The measurement of weather data for the aforementioned city is given courtesy of Marios Theristis, which was partially presented in his PhD thesis. For the three days (25/3/2015, 26/6/2015 and 3/8/2015), the data was acquired for all daylight hours. During these days, there were two days of a variation in the stochastic cover cloud, which resulted in a lower level of solar irradiance; and on one day, there was sunshine with a clear-sky.

The characterisation of the performance of the photovoltaic panels does not take into account the effects of such environmental factors as insulation level, solar spectrum, and other meteorological conditions. It is important, in the performance characterisation of photovoltaic solar cells, to consider the impact of the solar spectrum, the surrounding environment.

The solar spectrum is influenced by atmospheric parameters such as clouds, aerosol and perceptible water vapour, but the main factor that affects the solar spectrum is air mass, which subsequently affects the multi-junction solar cell's performance [191]. Increases in air mass weaken the solar irradiance over the entire short-wave spectrum, however, the relative weakening is greater in the spectral region of the top junction sub-cell [192]. The

height of the sun affects the *AM* and increases the scatter in the blue region. The increase of *AM* leads to significant deformation of the solar spectrum comprising global sunshine [124].

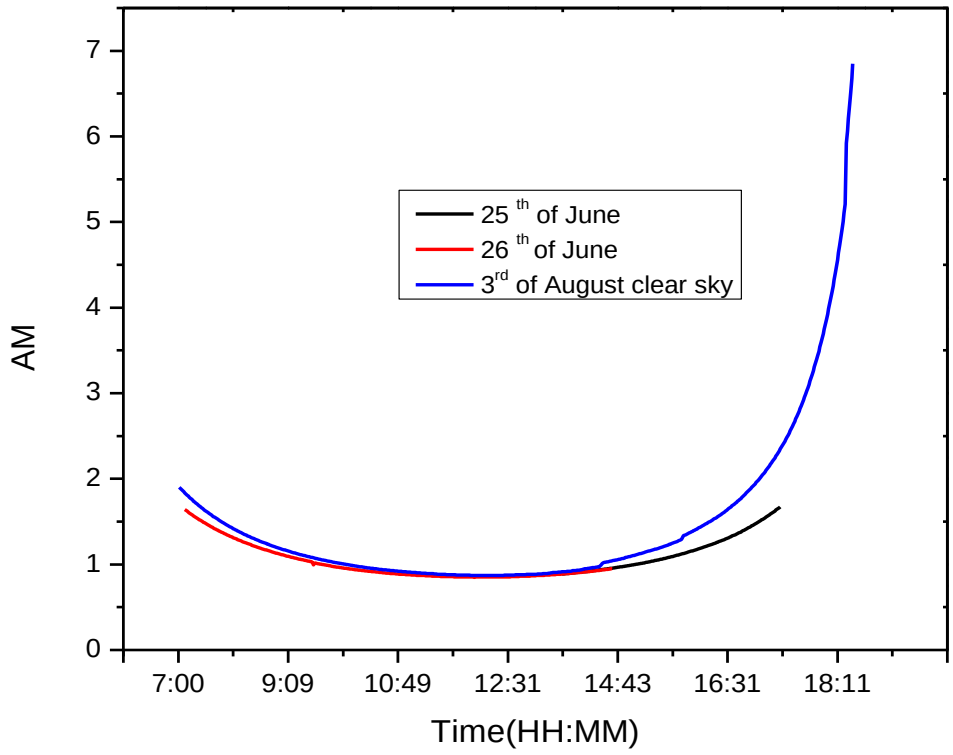

Figure 7-1 Variation of air mass *AM* versus daytime.

The *AM* is a measure of the atmospheric depth crossed by solar radiation. For clear-sky and cloudy weather measuring it is apparent, from the lower *AM* = 0.8D, that measuring at midday is the best choice for an optimized performance of cells, although during the morning and evening time the values of *AM* are significantly higher. Therefore, *AM* had significant effects on the wavelengths of solar radiation, also the magnitude of *DNI* at midday shows an optimum value. Figure 7-1 shows the variation of air mass versus daytime.

"The Clear-sky irradiance represents the global and direct irradiances-respectively, that are available at the Earth's surface for the considered location and time period in the absence of clouds" [193, 194]. It represents the boundary conditions with which the satellite-derived cloud-attenuation signal is superimposed. The Clear-sky irradiance is a function of Extra-terrestrial irradiance, with the position of the Sun in the sky quantified by the solar-zenith angle, and elevation above sea level [193].

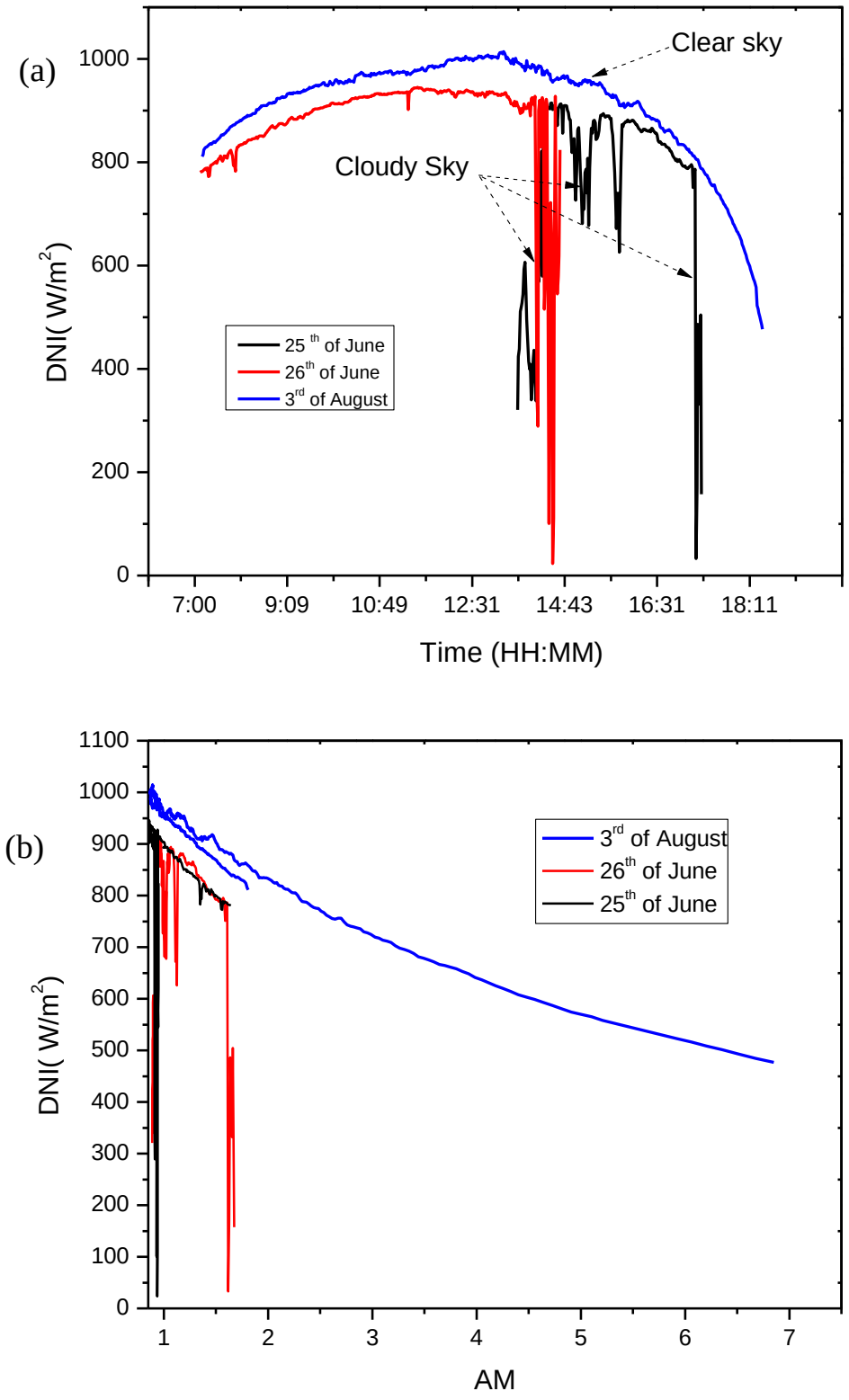

Figure 7-2 Daily metrological data (a) *DNI* versus daytime (b) *DNI* verses to different *AM* Air Mass values.

The variation of *DNI* daily profile data is presented at clear-sky and partly cloudy conditions; the *DNI* magnitude has a gradual increase from sunup until noontime, where

it reaches the peak. The afternoon time show that values began to decrease gradually until sunset. Figure 7-2 (a) illustrates daily metrological data of *DNI* versus daytime.

The variation of *DNI* on a daily basis with corresponding *AM*, gives an inversely proportional relationship, therefore as the values of *DNI* increase, the corresponding *AM* decreases. Figure 7-2 (b) illustrates the daily metrological data of *DNI* versus differences in *AM* Air Mass values.

The ambient temperature varied from a minimum value of 21°C (at sunrise) to 36°C peak (at midday). The environmental temperature is one of the parameters that play an essential role in PV performance. Figure 7-3 illustrates the fluctuation of the ambient temperature of the diurnal hours.

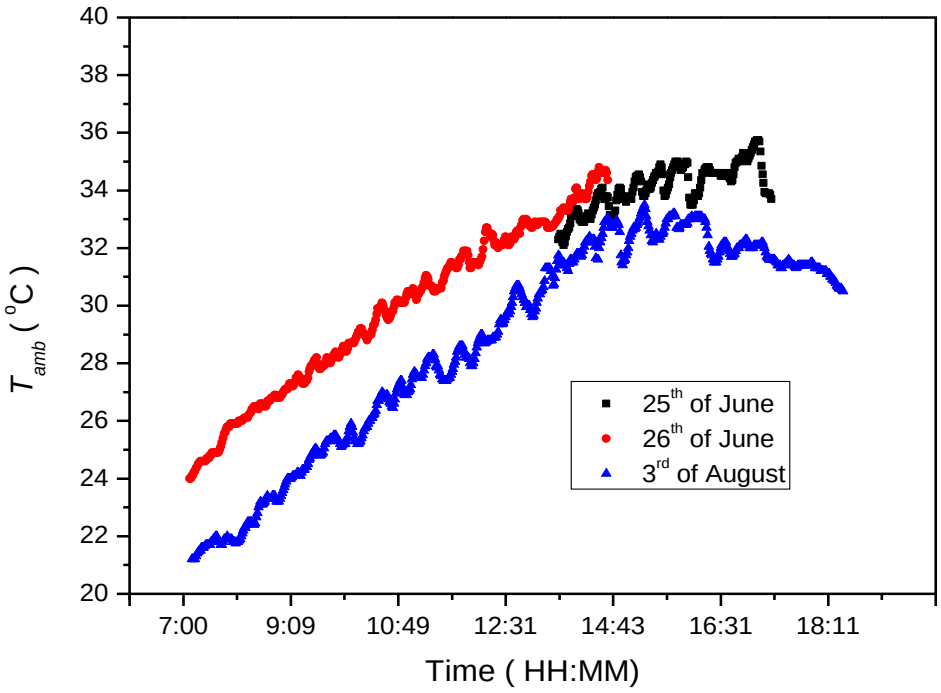

Figure 7-3 Ambient temperature versus daytime.

7.3.1 Effects of clouds on PV performance

The maximum amount of Direct Normal Irradiance (*DNI*) is taken into the account in this study: the *DNI* under a clear sky is typical for air transparency, while the mean of *DNI* represents the impact of the reflection of the clouds; the clouds arbitrarily affect the maximum ratio of *DNI*, despite the height of the Sun [124]. Besides, the average of the atmospheric clearness during the day can be determined by relative clearness index [195].

7.4 Thermal dynamic characterisation

The calculations illustrate the theoretical performance of triple-junction cells, nevertheless, the cells are sensitive to fluctuations of the solar spectrum. The heat power or heat flux is the magnitude of incident power on the top of the solar cells as a result of optical concentration. Heat power predicted (q_{heat}) is dependent on *DNI* and *AM*. Dynamic heat power generated by the solar cell is quantified by the given equation (59). It indicates that the heat power is influenced by *DNI* changes, so higher *DNI* results in higher q_{heat} values; through diurnal hours the peak is reached at midday (noon) time as illustrated in figure 7- 4 (a). The predicted heat power is also plotted versus the solar irradiation *DNI*, consequently, the lower values of *DNI* results in lower values of (q_{heat}) as illustrated in figure 7- 4 (b).

$$q_{heat(AM,DNI)} = DNI.(1-\eta_c).A_c.CR.\eta_{opt} \tag{59}$$

Where *DNI* is daily variable direct normal irradiance, η_c is conversion efficiency, and η_{opt} is the optic efficiency. The cell conversion efficiency is taken from a section 3 – 5 model results at CR=500x. To predict a dynamical cell temperature, the Equation (60) [173, 190] is used, where variable heat power, convection heat transfer, and ambient temperature.

$$T_{cell} = \alpha + \beta.q_{heat(DNI,AM)} + \gamma.h_{conv.} + \delta.T_{amb.} \tag{60}$$

Where q_{heat} is the heat generated by incident solar irradiance on the solar cells as a function of *DNI*, *AM*. The intercept and linear coefficients are $\alpha = 35.12°C$, $\beta = 1.80°C/W$, $\gamma = -0.02\ °C/(Wm^{-2}\ K^{-1})$, $\delta = 1.00$.[173, 190].

It is essential to indicate that the influence of Wind speed (*W*s), is not take into account in Equation (7-2). Based on experimental results, which established that the influence of *W*s on the prediction of cell temperature is relatively low, so it can be ignored in this estimations [190, 196]. For the location of Albuquerque, the average of *W*s is variable between (1 – 2*m*/s).

Spertino *et al.*[197] have performed a model to estimate cell temperature that depends on ambient temperature, solar irradiance and where the wind speed is neglected. Thus, the electrical efficiency has to be considered as a function of the cell temperature.

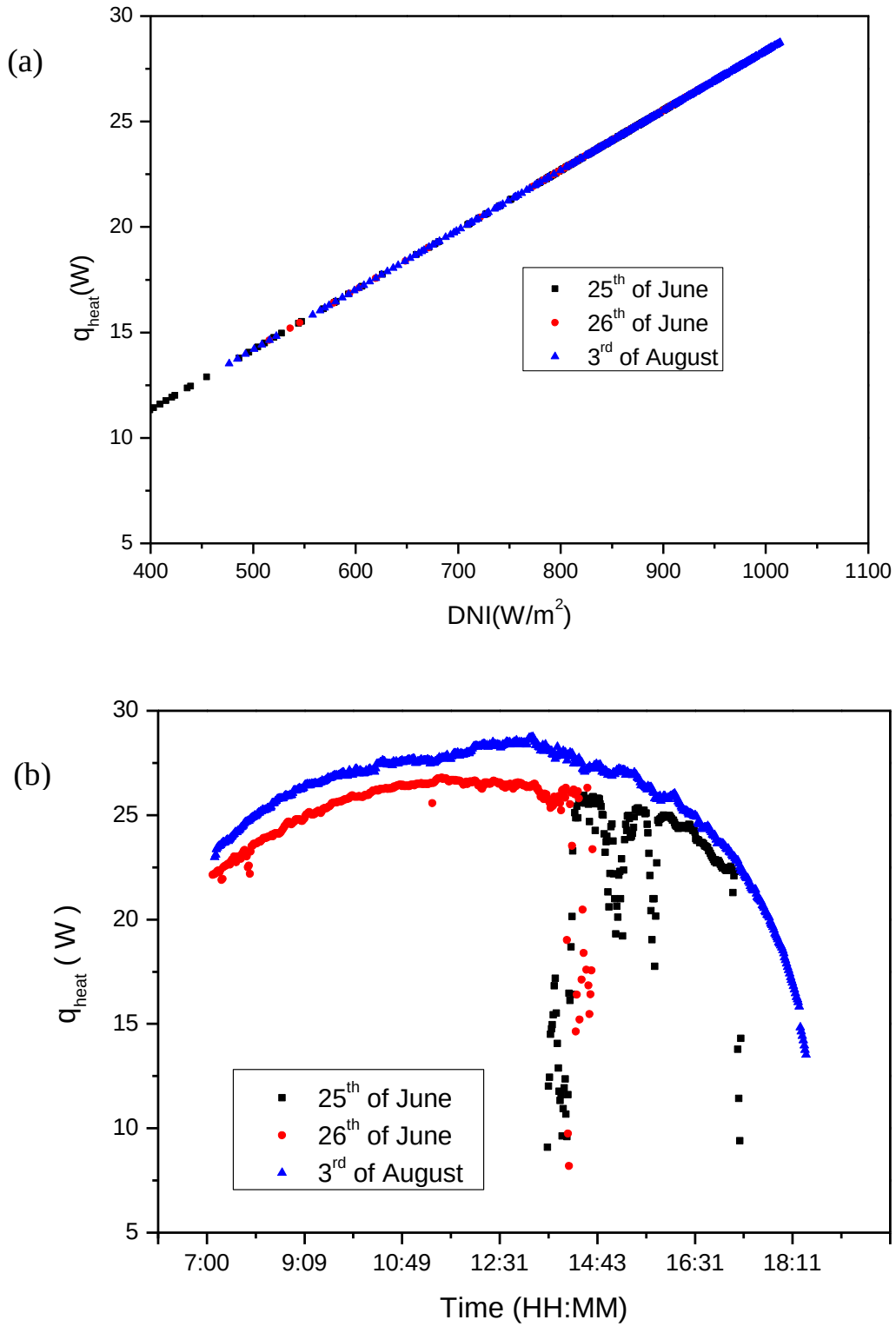

Figure 7-4 (a) heat power (q_{heat}) versus daytime, (b) heat power versus difference *DNI* values.

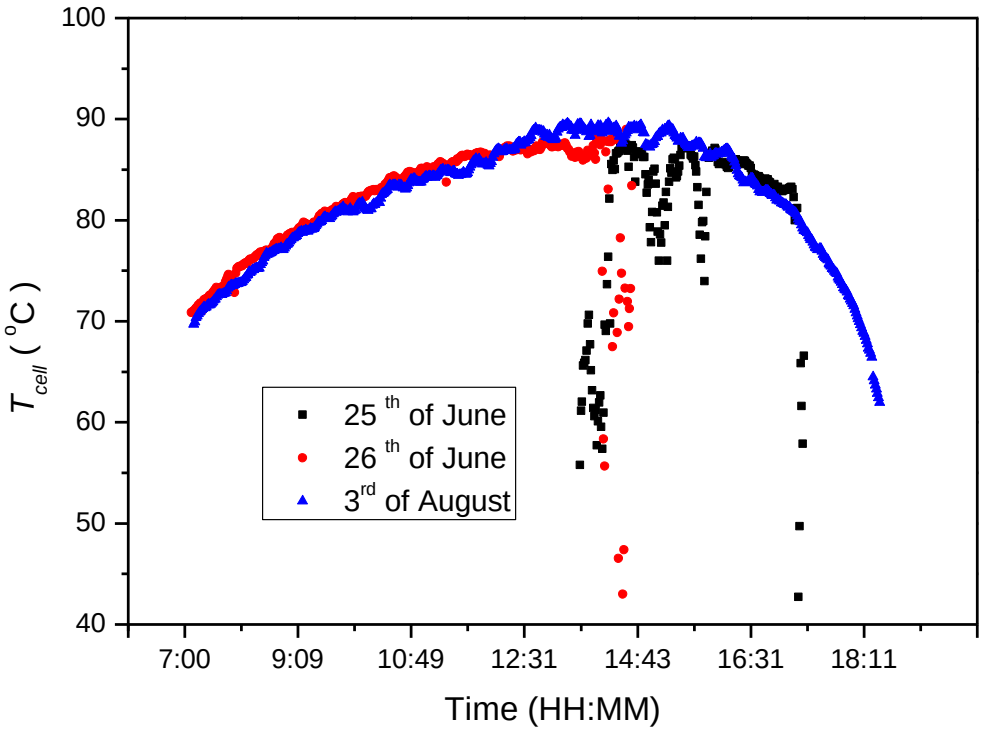

Figure 7-5 Cell temperature at convection heat transfer coefficient of 1400W/m^{2}K for different days.

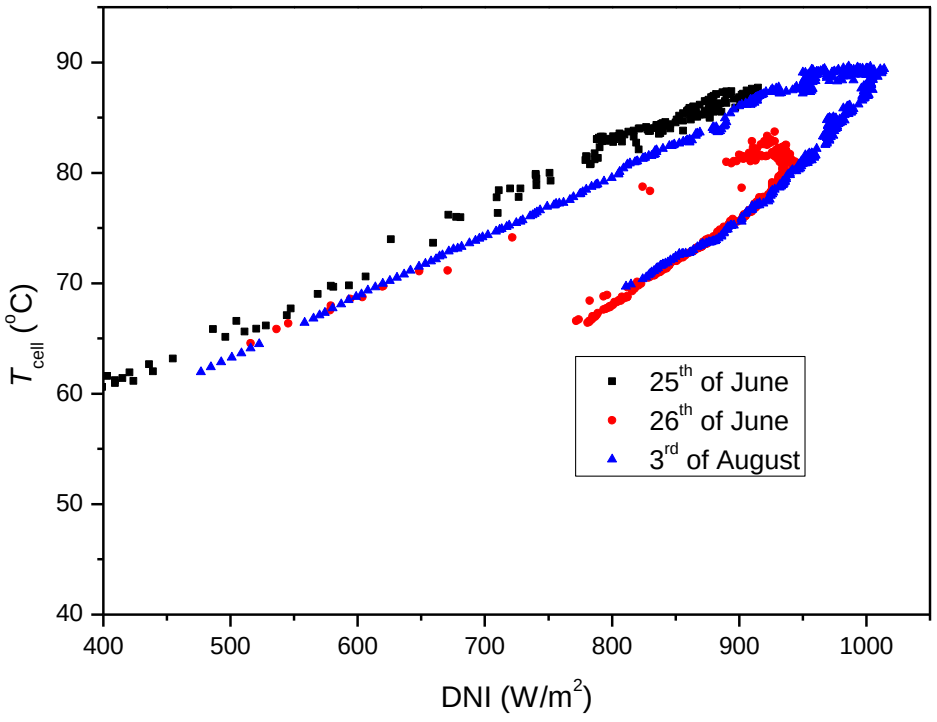

Figure 7-6 Cell temperature versus different values of direct normal irradiance.

The cell temperature (T_{cell}) reaches the highest value at midday, thus for lower values of *AM* and higher values of the *DNI* and ambient temperature, that, affect the system's performance. In contrast, high *AM* values result in lower cell temperatures because of the

lower corresponding *DNI*, and ambient temperature, which happens at sunrise and sunset. As seen in figure 7-5, it is significant that a cell's performance behaviour is volatile at various times of day, and is associated with the clearness of the atmosphere, as there is a variation in cell temperature at various times of the day and, longer-term, annually, for clear sky. A cooling requirement of CPV at 500x is analysed by [173], and is recommended for long-term operating of convection heat transfer h_{conv} >1400 W/m^{2}K. Based on real-time hours of environmental temperature, *DNI*, and *AM*, the cell temperature is simulated.

Figure 7-6 illustrates cell temperature versus different values of direct normal irradiance. Generally, when the solar irradiance intensity increases, the efficiency of the cell increases also, although, as cell temperature decreases, this leads to improvements in cell efficiency. While, at low solar irradiance, it has a big impact on cell temperature and efficiency. However, as the cell temperature rises, the positive influence of rising irradiance drops until finally, the efficiency begins to decrease. Figure 7-7 displays a cell temperature response to different scenarios of heat transfer coefficient. As the value of h_{conv} increases, the steady state cell temperature will decrease accordingly. Therefore, in this dynamic performance modelling, we must consider and review the various parameters of T_{amb}, *DNI* and *AM* on a daily basis.

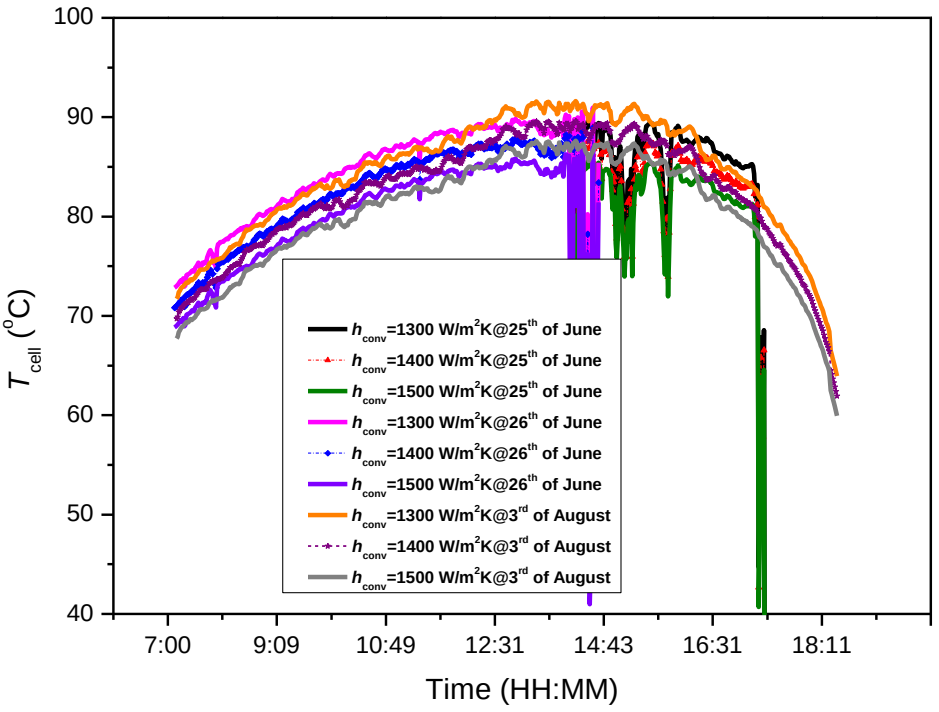

Figure 7-7 Cell temperature with variable convection heat transfer coefficient h_{conv} = 1300, 1400 and 1500 W/m^{2}K for different days.

7.5 Estimation of annual cell steady- state temperature

It important to consider the influence of weather conditions on the direct normal irradiance on a solar cell's performance behaviour, when knowing the hours of daily light irradiance can be evaluated together with monthly and annually irradiance. For long-term accurate predictions, the annual data is required to define cell temperature and annual variations of atmospheric parameters are considered. The predicted modelling results of annual cell temperature for Albuquerque by reference [190], follow up in the current study.

This data is taken from SAM[i] System Adviser Model which was introduced by NREL National Renewable Energy Laboratory databases [198]. The summary of annual weather is shown in figure 7-8 (a), and so is the average of *DNI* monthly profiles. In addition, the average ambient temperature is about 13.7^{o}C, as illustrated in figure 7-8 (b), and the average of the direct normal beam is 6.70kW/m^2 daily. In addition, the average daily sunshine hours are considered as listed in table 7-1.

As reported in reference [190], annual predicted peaks of cell temperature were at CR=500x for Albuquerque, New Mexico. As shown that, owing to the increase of cell temperature, during the summer season months, the mean cell temperature reaches about 83^{o}C, which should be born in mind during the design aspect.

7.6 Validation

Figure 7-9 shows a comparison between this study model with literature modelling results of annual cell temperature prediction. Therefore, it was found that the difference between the two model's cell temperatures in the Mean Bias Error (MBE) was 1.6%, by applying equation (61). Hence, the difference of the Root Mean Square Error (RMSE) was 2.2%, by applying equation (62).

$$MBE = \frac{1}{N}\sum_{i=1}^{N}(i_{current.\mathrm{mod.}} - i_{theristis.\mathrm{mod.}}) \tag{60}$$

$$RMSE = \sqrt{\frac{1}{N}\sum_{i=1}^{N}(i_{current.\mathrm{mod.}} - i_{theristis.\mathrm{mod.}})^2} \tag{62}$$

[i]SAM file, solar resource\USA NM Albuquerque Intl Arpt [isis] (TMY3).csv, this data at elevation 1619 m ,longitude 106.62 ^{o}W and latitude 35.04^{o}N.

Where $i_{\text{current mod.}}$ represents results of the current study model, $i_{\text{theristis mod.}}$ is the model results performed by (Theristis *et al.*[190]), and N is the number of data points matched.

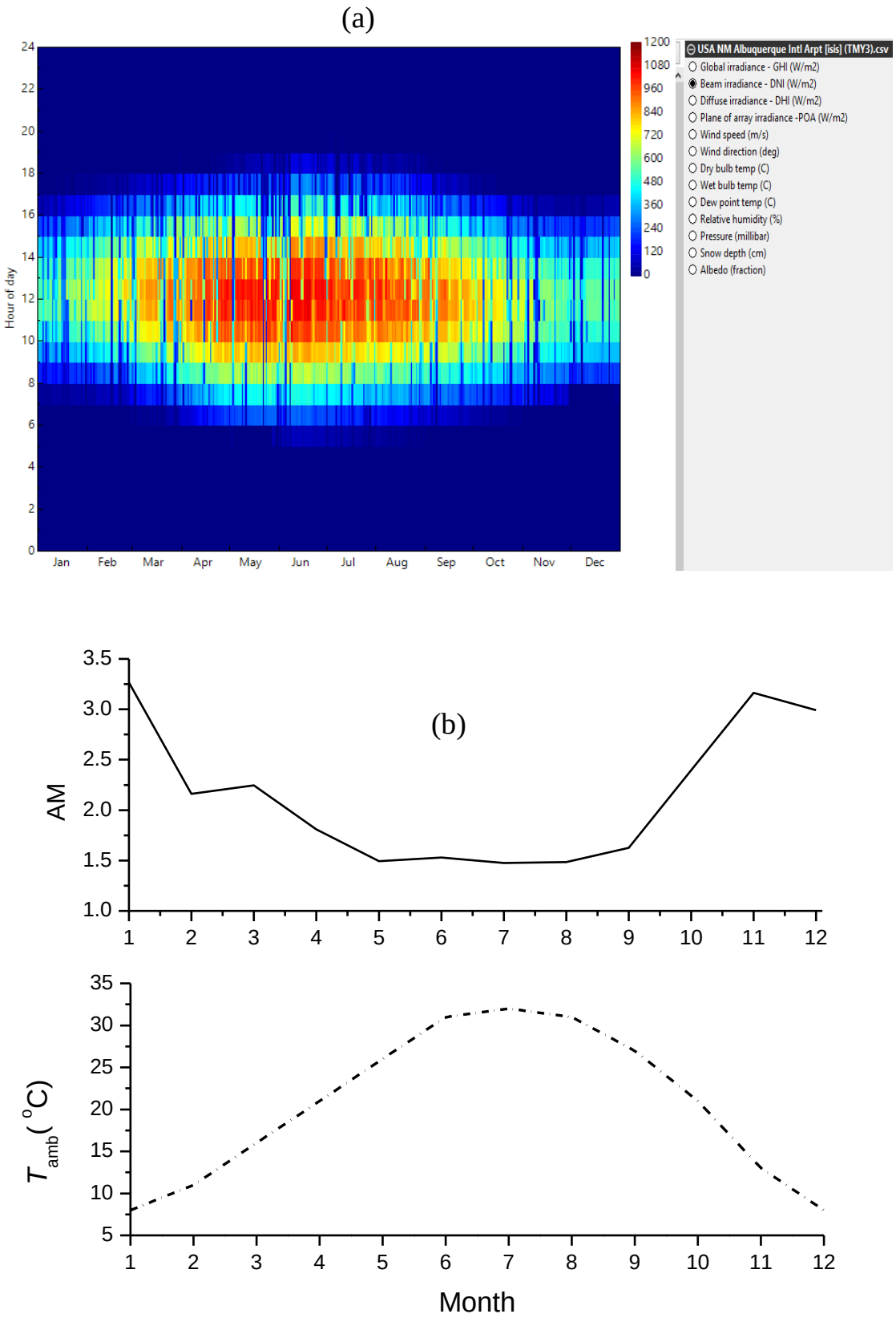

Figure 7-8 (a) annual beam irradiance *DNI* W/m^2 for NM Albuquerque [198], (b) an average of ambient temperature and *AM* of Albuquerque [190].

Table 7-1 Table average daily sunshine hours [198].

Month	1	2	3	4	5	6	7	8	9	10	11	12
No.Hours	7.05	7.57	9.00	10.08	10.58	12.10	10.36	10.17	10.28	9.03	8.26	7.27

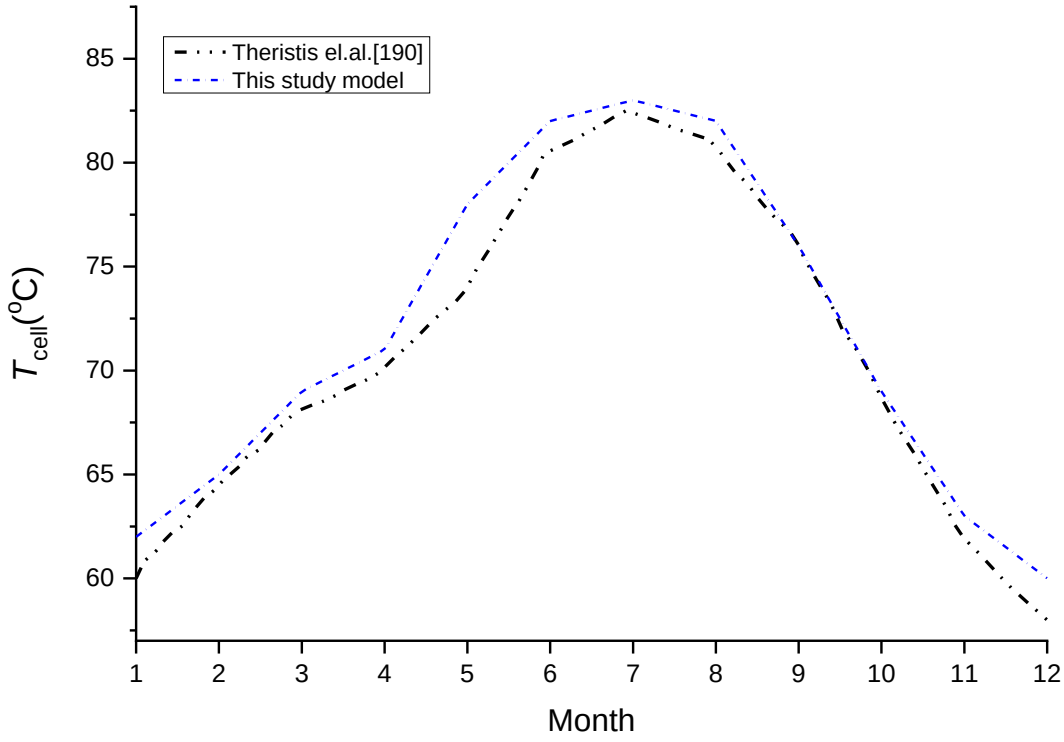

Figure 7-9 Compared this model with modelling results of annual cell temperature for Albuquerque, New Mexico US, data from Theristis *et al.*[190].

The annual maximum T_{cell}, as a function of different convective heat transfer coefficients (h_{conv}), has been predicted in this study. This determines the cooling requirement as design parameters: the value of h_{conv} = 1400Wm^{2}K is required for a maximum operating cell temperature of 83^{o}C. This maximum value appeared during the summer months, so high environment temperatures, lower values of *AM* and higher *DNI*.

Figure 7-10 shows the distribution of predicted cell temperature for a typical year of Albuquerque, New Mexico. The annual cell operating temperature is > 80^{o}C represents about 13% of the time which happened during the Summer season. Therefore, this highlighted high temperature in that period must be taken into account in any further designs. As is noted, the cell temperature between 65 – 70^{o}C is predominate in the Spring and Autumn season and represent about 24%, (the highest frequency). The cell temperature estimation in a CPV system is deemed as basic to quantify it's thermal and

electric energy production. It is important to mention that the direct beam of the sunlight is usually referred to as (*DNI)* Direct Normal Irradiance.

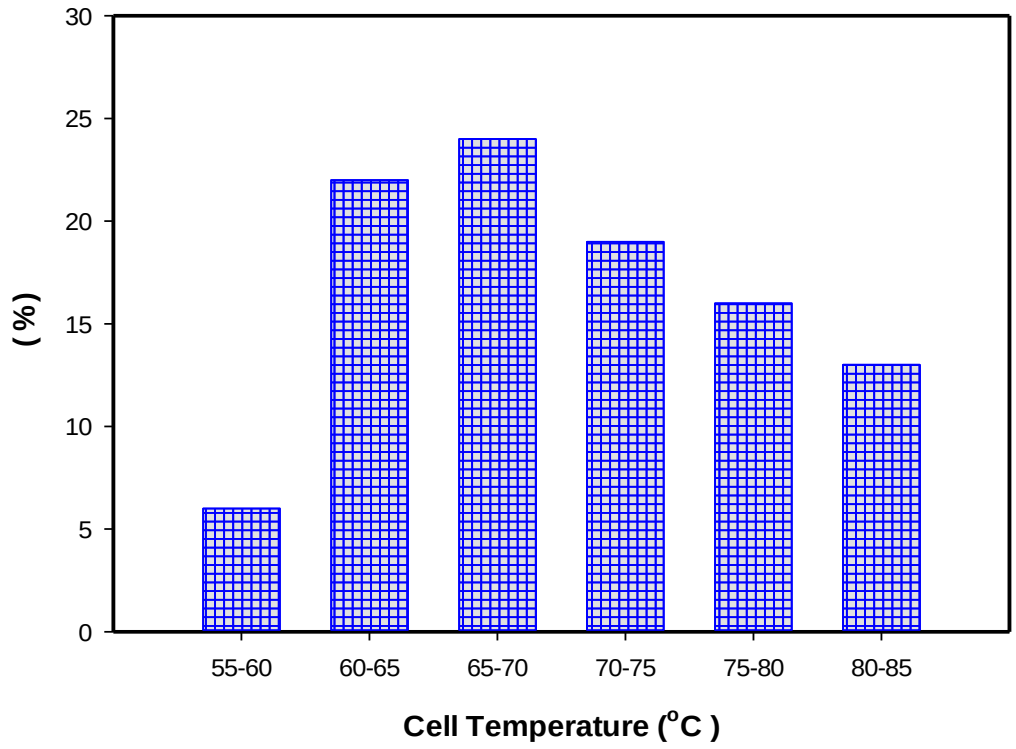

Figure 7-10 Typical year distribution percentage of predicted cell temperature.

The operation of a concentrating (500x) triple-junction solar cell during Summer season needs a convective heat transfer greater than 1400W/m^{2}K at the rear cell for safe operation. While, in a harsh environment, with a higher ambient temperatures has to be borne in mind, degradation is expected to occur. The exposure of PV solar cells to high temperatures (over the limit) for long-term will lead to performance degradation. The temperature increases can moreover result in a mechanical failure, such as a deformation of the cell.

7.7 Electrical dynamic characterisation

The performance behaviour of the (HCPV) cell/module in the field is complicated due to the diversity of interdependent elements and related operations, and because of the variation of operating conditions [169]. Convenient characterisation approaches are important for developing and optimising the efficiency of Triple-Junction solar cells, to

attain the peak efficiencies and energy harvest. Hence, characterisation is essential to indicate the critical parts of the CPV systems in actual operating conditions. Subsequently, in order to define the improvements needed to raise reliability of the system.

Obviously, the *DNI* is deemed the main influence on the electrical performance behaviour of a CPV solar cell. This influence is mainly noticeable by the effect of *DNI* on J_{sc} generated by cell, V_{oc} and output power. The current density dynamical predicted based on the temperature dependence as given [199, 200]:

$$J_{sc(DNI,T_c)} = J_{sc}^{*}\left(\frac{DNI}{DNI^{*}}\right) + \left(1 + \alpha(T_c - T_o\right) \tag{63}$$

Where J_{sc}^{*} is the current density at reference condition 1000W/m^2, *DNI* is a variety of direct normal irradiance for daytime, J_{sc} is the current density throughout daytime hours and α is the current density temperature coefficient. A single day short-circuit current density J_{sc} is plotted as a function of time and illustrates the variation of photo- current, which extracted from subcell current balances as the *AM* and *DNI* change. The rate of change in current density versus time as illustrated in figure (7-11). The dynamic open circuit voltage is predicted based on the temperature dependence as given [199]:

$$V_{oc(DNI,AM,T_c)} = V_{oc}^{\ *} + \left(\frac{n.k.T_c}{q}\right)\ln\left(\frac{DNI}{DNI^{*}}\right) + \beta_{Voc}(T_c - T_o) \tag{64}$$

Where K_b is a Boltzmann constant, *n* is a diode ideality factor, *q* is the electron charge and β_{Voc} is the open circuit voltage temperature coefficient. The concentration ratio CR of 500x is used; Figure (7-12) shows the variation of V_{oc} on a daily basis as a function of variable values of *DNI*, *AM* and T_{amb}.

As seen in the figures (7-13), the performance of the solar cell has the best power production at midday, where the values of *AM* are lower than 1.5D. In contrast, during sunrise and sunset, power production is low due to high *AM* and fewer *DNI* values; therefore, the cell's performance is optimised accordingly.

In conditions where the variations of *DNI* is influenced more by the cover of the cloud, (i.e. near step charge) the dynamic performance behaviour is very important [183].

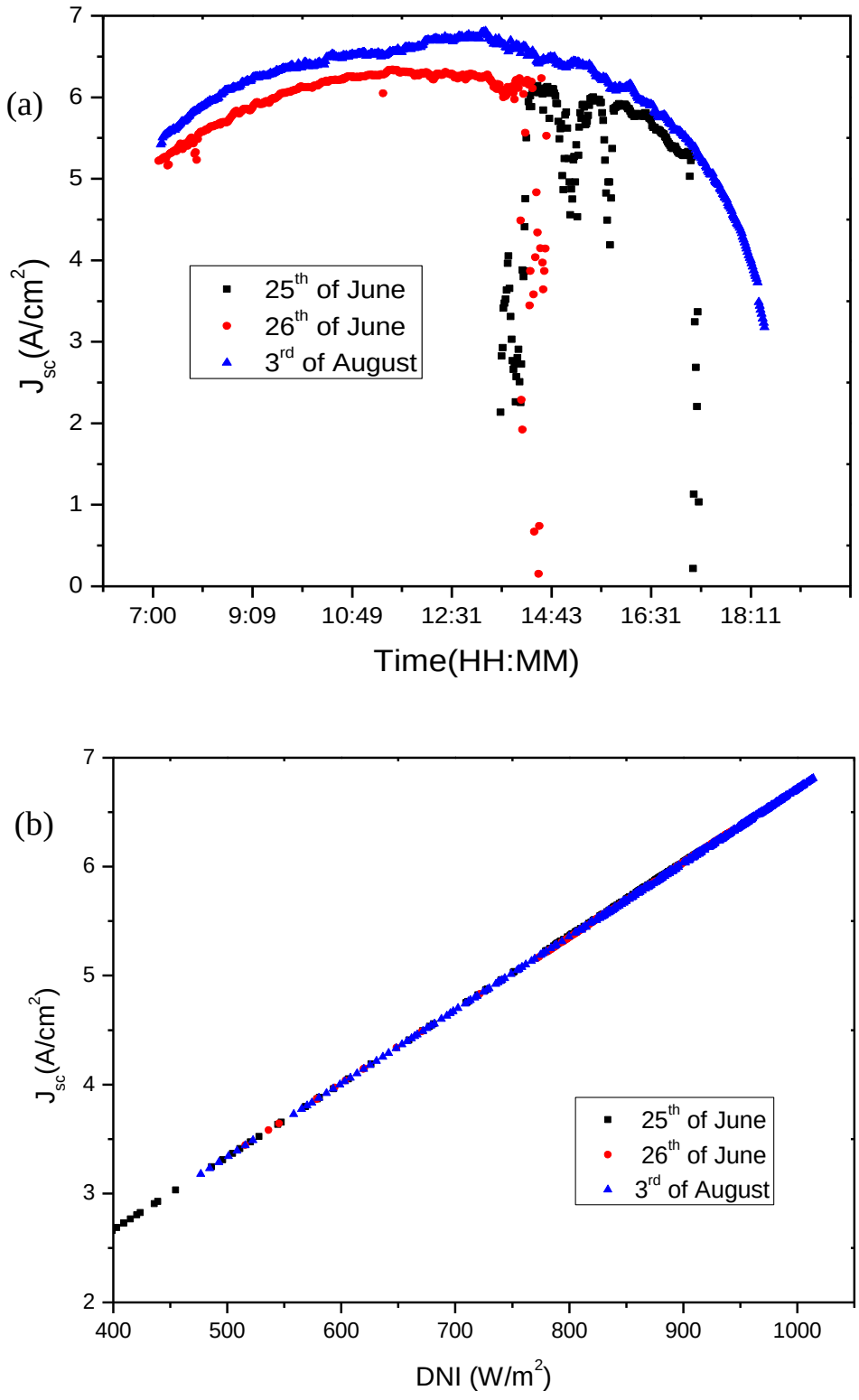

Figure 7-11 Changes of current density, (a) current density versus time, (b) current density versus the values of *DNI*.

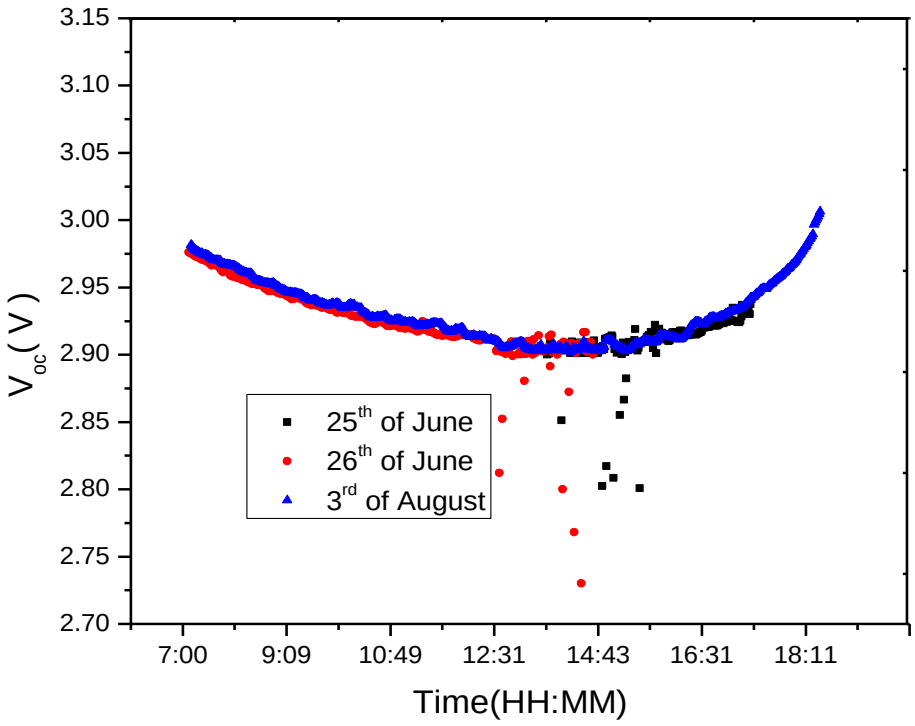

Figure 7-12 The open circuit's voltages depends on both the cell temperature and different *AM*.

The behaviour of maximum power under different atmospheric parameter of *DNI* and *AM* varies during daily hours. Subsequently, the maximum power is significantly influenced by such variation.

Power produced from the photovoltaic cell is proportional to the volatility of incident sunlight intensity on the solar cell's surface. Therefore, the output power varies significantly due to the variation in solar radiation intensity throughout the day and from one day to another. The prediction of power as a function of variable *DNI* and T_c can be estimated by using equation (65) [108, 201]:

$$P = P^{*}.\frac{DNI}{DNI^{*}}.[1+\delta(T_c - T_o)] \tag{65}$$

The variation of the maximum power of time of the day and long-term annual, for clear sky and can be integrated to be able to compare the performance of the seasonal, or annual, energy produced. Thus, it can give an overview for understanding performance and improving system design.

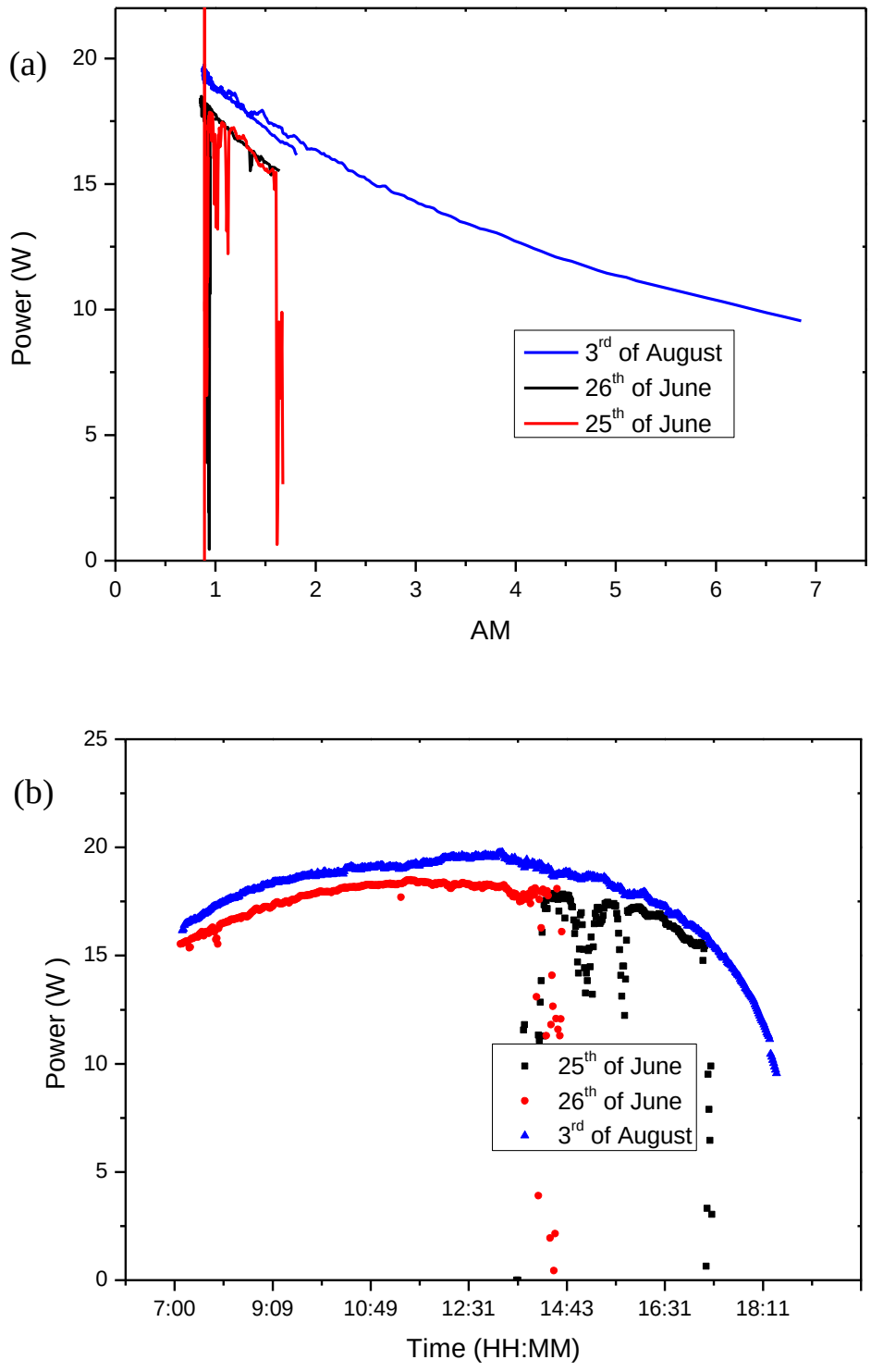

Figure 7-13 (a) estimation of maximum power versus to *AM*, (b) maximum power versus time.

By applying the dynamic model, the influence of variation in solar radiation on the power output of photovoltaic cells can be predicted. The output power from the cells is augmented based on the analysis of the dynamic model. Therefore, this provides a reference for assessing change of solar radiation and the device material.

The output power of the solar cell is a significant parameter because it enables knowing the energy harvest of a specific photovoltaic device. Therefore, the power produced by the high-efficiency triple-junction solar cell as a function of variable parameters of *DNI* and T_c will be performed accordingly.

7.8 Estimation of energy yield

The main motivation for the technologies of photovoltaic cells is to generate the electricity from the Sun's radiation, while performance analysis, or designing of a photovoltaic system, is essential in predicting an estimated annual energy yield. In order to do this, a thermal model is needed for the approximation of operating temperature based on environmental conditions such as solar radiation intensity and ambient temperature.

Like in any other kind of energy generation system, it is essential to recognise the performance of the system in terms of energy. The output power of the solar cell, under variable solar radiation, is predicted at CR = 500x. The energy produced (E_p) for every day is computed by integrating the output power every hour as expressed by (66):

$$E_p = \int_{t1}^{t2} P(t).dt \tag{66}$$

Where t_1 and t_2 is the time of sunrise and sunset, $P(t)$ is the average power as a function of time of the triple-junction cell at each time step, and dt is the means changes of time that is used as an input to the cell model.

In this study the daily energy generation is estimated from direct solar radiation. The predictions of energy generation are considered for two cases: first case at the clear sky and second case with a cloudy sky.

The annual sum of the energy produced is predicted by adding the energy produced for every day in the year. The generation of energy is predicted by the power over the period. Therefore, by integration of the outputs power over the year yield, a yearly energy generation can be estimated.

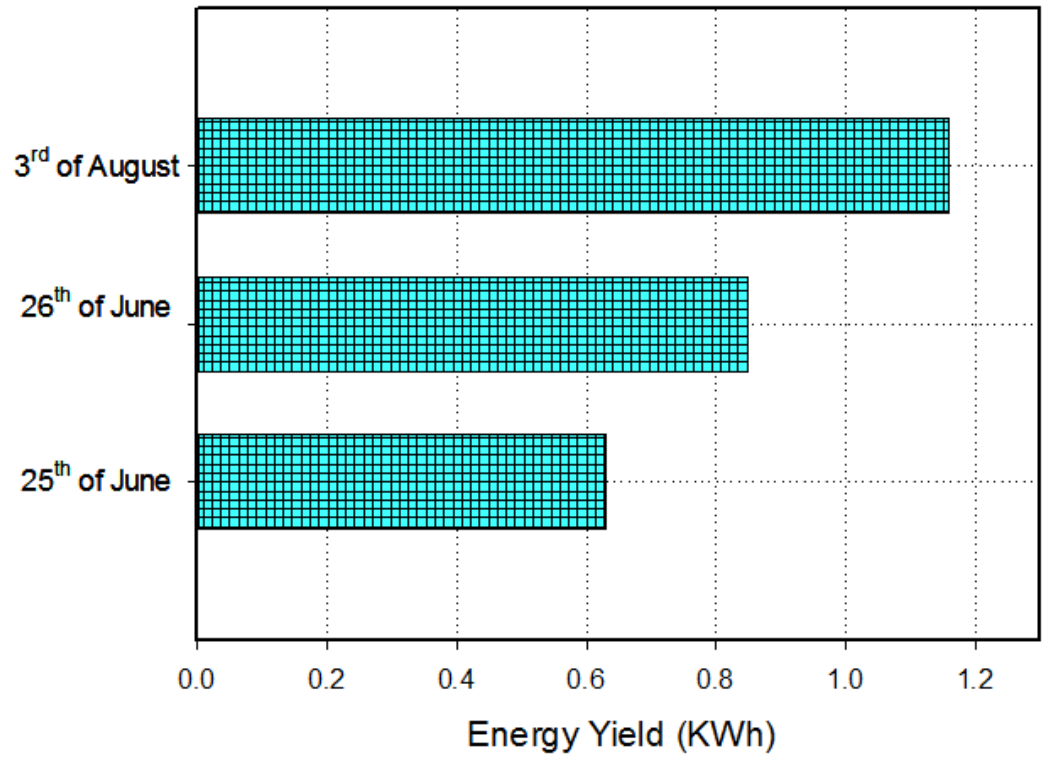

Figure 7-14 Estimations of daily energy yields of three days of summer 2015 generated from a single assembly.

On a day of sunshine, 3rd of August, the total energy production yields are about 1.16 kWh/day where Sunrise is at 7:30am and Sunset at 18:30pm. On the 26th of June, with Sunshine from 7:35am to 2:38pm, the energy produced is about 0.85 kWh/day (after 2:38pm, there were cloudy skies). While on 25th of June, with Sunshine from 1:25pm to 5:19pm, the energy generated was approximately 0.63kWh/day, because of cloudy skies when compared to a clear day, as shown in figure 7-14.

From an energy production perspective, this indicated that the average solar cell assembly generates more energy through the summer season, due to plentiful supply of the *DNI*. It is different between Winter, Autumn and Summer season, due to the period of sunshine in Winter and Autumn, while in summer, it is at the highest. The values of the *AM* and it's corresponding *DNI* also have influence. Therefore, higher *DNI* will lead to increases in the average energy production. Figure 7-15 summarised the prediction of the annual energy generation from a single assembly cell. Table 7-2 summarised the average monthly prediction of cell energy generated with a clear, and partially cloudy, sky.

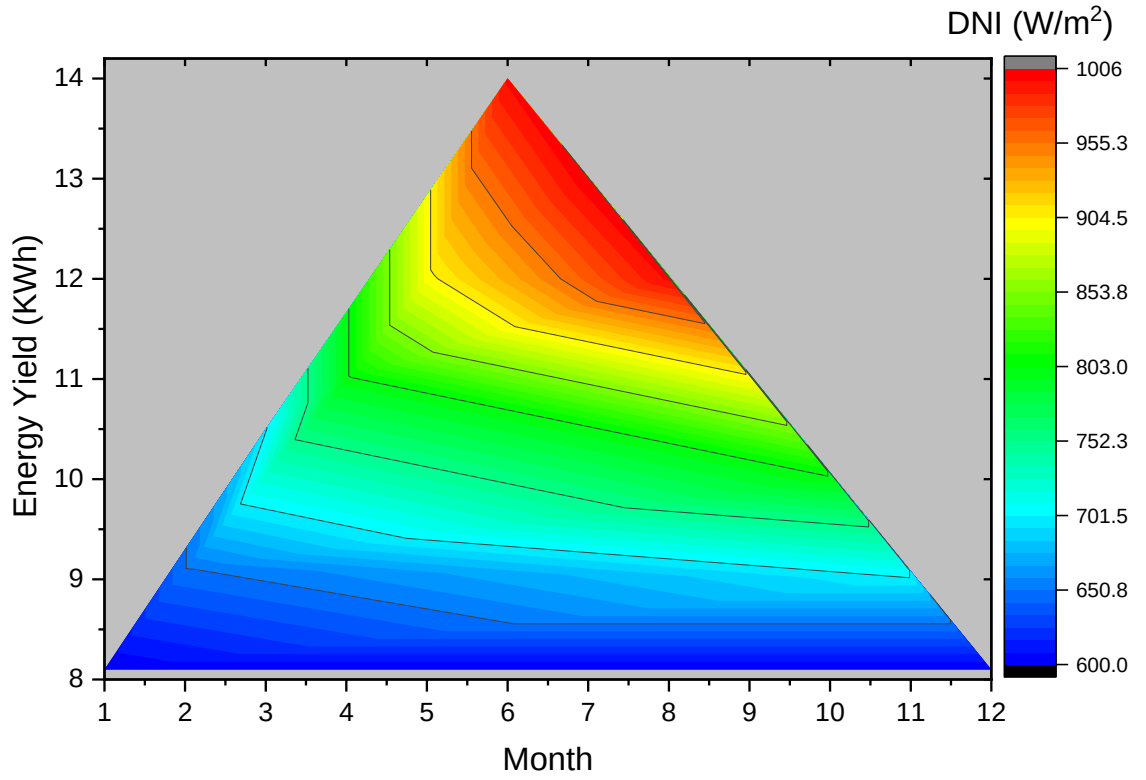

Figure 7-15 Predicted the average monthly of energy yield as a function of *DNI* at the clear sky.

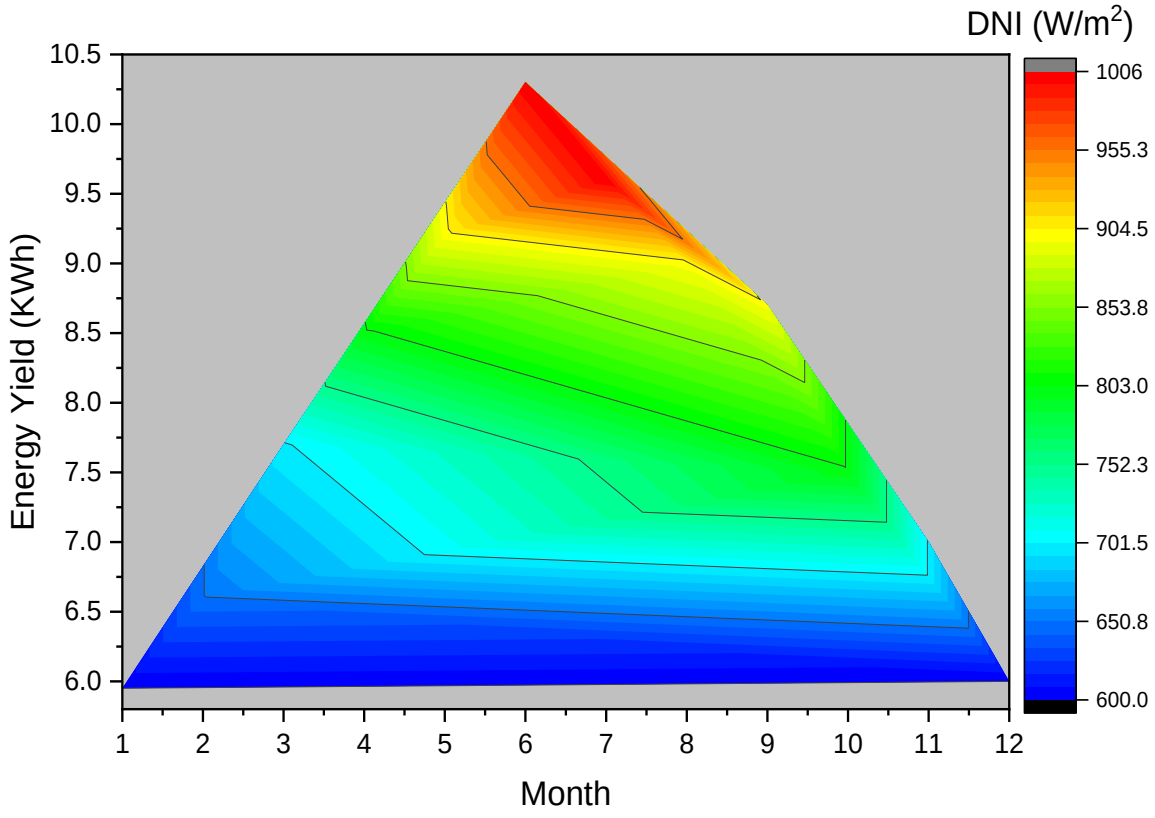

Figure 7-16 Predicted the average monthly of energy yield as a function of *DNI* at the partially cloudy sky.

Table 7-2 Estimations of monthly single assembly cell average energy yields at clear sky and energy yields at the partially cloudy sky.

	Estimation of energy production (kWh) at the clear sky		Estimation of energy production (kWh) at the partially cloudy sky	
	Minimum	Maximum	Minimum	Maximum
Monthly	8.1	14	5.9	10.2

Estimation of the maximum annual energy generated of a single assembly cell is about 128kWh, at the clear sky, and estimation of energy generated is 94kWh, for a partially cloudy sky. There was a significant energy difference between the example of clear and cloudy skies. Figure 7-16 illustrates the estimation of the average monthly value of energy generated as a function of *DNI* with a partially cloudy sky. Consequently, those energy losses must be considered when planning installations for the PV system.

Mi *et al*. [202] reported that the level of *DNI* was the predominant parameter which determines the quantity of energy generated, and also the performance of the HCPV system. The atmospheric parameters such as ambient temperature and wind speed need to be considered on system performance.

The impact of cloud shading shows an instantaneous decrease in incident solar irradiance and in turn, the output power will be affected for a short period, as has been observed. Although, in the harsh environment, the influence of dust accumulation has a long-period impact [203].

Summary

The sensitivity of spectral differences, cell temperature and high-energy output have been presented. The estimation of energy generation gives a plan to estimate the cost of long-time operations. In general, estimation of energy generation has been considered for a dynamic cell temperature. In addition, the photovoltaic power output is a dynamic change and it is dependent on the incident irradiation and the system's behaviour. However, this investigation had provided that the effect of higher temperature and the influence of variation in solar radiation affect cell's performance behaviour. The effects of cloud shading and variation of *AM* are taken into the account.

As the air mass increases, spectral attenuation has a significant effect on the thermal and electrical conversion efficiency of triple-junction solar cells. In addition, spectral change is one of the causes of the current mismatch in triple-junction cells. Thus, cell parameters such as short current density (J_{sc}), efficiency and output power are affected. Furthermore, as shown in the case of the cloud shadow limitation will have an influence on the distribution of incident solar radiation. Eventually, that will affect the power generation induced by photovoltaic solar cells.

In addition, this chapter describes the electrical parameter characterisation of the single cell assembly and outlines the influence light intensity changes have on the device's cell temperature. The dynamic performance is coupled with the *DNI, AM* and T_{amb} parameters on a daily basis. They significantly showed the variations in the behaviour of electrical performance parameters and energy production. For an optimum performance, the following parameters need to considered: a lower *AM*; lower T_{amb}; a higher *DNI* and a clear, cloud free, sky. The seasonal cell temperature variation has been predicted and compared with other research published results. Hence, the value of the Root Mean Square Error RMSE is about 2.2% and the Mean Bias Error (MBE) was 1.6%.

Consequently, the efforts have been assessed to understand the effect of temperature on the solar cell's performance, which can be used to for predict performance at a given temperature. This technique can be used in the optimum design of the solar cell, which maximizes the output power for variable temperature conditions throughout the operation.

Chapter 8: Conclusions and Recommendations

The motivation for the current research study is based on the growth in power demands in recent decades, and the fluctuation of oil and gas prices in international markets. Furthermore, to seek out clean and sustainable energy sources. Photovoltaics are one of the most promising technologies for cheaper, efficient electricity generation. The tools used in the numerical models are MATLAB and COMSOL Multiphysics, which have already proven their capability as powerful tools. The thermal-electrical characterisation of a CPV receiver assembly was studied in detail in chapters 3 –7.

8.1 Conclusions

This research study has presented and detailed the development of a computational technique which describes performance behaviour of an HCPV receiver. Theoretical investigations are considered through modelling; firstly, with an electrical model, then a thermal one. Hence, these created models are the cornerstones of the performance characteristic, an important tool in understanding the behaviour and which helps to describe the system.

The sensitivity of temperature on the semiconductors layer has been predicted, to determine the behaviour of the device, and to know the effects of temperature. The influence of cell temperature, rising from 25 to 125^{o}C, on a cell's electrical parameters, affects open circuit voltage, short circuit density, fill factor, power and efficiency has been studied. Therefore, the model gives details of temperature changes during different operating behaviours of the solar cell.

In this study, the effect of air mass on the performance of triple-junction solar cells is presented. The values of *AM* from (*AM* = 1 – 10D), CR = 1x were studied on the electrical model and the results are given in the form of *J-V*, *PV* curve characteristics and cell efficiency. Thus, the weakness of the solar spectrum leads to a reduction in performance parameters of the series connection of multi-junction solar cells. The challenge in characterising multi-junction cells is the sensitivity to the incident spectrum, because of the effects of changes in the air mass.

This research study presents an insight into the development of integrated numerical and thermal-electrical modelling. In addition, by utilising the multiphysics FEM approach,

the temperature distribution profile of the receiver can be visualised. Therefore, the 3D FEM of CPV receiver assembly model gives a better understanding of thermal performance behaviour. In addition, this illustrates the temperature distribution pattern on the receiver assembly profile.

The thermal performance of triple-junction solar cells with regard to temperature increase has been investigated. A temperature augmentation will result in a significant reduction in a material's bandgap; in turn, this will cause a slight rise in current density and a reduction in the open circuit voltage. In the stationary study of the numerical models, mathematical equations of the electrical and thermal performance were applied based on an iterative simulation technique. In order to retain the cell operating temperature at/or less than 80^{o}C, it was determined that the magnitude of the convection heat transfer coefficient $h_{conv} \geq 2.4$ KW/m^{2}K is needed, under the concentration ratio of 1000x.

Furthermore, the cell temperature is calculated by an iterative computational technique. A numerical thermal-electrical model has been developed using a convergent iterative technique. The efficiency dropped remarkably to approximately 3.5% as air mass decreased from 1.5 to 8D at the 1000x concentration ratio. This leads to a reduction in the convection heat transfer coefficient (h_{conv}) requirement and heat power generated by the solar cells.

The thermal response of the solar receiver at different atmospheric radiative and corresponding *AM* values from (*AM* = 1.5, 4 and 8D). The convergent cell temperature is $\leq 80^{o}$C at $T_{amb} = 25^{o}$C, and the h_{conv} between (2200 – 2400) W/m^{2}K. A parametric sweep study of $T_{amb} = 25 – 45^{o}$C, the $h_{conv} = 2200 – 3000$ W/m^{2}K, also (*AM* = 1.5, 4 and 8D) was conducted in order to retain a cell operating temperature lower 80 ^{o}C.

Thermal behaviour was studied with a variety of values for convective heat transfer, ambient temperature and air mass. The amount of heat transfer from the solar receiver ought to be maximised, in order to operate the cells more safely and at the lowest possible temperature. Thus, as deduced at high ambient temperature, there will be a requirement for high convective heat transfer coefficients to maintain a cell temperature below 80^{o}C. While, as *AM* decreases, the convective heat transfer coefficient values can decrease because the heat power decreases. From the modelling results, a better understanding of the thermal behaviour of the receiver assembly has been achieved. Therefore, this gives an overview of future engineering design of HCPV receivers and their long-term operating performance.

In addition, a model developed to characterise the dynamic behaviour of triple junction solar cells has been analysed. The influence of temperature and efficiency are investigated in dynamic patterns. The electrical and thermal performance of receiver assemblies at CR = 500x via a performed transient modelling of thermal and electrical performance has been reported. The significance of the transient model is the link between the ideal and environment experiment in order to understand the transient nature of CPV receivers. The behaviour of the triple-junction solar cell due to temperature rises has been discussed. Ultimately, thermal management, design and development is hugely important to the solar cell performance. A cell's stagnation temperature point is approximately 78.4^{o}C, in both the dynamic efficiency model and stationary efficiency model, and seeing the remarkable effects of increases and decreases of *DNI* at the steady-state cell temperature (T_{cell}). The electrical performance parameters of J_{sc}, V_{oc}, FF, and efficiency have been investigated under both transient and steady-state operating conditions.

From daily performance modelling, we can understand the CPV system design for different environments. Hence, as the values of *DNI*, T_{amb} increases, and the values of *AM* decrease, the thermal response needs more convective heat transfer to keep a cell operating safely. In addition, more energy yield is generated at the same time. On the other hand, lower values of *DNI*, T_{amb} and higher *AM* results in a lower operating temperature and proportional loss of power generation. Long-term performance evaluation, i.e. the average of monthly variations of atmospheric parameters throughout the year is taken into the account. Therefore, during the summer months of June, July and August, the effect of these aforementioned atmospheric parameters values requires more consideration. The thermal management of the receiver assembly also matters, and needs to improve during these summer months, in order to maintain a cell temperature below 80^{o}C.

Overall, the insight from these models can enhance the design of the devices' assembly and it can be simply adapted for wide-scale CPV arrays. This study's result present a valuable guidance for future engineering manufacturing and fabrication of solar concentrating photovoltaic technology. This study goes some way to improving the prediction of energy yield from HCPV. Ultimately, to reduce the cost of renewable energy from this source as it will reduce risk, increase investor confidence and therefore the cost of financing large capital investments. Thus, we have various norms while purchasing such equipment to operate in different environments. Arguably, an optimal utilisation will

allow the investors to choose a device that is the most efficient, has high reliability and one which requires the least expenditure.

8.2 Recommendation for further work

This study has contributed to a better understanding of: CPV receiver performance; triple-junction solar cells (consisting of three layers of different materials), and CPV receivers, through their modelling characterisation studies. In theoretical investigations and predictions of the operating framework for power generation, different environment parameters of *AM, DNI* and T_{amb} are taken into the account in the models. The overall dynamic solar radiation on a daily basis, from sunshine to sunset, is studied and predicted. In addition, annual energy production is estimated accordingly. The suggestions of further and extended works are listed below as follows:

- Comprehensive detailed cost analysis study based on the performance of annual energy production, this would be a fruitful area for more work.
- An outdoor experiential measurement studies of the harsh environmental effects, such as higher ambient temperature, dust and shading that have an effect on the performance behaviour of the thermal and electrical of CPV receivers. A further study could consider the long-term outdoor experimental work of different environment condition such as altitude, clearness index etc.
- Study of the tracking system on the performance of solar cells, which can include and integrated automatic daily and seasonal tracking system.
- Further study of high CR greater than 1000x in electrical-thermal performance, by considering an atmospheric factor daily, monthly and annually.
- Expand on the present study by the inclusion of densely packed array modules and CPV systems. Hence, this study focuses more on the modelling of a single cell assembly.
- From a thermal engineering point-view, the high thermal capacitance of the cell keeps the cell temperature high, so one must consider different materials, or consider adding more layers.

- Establishing performance monitoring systems through long-term analyses, which helps in diagnostics of performance degradation threat.
- Optical modelling of solar concentrators on electrical and thermal models by considering a different incidence ray angle.
- Thermal management and optimisation of heat generated in the receivers and reused the heat for another purpose rather than wasted to the environment.

The aforementioned recommendations can greatly improve the performance of the CPV system and enable cost reduction. Because of the time constraints in this research study, these above recommendations are not in the framework of this PhD project. These recommendations can be adapted in further research development projects. The concentrating CPV system will be a better choice for integration and optimisation in a module in the near future.

References

[1] R. G. Watts, *Engineering response to climate change*. CRC Press, 2013.

[2] B. Sorensen, *Renewable energy: physics, engineering, environmental impacts, economics and planning*. Elsevier Ltd, 2010.

[3] O. Edenhofer *et al.*, *Renewable energy sources and climate change mitigation: Special report of the intergovernmental panel on climate change*. Cambridge University Press, 2011.

[4] S. Roaf, S. Roaf, D. Crichton, and F. Nicol, *Adapting buildings and cities for climate change: a 21st century survival guide*. Routledge, 2009.

[5] R. E. Sims, "Renewable energy: a response to climate change," *Solar energy*, vol. 76, no. 1-3, pp. 9-17, 2004.

[6] T. Muneer, "Solar Radiation and Daylight Models, with a chapter on solar spectral radiation by C. Gueymard and H. Kambezidis," ed: Elsevier Butterworth-Heinemann, Oxford, UK, and Burlington, MA, 2004.

[7] O. Publishing, C.-o. Organisation for Economic, and Development, *OECD Green Growth Studies Energy*. OECD Publishing, 2012.

[8] Irena, "Global energy transformation: A roadmap to 2050," ed: International Renewable Energy Agency Abu Dhabi, 2018.

[9] "Turning Energy Systems Towards Sustainability," published by Earthscan. no. German Advisory Council on Global Change, , 2003.

[10] C. Kost *et al.*, "Levelized cost of electricity renewable energy technologies," *Fraunhofer Institute for Solar Energy Systems ISE*, 2018.

[11] A. Martí and A. Luque, *Next generation photovoltaics: high efficiency through full spectrum utilization*. CRC Press, 2003.

[12] F. Dimroth and S. Kurtz, "High-efficiency multijunction solar cells," *MRS bulletin*, vol. 32, no. 03, pp. 230-235, 2007.

[13] S. P. Philipps, A. W. Bett, K. Horowitz, and S. Kurtz, "Current status of concentrator photovoltaic (CPV) technology," National Renewable Energy Lab.(NREL), Golden, CO (United States), 2015.

[14] G. Sala, "Handbook of Photovoltaics," 2012. Elsevier.

[15] C. Algora and I. Rey-Stolle, *Handbook of concentrator photovoltaic technology*. John Wiley & Sons, 2016.

[16] J. H. Jo, R. Waszak, and M. Shawgo, "Feasibility of Concentrated Photovoltaic Systems (CPV) in Various United States Geographic Locations," *Energy Technology & Policy*, vol. 1, no. 1, pp. 84-90, 2014.

[17] Y. ABIKO, R. MIKAMI, K. IYATANI, S. TAMURA, K. SUGIYAMA, and M. UEYAMA, "Evaluation of Concentrator Photovoltaic System Power Plant," *SEI TECHNICAL REVIEW*, no. 86, p. 101, 2018.

[18] "Solargis s.r.o. [URL] http://solargis.com/assets/graphic/free-map/DNI/SolargisWorld-DNI-solar-resource-map-en.png."

[19] C. Honsberg and S. Bowden, "PV education," *ORG.(access April-June 2013) http://pveducation. org/pvcdrom/properties-of-sunlight/sun-position-calculator*, 2014.

[20] G. N. Tiwari, . Dubey, S,, "fundamental of photovoltaic models and their application," vol. book, Registered Charity Number 207890, 2010.

[21] M. A. Green, Y. Hishikawa, E. D. Dunlop, D. H. Levi, J. Hohl-Ebinger, and A. W. Ho-Baillie, "Solar cell efficiency tables (version 52)," *Progress in Photovoltaics*, vol. 26, no. 7, 2018.

[22] G. N. Tiwari and S. Dubey, *Fundamentals of photovoltaic modules and their applications*. Royal Society of Chemistry, 2009.

[23] V. Quaschning, "Understanding Renewable Energy Systems: Earthscan," ed: ISBN, 2005.
[24] K. Zweibel and P. Hersch, *Basic photovoltaic principles and methods*. Van Nostrand Reinhold Company, 1984.
[25] "renewables 2018 global status report - REN21," *www.ren21.net/wp-content/.../2018/06/17-8652_GSR2018_FullReport_web_final_.pdf*.
[26] "Annual Energy Outlook 2019 with projections to 2050," *January 24, 2019* *www.eia.gov/aeo*.
[27] A. A. Ghoneim, K. M. Kandil, T. H. Alzanki, and M. R. Alenezi, "Performance analysis of high-concentrated multi-junction solar cells in hot climate," *International Journal of Sustainable Energy*, vol. 37, no. 3, pp. 294-310, 2018.
[28] V. A. Antonio luque, " "Concentrator photovoltaic," *Springer series of optical since.* , 2007.
[29] G. Sala and A. Luque, "Past experiences and new challenges of PV concentrators," *SPRINGER SERIES IN OPTICAL SCIENCES*, vol. 130, p. 1, 2007.
[30] S. Bedair, M. Lamorte, and J. Hauser, "A two-junction cascade solar-cell structure," *Applied Physics Letters*, vol. 34, no. 1, pp. 38-39, 1979.
[31] S. R. Kurtz, P. Faine, and J. Olson, "Modeling of two-junction, series-connected tandem solar cells using top-cell thickness as an adjustable parameter," *Journal of Applied Physics*, vol. 68, no. 4, pp. 1890-1895, 1990.
[32] A. B. Maish, "Progress in the concentrator initiative program," in *Photovoltaic Specialists Conference, 1993., Conference Record of the Twenty Third IEEE*, 1993: IEEE, pp. 1203-1208.
[33] N. H. Karam *et al.*, "Recent developments in high-efficiency Ga0. 5In0. 5P/GaAs/Ge dual-and triple-junction solar cells: steps to next-generation PV cells," *Solar Energy Materials and Solar Cells*, vol. 66, no. 1-4, pp. 453-466, 2001.
[34] M. Wiesenfarth, I. Anton, and A. Bett, "Challenges in the design of concentrator photovoltaic (CPV) modules to achieve highest efficiencies," *Applied Physics Reviews*, vol. 5, no. 4, p. 041601, 2018.
[35] R. M. Swanson, "The promise of concentrators," *Progress in Photovoltaics: Research and Applications*, vol. 8, no. 1, pp. 93-111, 2000.
[36] S. P. Philipps, A. W. Bett, K. Horowitz, and S. Kurtz, "Current status of concentrator photovoltaic (CPV) technology," National Renewable Energy Lab.(NREL), Golden, CO (United States), 2017.
[37] R. King *et al.*, "Solar cell generations over 40% efficiency," *Progress in Photovoltaics: Research and Applications*, vol. 20, no. 6, pp. 801-815, 2012.
[38] E. F. Fernández, F. Almonacid, P. M. Rodrigo, and P. J. Pérez-Higueras, "CPV Systems," in *McEvoy's Handbook of Photovoltaics (Third Edition)*: Elsevier, 2017, pp. 931-985.
[39] "Fraunhofer Institute for Solar Energy Systems, ISE with support of PSE Conferences & Consulting GmbH," *Fraunhofer Institute for Solar Energy Systems, ISE*, no. report, Freiburg, 27 August 2018, Art no. www.ise.fraunhofer.de.
[40] D. Talavera, J. Ferrer-Rodríguez, P. Pérez-Higueras, J. Terrados, and E. Fernández, "A worldwide assessment of levelised cost of electricity of HCPV systems," *Energy Conversion and Management*, vol. 127, pp. 679-692, 2016.
[41] W. Shockley and H. J. Queisser, "Detailed balance limit of efficiency of p-n junction solar cells," *Journal of applied physics*, vol. 32, no. 3, pp. 510-519, 1961.
[42] V. Fthenakis, "Preface," in Third Generation Photovoltaics,," *V. Fthenakis*, no., Ed., ed: InTech, 2012,.

[43] I. Tobías and A. Luque, "Emerging High Efficiency Concepts for Concentrator Solar Cells," *Handbook of Concentrator Photovoltaic Technology*, p. 137, 2016.
[44] L. L. Kazmerski, "Solar photovoltaics R&D at the tipping point: A 2005 technology overview," *Journal of electron spectroscopy and related phenomena*, vol. 150, no. 2-3, pp. 105-135, 2006.
[45] M. Feteha and G. Eldallal, "The effects of temperature and light concentration on the GaInP/GaAs multijunction solar cell's performance," *Renewable Energy*, vol. 28, no. 7, pp. 1097-1104, 2003.
[46] A. Bett, F. Dimroth, and G. Siefer, "Multijunction concentrator solar cells," *Springer Series in Optical Sciences*, vol. 130, p. 67, 2007.
[47] A. Royne, C. J. Dey, and D. R. Mills, "Cooling of photovoltaic cells under concentrated illumination: a critical review," *Solar energy materials and solar cells*, vol. 86, no. 4, pp. 451-483, 2005.
[48] M. A. Green, M. J. Keevers, I. Thomas, J. B. Lasich, K. Emery, and R. R. King, "40% efficient sunlight to electricity conversion," *Progress in Photovoltaics: Research and Applications*, vol. 23, no. 6, pp. 685-691, 2015.
[49] S. P. Philipps and A. W. Bett, "III-V Multi-junction solar cells and concentrating photovoltaic (CPV) systems," *Advanced Optical Technologies*, vol. 3, no. 5-6, pp. 469-478, 2014.
[50] F. Dimroth, "High-efficiency solar cells from III-V compound semiconductors," *Physica Status Solidi C*, vol. 3, no. 3, pp. 373-379, 2006.
[51] J. P. Connolly, D. Mencaraglia, C. Renard, and D. Bouchier, "Designing III–V multijunction solar cells on silicon," *Progress in Photovoltaics: Research and Applications*, vol. 22, no. 7, pp. 810-820, 2014.
[52] N. Jain and M. K. Hudait, "III–V multijunction solar cell integration with silicon: Present status, challenges and future outlook," *Energy Harvesting and Systems*, vol. 1, no. 3-4, pp. 121-145, 2014.
[53] F. D. a. A. W. B. Simon P. Phillips, "high efficiency III-V Multi-junction solar cells". ," *Chapter IC-6. Solar Cells*, no. Second Edition, 2012.
[54] E. F. Fernández, A. J. García-Loureiro, and G. P. Smestad, "Multijunction concentrator solar cells: analysis and fundamentals," *High Concentrator Photovoltaics: Fundamentals, Engineering and Power Plants, Pérez-Higueras, Pedro and Fernández, Eduardo F.(Eds.) Springer*, pp. 9-37, 2015.
[55] P. Biwole, P. Eclache, and F. Kuznik, "Improving the performance of solar panels by the use of phase-change materials," in *World Renewable Energy Congress-Sweden; 8-13 May; 2011; Linköping; Sweden*, 2011, no. 57: Linköping University Electronic Press, pp. 2953-2960.
[56] A. Luque and S. Hegedus, *Handbook of photovoltaic science and engineering*. John Wiley & Sons, 2011.
[57] NREL., "National Center for Photovoltaics. Best research-cell efficiencies chart.," <*http://www.nrel.gov/ncpv/images/efficiency_chart.jpg*>. 2018.
[58] X. Zhang, X. Zhao, S. Smith, J. Xu, and X. Yu, "Review of R&D progress and practical application of the solar photovoltaic/thermal (PV/T) technologies," *Renewable and Sustainable Energy Reviews*, vol. 16, no. 1, pp. 599-617, 2012.
[59] A. Ramos, M. A. Chatzopoulou, I. Guarracino, J. Freeman, and C. N. Markides, "Hybrid photovoltaic-thermal solar systems for combined heating, cooling and power provision in the urban environment," *Energy conversion and management*, vol. 150, pp. 838-850, 2017.
[60] M. George, A. K. Pandey, N. A. Rahim, V. V. Tyagi, S. Shahabuddin, and R. Saidur, "Concentrated photovoltaic thermal systems: A component-by-component view on the developments in the design, heat transfer medium and applications," *Energy Conversion and Management*, vol. 186, pp. 15-41, 2019.

[61] Y. S. Kim, "Modeling of high-concentrator photovoltaic systems for utility-scale applications," in *High Concentrator Photovoltaics*: Springer, 2015, pp. 153-175.
[62] C. J. Riordan, R. Hulstrom, and D. Myers, *Influences of atmospheric conditions and air mass on the ratio of ultraviolet to total solar radiation*. Solar Energy Research Institute, 1990.
[63] J. A. Duffie and W. A. Beckman, *Solar engineering of thermal processes*. John Wiley & Sons, 2013.
[64] T. Muneer, "Solar radiation and daylight models. Elservier Butterworth," ed: Heinemann, Oxford, 2004.
[65] M. Theristis, "Development of a spectral dependent electrical & thermal model for High Concentrating Photovoltaic (HCPV) receivers," Heriot-Watt University, 2016.
[66] T. Markvart and K. Bogus, *Solar electricity*. John Wiley & Sons, 2000.
[67] R. Núñez *et al.*, "Determination of spectral variations by means of component cells useful for CPV rating and design," *Progress in Photovoltaics: Research and Applications*, vol. 24, no. 5, pp. 663-679, 2016.
[68] C. Domínguez and P. García-Linares, "Characterization of multijunction concentrator solar cells," in *High Concentrator Photovoltaics*: Springer, 2015, pp. 39-84.
[69] P. Pérez-Higueras and E. F. Fernández, *High concentrator photovoltaics: fundamentals, engineering and power plants*. Springer, 2015.
[70] "Spectral Characterisation of Photovoltaic Devices Technical Note. ," vol. https://www.bentham.co.uk/fileadmin/uploads/.../PVE300_Technical_Note.pdf.
[71] A. Rabl, "Comparison of solar concentrators," *Solar energy*, vol. 18, no. 2, pp. 93-111, 1976.
[72] R. Winston and W. T. Welford, "Design of nonimaging concentrators as second stages in tandem with image-forming first-stage concentrators," *Applied optics*, vol. 19, no. 3, pp. 347-351, 1980.
[73] A. Valera, E. F. Fernández, F. Almonacid, and P. M. Rodrigo, "Feasibility of flat-plate heat-sinks for ultra-high concentrations (> 2000 suns) using microscale solar cells," 2018: IEEE, pp. 1-4.
[74] C. Algora *et al.*, "III–V multijunction solar cells for ultra-high concentration photovoltaics," in *Photovoltaic Specialists Conference (PVSC), 2009 34th IEEE*, 2009: IEEE, pp. 001571-001575.
[75] L. Micheli, E. F. Fernández, F. Almonacid, K. Reddy, and T. K. Mallick, "Optimization of the least-material approach for passive Ultra-High CPV cooling," in *Photovoltaic Specialist Conference (PVSC), 2015 IEEE 42nd*, 2015: IEEE, pp. 1-6.
[76] L. M. Fraas and L. D. Partain, *Solar cells and their applications*. John Wiley & Sons, 2010.
[77] L. Micheli, N. Sarmah, X. Luo, K. Reddy, and T. K. Mallick, "Opportunities and challenges in micro-and nano-technologies for concentrating photovoltaic cooling: A review," *Renewable and Sustainable Energy Reviews*, vol. 20, pp. 595-610, 2013.
[78] A. Valera, E. F. Fernández, P. M. Rodrigo, and F. Almonacid, "Feasibility of flat-plate heat-sinks using microscale solar cells up to 10,000 suns concentrations," *Solar Energy*, vol. 181, pp. 361-371, 2019.
[79] C. Renno and F. Petito, "Design and modeling of a concentrating photovoltaic thermal (CPV/T) system for a domestic application," *Energy and buildings*, vol. 62, pp. 392-402, 2013.
[80] IEEE-SA Standards Board, "IEEE Recommended Practice for Qualification of Concentrator Photovoltaic (PV) Receiver Sections and Modules,," 2001.

[81] I. E. Commission, "Concentrator photovoltaic (CPV) modules and assemblies–design qualification and type approval," ed: IEC, 2007.
[82] L. Micheli, N. Sarmah, K. Reddy, X. Luo, and T. K. Mallick, "Design, development, and analysis of a densely packed 500x concentrating photovoltaic cell assembly on insulated metal substrate," *International Journal of Photoenergy*, vol. 2015, 2015.
[83] L. Micheli, "Enhancing electrical and heat transfer performance of high-concentrating photovoltaic receivers," *university of exeter, PhD Thesis*, 2015.
[84] I. García, M. Victoria, and I. Antón, "Temperature effects on CPV solar cells, optics and modules," *Handbook on Concentrator Photovoltaic Technology*, p. 245, 2016.
[85] K. Araki, "Annex: CPV modules and systems from daido steel," *Handbook of Concentrator Photovoltaic Technology*, pp. 413-418, 2016.
[86] K. Araki, H. Uozumi, and M. Yamaguchi, "A simple passive cooling structure and its heat analysis for 500/spl times/concentrator PV module," in *Photovoltaic Specialists Conference, 2002. Conference Record of the Twenty-Ninth IEEE*, 2002: IEEE, pp. 1568-1571.
[87] J. Jaus, R. Hue, M. Wiesenfarth, G. Peharz, and A. W. Bett, "Thermal management in a passively cooled concentrator photovoltaic module," *Fraunhofer Institut für System-und Innovationsforschung, Karlsruhe*, 2008.
[88] M. Martinez, I. Antón, and G. Sala, "Effect of wind in the cooling of a PV concentrator and in its energy production," in *Twenty second European PVSEC*, 2007, pp. 790-793.
[89] Y. Ota and K. Nishioka, "Estimation of operating temperature and energy output of concentrator photovoltaic module under concentration conditions," *Japanese Journal of Applied Physics*, vol. 53, no. 12, p. 122301, 2014.
[90] C. Renno and F. Petito, "Triple-junction cell temperature evaluation in a CPV system by means of a Random-Forest model," *Energy Conversion and Management*, vol. 169, pp. 124-136, 2018.
[91] Y. Zhangbo, L. Qifen, Z. Qunzhi, and P. Weiguo, "The cooling technology of solar cells under concentrated system," in *Power Electronics and Motion Control Conference, 2009. IPEMC'09. IEEE 6th International*, 2009: IEEE, pp. 2193-2197.
[92] M. A. Steiner, J. F. Geisz, D. J. Friedman, W. J. Olavarria, A. Duda, and T. E. Moriarty, "Temperature-dependent measurements of an inverted metamorphic multijunction (IMM) solar cell," in *Photovoltaic Specialists Conference (PVSC), 2011 37th IEEE*, 2011: IEEE, pp. 002527-002532.
[93] F. Gualdi, O. Arenas, A. Vossier, A. Dollet, V. Aimez, and R. Arès, "Determining passive cooling limits in CPV using an analytical thermal model," in *9TH INTERNATIONAL CONFERENCE ON CONCENTRATOR PHOTOVOLTAIC SYSTEMS: CPV-9*, 2013, vol. 1556, no. 1: AIP Publishing, pp. 10-13.
[94] P. Espinet-González *et al.*, "Evaluation of the reliability of commercial concentrator triple-junction solar cells by means of accelerated life tests (ALT)," in *AIP Conference Proceedings*, 2013, vol. 1556, no. 1: AIP, pp. 222-225.
[95] M. Muller, S. Kurtz, M. Steiner, and G. Siefer, "Translating outdoor CPV I–V measurements to a CSTC power rating and the associated uncertainty," *Progress in photovoltaics: Research and Applications*, vol. 23, no. 11, pp. 1557-1571, 2015.
[96] M. Muller, C. Deline, B. Marion, S. Kurtz, and N. Bosco, "Determining outdoor CPV cell temperature," in *AIP conference proceedings*, 2011, vol. 1407, no. 1: AIP, pp. 331-335.

[97] E. F. Fernández, F. Almonacid, P. Rodrigo, and P. Pérez-Higueras, "Calculation of the cell temperature of a high concentrator photovoltaic (HCPV) module: a study and comparison of different methods," *Solar Energy Materials and Solar Cells*, vol. 121, pp. 144-151, 2014.
[98] F. Almonacid, E. F. Fernandez, A. Mellit, and S. Kalogirou, "Review of techniques based on artificial neural networks for the electrical characterization of concentrator photovoltaic technology," *Renewable and Sustainable Energy Reviews*, vol. 75, pp. 938-953, 2017.
[99] E. F. Fernández, P. Rodrigo, F. Almonacid, and P. Pérez-Higueras, "A method for estimating cell temperature at the maximum power point of a HCPV module under actual operating conditions," *Solar Energy Materials and Solar Cells*, vol. 124, pp. 159-165, 2014.
[100] L. Breiman, "Random forests," *Machine learning*, vol. 45, no. 1, pp. 5-32, 2001.
[101] L. Lin, F. Wang, X. Xie, and S. Zhong, "Random forests-based extreme learning machine ensemble for multi-regime time series prediction," *Expert Systems with Applications*, vol. 83, pp. 164-176, 2017.
[102] P. Espinet-González *et al.*, "Temperature accelerated life test on commercial concentrator III–V triple-junction solar cells and reliability analysis as a function of the operating temperature," *Progress in Photovoltaics: Research and Applications*, vol. 23, no. 5, pp. 559-569, 2015.
[103] M. Theristis and T. S. O'Donovan, "Electrical-thermal analysis of III–V triple-junction solar cells under variable spectra and ambient temperatures," *Solar Energy*, vol. 118, pp. 533-546, 2015.
[104] C. Renno, G. Landi, F. Petito, and H. Neitzert, "Influence of a degraded triple-junction solar cell on the CPV system performances," *Energy Conversion and Management*, vol. 160, pp. 326-340, 2018.
[105] A. Muron, S. Chowa, J. Wheeldona, K. Hinzera, and H. Schriemera, "Thermal optimization of a solar cell carrier for concentrator systems," in *Proc. of SPIE Vol*, 2011, vol. 8007, pp. 800722-1.
[106] L. Micheli, E. F. Fernández, F. Almonacid, T. K. Mallick, and G. P. Smestad, "Performance, limits and economic perspectives for passive cooling of High Concentrator Photovoltaics," *Solar Energy Materials and Solar Cells*, vol. 153, pp. 164-178, 2016.
[107] F. Ghani, E. Fernandez, F. Almonacid, and T. O'Donovan, "The numerical computation of lumped parameter values using the multi-dimensional Newton-Raphson method for the characterisation of a multi-junction CPV module using the five-parameter approach," *Solar Energy*, vol. 149, pp. 302-313, 2017.
[108] P. M. Rodrigo, R. Velázquez, E. F. Fernández, F. M. Almonacid, and A. Lay-Ekuakille, "A method for the outdoor thermal characterisation of high-concentrator photovoltaic modules alternative to the IEC 62670-3 standard," *Energy*, vol. 148, pp. 159-168, 2018.
[109] F. Almonacid, E. F. Fernández, B. Almonacid-Cruz, and P. M. Rodrigo, "Spectral-matching-ratio modelling based on ANNs and atmospheric parameters for the electrical characterization of multi-junction concentrator PV systems," *Energy*, vol. 156, pp. 409-417, 2018.
[110] M. Theristis, E. F. Fernández, G. E. Georghiou, and T. S. O'Donovan, "Performance of a concentrating photovoltaic monomodule under real operating conditions: Part I–Outdoor characterisation," *Energy Conversion and Management*, vol. 154, pp. 311-321, 2017.
[111] C. Renno, F. Petito, G. Landi, and H. Neitzert, "Experimental characterization of a concentrating photovoltaic system varying the light concentration," *Energy Conversion and Management*, vol. 138, pp. 119-130, 2017.

[112] Z. Wang, H. Zhang, D. Wen, W. Zhao, and Z. Zhou, "Characterization of the InGaP/InGaAs/Ge triple-junction solar cell with a two-stage dish-style concentration system," *Energy Conversion and Management,* vol. 76, pp. 177-184, 2013.
[113] N. Xu, J. Ji, W. Sun, L. Han, H. Chen, and Z. Jin, "Outdoor performance analysis of a 1090× point-focus Fresnel high concentrator photovoltaic/thermal system with triple-junction solar cells," *Energy conversion and management,* vol. 100, pp. 191-200, 2015.
[114] D. K. Gupta, M. Barink, and M. Langelaar, "CPV solar cell modeling and metallization optimization," *Solar Energy,* vol. 159, pp. 868-881, 2018.
[115] T. Sweet *et al.*, "Design and characterization of hybrid III–V concentrator photovoltaic–thermoelectric receivers under primary and secondary optical elements," *Applied Energy,* vol. 226, pp. 772-783, 2018.
[116] M. Bonnet-Eymard, M. Boccard, G. Bugnon, F. Sculati-Meillaud, M. Despeisse, and C. Ballif, "Optimized short-circuit current mismatch in multi-junction solar cells," *Solar Energy Materials and Solar Cells,* vol. 117, pp. 120-125, 2013.
[117] I. Rey-Stolle, J. M. Olson, and C. Algora, "Concentrator Multijunction Solar Cells," *Handbook on Concentrator Photovoltaic Technology,* p. 59, 2016.
[118] M. Steiner *et al.*, "FLATCON® CPV module with 36.7% efficiency equipped with four-junction solar cells," *Progress in Photovoltaics: Research and Applications,* vol. 23, no. 10, pp. 1323-1329, 2015.
[119] G. Segev, G. Mittelman, and A. Kribus, "Equivalent circuit models for triple-junction concentrator solar cells," *Solar Energy Materials and Solar Cells,* vol. 98, pp. 57-65, 2012.
[120] Y. P. Varshni, "Temperature dependence of the energy gap in semiconductors," *Physica,* vol. 34, no. 1, pp. 149-154, 1967.
[121] X. Han, Y. Guo, Q. Wang, J. Qu, and P. Phelan, "Investigations of III–V concentrator solar cells with liquid immersion for high concentrating photovoltaic systems," *Solar Energy,* vol. 158, pp. 728-736, 2017.
[122] G. Peharz, G. Siefer, and A. Bett, "A simple method for quantifying spectral impacts on multi-junction solar cells," *Solar Energy,* vol. 83, no. 9, pp. 1588-1598, 2009.
[123] B. García-Domingo, J. Aguilera, J. De la Casa, and M. Fuentes, "Modelling the influence of atmospheric conditions on the outdoor real performance of a CPV (Concentrated Photovoltaic) module," *Energy,* vol. 70, pp. 239-250, 2014.
[124] K. Araki and M. Yamaguchi, "Influences of spectrum change to 3-junction concentrator cells," *Solar energy materials and solar cells,* vol. 75, no. 3, pp. 707-714, 2003.
[125] P. Verlinden and J. Lasich, "Energy rating of concentrator PV systems using multi-junction III–V solar cells," in *Photovoltaic Specialists Conference, 2008. PVSC'08. 33rd IEEE,* 2008: IEEE, pp. 1-6.
[126] G. S. Kinsey and K. M. Edmondson, "Spectral response and energy output of concentrator multijunction solar cells," *Progress in Photovoltaics: Research and Applications,* vol. 17, no. 5, pp. 279-288, 2009.
[127] E. F. Fernández, A. J. García-Loureiro, and G. P. Smestad, "Multijunction concentrator solar cells: analysis and fundamentals," in *High Concentrator Photovoltaics*: Springer, 2015, pp. 9-37.
[128] D. Friedman, J. Olson, and S. Kurtz, "High-Efficiency III–V Multijunction Solar Cells," *Handbook of Photovoltaic Science and Engineering,* pp. 314-364, 2010.
[129] A. R. Jha, *Solar cell technology and applications*. CRC press, 2009.

[130] A. W. Walker, "Bandgap engineering of multi-junction solar cells using nanostructures for enhanced performance under concentrated illumination," University of Ottawa (Canada), 2013.
[131] M. Green, K. Emery, Y. Hishikawa, W. Warta, and E. Dunlop, "Solar Cell Efficiency Tables (Version 38)," *Progress in Photovoltaics: Research and Applications,* vol. 19, no. NREL/JA-5200-52449, 2011.
[132] C. Gueymard, "Simple model of the atmospheric radiative transfer of sunshine (SMARTS2): algorithms and performance assessment," *Florida: Solar Energy Center,* 1995.
[133] C. A. Gueymard, "Parameterized transmittance model for direct beam and circumsolar spectral irradiance," *Solar Energy,* vol. 71, no. 5, pp. 325-346, 2001.
[134] F. Kasten and A. T. Young, "Revised optical air mass tables and approximation formula," *Applied optics,* vol. 28, no. 22, pp. 4735-4738, 1989.
[135] C. A. Gueymard and D. Myers, "Solar resource for space and terrestrial applications," *Solar Cells and Their Applications,* vol. 217, p. 427, 2010.
[136] D. R. Myers, K. Emery, and C. Gueymard, "Revising and validating spectral irradiance reference standards for photovoltaic performance evaluation," *Journal of solar energy engineering,* vol. 126, no. 1, pp. 567-574, 2004.
[137] J. A. Ruiz-Arias and C. A. Gueymard, "Solar Resource for High-Concentrator Photovoltaic Applications," in *High Concentrator Photovoltaics*: Springer, 2015, pp. 261-302.
[138] E. F. Fernández *et al.,* "Analysis of high concentrator photovoltaic modules in outdoor conditions: influence of direct normal irradiance, air temperature, and air mass," *Journal of Renewable and Sustainable Energy,* vol. 6, no. 1, p. 013102, 2014.
[139] E. F. Fernández *et al.,* "Quantifying the effect of air temperature in CPV modules under outdoor conditions," in *8TH INTERNATIONAL CONFERENCE ON CONCENTRATING PHOTOVOLTAIC SYSTEMS: CPV-8,* 2012, vol. 1477, no. 1: AIP Publishing, pp. 194-197.
[140] M. Meusel, R. Adelhelm, F. Dimroth, A. Bett, and W. Warta, "Spectral mismatch correction and spectrometric characterization of monolithic III–V multi-junction solar cells," *Progress in Photovoltaics: Research and Applications,* vol. 10, no. 4, pp. 243-255, 2002.
[141] H. Cotal *et al.,* "III–V multijunction solar cells for concentrating photovoltaics," *Energy & Environmental Science,* vol. 2, no. 2, pp. 174-192, 2009.
[142] P. Mialhe, B. Affour, K. El-Hajj, and A. Khoury, "High Injection Effects on Solar Cell Performances," *Active and Passive Electronic Components,* vol. 17, no. 4, pp. 227-232, 1995.
[143] R. R. King, R. A. Sinton, and R. M. Swanson, "Doped surfaces in one sun, point-contact solar cells," *Applied Physics Letters,* vol. 54, no. 15, pp. 1460-1462, 1989.
[144] M. Ochoa, E. Barrigón, L. Barrutia, I. García, I. Rey-Stolle, and C. Algora, "Limiting factors on the semiconductor structure of III–V multijunction solar cells for ultra-high concentration (1000–5000 suns)," *Progress in Photovoltaics: Research and Applications,* vol. 24, no. 10, pp. 1332-1345, 2016.
[145] G. S. Kinsey, P. Hebert, K. E. Barbour, D. D. Krut, H. L. Cotal, and R. A. Sherif, "Concentrator multijunction solar cell characteristics under variable intensity and temperature," *Progress in Photovoltaics: Research and Applications,* vol. 16, no. 6, pp. 503-508, 2008.
[146] S. Yoon and V. Garboushian, "Reduced temperature dependence of high-concentration photovoltaic solar cell open-circuit voltage (Voc) at high concentration levels," in *Photovoltaic Energy Conversion, 1994., Conference*

Record of the Twenty Fourth. IEEE Photovoltaic Specialists Conference-1994, 1994 IEEE First World Conference on, 1994, vol. 2: IEEE, pp. 1500-1504.

[147] C. Min, C. Nuofu, Y. Xiaoli, and Z. Han, "Fabrication and Temperature dependence of a GaInP/GaAs/Ge tandem solar cell," *Journal of Semiconductors,* vol. 33, no. 2, p. 024006, 2012.

[148] R. I. Rabady, "Optimized multi-junction photovoltaic solar cells for terrestrial applications," *Solar Energy*, vol. 106, pp. 72-81, 2014.

[149] S. M. Sze and K. K. Ng, *Physics of semiconductor devices*. John wiley & sons, 2006.

[150] G. F. Xing J, . "An improvement temperature estimation method for solar cell operating at high concentrations" *solar energy*, 2013.

[151] H. Cotal and R. Sherif, "Temperature dependence of the IV parameters from triple junction GaInP/InGaAs/Ge concentrator solar cells," in *Photovoltaic Energy Conversion, Conference Record of the 2006 IEEE 4th World Conference on*, 2006, vol. 1: IEEE, pp. 845-848.

[152] K. Nishioka, T. Takamoto, T. Agui, M. Kaneiwa, Y. Uraoka, and T. Fuyuki, "Evaluation of temperature characteristics of high-efficiency InGaP/InGaAs/Ge triple-junction solar cells under concentration," *Solar energy materials and solar cells,* vol. 85, no. 3, pp. 429-436, 2005.

[153] P. Singh and N. M. Ravindra, "Temperature dependence of solar cell performance—an analysis," *Solar Energy Materials and Solar Cells,* vol. 101, pp. 36-45, 2012.

[154] H. Helmers, M. Schachtner, and A. W. Bett, "Influence of temperature and irradiance on triple-junction solar subcells," *Solar Energy Materials and Solar Cells,* vol. 116, pp. 144-152, 2013.

[155] G. Siefer and A. W. Bett, "Analysis of temperature coefficients for III–V multi-junction concentrator cells," *Progress in Photovoltaics: Research and Applications,* vol. 22, no. 5, pp. 515-524, 2014.

[156] A. O. Maka and T. S. O'Donovan, "Analysis of thermal response and electrical characterisation of triple-junction solar cells based on variable solar spectral irradiance and air mass," *Thermal Science and Engineering Progress,* 2019.

[157] G. A. Landis and E. Haag, "Analysis of Solar Cell Efficiency for Venus Atmosphere and Surface Missions," in *11th International Energy Conversion Engineering Conference, San Jose CA*, 2013.

[158] L. Z. Broderick, B. R. Albert, B. S. Pearson, L. C. Kimerling, and J. Michel, "Design for energy: Modeling of spectrum, temperature and device structure dependences of solar cell energy production," *Solar Energy Materials and Solar Cells,* vol. 136, pp. 48-63, 2015.

[159] A. O. Maka and T. S. O'Donovan, "Modelling of the thermal behaviour of solar high concentrating photovoltaic receiver," *Thermal Science and Engineering Progress,* vol. 9, pp. 281-288, 2019.

[160] N. S. Kumar *et al.*, "Experimental validation of a heat transfer model for concentrating photovoltaic system," *Applied Thermal Engineering,* vol. 33, pp. 175-182, 2012.

[161] A. Aldossary, S. Mahmoud, and R. Al-Dadah, "Technical feasibility study of passive and active cooling for concentrator PV in harsh environment," *Applied Thermal Engineering,* vol. 100, pp. 490-500, 2016.

[162] F. Fernández *et al.*, "Calculation of cell temperature in a HCPV module using V oc," in *Electron Devices (CDE), 2013 Spanish Conference on*, 2013: IEEE, pp. 317-320.

[163] H. Lv, F. Sheng, J. Dai, W. Liu, C. Cheng, and J. Zhang, "Temperature-dependent model of concentrator photovoltaic modules combining optical elements and III–V multi-junction solar cells," *Solar Energy*, vol. 112, pp. 351-360, 2015.
[164] F. Sarhaddi, S. Farahat, H. Ajam, A. Behzadmehr, and M. M. Adeli, "An improved thermal and electrical model for a solar photovoltaic thermal (PV/T) air collector," *Applied Energy*, vol. 87, no. 7, pp. 2328-2339, 2010.
[165] İ. Ceylan, A. E. Gürel, A. Ergün, and A. Tabak, "Performance analysis of a concentrated photovoltaic and thermal system," *Solar Energy*, vol. 129, pp. 217-223, 2016.
[166] Y. Ota, H. Nagai, K. Araki, and K. Nishioka, "Thermal transfer simulation for concentrator photovoltaic receiver under concentration condition," in *9TH INTERNATIONAL CONFERENCE ON CONCENTRATOR PHOTOVOLTAIC SYSTEMS: CPV-9*, 2013, vol. 1556, no. 1: AIP Publishing, pp. 18-21.
[167] L. M. Jiji and L. M. Jiji, *Heat convection*. Springer, 2006.
[168] C. Multiphysics, "COMSOL multiphysics user guide (Version 4.3 a)," *COMSOL, AB*, pp. 39-40, 2012.
[169] P. Rodrigo, L. Micheli, and F. Almonacid, "The high-concentrator photovoltaic module," in *High concentrator photovoltaics*: Springer, 2015, pp. 115-151.
[170] W. Frei, "Solutions to Linear Systems of Equations: Direct and Iterative Solvers," *COMSOL Blog*, 2013.
[171] T. L. Chou, Shih, Z.H., Hong, H.F., Han, C.N.," Chiang, K.N.,, "Thermal performance assessment and validation of high-concentration photovoltaic solar cell module," *IEEE Trans. Comp. Packag. Manuf. Technol*, vol. 2, pp. 578–586, 2012.
[172] L. Micheli, N. Sarmah, X. Luo, K. Reddy, and T. K. Mallick, "Design of a 16-cell densely-packed receiver for high concentrating photovoltaic applications," *Energy Procedia*, vol. 54, pp. 185-198, 2014.
[173] M. Theristis, C. Stark, and T. S. O'Donovan, "Determination of the cooling requirements for single cell photovoltaic receivers under variable atmospheric parameters," in *Photovoltaic Specialist Conference (PVSC), 2015 IEEE 42nd*, 2015: IEEE, pp. 1-5.
[174] G. Peharz, J. P. Ferrer Rodríguez, G. Siefer, and A. W. Bett, "Investigations on the temperature dependence of CPV modules equipped with triple-junction solar cells," *Progress in Photovoltaics: Research and Applications*, vol. 19, no. 1, pp. 54-60, 2011.
[175] H. Baig, K. C. Heasman, and T. K. Mallick, "Non-uniform illumination in concentrating solar cells," *Renewable and Sustainable Energy Reviews*, vol. 16, no. 8, pp. 5890-5909, 2012.
[176] M. Wiesenfarth, S. Gamisch, P. Jakob, M. Steiner, and A. W. Bett, "Systematic design evaluation on the example of a concentrator photovoltaic module with mirror optics and passive heat dissipation," *Progress in Photovoltaics: Research and Applications*.
[177] D. Talavera, P. Pérez-Higueras, J. Ruíz-Arias, and E. Fernández, "Levelised cost of electricity in high concentrated photovoltaic grid connected systems: spatial analysis of Spain," *Applied Energy*, vol. 151, pp. 49-59, 2015.
[178] S. Kurtz and J. Geisz, "Multijunction solar cells for conversion of concentrated sunlight to electricity," *Optics express*, vol. 18, no. 101, pp. A73-A78, 2010.
[179] F. Dimroth *et al.*, "Wafer bonded four-junction GaInP/GaAs//GaInAsP/GaInAs concentrator solar cells with 44.7% efficiency," *Progress in Photovoltaics: Research and Applications*, vol. 22, no. 3, pp. 277-282, 2014.
[180] Y. A. Cengel, *Heat transfer: a practical approach*. WBC McGraw-Hill, 1998.

[181] N.-Y. Wang, S.-Y. Chiang, T.-L. Chou, Z.-H. Shih, H.-F. Hong, and K.-N. Chiang, "Transient thermal analysis of high-concentration photovoltaic cell module subjected to coupled thermal and power cycling test conditions," in *Thermal and Thermomechanical Phenomena in Electronic Systems (ITherm), 2010 12th IEEE Intersociety Conference on*, 2010: IEEE, pp. 1-6.
[182] D. Torres-Lobera and S. Valkealahti, "Inclusive dynamic thermal and electric simulation model of solar PV systems under varying atmospheric conditions," *Solar Energy*, vol. 105, pp. 632-647, 2014.
[183] L. Migliorini, L. Molinaroli, R. Simonetti, and G. Manzolini, "Development and experimental validation of a comprehensive thermoelectric dynamic model of photovoltaic modules," *Solar Energy*, vol. 144, pp. 489-501, 2017.
[184] K. Nishioka, T. Sueto, M. Uchida, and Y. Ota, "Detailed analysis of temperature characteristics of an InGaP/InGaAs/Ge triple-junction solar cell," *Journal of electronic materials*, vol. 39, no. 6, pp. 704-708, 2010.
[185] M. Theristis, N. Sarmah, T. K. Mallick, and T. S. O'Donovan, "Design and numerical analysis of enhanced cooling techniques for a high concentration photovoltaic (HCPV) system," 2012, pp. 260-265.
[186] " Azurspace, triple junction solar cell assembly – Type 3C42A," *data sheet* 2014.
[187] H. Cotal and J. Frost, "Heat transfer modeling of concentrator multijunction solar cell assemblies using finite difference techniques," in *Photovoltaic Specialists Conference (PVSC), 2010 35th IEEE*, 2010: IEEE, pp. 000213-000218.
[188] A. Sharpe, P. Eames, F. Dimroth, K. Araki, and I. Antón, "Modelling of multijunction cell temperature distributions subject to realistic operating conditions," in *AIP Conference Proceedings*, 2013, vol. 1556, no. 1: AIP, pp. 142-146.
[189] S. Jakhar, M. Soni, and N. Gakkhar, "Historical and recent development of concentrating photovoltaic cooling technologies," *Renewable and Sustainable Energy Reviews*, vol. 60, pp. 41-59, 2016.
[190] M. Theristis, E. F. Fernández, C. Stark, and T. S. O'Donovan, "A theoretical analysis of the impact of atmospheric parameters on the spectral, electrical and thermal performance of a concentrating III–V triple-junction solar cell," *Energy Conversion and Management*, vol. 117, pp. 218-227, 2016.
[191] P. Faine, S. R. Kurtz, C. Riordan, and J. Olson, "The influence of spectral solar irradiance variations on the performance of selected single-junction and multijunction solar cells," *Solar cells*, vol. 31, no. 3, pp. 259-278, 1991.
[192] E. F. Fernández, F. Almonacid, J. Ruiz-Arias, and A. Soria-Moya, "Analysis of the spectral variations on the performance of high concentrator photovoltaic modules operating under different real climate conditions," *Solar Energy Materials and Solar Cells*, vol. 127, pp. 179-187, 2014.
[193] R. Perez, T. Cebecauer, and M. Šúri, "Semi-empirical satellite models," *Solar energy forecasting and resource assessment*, pp. 21-48, 2013.
[194] R. Chauvin, J. Nou, J. Eynard, S. Thil, and S. Grieu, "A new approach to the real-time assessment and intraday forecasting of clear-sky direct normal irradiance," *Solar Energy*, vol. 167, pp. 35-51, 2018.
[195] E. Roumpakias and A. Stamatelos, "Comparative performance analysis of grid-connected photovoltaic system by use of existing performance models," *Energy Conversion and Management*, vol. 150, pp. 14-25, 2017.
[196] F. Almonacid, P. Pérez-Higueras, E. F. Fernández, and P. Rodrigo, "Relation between the cell temperature of a HCPV module and atmospheric parameters," *Solar Energy Materials and Solar Cells*, vol. 105, pp. 322-327, 2012.

[197] F. Spertino, A. D'angola, D. Enescu, P. Di Leo, G. V. Fracastoro, and R. Zaffina, "Thermal–electrical model for energy estimation of a water cooled photovoltaic module," *Solar Energy,* vol. 133, pp. 119-140, 2016.
[198] N. Blair *et al.*, "System advisor model, sam 2014.1. 14: General description," National Renewable Energy Laboratory (NREL), Golden, CO., 2014.
[199] F. Almonacid, A. Mellit, and S. A. Kalogirou, "Applications of ANNs in the Field of the HCPV Technology," in *High Concentrator Photovoltaics*: Springer, 2015, pp. 333-351.
[200] A. K. Tossa, Y. Soro, Y. Azoumah, and D. Yamegueu, "A new approach to estimate the performance and energy productivity of photovoltaic modules in real operating conditions," *Solar energy,* vol. 110, pp. 543-560, 2014.
[201] E. F. Fernández, F. Almonacid, T. Mallick, and P. Pérez-Higueras, "Analytical modelling of high concentrator photovoltaic modules based on atmospheric parameters," *International Journal of Photoenergy,* vol. 2015, 2015.
[202] Z. Mi *et al.*, "Performance Analysis of a Grid-connected High Concentrating Photovoltaic System under Practical Operation Conditions," *Energies,* vol. 9, no. 2, p. 117, 2016.
[203] A. Bonkaney, S. Madougou, and R. Adamou, "Impacts of Cloud Cover and Dust on the Performance of Photovoltaic Module in Niamey," *Journal of Renewable Energy,* vol. 2017, 2017.